DELAY-LINE STABILIZED MICROWAVE OSCILLATOR WITH FREQUENCY CONTROL

A thesis submitted for the degree of Doctor of Philosophy

by

Charles Edward Free

Department of Electrical & Electronic Engineering,
Brunel University

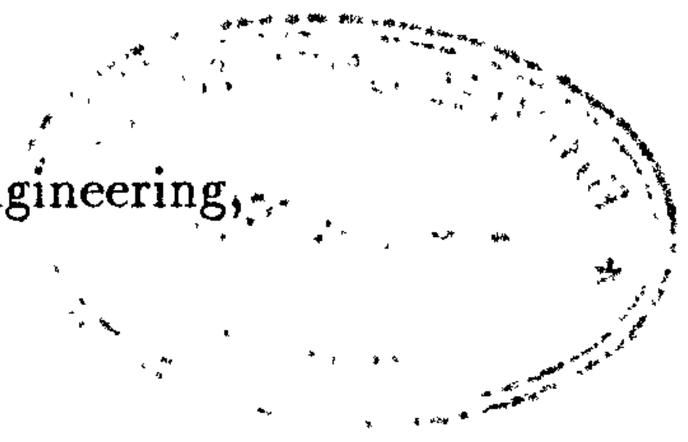

April 1997

Abstract

The technique whereby the frequency of an oscillator is stabilized using an external feedback network incorporating a delay-line is extended in this thesis to provide digital control of the frequency of the oscillator.

Novel circuit techniques have been developed and analysed to permit the implementation of the proposed frequency control technique in a compact format, suitable for implementation in either hybrid or monolithic microwave integrated circuits. Two new microstrip circuits have been introduced, namely the three-port ring discriminator and the single PIN diode phase shifter.

Frequency control of an oscillator is achieved by digitally controlling the time delay through phase shifters in the feedback path of the oscillator's stabilization circuit. A new microstrip phase shifting circuit has been developed which has the advantage of requiring only one active switching element to achieve each digital bit of phase change. The circuit has been analysed in detail and results obtained at X-band to support the theoretical predictions. As part of the analysis of this new component, and in order to permit a greater degree of precision in the design of the phase changes, some new microstrip design techniques have been introduced. These have led to a more exact design for coupled line phase shifters and to an equivalent circuit to represent the excess phase in microstrip DC breaks.

Delay-line stabilization of an oscillator requires the use of a phase sensitive network, or frequency discriminator. Whilst this could be realised on microstrip using conventional circuitry, by interconnecting two hybrid rings, a new circuit component, namely the three-port ring discriminator, was developed to provide a simpler, more compact solution. A rigorous analysis of the new circuit is presented, and the behaviour verified through measurements over the frequency range 8-12GHz.

The new single PIN diode phase shifter has been incorporated in the delay

path of a three-port ring discriminator, and used to control the frequency of an oscillator. Results are presented for circuits at X-band which show the degree of frequency stabilization that has been obtained, together with the reduction in oscillator phase noise. In addition, the original concept of delay-line switching to control the frequency of an oscillator has been extended to yield a further new circuit, based on a three-port ring with a switched-feed mechanism; results are presented which verify the operation of this new circuit both theoretically and through practical measurement.

New techniques for controlling the frequency of microstrip oscillators have thus been established, both theoretically and through practical measurement, which combine simple methods of frequency selection with inherent low-noise performance.

Contents

List of Figures

Acknowledgments

The author is indebted to his supervisor, Prof. C.S. Aitchison, for his help and encouragement throughout the duration of the project.

Author's Declaration

The work described in this thesis is based on original study carried out by the author under the guidance of his supervisor. Where known or published material has been included, appropriate references have been cited.

Introduction

Oscillators which offer digital frequency control together with low noise performance are increasing in demand in modern communication systems. Moreover, for many such systems, particularly those designed for commercial applications, cost is also a premium factor. Whilst frequency synthesizer techniques can yield oscillators with extremely high performance, in terms of frequency selection and low phase noise, they tend to be expensive, particularly at microwave frequencies. The purpose of this study was to investigate a new technique for implementing control of the frequency of an oscillator using a switched delay line technique.

Delay line techniques for stabilizing the frequency of an oscillator are well known at frequencies up to the low microwave region. The work described in this report extends the technique to higher microwave frequencies than have hitherto been reported in the literature, and includes the effect of delay line switching to achieve frequency control. The principal intention was to implement the new technique as a hybrid microwave integrated circuit, using microstrip techniques. Whilst this would be relatively straightforward using standard microstrip components, a number of new microstrip circuit configurations, notably the single PIN diode phase shifter and the three-port ring discriminator, were introduced to minimise circuit complexity and provide a low cost solution, which was both economically and technically viable.

In order to obtain a rigorous understanding of the behaviour of these new circuit elements, some new theoretical methods of circuit analysis have been introduced, and these are discussed in some detail in the appropriate chapters.

Chapter 1. Review of Previous Work Starting with a description of existing delay line techniques for stabilizing an oscillator, the discussion is extended to consider the methods of fabrication which have been employed and the resulting implications in terms of frequency and noise performance. Since the intention of the present work is to implement circuits in a microstrip format a review is presented of relevant microstrip devices, namely phase shifters, delay lines and discriminators.

Chapter 2. Single PIN Diode Phase Shifter. The theory and practical results for a new type of microstrip phase shifter, which uses a single PIN diode to achieve the switching function, is described. In the course of the discussion a new and more accurate theory is presented for the analysis of coupled microstrip lines. The phase shifting circuits which are described include planar DC breaks to permit DC biasing of the PIN diodes. A hitherto unknown excess phase associated with these breaks is identified and an equivalent circuit model developed to permit precise transmission phase calculations.

Chapter 3. Three-Port Ring Discriminator A new type of microstrip discriminator, based on a three-port ring, is presented. The concept of the three-port ring is explained and expanded into numerical detail using conventional odd and even equivalent circuit analysis. Modifications to existing theory are given to permit the analysis of asymmetric ring structures. Practical results at X-band are given to support the proposed circuit. Consideration is also given to the effects of circuit discontinuities on the discriminator performance.

Chapter 4. Extended Analysis of Microstrip Ring Circuits. A new method of analysis of microstrip ring structures is introduced. The method makes use of a current summing technique which is shown to be particularly useful for analysing asymmetric ring structures. Theoretical results are presented for the three-port ring structures introduced in chapter 3, and the results are extended to consider the effects of simultaneously feeding a ring structure at a number of different positions. In order to demonstrate the validity of the new analytical technique, it is applied to the well known four port hybrid ring.

Chapter5. Microwave Oscillator Control using a Single Switched Delay-Line. The construction and performance of an oscillator control circuit which combines the three port ring discriminator and the single PIN diode phase shifter is described. The circuit is based on the idea of delay line switching in a microwave discriminator which was initially described in the introduction. Results are presented which show how the frequency of the oscillator can be controlled by switching the PIN diode phase shifter, thereby causing variations in the delay path of the three port discriminator. Included in the results are phase noise responses which show the effect of circuit stabilization and demonstrate the ability of the circuit to reduce the close carrier noise of the oscillator.

Chapter 6. A Digitally Controlled Microwave Oscillator. The results of the new theory introduced in chapter 4 are exploited to produce a circuit for controlling digitally the frequency of an oscillator. The results for a dual-fed microstrip circuit at X-band are described. In addition to demonstrating the frequency selection capabilities of the circuit, phase noise responses show how the circuit stabilization properties are maintained as the frequency of the oscillator is switched. Also presented are time domain responses which provide an indication of the settling time of the oscillator together with the effects of transient overshoot.

Chapter 7. Overview Discussion. A short discussion of some of the general aspects of the work is given to supplement the detailed discussions on the individual activities which are are presented at the ends of chapters 2 through 6.

Chapter 8. Conclusions and Suggestions for Further Work. This provides a summary of the main outcomes of the work, and is supplemented in Appendix C by details of the publications which have resulted from the project. Some suggestions are provided for a more detailed analysis of the noise aspects of the frequency control systems investigated and for the expansion of the circuits to provide greater design flexibility.

Chapter 1

Review of Previous Work

1.1 Summary

The main aim of the present work is to extend the concept of the delay-line stabilised oscillator to include control of the oscillator frequency. It is intended that the arrangement will be implemented in microstrip and that the control function will be achieved by including a switched, microstrip phase shifter in the time delay path of the stabilisation circuit. Thus the review of previous work has been divided into three sections. The first concentrates on work which has been reported on delay-line stabilised oscillators. The second section considers how the basic, single frequency delay-line stabilisation circuit could be implemented in microstrip, using existing components. The last section is devoted to microstrip techniques which have been reported for the implementation of digitally-controlled phase shifters.

1.2 Delay-line stabilised oscillators

The concept of a delay-stabilised variable frequency oscillator was first introduced by UNDERHILL [1]. He described a technique whereby the frequency of an oscillator could be continuously tuned over a 2:1 frequency range, whilst maintaining a frequency stability approaching that of a quartz-crystal oscillator. The oscillator system used is shown in Fig. 1.1, p. 22. The essential principle is that the output from the oscillator is split in a feedback network. One half of the split signal is applied directly to a phase detector (PD) and

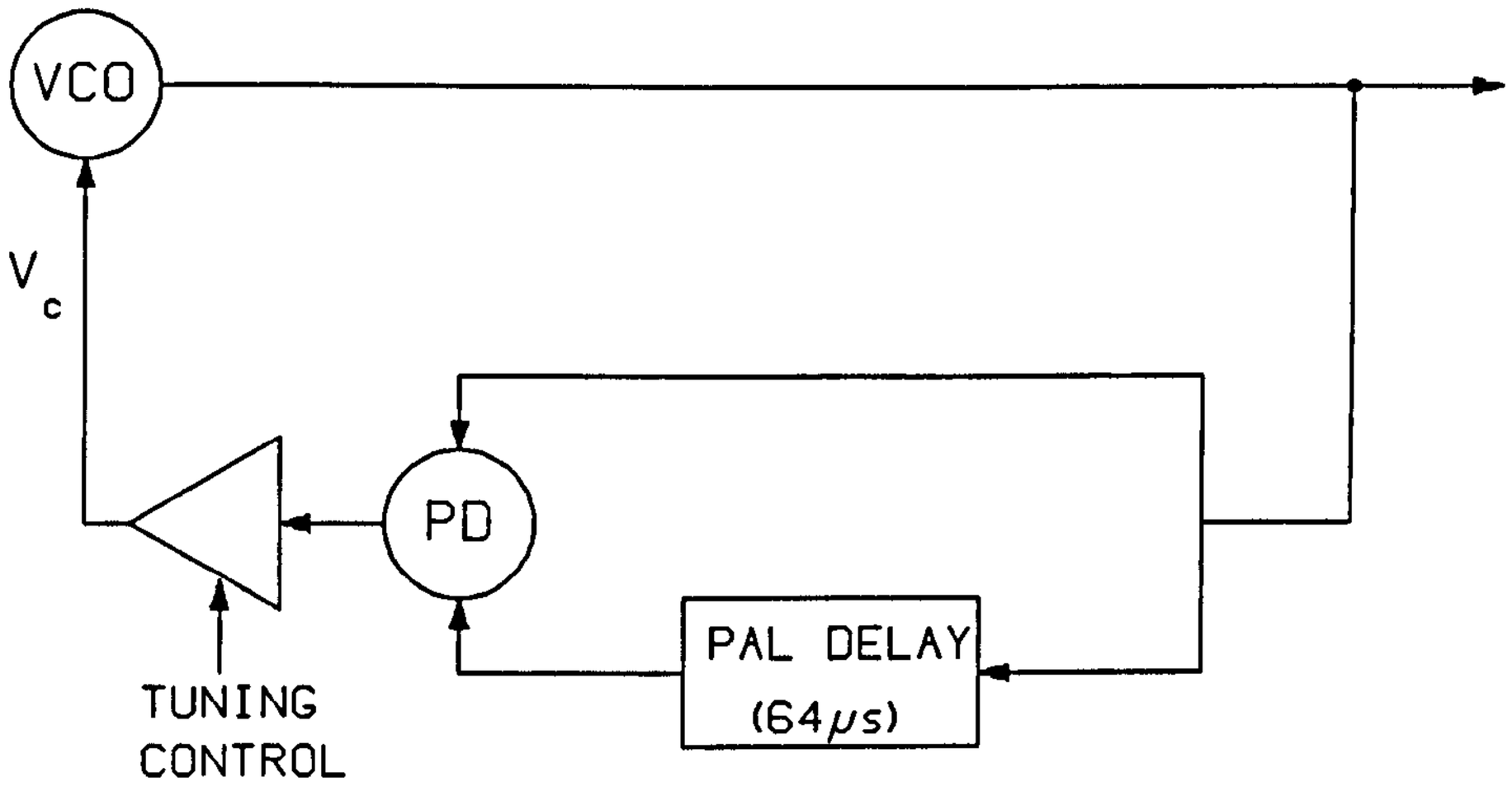

Figure 1.1: **Low-frequency delay-line stabilised oscillator**

the other signal is connected to the detector though a delay-line. Since the delay line provides a phase shift which is proportional to frequency the use of a linear phase detector will provide an output voltage which is linearly proportional to frequency. In the arrangement shown in Fig. 1.1, above, the output from the phase detector is compared with a reference voltage in a differential amplifier, whose output is then used as the frequency controlling signal for the voltage controlled oscillator (VCO). A tuning voltage is shown which provides a variable reference level and hence allows the frequency of the system to be externally tuned. Whilst the stability of the this arrangement depends primarily on the stability of the delay-line, it is also dependent on the stability of the tuning voltage. Underhill does not address this aspect directly, but assumes that the tuning voltage contributes no error. Results are presented for an oscillator working over the range 3-6MHz, using a PAL delay line giving a delay of approximately $64\mu s$. Spectral responses are given which show a significant reduction in close-carrier noise, although this has not been quantified. The general conclusion from the paper was that the

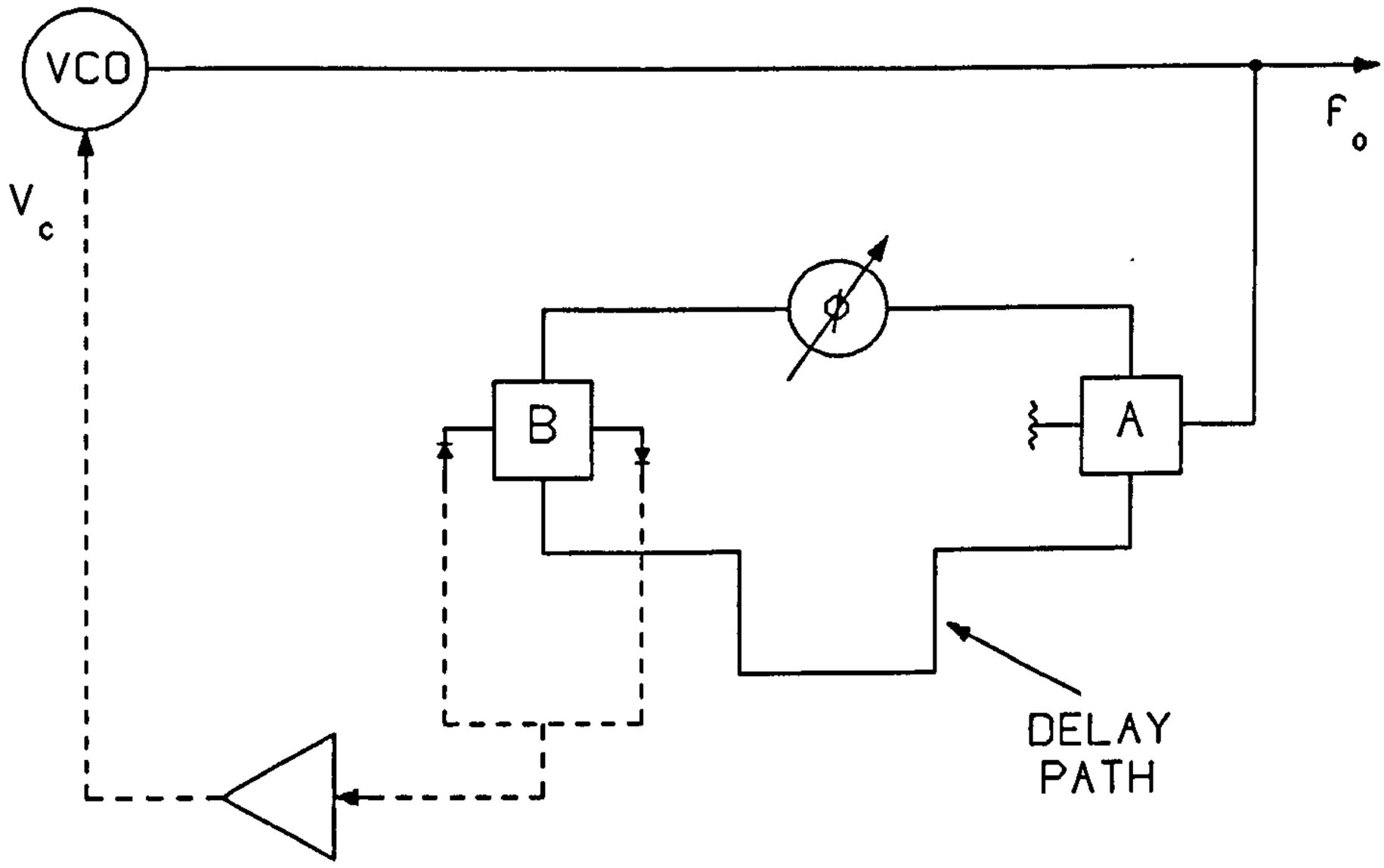

Figure 1.2: **Microwave delay-line stabilised oscillator.**

delay-line stabilisation technique offered performance between that of fully variable, but not very stable LC oscillators, and that of highly stable discretely stepped frequency synthesisers.

Subsequently, AITCHISON AND BATLIWALA [2] showed that the principle established by UNDERHILL [1] could be extended to microwave frequencies. At these frequencies the required time delay can be achieved by a relatively short length of microwave transmission line. The experimental circuit reported by AITCHISON AND BATLIWALA [2] is shown in Fig. 1.2, above. For clarity, the non-microwave connections are represented by broken lines. The circuit was built using standard WG16 waveguide. The principle of operation was essentially the same as that for Underhill's system. A hybrid -T junction (A) was used to split the oscillator output into the two paths to the phase detector. One path contained an additional length of waveguide to provide the delay, and the other a variable phase changer to set the frequency of

operation. In this arrangement the phase detector was formed by a second hybrid-T junction (B) and two detector diodes connected in anti-phase. Convincing results were presented which gave a stabilisation ratio of 23 and a significant reduction in close carrier noise. One difference between the work reported in this paper and that from Underhill is that the authors here do not consider the effect of circuit tuning or frequency switching. The authors conclude that the low-frequency technique demonstrated by Underhill is viable at microwave frequencies and, moreover, that the technique is suitable for transfer to microstrip. With regard to microstrip they make the further point that low-temperature-dependent substrates should be used. In a subsequent paper the same authors BATLIWALA AND AITCHISON [3] present information on the temperature dependence of a modified zirconate substrate, but they do not relate these results to the delay-line stabilisation circuit.

It was around the time that AITCHISON AND BATLIWALA [2] demonstrated the feasibility of applying delay-line stabilisation at microwave frequencies, that a number of authors reported results of similar experiments. GLANCE AND SNELL [4] described the results for a discriminator-stabilised microstrip oscillator, which used an octagonal microstrip resonator. The resonator was designed to give two orthogonally polarised resonances which were coupled to reversed diode pair, whose combined output yielded a discriminator function. The paper describes results for the technique applied to a Gunn diode oscillator working at 5.2GHz. A measured stabilisation ratio of 1000 was quoted, although it is difficult to relate this to the results of other authors because of a lack of information about frequency performance. However, the authors point out that frequency tuning is achievable by either adjusting the resonator lengths or by dielectric loading of the resonator. In either case this would indicate an effectively fixed frequency device.

In 1977, AMBLARD AND PEYRAT [5] described an X-band bulk-wave delay-line stabilised oscillator, using the principle established by AITCHISON AND BATLIWALA [2], whom they reference. Amblard and Peyrat use a $0.5\mu s$ acoustic bulk-wave delay-line in the general interferometer arrangement discussed earlier. Their reasons for choosing this type of delay line were that it exhibits high Q, wide frequency range of operation and has a low vibration sensitivity. This makes the bulk-wave stabilisation technique particularly suitable for airborne and similar applications where there are hard temper-

ature and vibration requirements. However, the drawback of the technique, compared to transmission line arrangements, is that the frequency of operation is limited by the bulk-wave device. Such devices are only available up to low microwave frequencies. Amblard and Peyrat present results for a stabilised Gunn diode oscillator, with a phase noise performance comparable with a crystal stabilised source. Although the main thrust of this paper is towards the demonstration of the stabilisation properties of bulk wave systems, it is worth noting that the absolute values of phase noise quoted are rather high for an X-band device.

The delay-line stabilisation technique, although attractive in terms of its quality and simplicity, does not appear to have been seriously addressed in the recent literature. Moreover, where delay-line techniques are mentioned, it tends to be in terms of surface acoustic wave delay devices. Certainly there has been been no attempt to extend the capability of the delay-line technique to make a digitally controlled oscillator by digitally switching the delay time.

1.3 Microstrip implementation

The main thrusts of the present work are to implement in microstrip the microwave delay-line stabilisation technique established in waveguide by AITCHISON AND BATLIWALA [2] and to extend the technique to provide digital control of the frequency of an oscillator.

Implementing in microstrip the circuit shown in Fig. 1.2, p. 23 is relatively straightforward using standard microstrip components. The hybrid-T junctions can be replaced by hybrid rings and the remainder of the interconnections by microstrip transmission lines, with a difference (δ) in the length of the two lines interconnecting the hybrid rings so as to provide an effective delay in one path. The value of δ would be set to λ_s, where λ_s is the substrate wavelength at the design frequency. This would then provide the necessary delay of one period to centre the discriminator response at the design frequency. A basic microstrip arrangement is shown schematically in Fig. 1.3, p. 26. This differs from the circuit of Fig. 1.2, p. 23 in that there is no variable phase shifter. Using microstrip CAD software, which includes discontinuity compensation, it should be possible for a simple microstrip circuit to be designed for a precise frequency, without the need for circuit tuning, and so

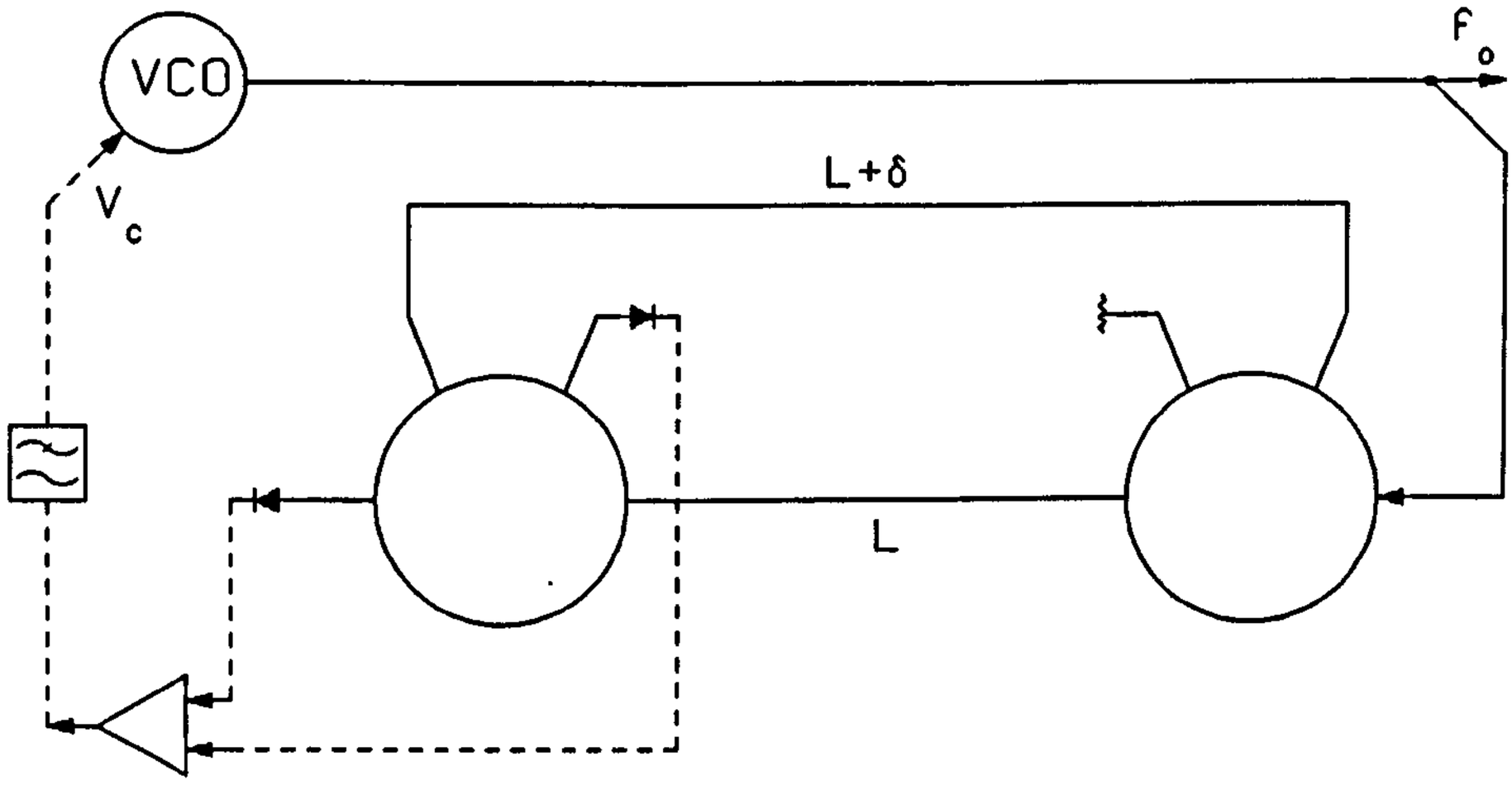

Figure 1.3: **Microstrip implementation of delay-line stabilisation circuit using standard microstrip components**

alleviating the need for a continuously variable phase shifter. It should be noted that a hybrid ring is preferred to 3-port Wilkinson power splitter to achieve the 3dB signal division at the input , since there is zero loss at the design frequency. Hybrid rings are well established devices with little recent development reported in the literature, apart from modifications to achieve broadband performance. KIM AND NAITO [6] showed that by modifying the widths of the ring it was possible to improve the 3dB performance of a conventional hybrid ring structure by a factor of 1.84.

However, the aim of the present work was not just to implement the delay-technique in microstrip at a single frequency, but rather to change the delay time so as to produce an offset voltage at the amplifier output which could then be used to provide a step change in the oscillator frequency. Clearly, if the delay time could be digitally controlled this would in turn provide digital control of the oscillator frequency. Changing the delay digitally requires the inclusion of a digital phase shifter in the effective delay path as shown in Fig. 1.4, p. 27.

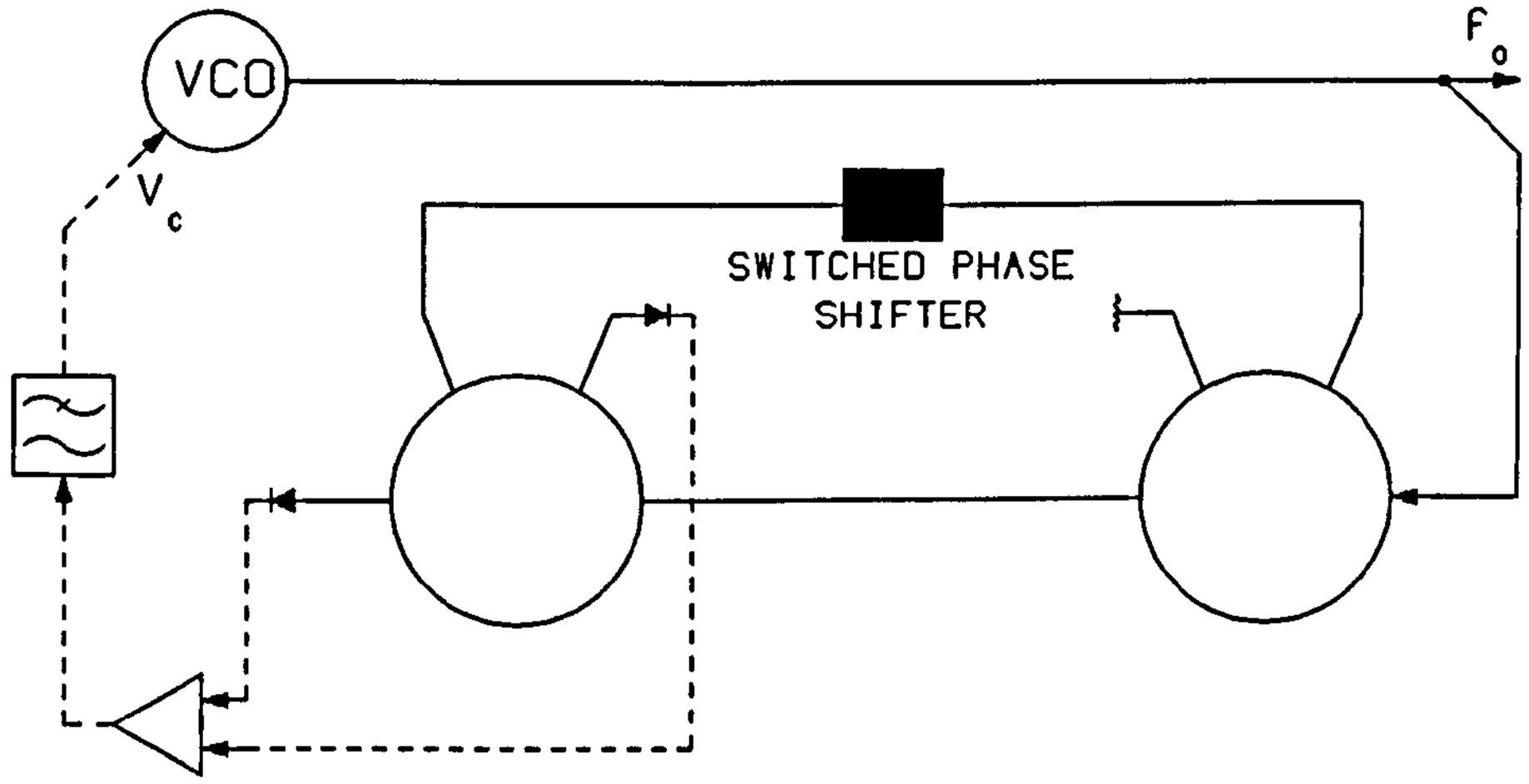

Figure 1.4: **Microstrip stabilisation circuit with digital control.**

1.3.1 Digitally controlled microstrip phase shifters.

There are three established techniques for switching the phase in a microstrip circuit. They make use of switched lines, reactively loaded lines and reflections from reactively loaded 3dB hybrids. Thorough descriptions of these techniques, together with practical performance data can be found in WHITE [12] and FOOKS AND ZAKAREVICIUS [22]. The switched phase shifters so far reported in the literature, both for hybrid and monolithic circuits, have used these techniques either singly or in combination.

The switched line phase shifter is the simplest of the three types to design and implement. A typical microstrip layout is shown in Fig. 1.5, p. 28. A signal entering at port 1 is routed either through path X, by switching the PIN diodes D_1 and D_2 on, and D_3 and D_4 off, or through path Y by switching D_1 and D_2 off, and D_3 and D_4 on. Since the transmission phase is proportional to the line length there will be a change in phase proportional to the differ-

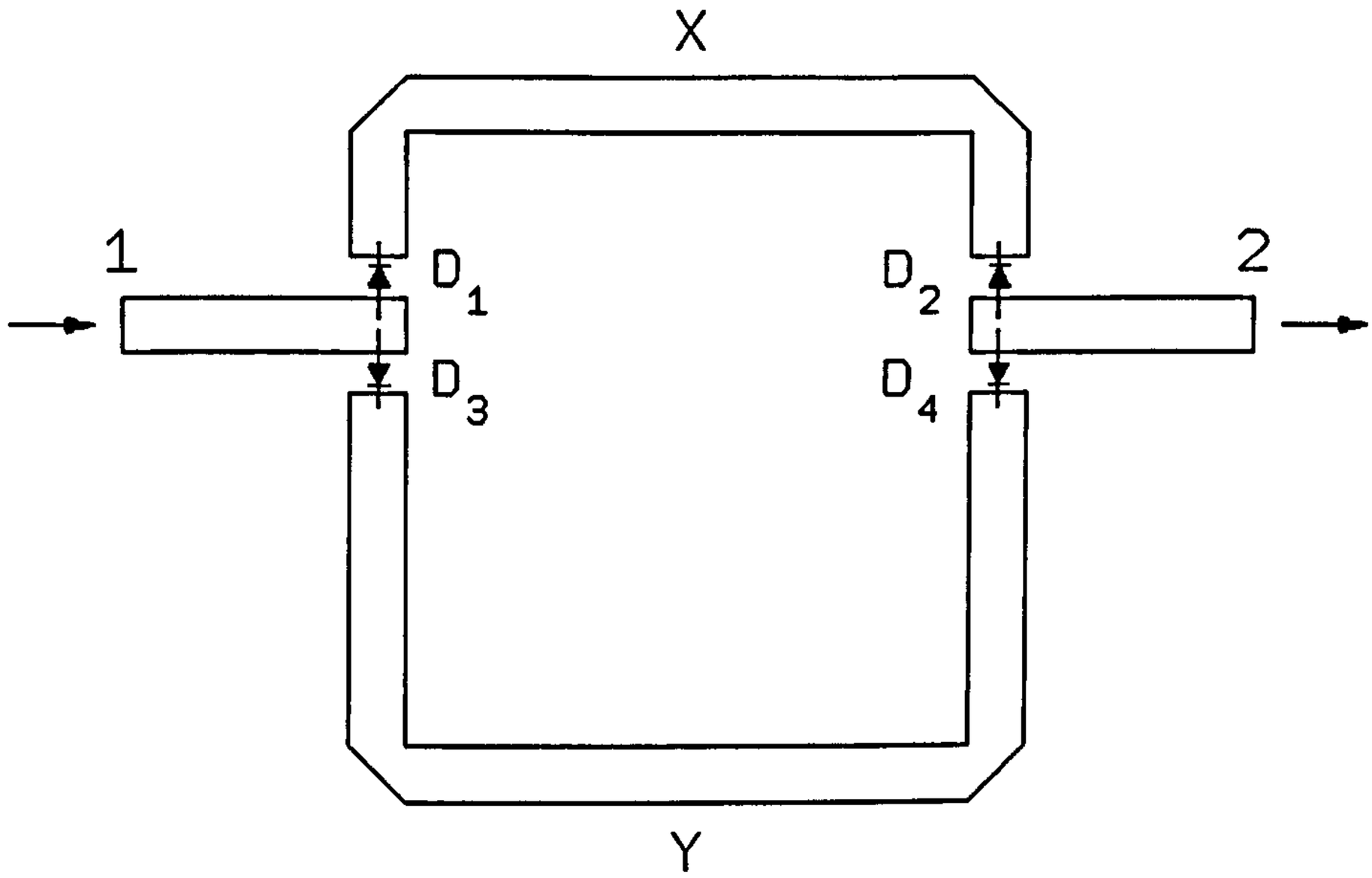

Figure 1.5: **Switched-line phase shifter.**

ence in the lengths of paths X and Y. As the difference in length is set at the mask making stage of the fabrication process the resulting phase change can be set quite precisely. There are also no inherent frequency limitations to the circuit, which should exhibit wide bandwidth performance. Nor are there any limitation on the size of phase change that can be achieved. However, there are some significant disadvantages. There are always two switching diodes in the transmission path of the signal, which means that the transmission properties of the circuit are a function of the transmission characteristics of the diodes and their mounting, and include errors due variations in diode performance due to poor manufacturing. Furthermore, the circuit occupies a lot of substrate area. These disadvantages become more significant when one considers a digital device. Each cell requires 4 diodes, so, for example, a 4-bit device requires 16 active devices and occupies a significant area of substrate.

A popular alternative to the switched-line phase shifter is the loaded-line circuit shown in Fig. 1.6, p. 29. The main line is loaded by two reactive stubs,

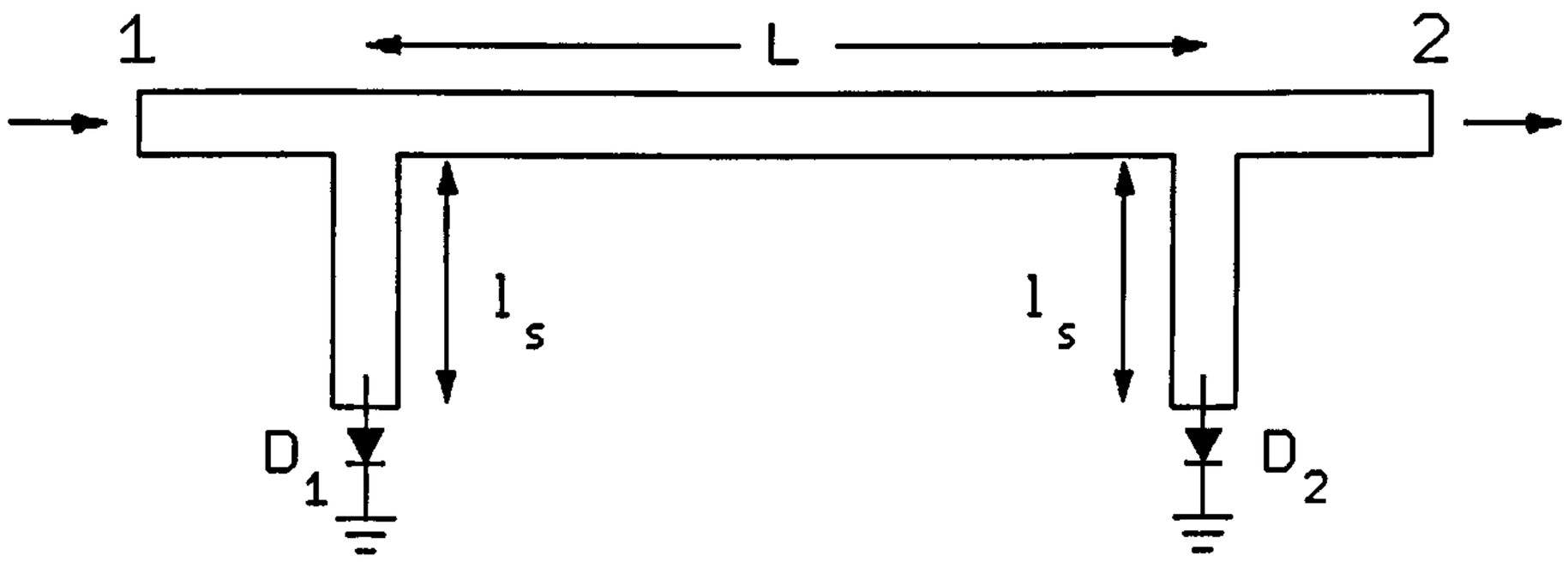

Figure 1.6: **Loaded line phase shifter**

which are terminated by PIN diodes D_1 and D_2. A signal travelling along the main line from port 1 to port 2 is perturbed by the two reactances, and experiences a change in transmission phase. If the separation (L) between the stubs is made equal to $\lambda_s/4$ at the design frequency, the reflections on the main line due to the two stubs will cancel at the input port. Thus the device will be frequency matched. The shunt susceptance presented to the main line can be controlled by switching the diodes loading the stub ends to provide nominal open or short circuit terminations. The phase change which is achievable, with an acceptable bandwidth, depends upon the lengths of the stubs and their characteristic impedances. Using this technique it is thus possible to realise a digitally controlled phase shifter, using only two switching elements per bit of phase change. It should be noted, however, that the frequency dependent input match of this circuit tends to worsen with the size of the phase step. Thus practical designs of multi-bit phase shifter, covering a wide range of phase tend to use a combination of the switched line method and the loaded technique. AYASLI ET AL [7] in designing a monolithic X-band 4-bit phase shifter covering the range 0° to 360°, used two switched-line cells for the most significant bits and two loaded-line cells for the least significant bits. The authors concluded that the performance of the phase shifter was satisfactory for phased array applications, but some of the

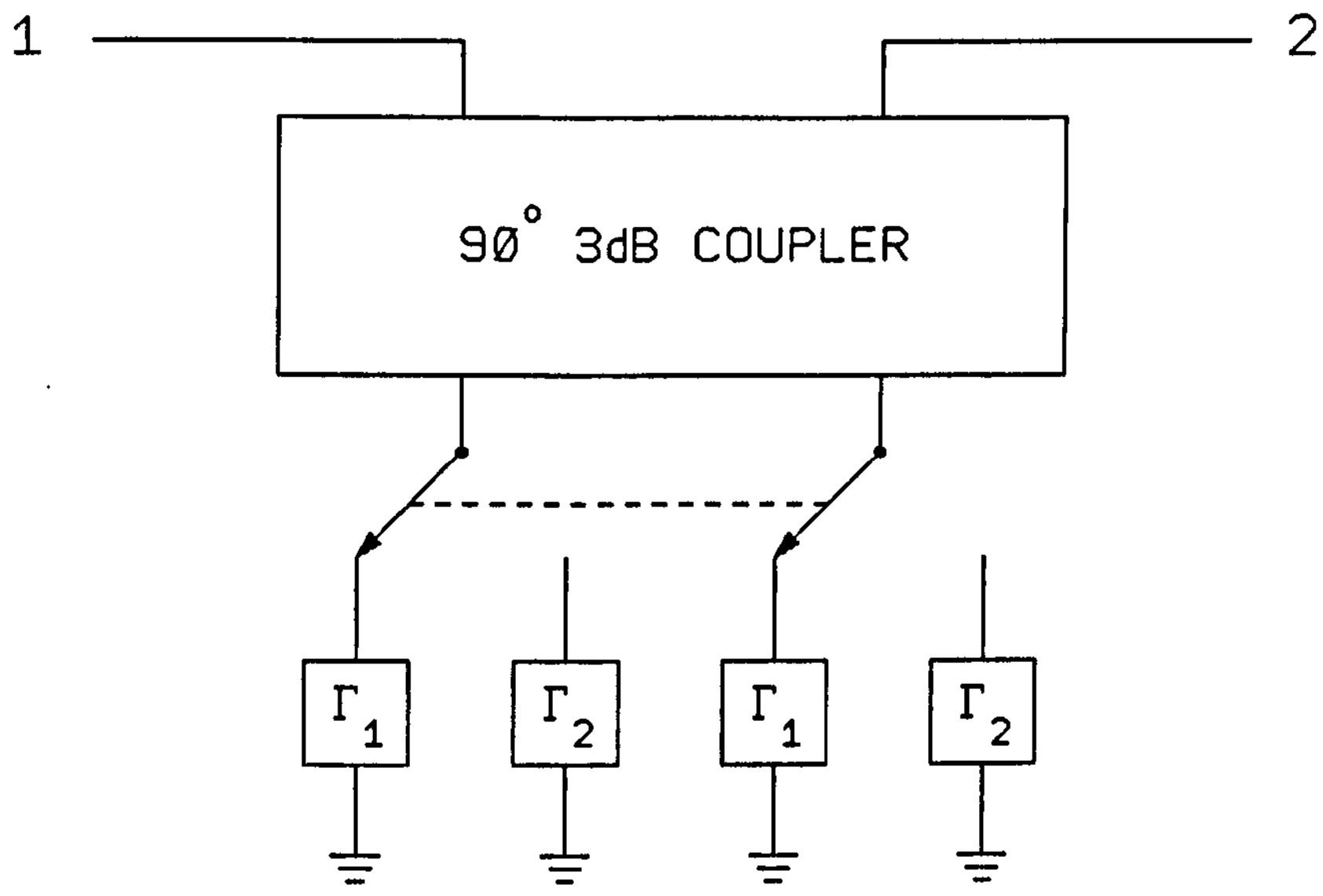

Figure 1.7: **Reflection type phase shifter.**

difficulties in making this type of circuit are evident from a closer examination of the results. The overall loss was quoted as 5.1 ± 0.6dB and nowhere over the measured band of 8.5-11GHz were there uniform 22.5° intervals between the 15 non-zero states. While this level of performance might be suitable for phase array radars where errors in the individual phase errors may have a relatively small effect on the radiated beam characteristics it would be unacceptable for an n-bit PSK communication system and certainly not acceptable for frequency control of an oscillator using the modified delay-line stabilisation arrangement proposed earlier. If the phase steps quoted in the Ayasli paper were translated to frequency steps from an oscillator employing the proposed switched delay-line stabilisation technique, the results would be grossly inferior to those obtainable from a simple synthesiser.

The last type of phase shifter, the reflective type, is the one most frequently reported in the literature. It consists of a 3dB hybrid coupler with phase controllable reflective terminations. This is shown schematically in Fig. 1.7, above. It can be implemented in microstrip using various forms of

hybrid coupler, such as the branch line coupler, hybrid ring and backward wave coupler. In the case of the hybrid ring, an additional quarter-wave section is required in one of the reflection ports to provide the required 90° phase difference between the nominal output ports. The phase-controllable, reflective terminations on the output ports can be realised using PIN diode switching elements. WHITE [12] provides a comprehensive design analysis for these terminations. This type of phase shifter has several advantages over the types already discussed. In particular, it requires only two active elements for each bit of phase shift. Furthermore, it can provide large phase changes and it can maintain a good input match over a wide range of frequencies. GLANCE [8], reported on the performance of a 14GHz 4-bit phase shifter using this reflection technique, with significantly better results than AYASLI ET AL [7]. Glance's results showed well defined phase intervals over the range 0° to 360°, and this performance was maintained over a 500MHz bandwidth. Moreover, the insertion loss reported by Glance over this bandwidth was only $1.4dB \pm 0.1dB$.

Other authors have reported different types of switched phase shifter, but they tend to be variations of the three basic methods which have been discussed. WILSON ET AL [9] describe a novel MMIC X-band phase shifter which uses a hybrid coupler and two tapped delay lines. There was no significant improvement in performance compared with the Glance design, as far as linearity of the frequency steps was concerned, but there was a significant improvement in percentage bandwidth. The Wilson phase shifter gave well defined frequency steps over much of the 8-12GHz band. However, there was a significant absolute insertion loss and, more importantly, there was a significant change in insertion loss between states.

1.4 Conclusions

There has been no attempt to exploit the concept of the microwave delay-line stabilised oscillator, using transmission line components, since it was established by AITCHISON AND BATLIWALA [2] in the mid 1970s. In particular, there has been no reported attempt to introduce some form of programmable phase control into the delay-line path so as to control the the frequency of the oscillator. Where the general technique of AITCHISON AND BATLIWALA [2]

PAGES MISSING IN ORIGINAL

Chapter 2

Single PIN Diode Phase Shifter

2.1 Summary

The conventional designs of digitally controlled phase shifters which have been reported in the literature, and which were summarized in chapter1, require the use of at least two switching elements per bit of phase shift. These designs have two principal disadvantages: they are expensive in terms of the number of switching elements that are required, and they occupy relatively large areas of substrate. Furthermore, although the active elements are functioning purely as switching devices, they are in the path of the microwave signal and consequently the behaviour of the the phase changer is to some extent dependent upon the transmission properties of these switches. Clearly, the greater the number of these switching elements that are involved, the less precise will be the selection of the phase states.

In this chapter a new circuit is proposed which uses only one switching element (PIN diode) to achieve each digital bit of phase change. Whilst the circuit makes use of some standard microstrip circuit geometries, it has been necessary to significantly extend the previously published theory relating to certain microstrip circuit elements in order to design precise phase changes. In particular, this has led to more precise design equations for coupled line structures and to a better understanding of the transmission phase of microstrip DC breaks.

A number of representative circuits have been built and tested to support the proposed design and justify the use of new theory.

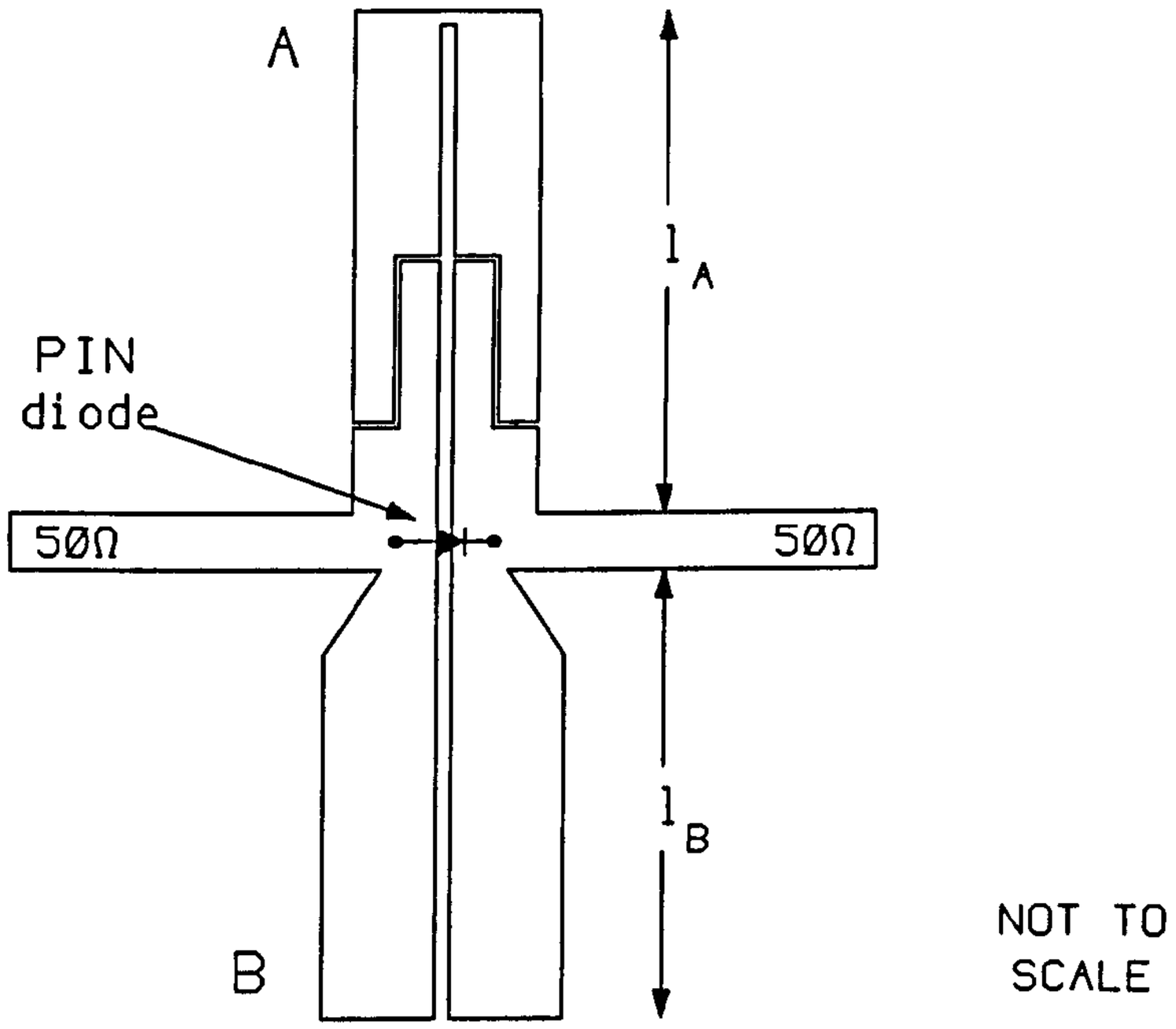

Figure 2.1: Single PIN Diode Phase Shifter

2.2 Concept of the single PIN diode phase shifter

The proposed circuit of a single-bit microstrip phase shifter is shown in Fig. 2.1, above.

The arrangement consists of two coupled line sections , A and B, with a PIN diode mounted at their intersection with the main 50Ω line. Section A, in which the lines are connected at the remote end to form a short circuit for the odd mode, contains two DC breaks in the form of zig-zag slits. These permit DC biasing of the PIN diode. Section B is a high impedance matching section. It will be observed that section A, without the DC breaks, forms an all-pass filter of the type described by JONES & BOLLJAHN [10] and sub-

sequently employed by SCHIFFMAN [11] in the design of passive differential phase shifters. The widths and spacing of the coupled lines forming section A determines the values of the odd and even mode impedances for this section. These values control the input impedance of the coupled-line section, and also the linearity of the phase frequency response. In a practical design the values of the impedances would be chosen so that input impedance of the coupled-line section matched that of the main line, 50Ω in this instance. The widths and spacing of the coupled lines forming section B will not necessarily have the same values as section A. For reasons which will be discussed later it is convenient to use lines of a wider width in section B. In order that these lines should have a more precise point of action on the main line they have been tapered where they join the 50Ω main path, as can be seen in Fig. 2.1, p. 34. The tapering is fairly gradual and does not enter into the design calculations.

A specified phase change is obtained by switching the PIN diode and the frequency response is then simply the difference between the phase-frequency responses of the circuit in the two diode states. The circuit is designed to be matched to the main 50Ω line, at the centre frequency, in both states.

Considering the operation in more detail, starting with the diode in the off state, it can be seen that the two coupled line sections are effectively in parallel. The input impedance of the B section is designed to be high so that most of the input signal will be transmitted through section A with a transmission phase change determined primarily by the length, l_A. The equivalent circuit is shown in Fig. 2.2, p. 36.

With the PIN diode in the on state, a nominal short circuit exists across the centre of the coupled lines. This will inhibit the formation of the odd mode on the coupled lines and therefore the A and B sections will behave as shunt connected stubs, each supporting an even mode. The resulting equivalent circuit is also shown in Fig. 2.2, p. 36. The circuit parameters are chosen so that the stubs present equal and opposite input susceptances to the main line at the centre frequency, so that their effects cancel. However, it is desirable that the overall length, $l_A + l_B$, of the structure should not create an electrical length which is a multiple of π, to avoid resonances. This implies $Z_{oeA} \neq Z_{oeB}$ which accounts for the difference in line geometries on sections A and B which was referred to earlier in the discussion.

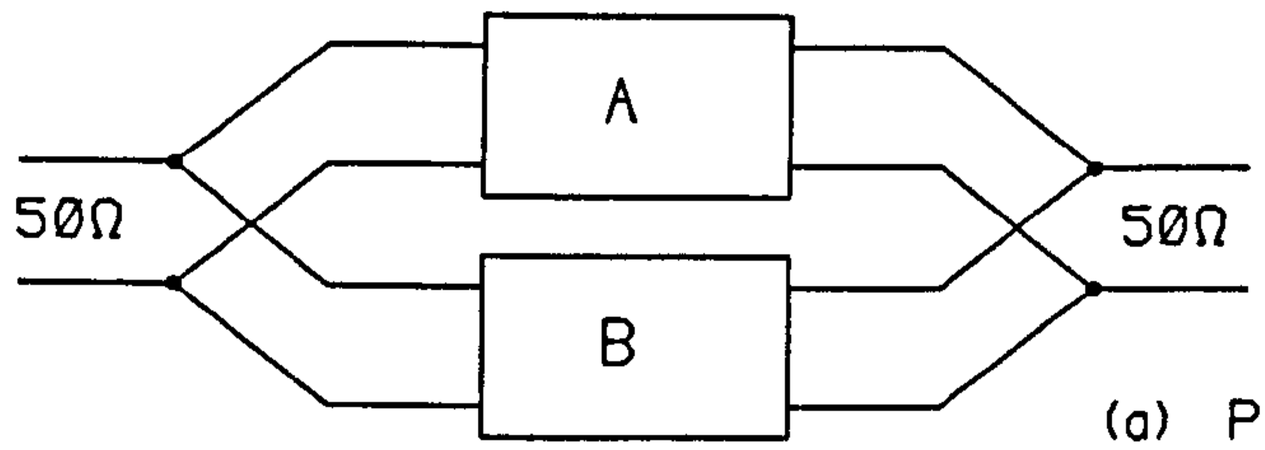

(a) PIN diode off

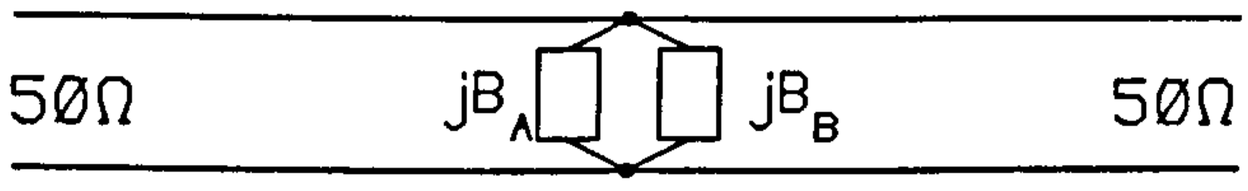

(b) PIN diode on

Figure 2.2: **Equivalent circuits for both diode states**

It is the action of the PIN diode in creating different propagating conditions in the two states that is crucial to the operation of the device.

2.3 Phase shift element

The phase change provided by the single PIN diode phase shifter is primarily determined by the transmission phase through section A of Fig. 2.1, p. 34. It is therefore necessary to develop an accurate model for the microstrip coupled lines forming this section, both in terms of the signals propagating along the lines, and including the effects of the inherent discontinuities associated with the structure.

The coupled section in question is shown in more detail in Fig. 2.3, p. 37, together with the essential parameters of the line geometry.

The transmission phase change between ports 1 and 2 is a function of the coupled length, l_A. This configuration of microstrip lines is often referred to as a Schiffman coupler, following from that author's use of the design in differential phase shifters, see SCHIFFMAN [11]. However, Schiffman's original

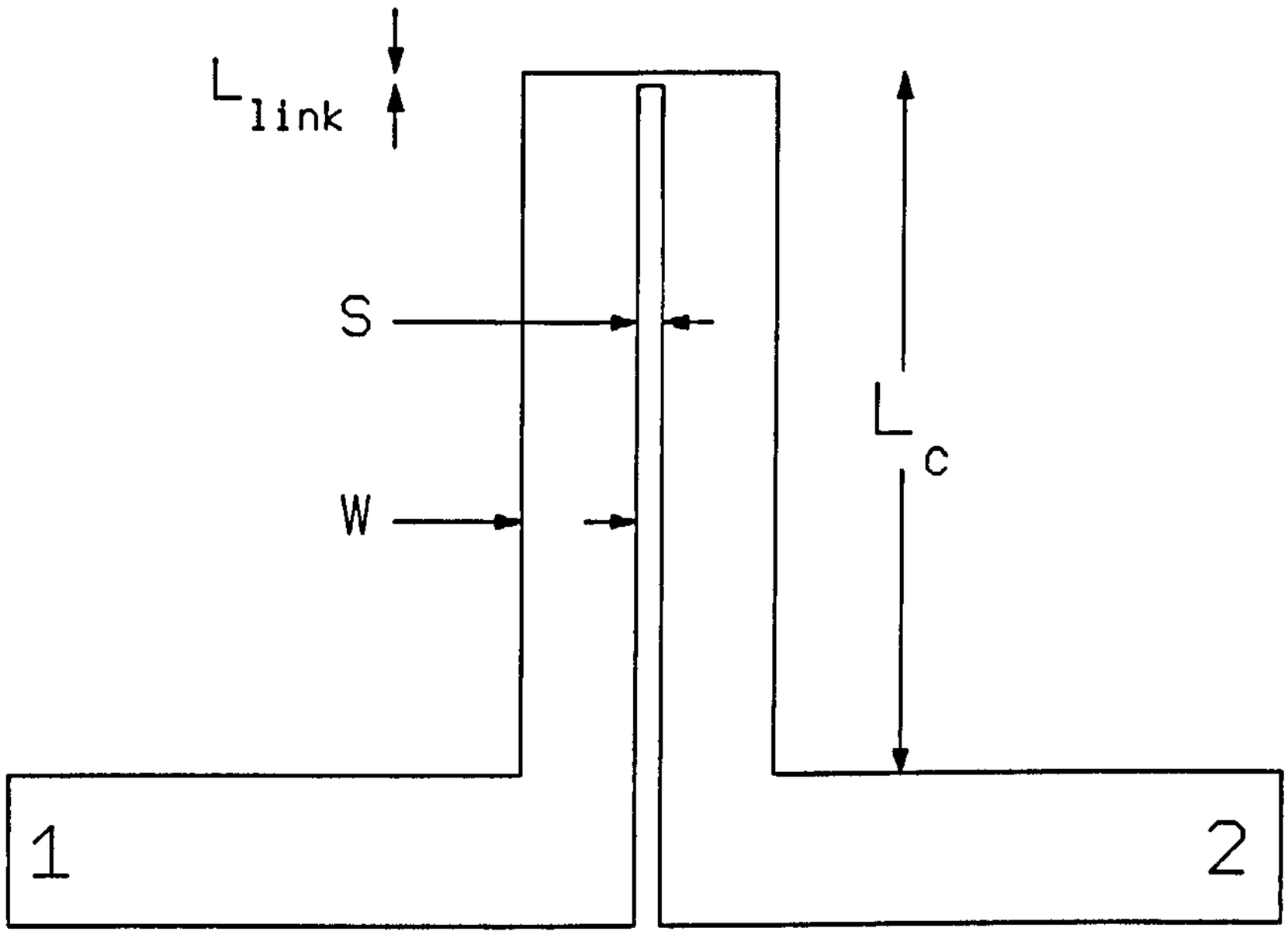

Figure 2.3: **Configuration of coupled-line phase shifter**

work was based on stripline transmission structures, where the odd and even modes propagating along the coupled line structure have equal phase velocities. Thus Schiffman was able to make use of the well known expressions for coupled-line filters developed by JONES & BOLLJAHN [10]. When this type of circuit has been designed in microstrip the same transmission equations are usually quoted, as in WHITE [12], and the unequal odd and even mode velocities averaged to provide, theoretically, a well-behaved characteristic with zero insertion loss at all frequencies.

In this section a new and more exact analysis in terms of the independent odd and even mode velocities is presented, which shows that for certain values of the length, L_C, the insertion phase departs significantly from the ideal (average mode velocity) characteristic, and the microstrip structure presents a significant mismatch at the input port. Some authors, notably SCHIEK & KOHLER [13], have recognized the problem and suggested modifications to the basic design to compensate for the difference in the odd and even mode velocities, but there does not appear to have been any extended theoretical

consideration in the literature of the simple coupled-line section to show the extent of the problem.

There is a further problem which does not appear to have been addressed in the literature, namely that of establishing the actual coupled length that should be used in the design expressions. So, after considering the limitations that exist in the analysis of coupled microstrip lines, this chapter concludes with an investigation of the modifications that need to be made to compensate for discontinuities in the coupled-line structure.

2.3.1 Theory of coupled microstrip lines

The method of analysis used here follows the conventional approach adopted for coupled microstrip lines, whereby the total voltages and currents on the structure are obtained from the summation of the odd and even mode solutions. However, unlike the conventional method which has been applied to this structure previously in the literature, the electrical length of each equivalent circuit is specified here in terms of the independent odd and even mode velocities. Thus the configuration of the structure shown in Fig. 2.3, p. 37 can be reduced to two equivalent circuits as shown in Fig. 2.5, p. 40, where θ_e is the electrical length for the even mode and θ_o is the electrical length for the odd mode.

Each of the lines shown in the equivalent circuit may be analysed using simple transmission line theory. Thus the currents and voltages at terminals 1 and 4 for the two modes are related by

$$\begin{bmatrix} V_{1e} \\ I_{1e} \end{bmatrix} = \begin{bmatrix} \cos\theta_e & jZ_{oe}\sin\theta_e \\ jY_{oe}\sin\theta_e & \cos\theta_e \end{bmatrix} \begin{bmatrix} V_{4e} \\ I_{4e} \end{bmatrix} \tag{2.1}$$

and

$$\begin{bmatrix} V_{1o} \\ I_{1o} \end{bmatrix} = \begin{bmatrix} \cos\theta_o & jZ_{oo}\sin\theta_o \\ jY_{oo}\sin\theta_o & \cos\theta_o \end{bmatrix} \begin{bmatrix} V_{4o} \\ I_{4o} \end{bmatrix} \tag{2.2}$$

where Z_{oe} and Z_{oo} are the even and odd mode impedances, and Y_{oe} and Y_{oo} are the corresponding admittances. The relationships between the voltages and currents on the line joining ports 2 and 3 can then be deduced from symmetry. On the microstrip structure being considered, ports 3 and 4 are connected by a narrow conducting link. The link is designed to be narrow so that there will be no propagation around the end of the coupled section, but

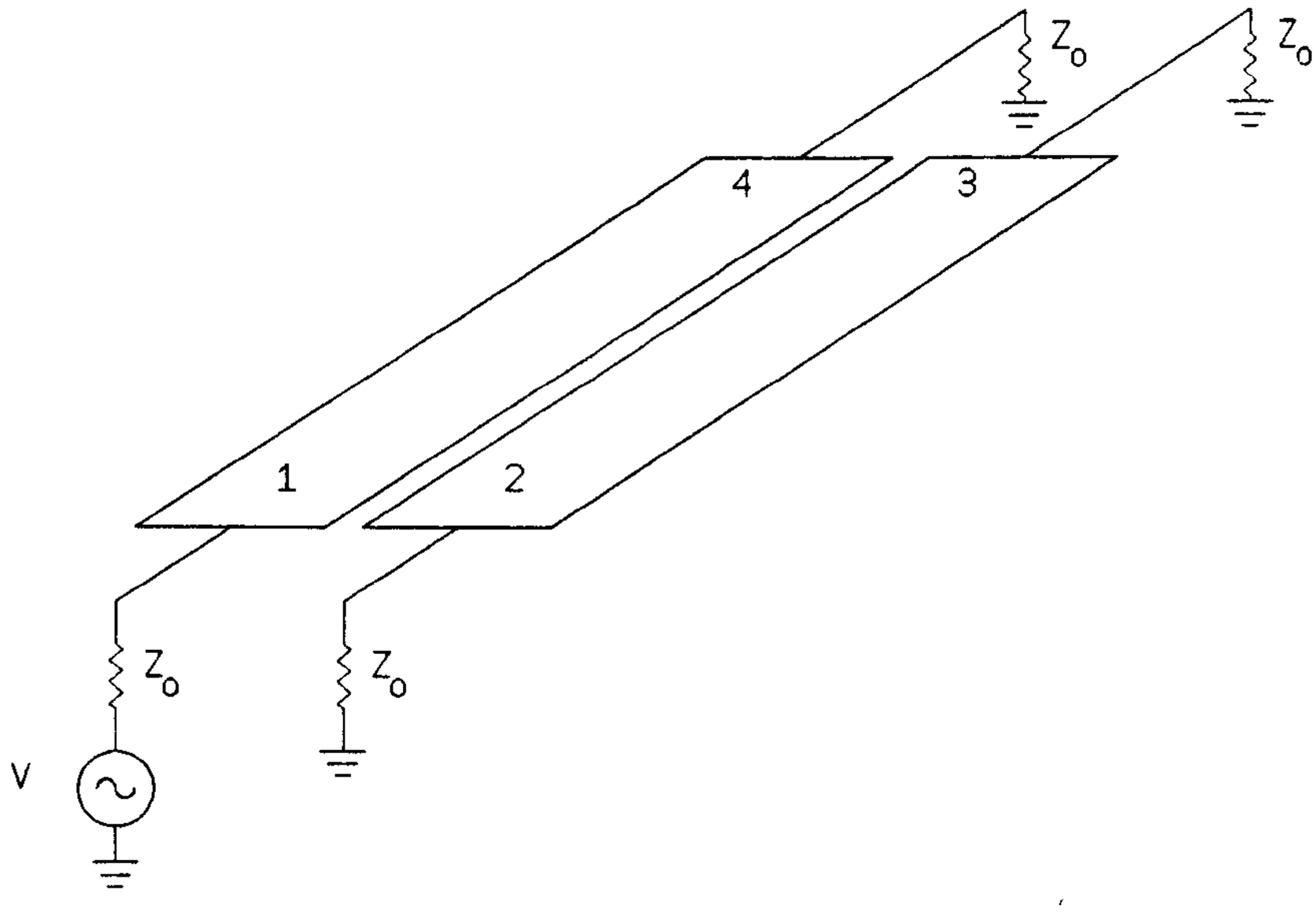

Figure 2.4: **Coupled microstrip lines showing port configurations**

rather that the even and odd modes will be terminated by open and short circuits, respectively.

Thus the boundary conditions for the structure may be written as

$$I_{3e} = I_{4e} = 0 \tag{2.3}$$

$$V_{3o} = V_{4o} = 0. \tag{2.4}$$

The transmission coefficient, V_2/V_1, for the circuit is obtained from

$$\frac{V_2}{V_1} = \frac{V_{2e} + V_{2o}}{V_{1e} + V_{1o}} \tag{2.5}$$

It follows, from considerations of symmetry, that the transmission coefficient can also be written as

$$\frac{V_2}{V_1} = \frac{V_{1e} - V_{1o}}{V_{1e} + V_{1o}} \tag{2.6}$$

giving, after substitution for terminal voltages in terms of the line characteristic impedances

$$\frac{V_2}{V_1} = \frac{-jZ_o(Z_{oe}\cot\theta_e + Z_{oo}\tan\theta_o)}{2Z_{oe}Z_{oo}\tan\theta_o\cot\theta_e - jZ_o(Z_{oe}\cot\theta_e - Z_{oo}\tan\theta_o)} \tag{2.7}$$

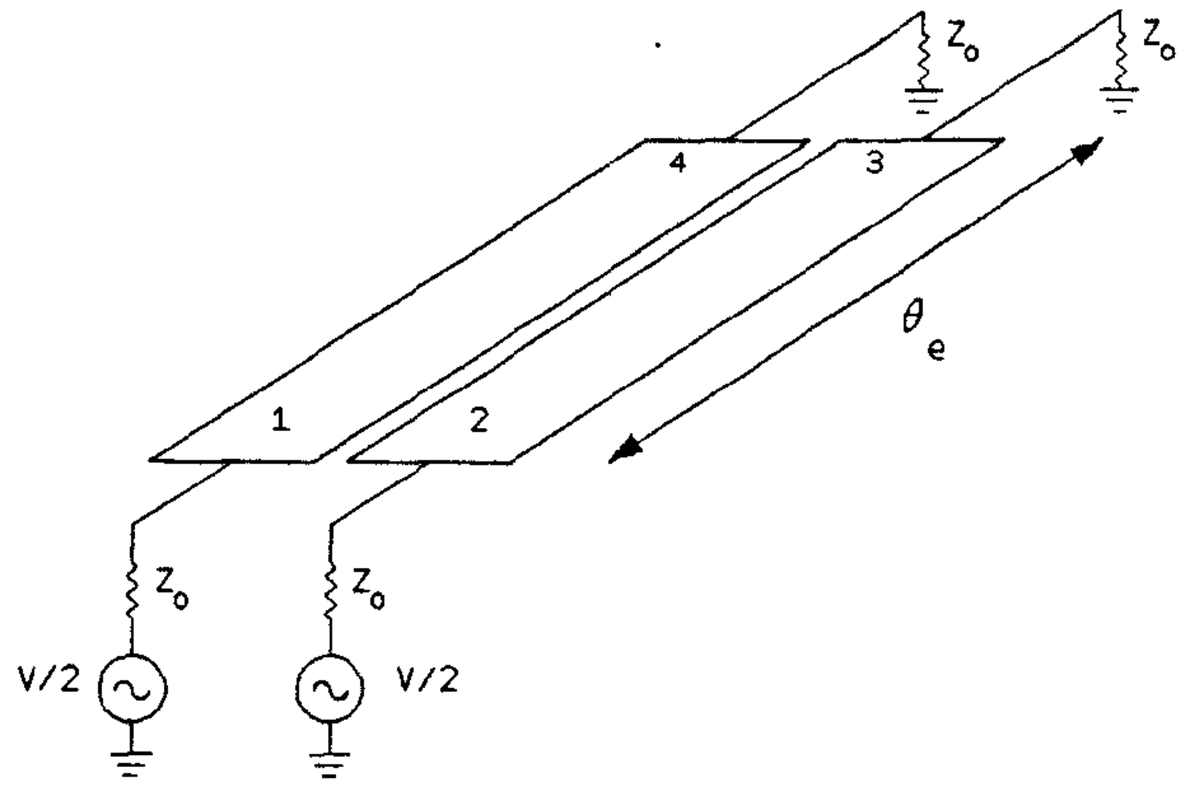

Even mode

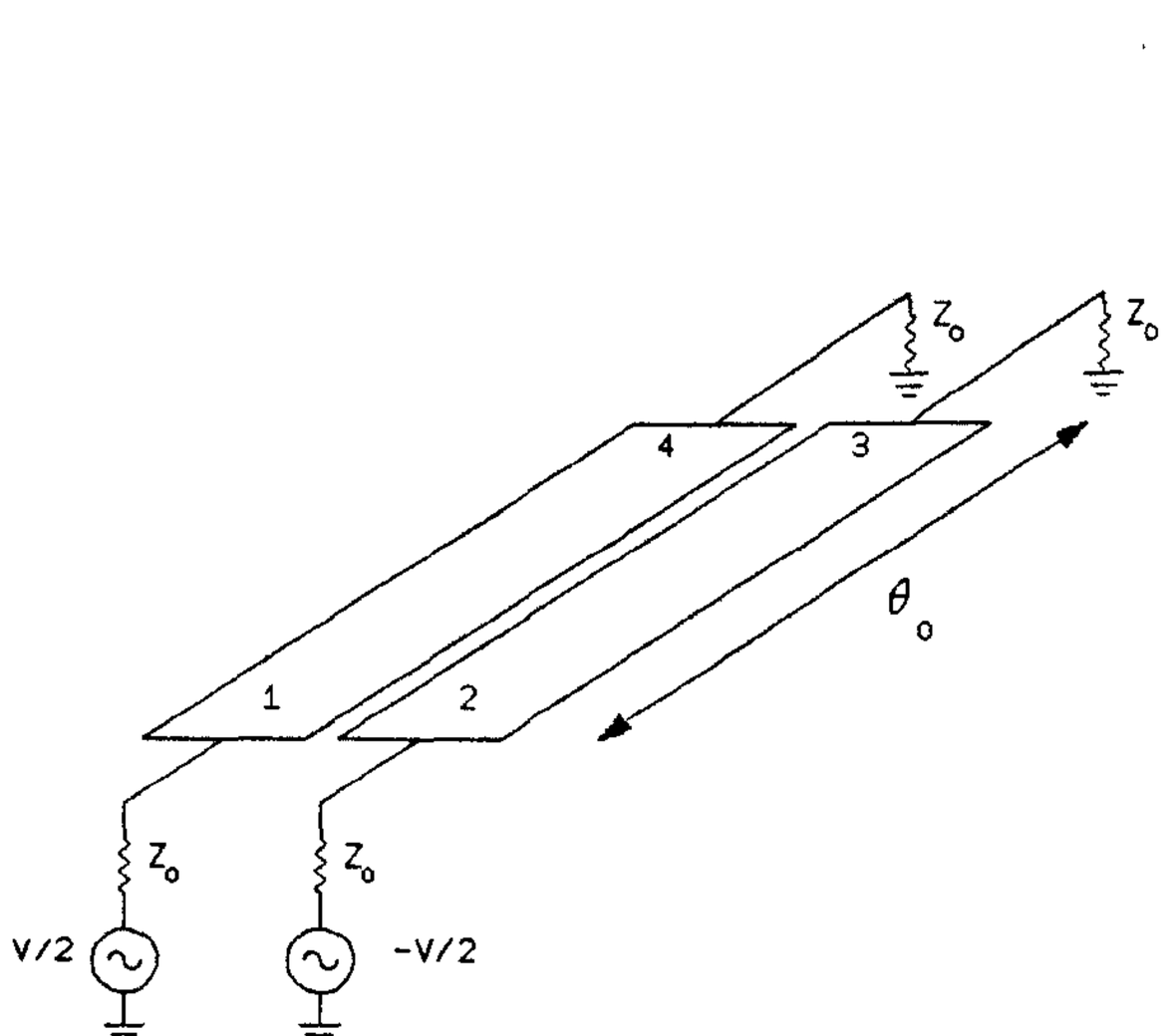

Odd mode

Figure 2.5: Equivalent circuits for odd and even modes

from which the transmission phase change is obtained as

$$\phi = \frac{\pi}{2} + \tan^{-1}\left[\frac{Z_o(Z_{oo}\tan\theta_o - Z_{oe}\cot\theta_e)}{2Z_{oe}Z_{oo}\tan\theta_o\cot\theta_e}\right] \tag{2.8}$$

The detailed derivations of 2.7 and 2.8 can be found in appendix A.

If it is assumed that the odd and even modes have equal velocities of propagation, i.e. $\theta_o = \theta_e = \theta$, then 2.8 reduces to

$$\phi = \cos^{-1}\left[\frac{\frac{Z_{oe}}{Z_{oo}} - \tan^2\theta}{\frac{Z_{oe}}{Z_{oo}} + \tan^2\theta}\right] \tag{2.9}$$

which is the form quoted by SCHIFFMAN [11], and usually employed as an approximation in microstrip designs.

The approximations usually made in coupled-line phase shifter design also extend to the match of the circuit, wherein it is assumed that the input impedance is given by

$$Z_o = \sqrt{Z_{oe}Z_{oo}}. \tag{2.10}$$

It is shown in appendix A that if an exact analysis, using the individual odd and even mode velocities is performed, the input impedance at port 1 is frequency dependent and given by

$$Z_1 = \frac{2Z_{oe}Z_{oo}\cot\theta_e\tan\theta_o - jZ_o(Z_{oe}\cot\theta_e - Z_{oo}\tan\theta_o)}{2Z_o - j(Z_{oe}\cot\theta_e - Z_{oo}\tan\theta_o)}. \tag{2.11}$$

2.3.2 Effects of dispersion

In the previous section, the electrical length (θ_n) of the coupler for each mode is related to the frequency of operation (f) through

$$\theta_n = \frac{2\pi f l}{v_{p,n}} \tag{2.12}$$

where $v_{p,n}$ is the velocity of propagation of the appropriate mode. However, it is well known that for frequencies above a few GHz dispersion effects become significant, and therefore an appropriate frequency dependent expression for $V_{p,n}$ must be used. A number of authors have addressed the issue of dispersion in coupled microstrip lines and a variety of frequency dependent design equations have been published for the effective relative permittivity, $\epsilon_{r,eff}$, applying to each of the odd and even modes. In the present analysis the dispersion relationships due to GETSINGER [14] were used. These are reproduced for reference in appendix A.2.

2.3.3 Discontinuity analysis

The previous discussion has considered the propagation aspects of signals on coupled microstrip line structures. If these structures are to yield precise, predictable phase changes the analysis must be extended to consider discontinuity effects. There are two principal discontinuities associated with the coupled line structure shown in Fig. 2.3, p. 37, namely the fringing at the remote end of the coupler, and the discontinuity formed by the right-angled entry to the coupler.

The link which terminates the remote end of the coupler provides an effective short circuit for the odd mode. There will be some penetration of the odd mode current into the terminating link, but this can be accounted for by using the full length of the coupler for the odd mode. The principal fringing effect will thus be that due to the even mode. Therefore, in the foregoing analysis the length used for the even mode was extended by δl, where δl is the effective line extension due to the open-end fringing effect. The value of δl was computed from the well known expression due to HAMMERSTAD AND BEKKADAL [15], namely

$$\delta l = 0.412h \left(\frac{\epsilon_{r,eff} + 0.3}{\epsilon_{r,eff} - 0.258} \right) \left(\frac{\frac{w_t}{h} + 0.262}{\frac{w_t}{h} + 0.813} \right) \tag{2.13}$$

where h is the thickness of the substrate, $\epsilon_{r,eff}$ is the effective relative permittivity and where, in the present analysis, $w_t = 2w + s$ since the even mode extends over the full width of the coupled line structure.

The discontinuity effect associated with the right-angle entry to the coupler is less easy to quantify. Whilst right-angle bends in single microstrip lines have been extensively investigated in the literature, and a variety of discontinuity models developed, there have been no discontinuity studies reported which consider the combined effects of bends and coupling. In the present work a suitable specification for the coupled length was determined empirically.

2.4 Matching stub

The matching stub (section B in Fig. 2.1, p. 34) is required to perform two distinct functions. Firstly, with the diode in the off state, it must provide

a high input impedance so that the signal is transmitted through section A and secondly, with the diode in the on state, it must provide a shunt stub whose input admittance matches out that of section A. There are sufficient degrees of freedom in the design to allow both of these requirements to be satisfied. This is mainly because, with the diode off, both the odd and even modes exist on the coupled line structures, and with the diode on, only the even mode exists. Thus the stub exhibits quite different behaviour in the two diode states. If necessary this difference can be increased by choosing different track widths and spacings for the two sections, A and B.

The initial step in designing a single PIN diode phase shifter is to choose the length, l_c, of section A to give the required phase change. This length is then used to compute the input admittance, Y_A, of section A assuming that only the even mode is present. The length of the stub is then calculated to make the input admittance of the stub equal to the conjugate of Y_A. That is, the stub length is calculated from

$$Y_A = -Y_B \tag{2.14}$$

$$jY_{oe,A} \tan \beta_A l_c = -jY_{oe,B} \tan \beta_B l_s \tag{2.15}$$

leading to

$$l_s = \frac{1}{\beta_B} \tan^{-1} \left[-\frac{Y_{oe,A}}{Y_{oe,B}} \tan \beta_A l_c \right] \tag{2.16}$$

where $Y_{oe,A}$ and $Y_{oe,B}$ are the characteristic even mode admittances, and β_A and β_B the phase propagation constants, on sections A and B respectively. This will ensure that the phase shifter is matched in the on state, with nominally zero transmission phase, although the actual transmission phase in this condition will depend on the characteristics of the PIN diode and the microstrip gap. However, having set the length of the stub in this way, it is necessary to check that it still provides the required high input impedance in the off state. If this is not initially achieved the stub can be redesigned with a different track geometry. Since the odd mode is not present in both states, changing the relative values of track widths and spacing will have the effect of changing the relative values of the velocity of propagation in both states, thus enabling both matching conditions to be achieved.

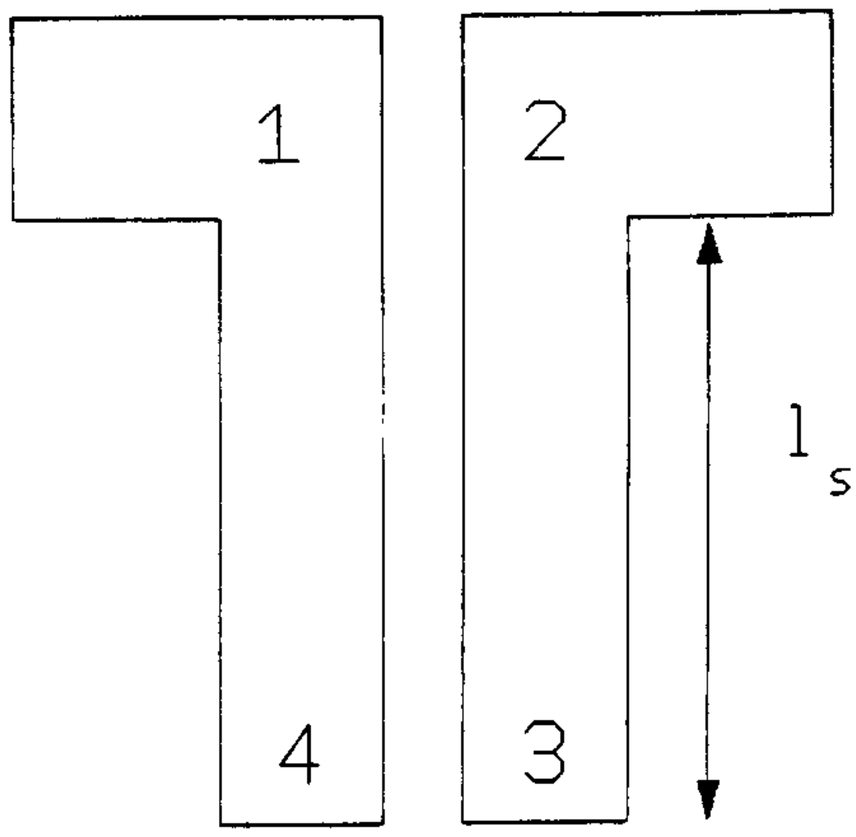

Figure 2.6: **Port nomenclature for open-circuit, couple-line stub**

2.4.1 Theory of open-circuit stub with both modes present

The essential stub geometry is shown in Fig. 2.6, above.

With both modes present, corresponding to the diode in the off state in the phase shifter, the boundary conditions are

$$I_{3e} = I_{4e} = 0 \tag{2.17}$$

$$I_{3o} = I_{4o} = 0. \tag{2.18}$$

Substituting these boundary conditions into the basic transmission line equations 2.1 and 2.2 we obtain, for the odd mode

$$V_{1o} = V_{4o} \cos\theta_o \tag{2.19}$$

$$I_{1o} = jY_{oo}V_{4o} \sin\theta_o. \tag{2.20}$$

Hence, we obtain the input impedance at port 1 for the odd mode, Z_{1o}, as

$$Z_{1o} = \frac{V_{1o}}{I_{1o}} = -jZ_{oo} \cot\theta_o \tag{2.21}$$

Similarly, for the even mode

$$V_{1e} = V_{4e} \cos\theta \tag{2.22}$$

$$I_{1e} = jY_{oe}V_{4e} \sin\theta_e \tag{2.23}$$

leading to the input impedance, Z_{1e}, for the even mode at port 1 as

$$Z_{1e} = \frac{V_{1e}}{I_{1e}} = -jZ_{oe}\cot\theta_e. \tag{2.24}$$

The net input impedance at port 1 is then obtained as

$$Z_1 = \frac{V_{1e} + V_{1o}}{I_{1e} + I_{1o}} \tag{2.25}$$

where

$$V_{1e} = \frac{Z_{1e}}{Z_{1e} + Z_o}V \tag{2.26}$$

and

$$V_{1o} = \frac{Z_{1o}}{Z_{1o} + Z_o}V \tag{2.27}$$

and where V is the applied signal level and Z_o is the loading impedance on ports 1 and 2. Thus we obtain

$$Z_1 = \frac{\frac{Z_{1e}}{Z_{1e}+Z_o} + \frac{Z_{1o}}{Z_{1o}+Z_o}}{\frac{1}{Z_{1e}+Z_o} + \frac{1}{Z_{1o}+Z_o}} \tag{2.28}$$

$$= \frac{2Z_{1e}Z_{1o} + Z_o(Z_{1e} + Z_{1o})}{2Z_o + Z_{1e} + Z_{1o}} \tag{2.29}$$

Substituting for Z_{1e} and Z_{1o} into equation 2.29 gives the input impedance at port 1 of the open circuit, coupled-line section as

$$Z_1 = \frac{-2Z_{oe}Z_{oo}\cot\theta_e\cot\theta_o - jZ_o(Z_{oo}\cot\theta_o + Z_{oe}\cot\theta_e)}{2Z_o - j(Z_{oo}\cot\theta_o - Z_{oe}\cot\theta_e)} \tag{2.30}$$

2.4.2 Even mode loading

The key aspect of the stub design is that there should be a significant difference in the behaviour of the stub with both modes present compared with only the even mode present. It would therefore be advantageous to maximize this difference by modifying the stub geometry. One possible technique would be to provide even mode loading at the remote end of the coupled section as shown in Fig. 2.7, p. 46.

The two addition stubs which provide the loading will affect the even mode performance, but should have little effect on the odd mode, which is confined the gap between the coupled lines.

The boundary conditions for the new stub geometry are, for the odd mode

$$I_{3o} = I_{4o} = 0 \tag{2.31}$$

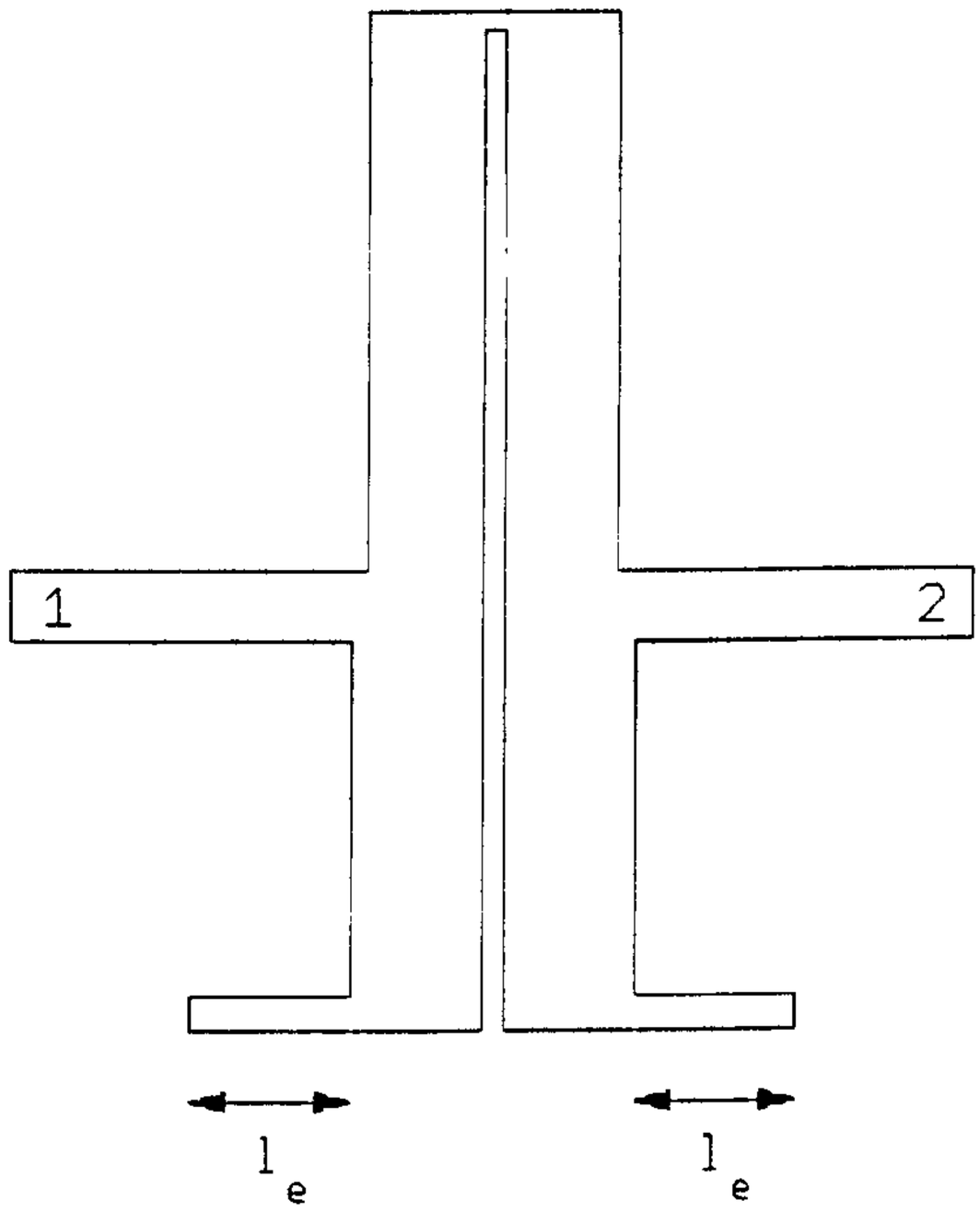

Figure 2.7: **Microstrip layout of single PIN diode phase shifter showing even mode loading on the matching stub**

and for the even mode

$$\frac{V_{4e}}{I_{4e}} = jX \tag{2.32}$$

where X represents the reactive loading on the even mode, and where the magnitude and sign of X depend on the width and length (l_e) of the loading stub. Substituting the odd mode boundary condition into the transmission line equations 2.1 and 2.2 we obtain, as in section 2.3.1, the input impedance of the odd mode as

$$Z_{1o} = -jZ_{oo}\cot\theta_o. \tag{2.33}$$

Similarly, from equations 2.1 and 2.2 we have, for the even mode

$$Z_{1e} = \frac{V_{1e}}{I_{1e}} \tag{2.34}$$

$$= \frac{V_{4e}\cos\theta_e + jI_{4e}Z_{oe}\sin\theta_e}{jY_{oe}V_{4e}\sin\theta_e + I_{4e}\cos\theta_e} \tag{2.35}$$

$$= \frac{jX\cos\theta_e + jZ_{oe}\sin\theta_e}{-Y_{oe}X\sin\theta_e + \cos\theta_e} \tag{2.36}$$

i.e.

$$Z_{1e} = \frac{j(X + Z_{oe}\tan\theta_e)}{1 - Y_{oe}X\tan\theta_e}. \tag{2.37}$$

Substituting for Z_{1o} and Z_{1e} into 2.29 gives the input impedance at port 1 of the structure as

$$Z_1 = \frac{j[X(Z_o - 2) + Z_o(Z_{oe}\tan\theta_e - Z_{oo}\cot\theta_o) + Z_{oo}\cot\theta_o\tan\theta_e(2Z_{oe} - XY_{oe}Z_o)]}{2(1 - Y_{oe}X\tan\theta_e) + j(X + Z_{oe}\tan\theta_e - Z_{oo}\cot\theta_o + Y_{oe}XZ_{oo}\cot\theta_o\tan\theta_e)} \tag{2.38}$$

2.5 Microstrip DC breaks

The single PIN diode phase shifter shown in Fig. 2.1, p. 34 uses a PIN diode connected across the entry to the coupled-line sections to control the phase change. It is clear from this figure that section A creates a DC short across the diode and prevents a DC control voltage being applied. There are two possible strategies that can be used to prevent DC shorting: (a) a surface mount chip capacitor could be connected across the end of section A in place of the shorting link; (b) planar DC breaks could be introduced into the microstrip lines forming section A.

The use of a capacitor is the less attractive of the two solutions, because in practical circuit fabrication it represents an additional surface mount operation and, more importantly, it could introduce a significant discontinuity. Therefore the use of planar DC breaks in the coupled-line section forming section A of the single PIN diode phase shifter was investigated. Since the design of the phase shifter requires a precise understanding of the transmission phase through section A, it is particularly important that the inclusion of a DC break within this section should not create significant mismatches nor introduce any unknown transmission phase changes.

2.5.1 DC break geometry

The planar microstrip DC break originally proposed by LACOMBE AND COHEN [17] consisted of two coupled microstrip fingers as shown in Fig. 2.8, p. 48. This structure was a application of the band-pass filter proposed by JONES AND BOLLJAHN [10]. The shape of the structure is dictated by the need to provide a nominal wideband match, and this can be made in excess

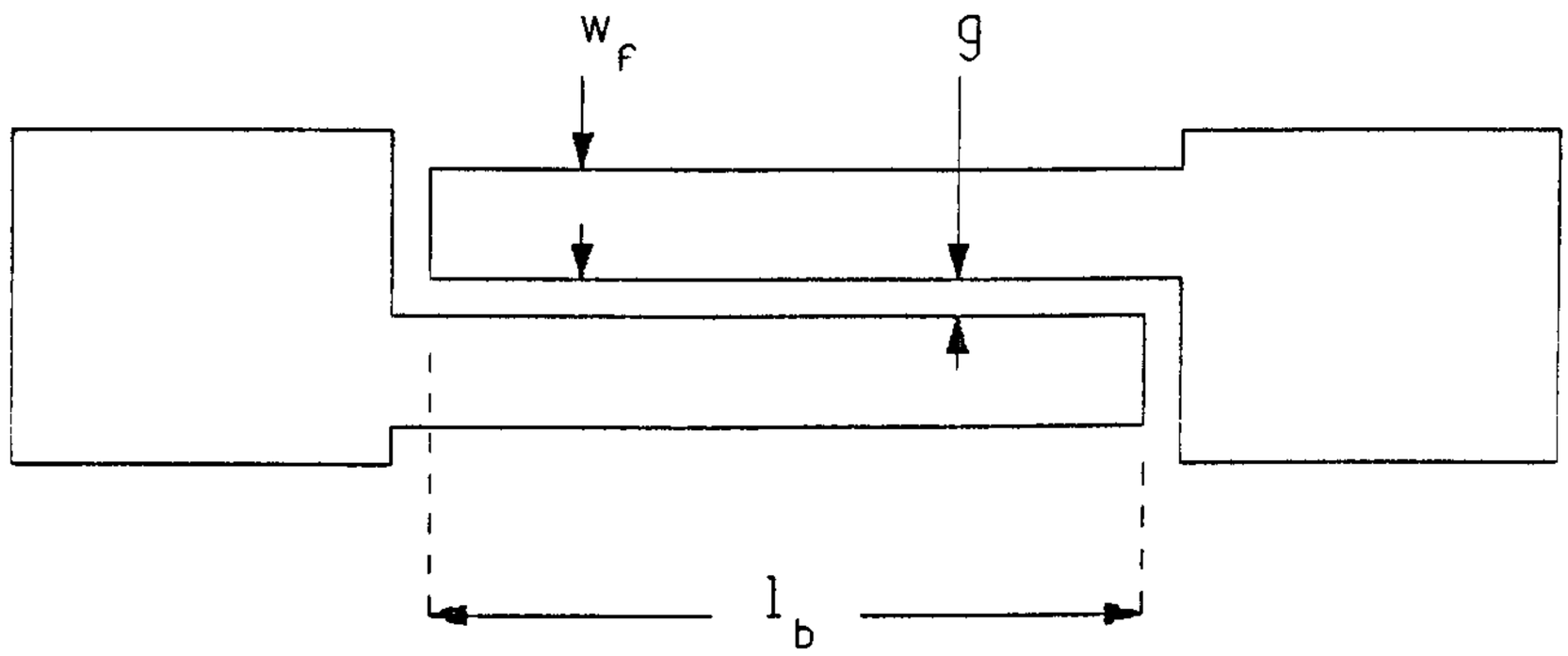

Figure 2.8: **Geometry of conventional microstrip planar DC break**

of one octave. In the present application the DC break must be included in the coupled section A. However, in order to maintain symmetry two DC breaks are used as shown in Fig. 2.9, p. 49.

It is expected that the DC break will introduce some excess phase into each microstrip line, and if only one such break were used it would cause some imbalance in the even mode on each side of the coupler. Whilst this finger shape of DC break is quite acceptable for single microstrip lines it poses an additional problem for the coupler, in that the spacing between the two coupled lines, which is crucial in establishing a particular phase change, exhibits a discontinuity in the vicinity of the breaks. That is, the coupling gap widens for the length of the break. Thus for the present application some modifications to the shape of the DC break were investigated.

Two alternative DC break geometries are shown in Fig. 2.10, p. 50. The simple zigzag slit is attractive for the current work as it can be inserted without causing any significant discontinuity to the odd mode. However, it is not as well matched as the finger break because of the increased w/h ratio in the vicinity of the break, which means that it is not possible to select a gap size which will maintain the basic $Z_o = \sqrt{Z_{oe}Z_{oo}}$ matching condition. The other possibility shown in Fig. 2.10, p. 50 is to use a simple slanting slit. Whilst tapered sections of microstrip line are not amenable to simple

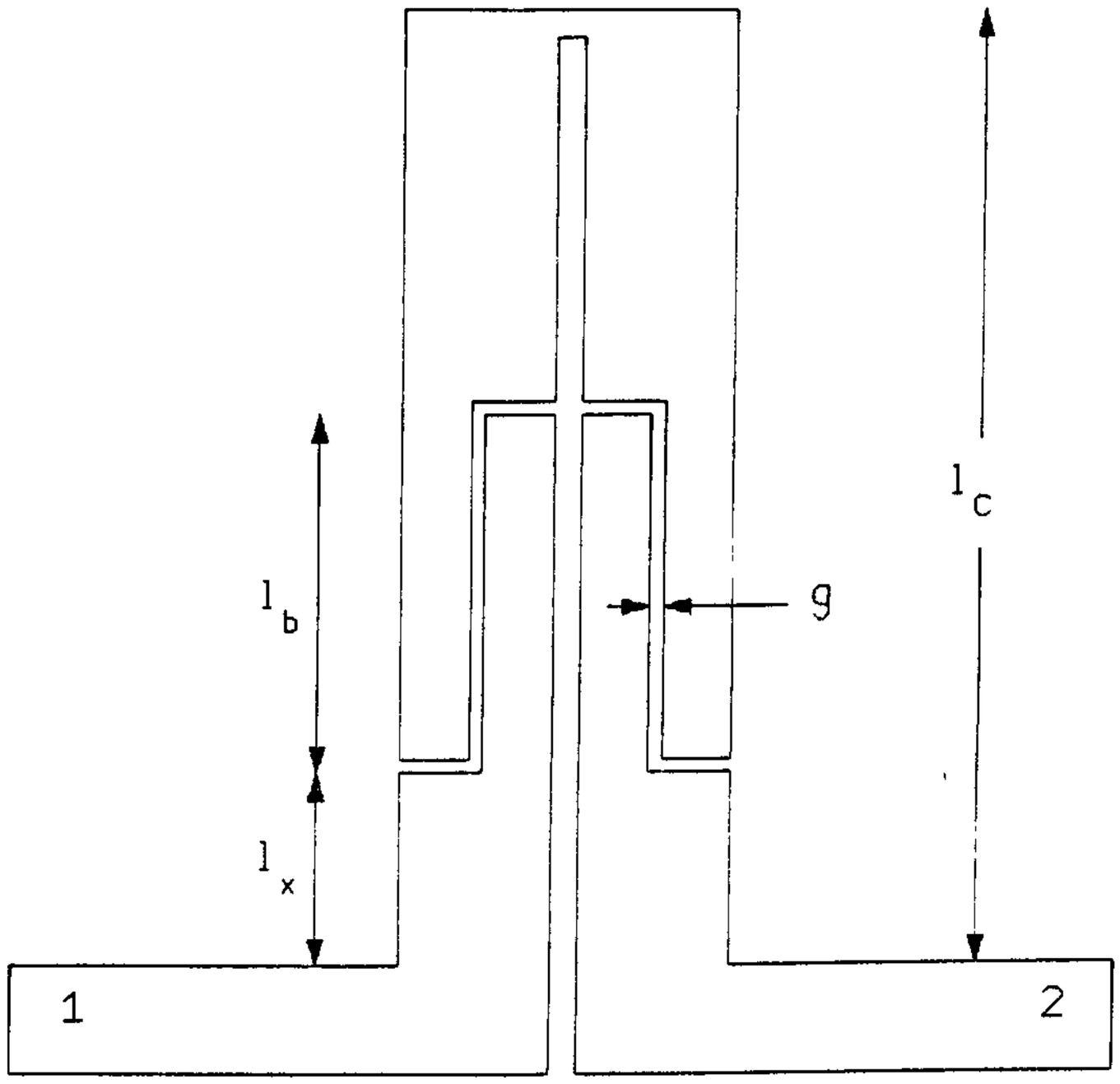

Figure 2.9: **Inclusion of DC breaks in coupled-line phase shifter**

analysis, two elementary design rules can be employed. Firstly, if the axial length of the slit is made $\lambda/4$, then any reflections from the discontinuities at the ends of the slit will cancel and, secondly, by making the gap as small as practical good coupling should be ensured. The problem, however, is that while this design strategy may lead to a DC break with low insertion loss, the difficulty of precise analysis leads to an indeterminate transmission phase change through the device, which is a critical parameter in the present work.

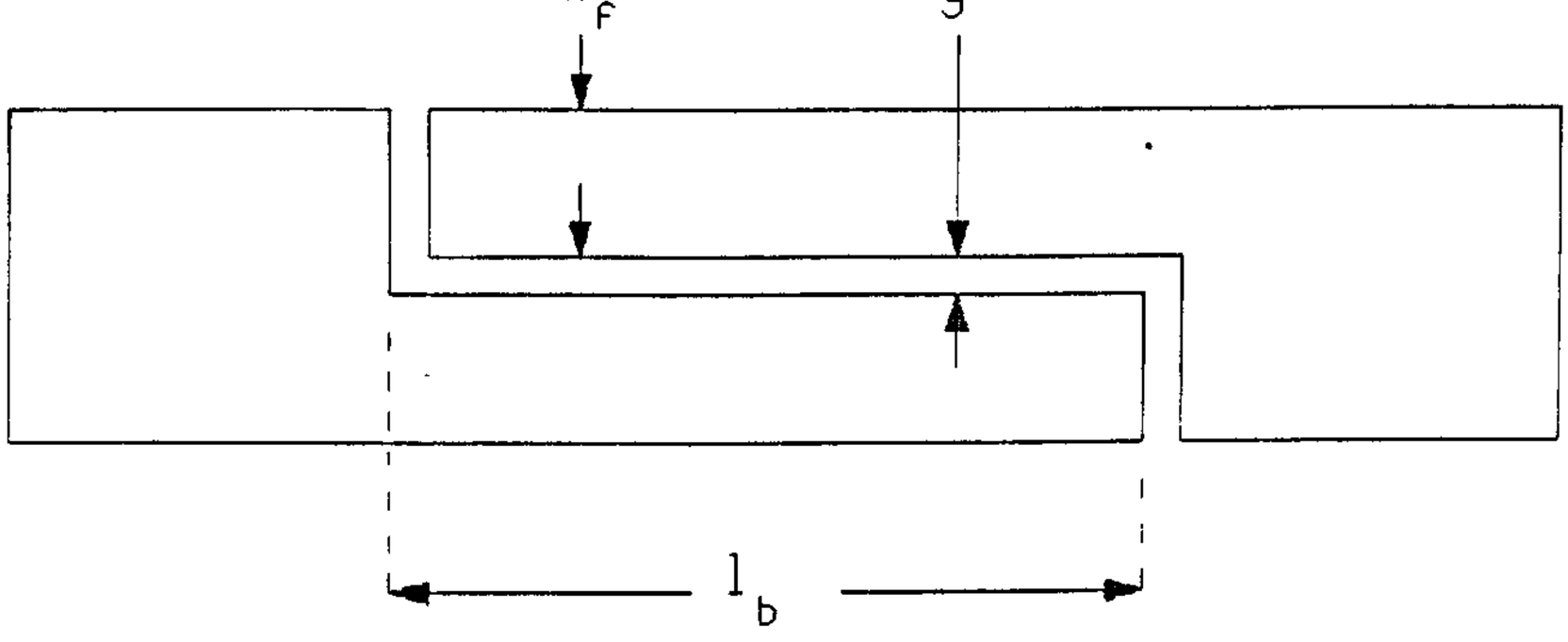

Zig-zag break

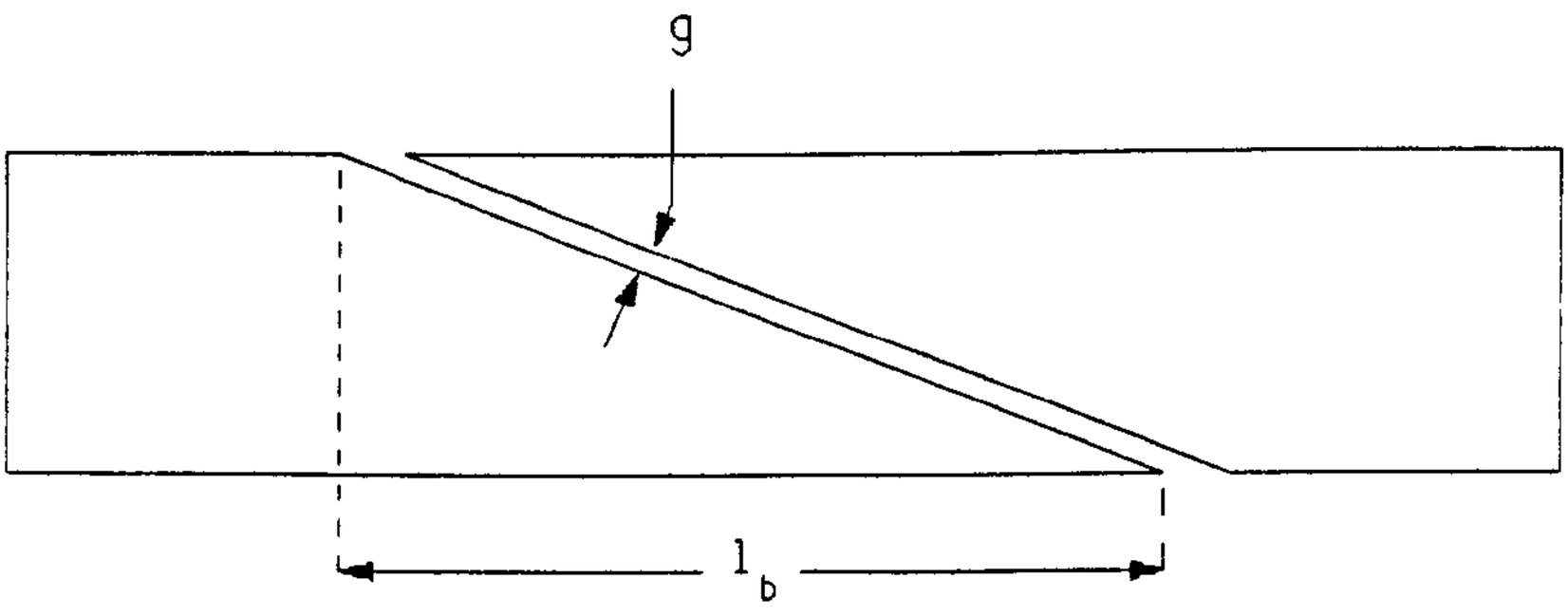

Slant break

Figure 2.10: **Alternative DC break geometries**

2.5.2 Theory of planar microstrip DC breaks

The finger break proposed by LACOMBE AND COHEN [17] is amenable to precise analysis. They showed that the coefficient S_{21} is readily obtained

from the z-parameters of the circuit as

$$S_{21} = \frac{2Z_{21}}{(Z_{11}+1)(Z_{22}+1) - Z_{12}Z_{21}} \tag{2.39}$$

where

$$Z_{11} = Z_{22} = -j\frac{Z_{oe}+Z_{oo}}{2}\frac{\cot\theta}{Z_o} \tag{2.40}$$

$$Z_{12} = Z_{21} = -j\frac{Z_{oe}-Z_{oo}}{2}\frac{\csc\theta}{Z_o} \tag{2.41}$$

and Z_o is the characteristic impedance of the main microstrip line, θ is the electrical length of the coupled section and Z_{oe} and Z_{oo} are the even and odd mode characteristic impedances for the coupled lines.

Similarly, the reflection coefficient S_{11} is obtained from

$$S_{11} = \frac{(Z_{11}-1)(Z_{11}+1) - Z_{12}Z_{21}}{(Z_{11}+1)^2 - Z_{12}^2} \tag{2.42}$$

The value of θ in these expressions is simply related to the coupled line length, l, by

$$\theta = \beta l = \frac{2\pi}{\lambda} l \tag{2.43}$$

To achieve a satisfactory match the length, l, is made equal to $\lambda_{av}/4$ at the design centre frequency. The wavelength, λ_{av}, is the average of the odd and even mode wavelengths and as such suffers the same error previously discussed for the coupled lines in the basic phase shifter.

2.5.3 Excess phase in microstrip DC breaks

Whilst the use of the conventional microstrip finger break is widespread in microwave circuit designs, one aspect of the finger break performance that does not appear to have been addressed in the literature is that of excess phase. The excess phase is the difference between the phase change through the break and through the same physical length of 50Ω microstrip line. Clearly in the present application a precise knowledge of the total phase change though the DC breaks is crucial to the design of the phase shifting element. The total phase change through a finger break may conveniently be divided into two parts: (a) the phase change through the coupled line section; (b) the additional phase due to the end discontinuities. The calculation of the

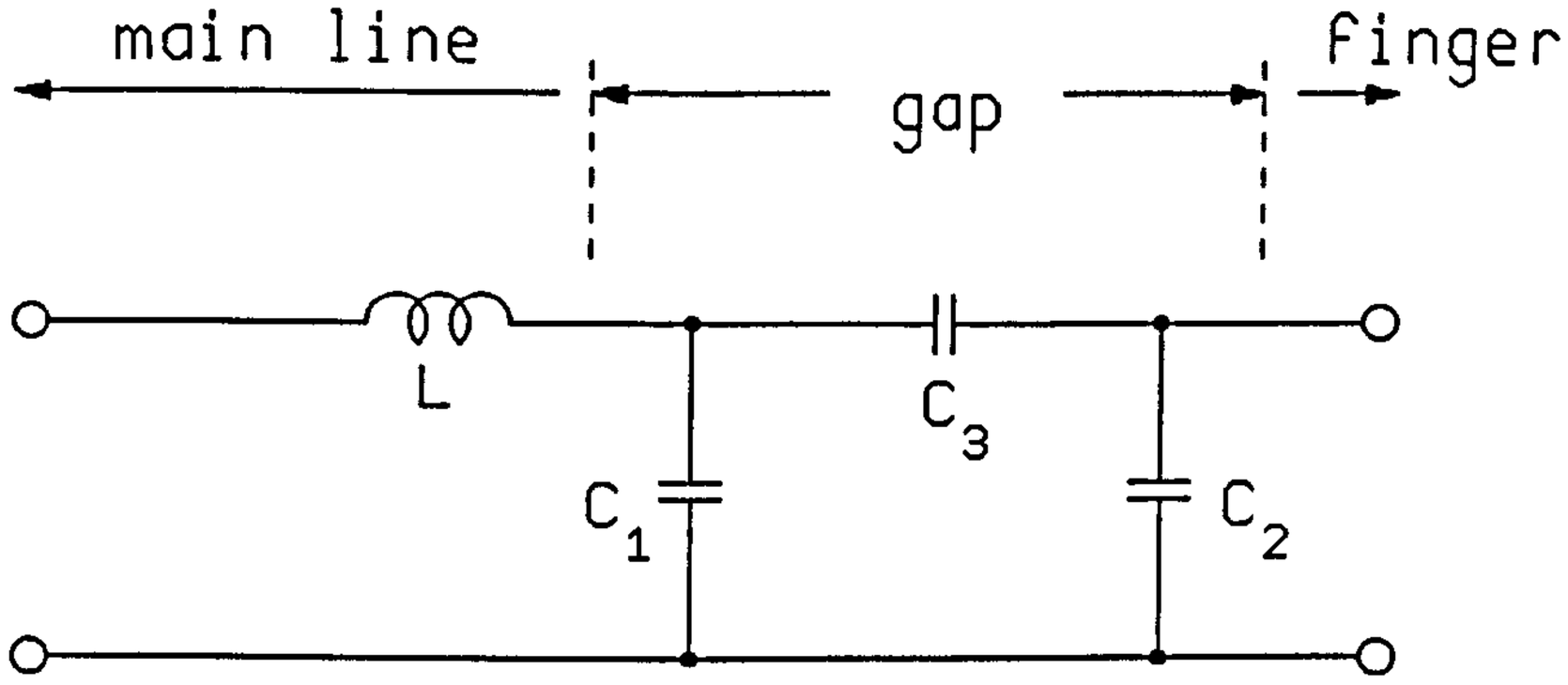

Figure 2.11: **Equivalent circuit for coupled-line end discontinuities**

phase change through the coupled section has already been covered and it remains to find the phase change due to the end discontinuities.

Three discontinuity components may be identified as being associated with each finger end, namely: (i) an inductive component related to the narrowing of the main microstrip track to form the finger; (ii) capacitive coupling between the finger end and the adjacent main microstrip track end; (iii) fringing capacitances at the track ends. An equivalent circuit of the form shown in Fig. 2.11, above may be deduced to represent the discontinuity at each finger end. It should be noted that, in the case of the finger break, C_1 and C_2 have different values since C_2 represents the fringing from a narrow finger end and C_1 the fringing from a rather larger region formed by the end of the main microstrip line. HAMMERSTAD AND BEKKADAL [15] have given expressions which enable the individual elements of the circuit in Fig. 2.11, above to be calculated from the microstrip geometry and hence to be represented by some equivalent line lengths.

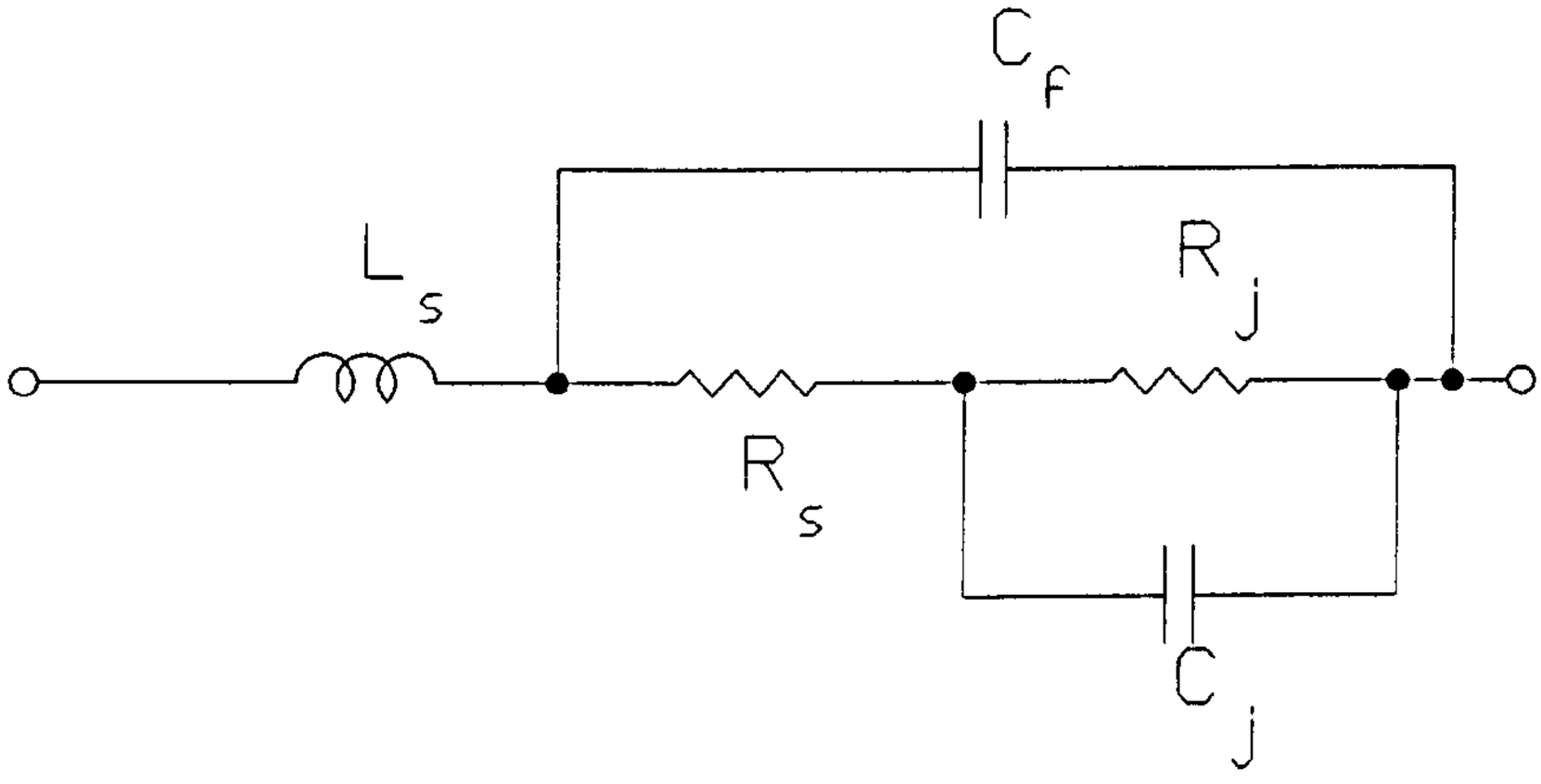

Figure 2.12: Equivalent circuit of beam-lead PIN diode

2.6 PIN diode requirements

The PIN diode mounted across the entry to the coupled lines in Fig. 2.1, p. 34 serves to control the modes present on the coupled lines. It should therefore function as a simple switch, presenting an open-circuit in the OFF state and a short-circuit in the ON state. However, if the circuit is to be designed to give precise phase changes it is necessary to establish values for the transmission though the diode in the two states, due to its non-ideal properties. It is well known, for example, that a series mounted PIN diode will provide low insertion loss but relatively poor isolation. The insertion loss and isolation, together with the corresponding transmission phase changes, can be found by modelling an equivalent circuit of the diode mounted across the effective microstrip gap at the entry to the coupled sections in Fig. 2.1, p. 34.

2.6.1 PIN diode model

The PIN diode used in the present investigation, was a low-loss beam-lead device whose equivalent circuit is shown in figure Fig. 2.12, above. This is a standard diode model where C_j is the junction capacitance, R_j the

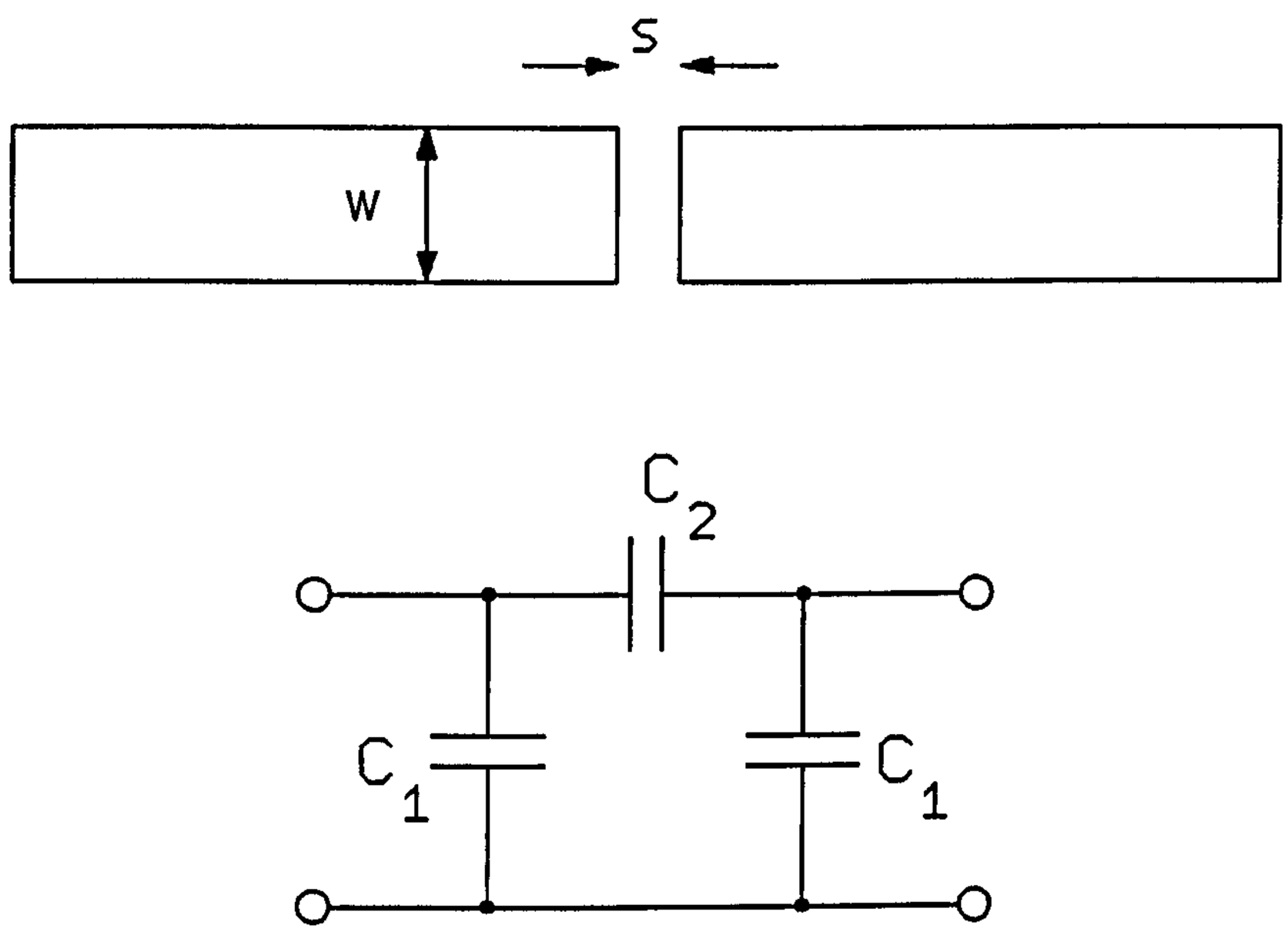

Figure 2.13: **Microstrip series gap and equivalent circuit**

junction resistance, R_s the combined bulk semiconductor and lead resistance, L the beam-lead inductance and C_f the packaging capacitance. The values for the Hewlett-Packard (5082-3900) diode used in this investigation were: $C_j = 0.2pF$; $R_s = 6\Omega$; $R_j = 10k\Omega$; $C_f = 0.01pF$; $L_s = 0.5nH$. The last parameter was not specified by the manufacturer but was estimated on the basis of beam-leads contributing approximately 1nII/mm of series lead inductance.

2.6.2 Microstrip gap model

A series gap in a microstrip line can be modelled as a π network of capacitors as shown in Fig. 2.13, above. A number of authors have addressed the problem of gap capacitance evaluation, but the results due to BENEDEK AND

SILVESTER [18] are generally taken to be the most accurate. By considering the excess charge distribution in the vicinity of a discontinuity they were able to produce graphical data for the elements in the capacitive π-model used to represent gap discontinuities. Whilst the rigorous mathematical approach of BENEDEK AND SILVESTER [18] leads to precise results, circuit designers require simple expressions for the capacitance values in terms of the odd and even mode capacitances, C_o and C_e, and the microstrip geometry. GARG AND BAHL [19] used curve-fitting techniques to generate closed-form expressions to represent the results of the BENEDEK AND SILVESTER [18] analysis. These expressions relate the element values of the equivalent circuit to the microstrip dimensions. The expressions are reproduced in appendix A.

2.7 Design of single PIN diode phase shifter

The microstrip track geometries for the single PIN diode phase shifters were designed using the foregoing theory. In the diode OFF state, it was assumed that there was no direct transmission through the PIN and that the circuit could theoretically be modelled as two transmission networks in parallel. One network representing section A, which provided the nominal phase change, and the other representing the matching stub (section B), through which there would naturally be some small transmission, which would modify the phase response in the OFF state. To perform the theoretical analysis each section was modelled in terms of y-parameters, which were summed and converted to S-parameters to give the overall result in the most convenient format.

In order to account for the presence of the DC breaks in the coupled section, this was modelled initially as three networks in series. The first representing the coupled line between the entry point and the DC break, the second the transmission through the DC break and lastly a network to represent the coupled line between the DC break and the terminating link. The networks were summed using ABCD transmission parameters so as to include the effects of mismatch due to the DC break.

In the diode ON state the circuit was modelled as two shunt connected stubs, formed by the even mode transmission through sections A and B, and by a series network to represent the transmission through the diode (mounted

across a microstrip gap) in the ON state, which would contribute both loss and a small phase change.

2.8 Fabrication and measurement

All of the test circuits were fabricated on RT/duroid 6010, which was coated with 1/8oz EDP copper, giving a copper track thickness of $4.5\mu m$. The substrate was $635\mu m$ thick and had a relative permittivity of 10.4. A conventional wet etching process was used to fabricate the circuits, with appropriate allowances being made for undercutting.

The test circuits were mounted in a Wiltron 2500 test jig and the measurements made with an HP8410 vector network analyser.

2.9 Results and discussion

In order to establish the behaviour of the single PIN diode phase changer, and to develop design procedures which give precise changes in phase, each of the constituent parts of the phase shifter was first investigated both theoretically and through practical measurement. Finally, practical measurements were performed on various electronically switched circuits.

2.9.1 Behaviour of coupled microstrip lines

It was pointed out in section 2.3 that the normal method of analysis of coupled microstrip lines involves an approximation, in that the average of the odd and even modes is used. Fig. 2.14, p. 57 shows the theoretical insertion phase, computed as a function of the coupler length at 12 GHz, for the basic phase change element shown in Fig. 2.3, p. 37. The graph shows the responses obtained using both the approximate and exact methods of analysis. It can be seen that the exact response departs significantly from the approximate characteristic for certain lengths and, as would be expected, the difference tends to increase with the length of the coupled section. This is demonstrated more clearly in Fig. 2.15, p. 58, where the magnitude of the difference between the responses has been plotted as a function of the length, and shows that the difference can be up to 60°.

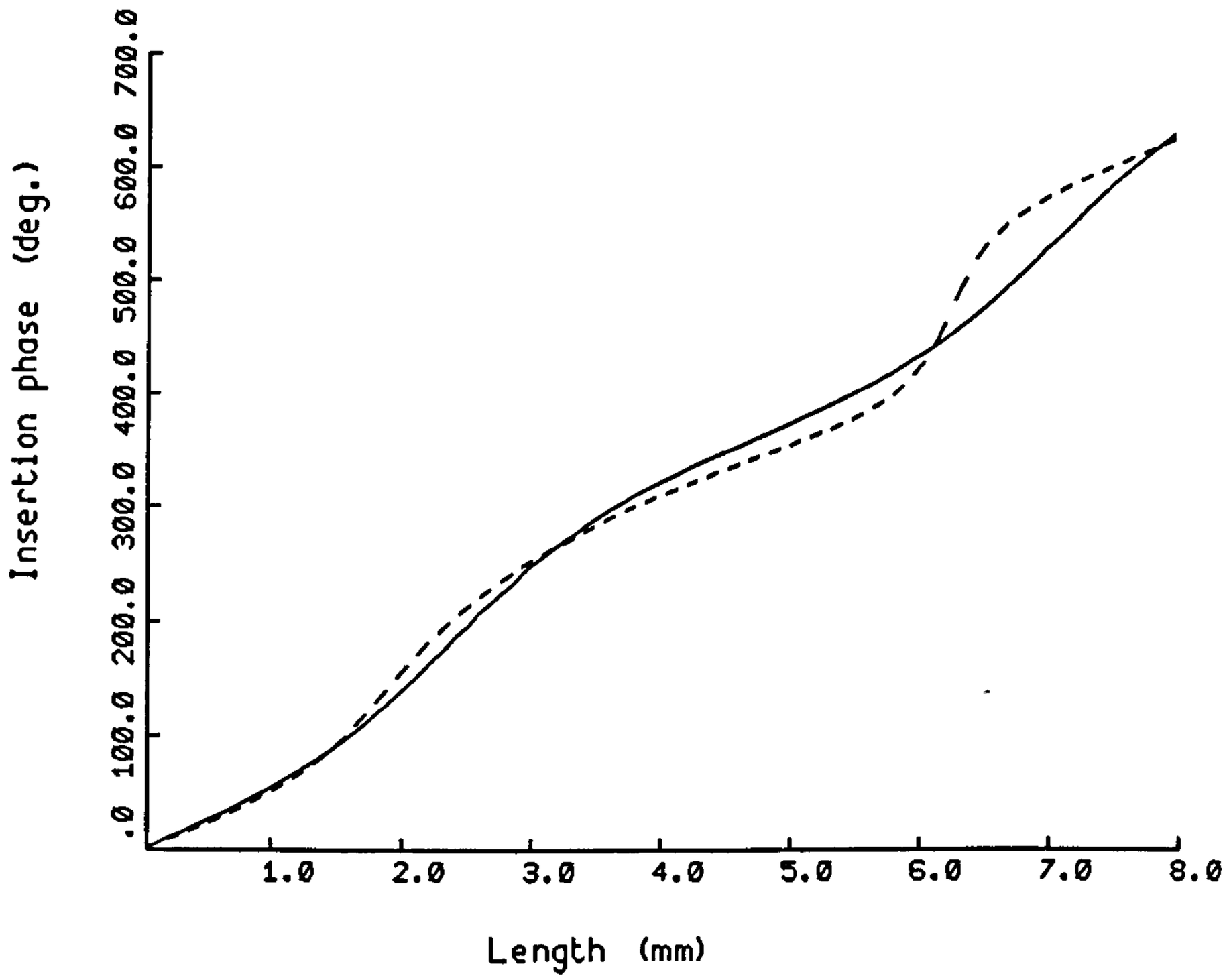

Figure 2.14: **Theoretical insertion phase at 12GHz**

The approximate theory assumes that the match of the circuit is perfect, and frequency invariant. It can be seen from Fig. 2.16, p. 59 that the exact analysis predicts significant insertion loss, due to circuit mismatch. As would be expected the highest loss occurs in the same region as the highest phase difference. In order to establish the validity of the new exact theory a number of coupled-line phase shifters of arbitrary length were designed and tested at X-band. The coupled-line geometry was chosen to give nominal input and output impedances of 50Ω, using $Z_o = \sqrt{Z_{oe} Z_{oo}}$. There is no unique combination of track width (w) and spacing (s) to satisfy this relationship and the actual values were selected so as to make the fabrication relatively noncritical. In calculating the values of θ_e and θ_o the GETSINGER [14] model

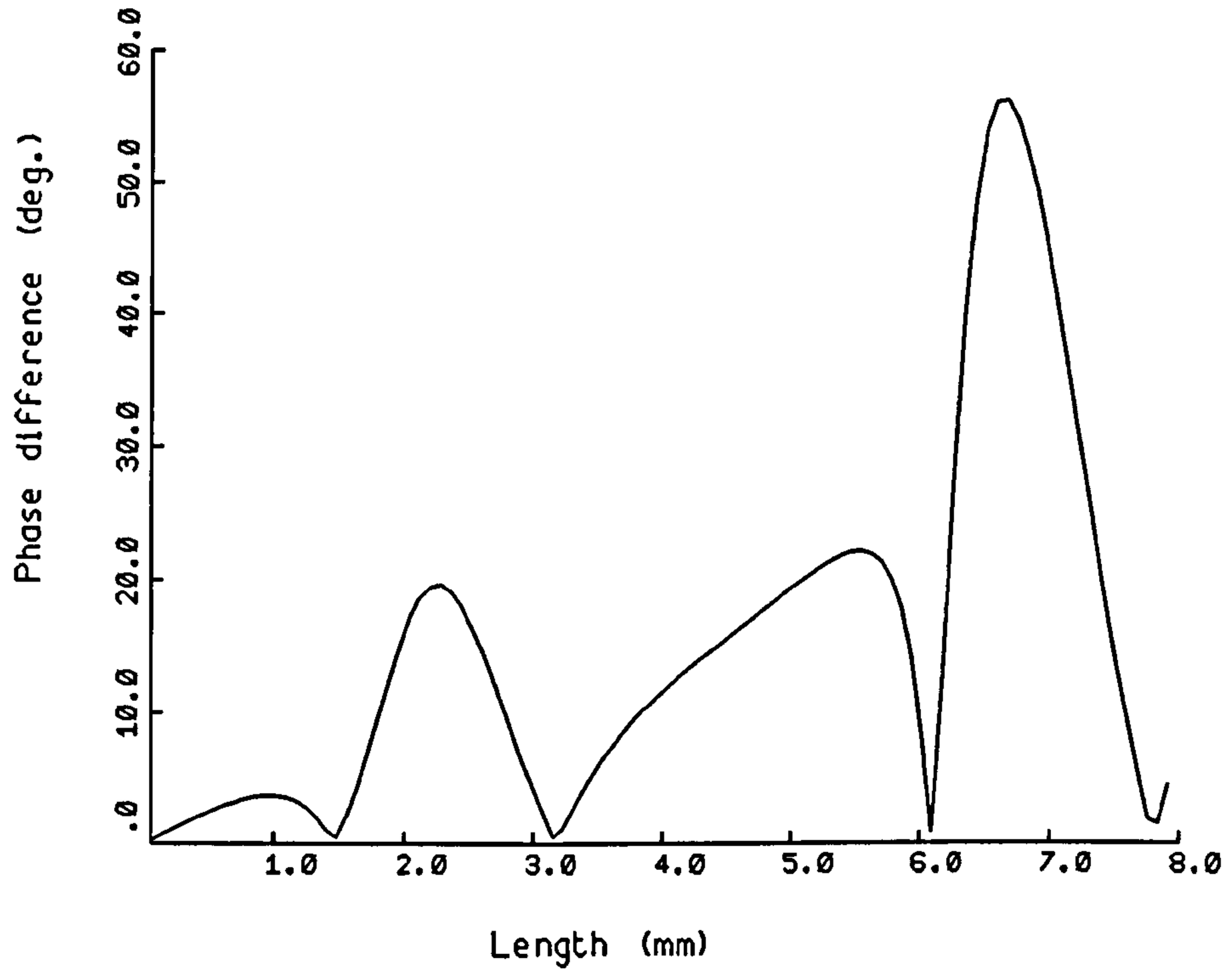

Figure 2.15: **Difference between exact and approximate theoretical insertion phase at 12GHz**

was used to account for dispersive effects. The effective length of the coupled region for the even mode was taken to be $L_c + l_{eo}$, where l_{eo} represents the effect of fringing at the remote end of the coupler and was evaluated from the HAMMERSTAD AND BEKKADAL [15] expressions. In the calculation for L_{eo} the effective width of the line for the even mode was taken to be $2w + s$. Since the odd mode is fairly precisely terminated by the link at the remote end of the coupler no allowance was made for for fringing of this mode, other than to use the full value of L_c, including l_{link}, on the basis that there will be some slight extension of the odd mode length due to the effective inductance caused by the odd mode penetrating into the narrow link.

In Fig. 2.18, p. 60, Fig. 2.19, p. 61, Fig. 2.20, p. 62, Fig. 2.21, p. 63, Fig. 2.22, p. 64 comparisons are presented between the theoretical insertion

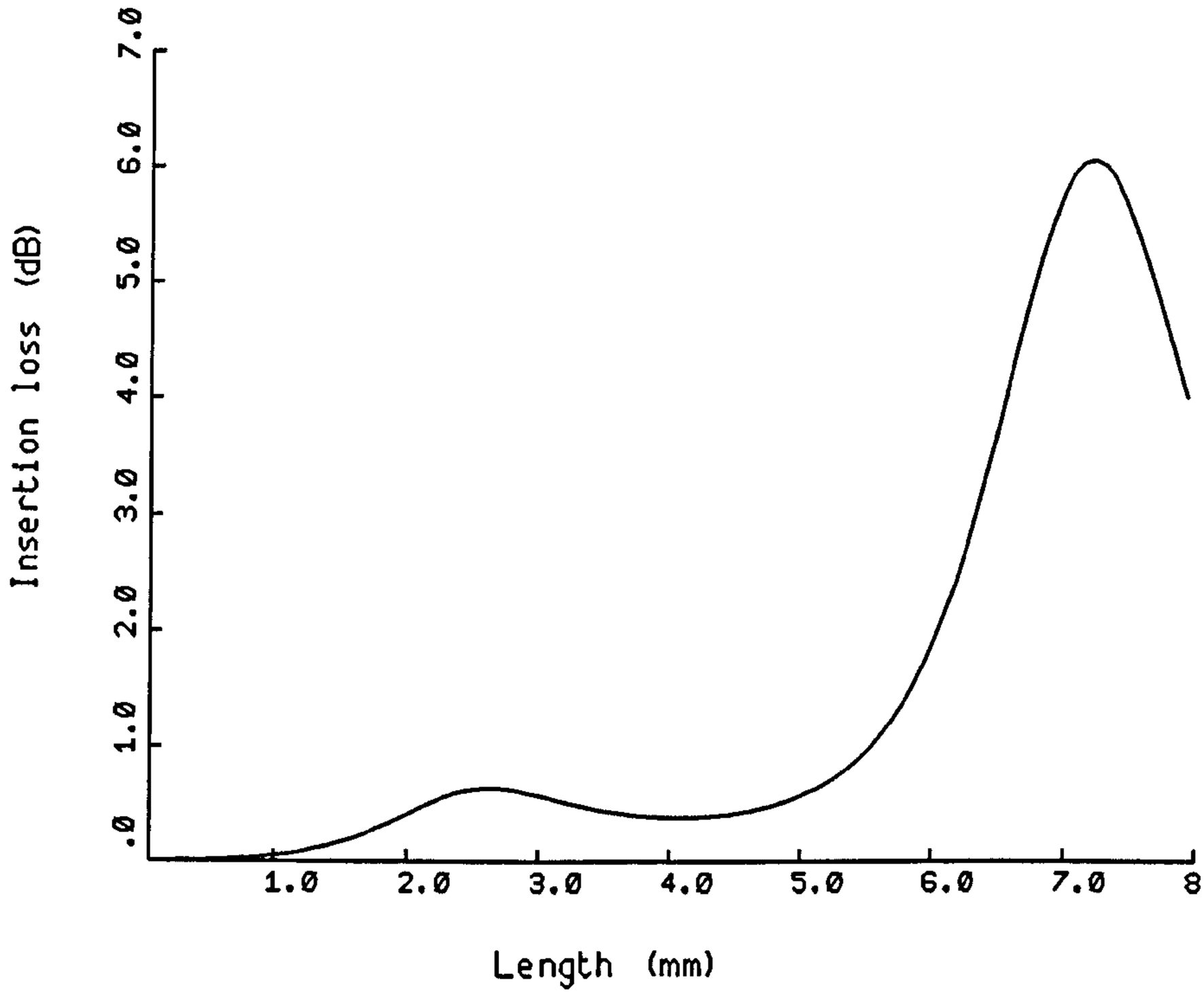

Figure 2.16: **Theoretical insertion loss for phase shifter at 12GHz using exact analysis**

phase and measured data over the X-band frequency range for five couplers having different lengths. The dimensions of the five test circuits are given in Fig. 2.17, below.

CIRCUIT	L_c	L_{link}	w	s
1	759	26	465	100
2	1257	47	476	95
3	1784	30	470	103
4	4650	52	477	109
5	6672	54	469	109

Figure 2.17: **Table of test circuit dimensions** [μm]

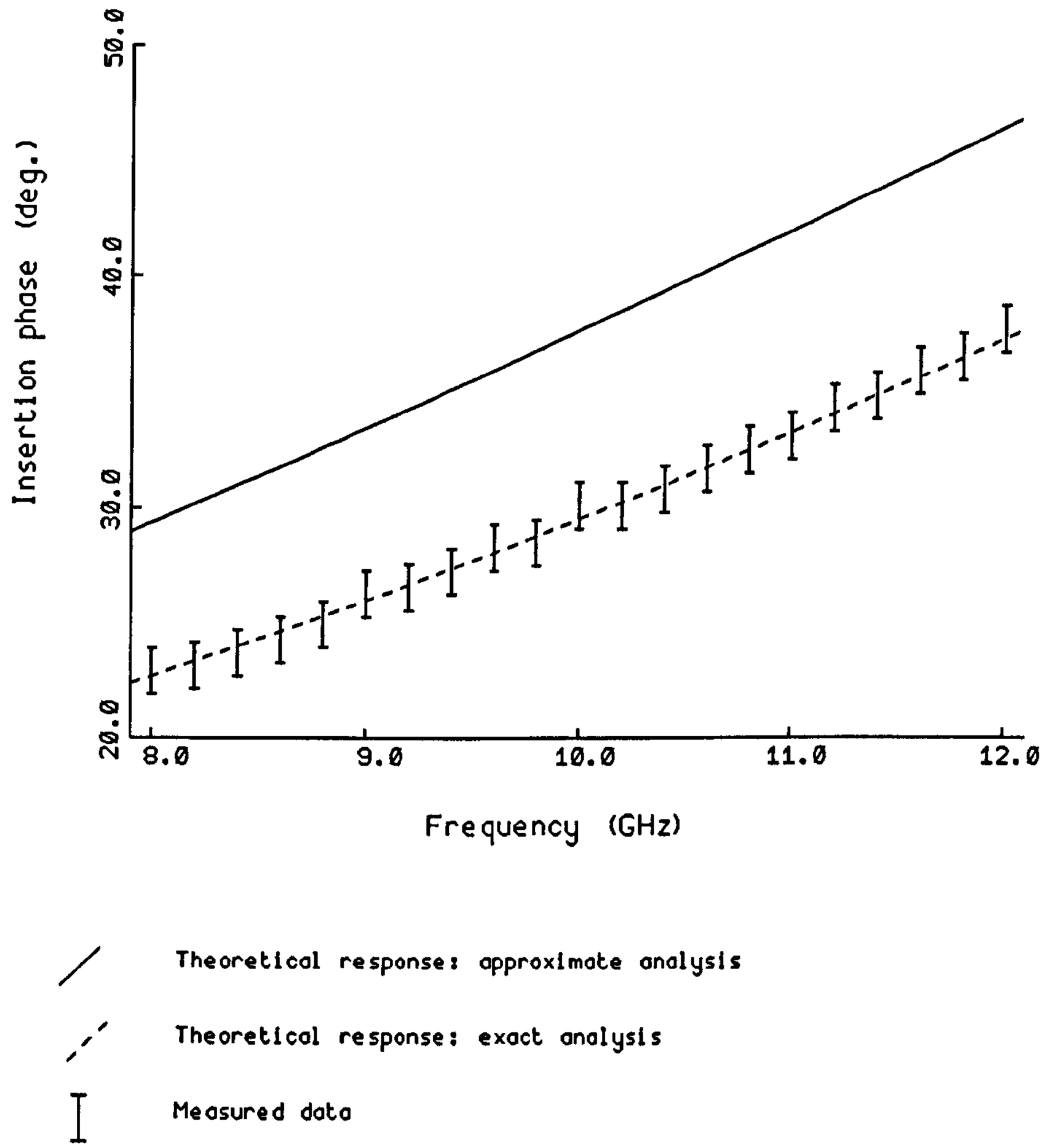

Figure 2.18: **Comparison of measured and theoretical insertion phase data for circuit 1.**

The lengths of the couplers were chosen to cover a wide range of phases, in arbitrary steps. The error bars associated with the measured data show a $\pm 1°$ measurement uncertainty. It can be seen that in all cases there is good agreement between the measured data and the predicted response based on an exact analysis. For circuit 1, with the shortest coupled length, the agreement is particularly good with the exact responses well within the 1° error

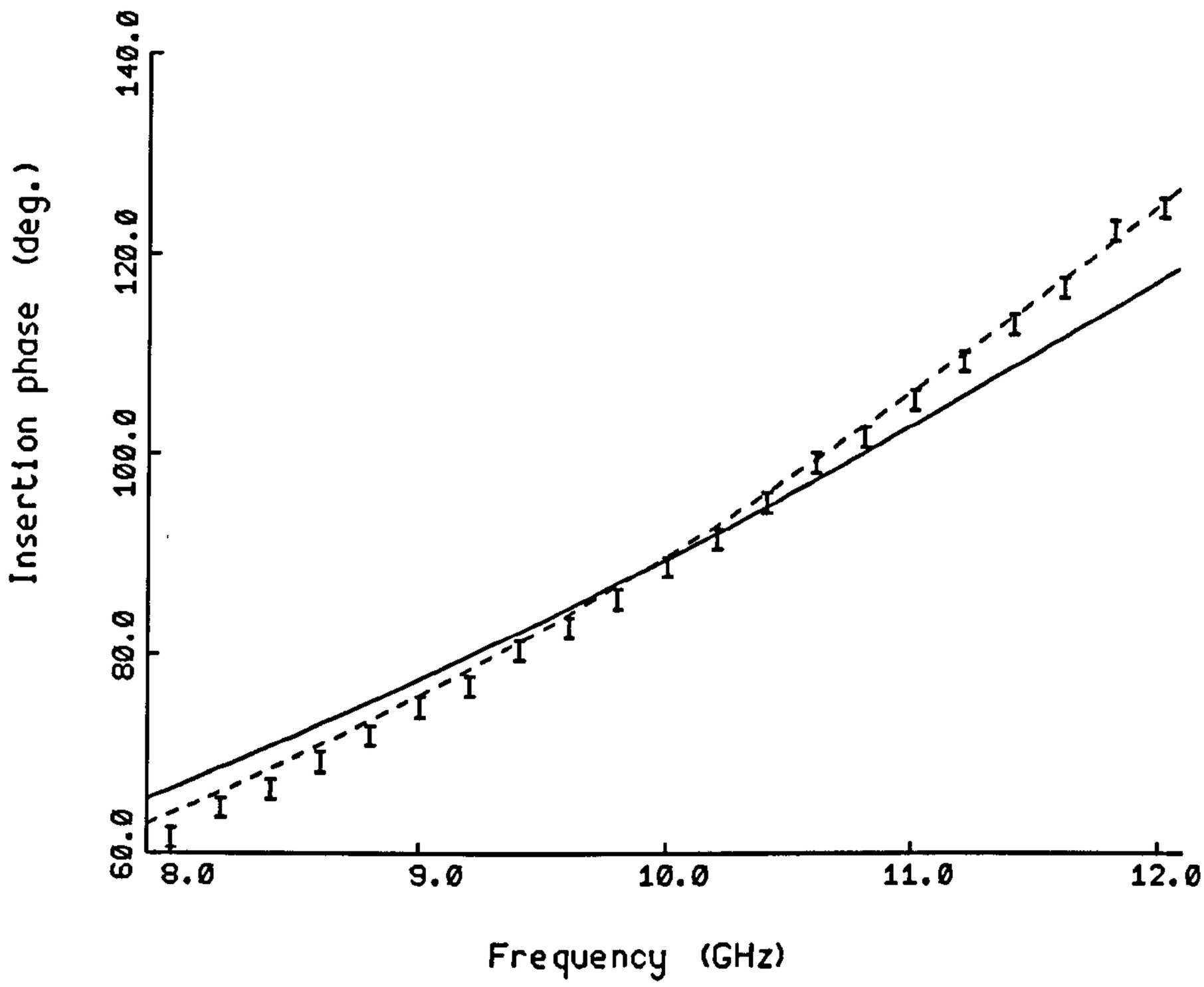

Figure 2.19: **Comparison of measured and theoretical insertion phase data for circuit 2.**

bounds of the measured data. For the other responses, even when the exact response lies outside the error bounds of the measured data the departure is small compared to the difference between the exact and approximate values. The agreement between the measured data and the exact response is emphasized by considering the shape of the responses. There are significant differences between the shapes of the approximate and exact responses, par-

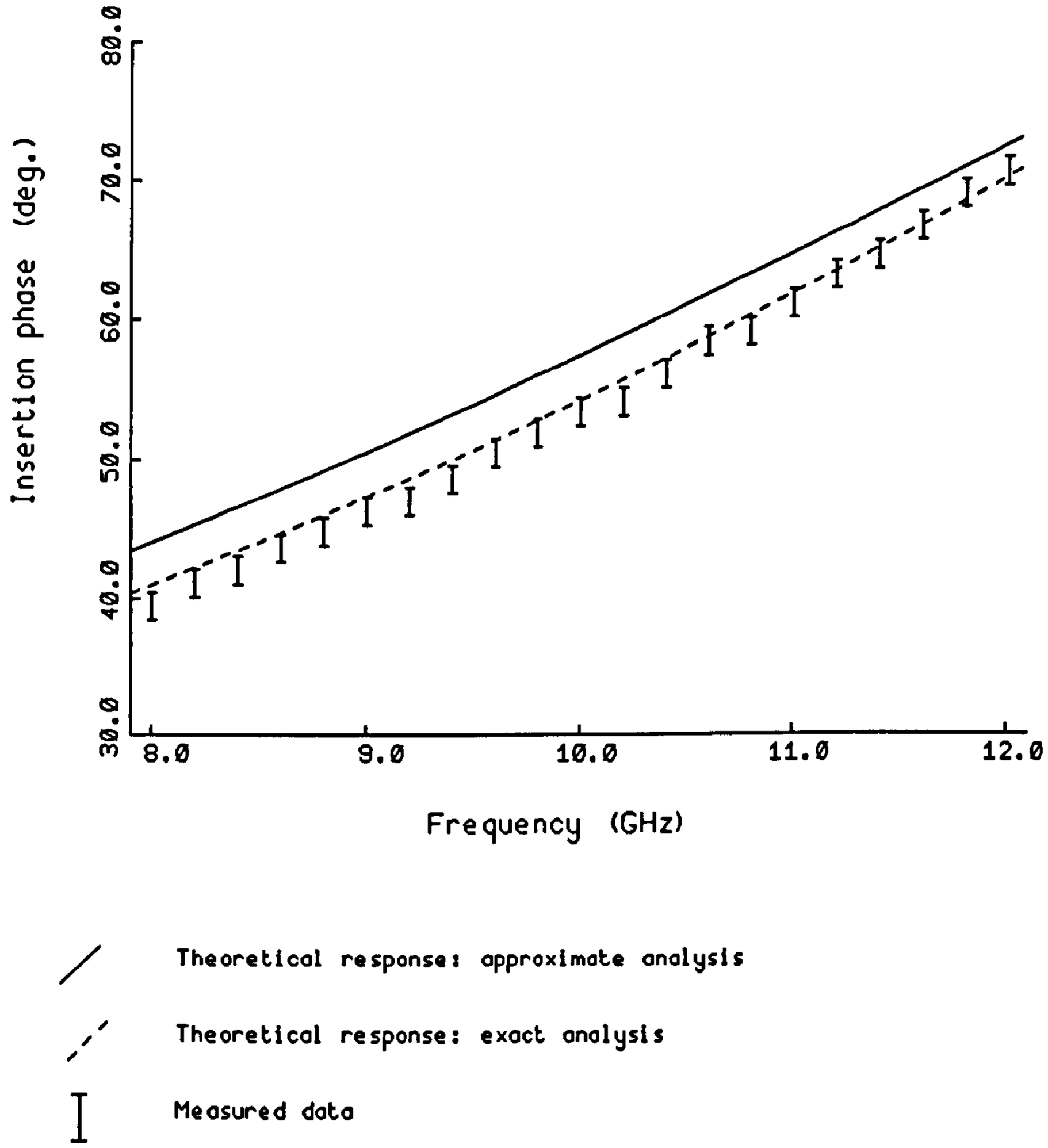

Figure 2.20: Comparison of measured and theoretical insertion phase data for circuit 3.

ticularly for the longer coupled lengths, but in all cases the measured data points follow closely the shape of the exact response.

Fig. 2.21, p. 63 and Fig. 2.22, p. 64, which represent the longer coupled sections, show that the agreement between the measured data and the exact response tends to worsen at the top end of the frequency band. This suggests that some dispersive effect is involved, which would naturally become more

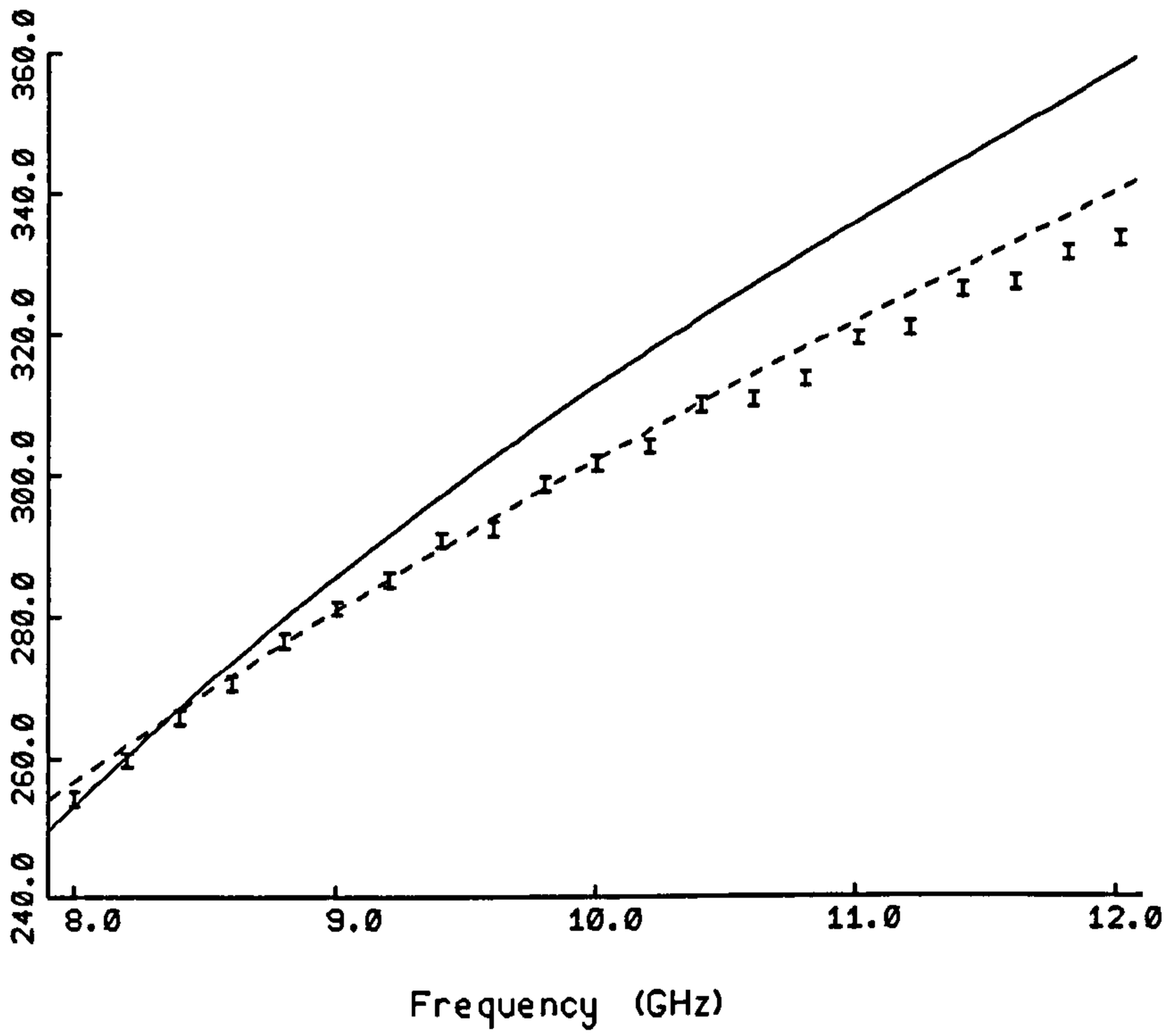

Figure 2.21: Comparison of measured and theoretical insertion phase data for circuit 4.

significant as the length of the coupled section increased. The model due to GETSINGER [14] was used to account for dispersion, but some authors, notably EASTER AND GUPTA [20], have suggested that this model gives a slight overestimate of the effect of dispersion. This would be consistent with the results shown in Fig. 2.21, above and Fig. 2.22, p. 64, where the predicted insertion phase is slightly higher than the measured data at the top end of the

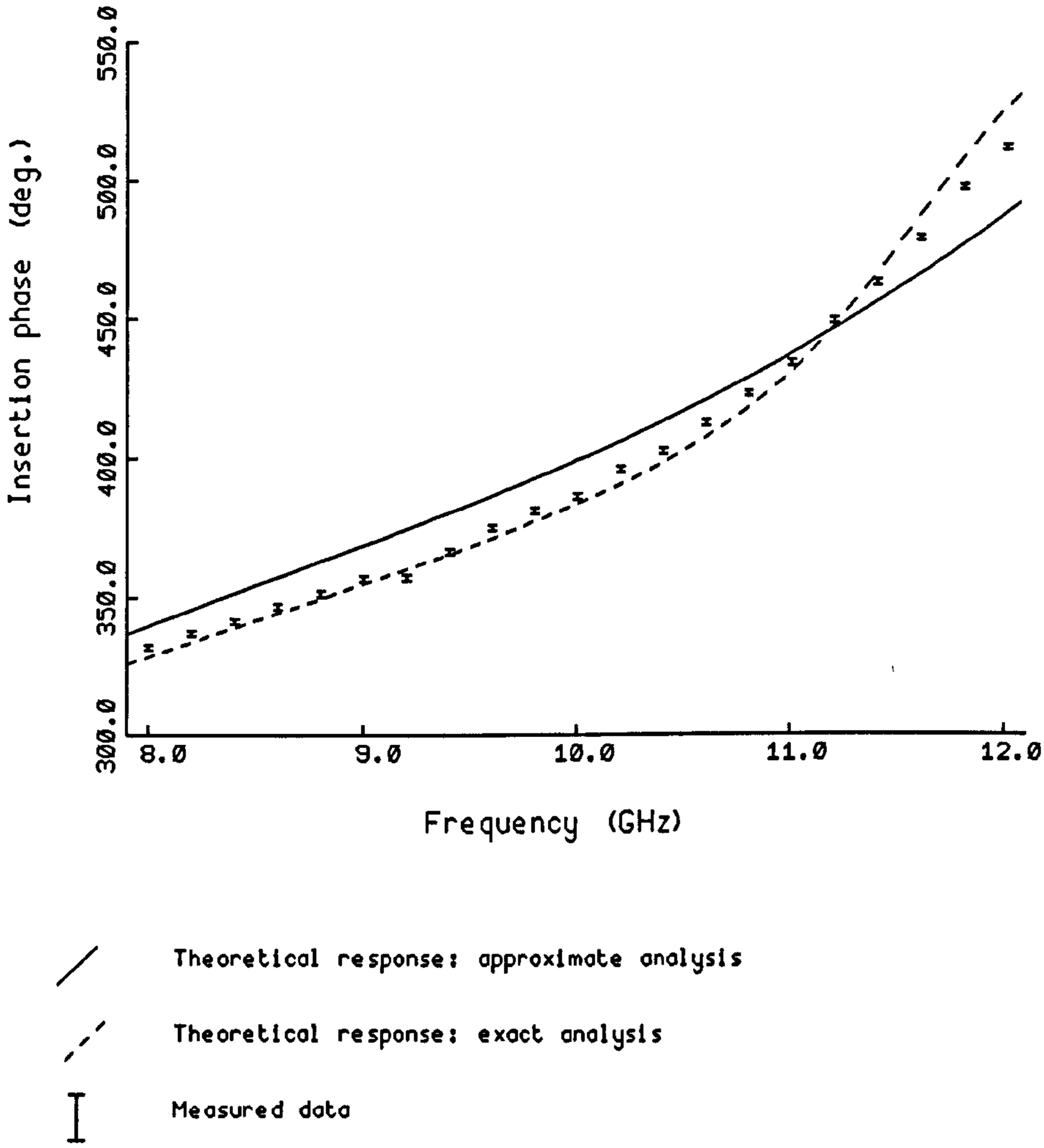

Figure 2.22: **Comparison of measured and theoretical insertion phase data for circuit 5.**

band. A more recent dispersion model, from KIRSCHNING AND JANSEN [21] claims to provide a more accurate prediction of dispersion effects at higher frequencies, and could possibly improve the fit between the measured data and the exact theory in the 11-12GHz region.

In calculating the theoretical responses no attempt was made to model the discontinuities formed by the 90° bends at the entry to the coupled region.

Indeed there do not appear to exist in the literature discontinuity models which include the combined effect of bends and coupling. However, it would appear from the results that this is an unnecessary refinement for the circuit designer and that adequate prediction of the insertion phase results from using the nominal length, L_c, together with small compensations for fringing at the remote end of the device.

It is not thought that the bend discontinuity contributed to the departure of the measured data from the exact response at the higher end of the measured frequency band, since this effect was only noticeable for the longer coupled sections and suggested a purely length dependent effect.

While the insertion phase exhibits some degree of nonlinearity with frequency, the simple coupled-line section, without the changes in line geometry which have been introduced by some authors, such as SCHIEK AND KOHLER [13], to overcome problems associated with different mode velocities, provides a simple component capable of yielding very predictable results. Moreover, its simple geometry would seem to be attractive for use at higher microwave frequencies where changes in line geometry, introduced for mode velocity compensation, would themselves introduce significant discontinuities.

2.9.2 Matching stub

The matching stub in the single PIN diode phase shifter is required to provide a particular input reactance with the PIN diode in the on state, i.e. with only the even mode present, and to always have a high input impedance with the PIN diode off, i.e. with both modes present. Whilst the open-circuited stub would be expected to yield a high input impedance when its length was in the vicinity of $\lambda/2$ it is of interest to know how the input impedance changes with length, since this directly affects the range of phase changes that can be achieved with the single PIN diode phase changer, and over a range of frequencies. Theoretical values for input impedance as a function of the stub length are shown in Fig. 2.23, p. 66, Fig. 2.24, p. 67 and Fig. 2.25, p. 68 , for a range of lengths around the $\lambda/2$ value. For the stub being simulated to give these theoretical responses, the track geometry led to the average of the odd and even mode wavelengths being approximately 11.8mm at 10GHz.

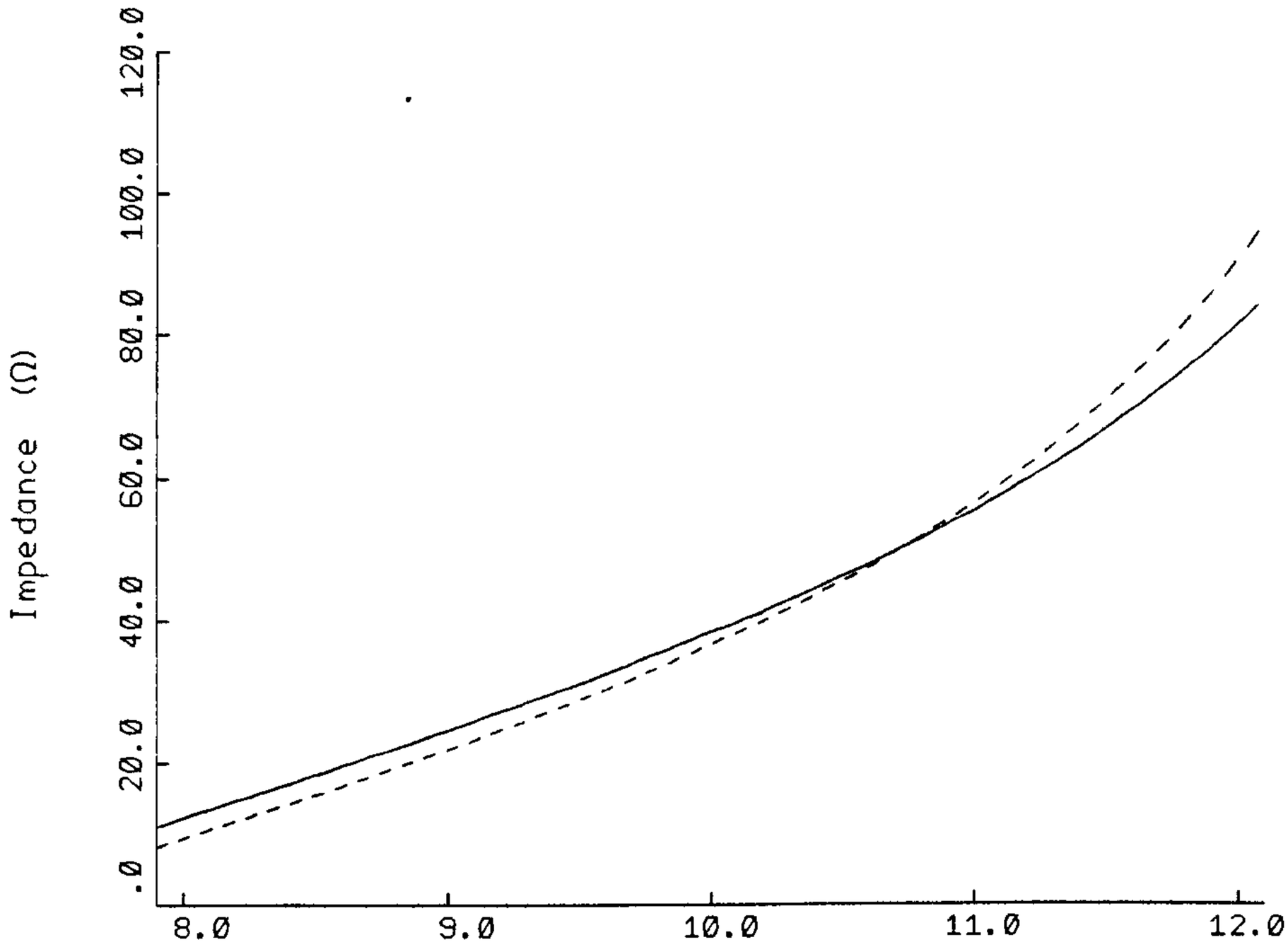

Figure 2.23: Theoretical responses showing the variation of input impedance of an open-circuited stub, 4mm in length, as a function of frequency

This is consistent with the result shown in Fig. 2.24, p. 67 which shows the highest input impedance is obtained with the 6mm stub, and tends to infinity at the frequency which gives a length of $\lambda/2$. The responses also show the effect on the impedance of using an exact analysis rather than one based

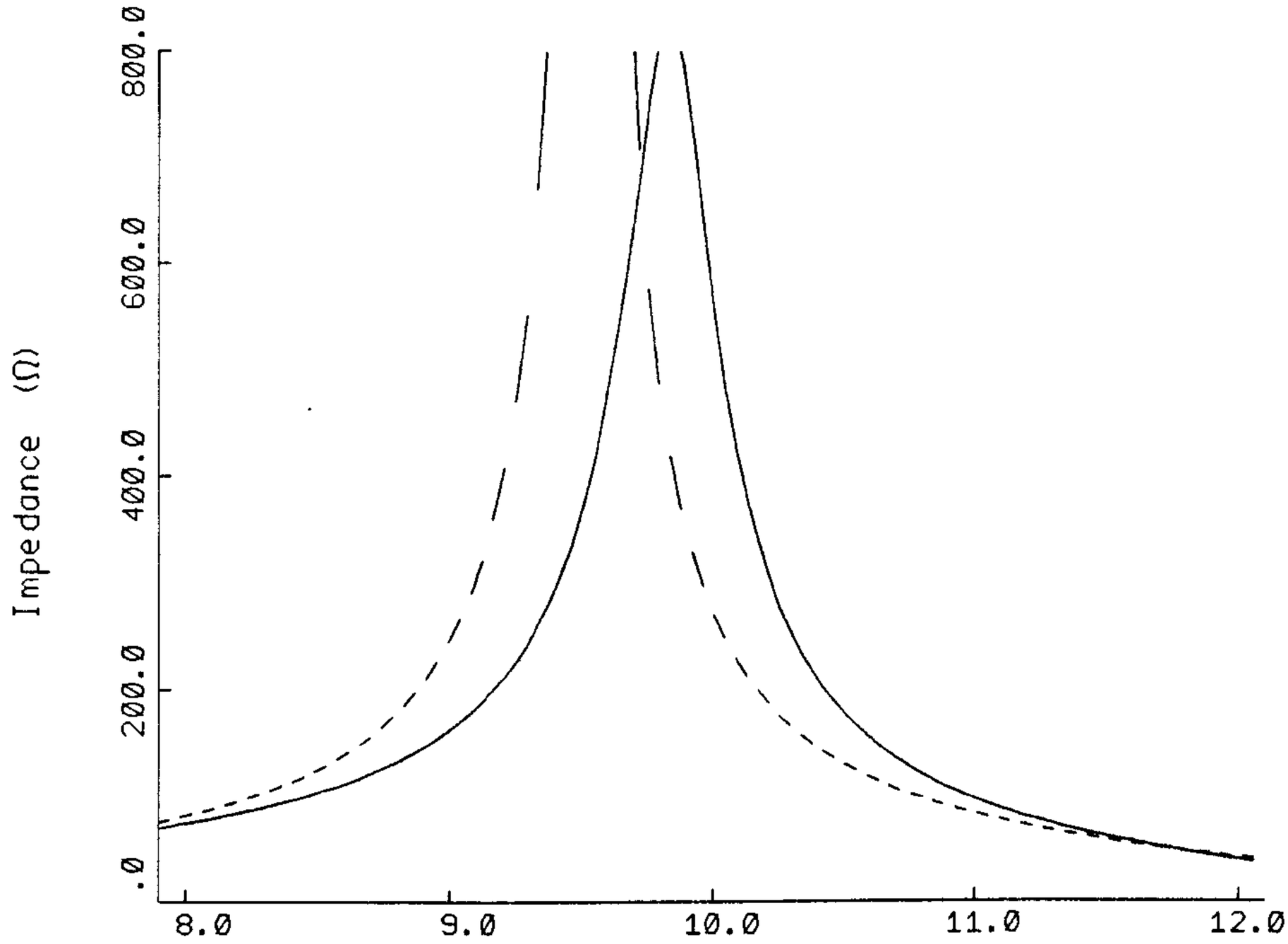

Figure 2.24: Theoretical responses showing the variation of input impedance of an open-circuited stub, 6mm in length, as a function of frequency

on averaging the odd and even mode propagation velocities. The difference between the two methods is particularly noticeable when the stub length is in the vicinity of $\lambda/2$. This is particularly significant for the present application which requires the stub to work in the high impedance region. It can be seen

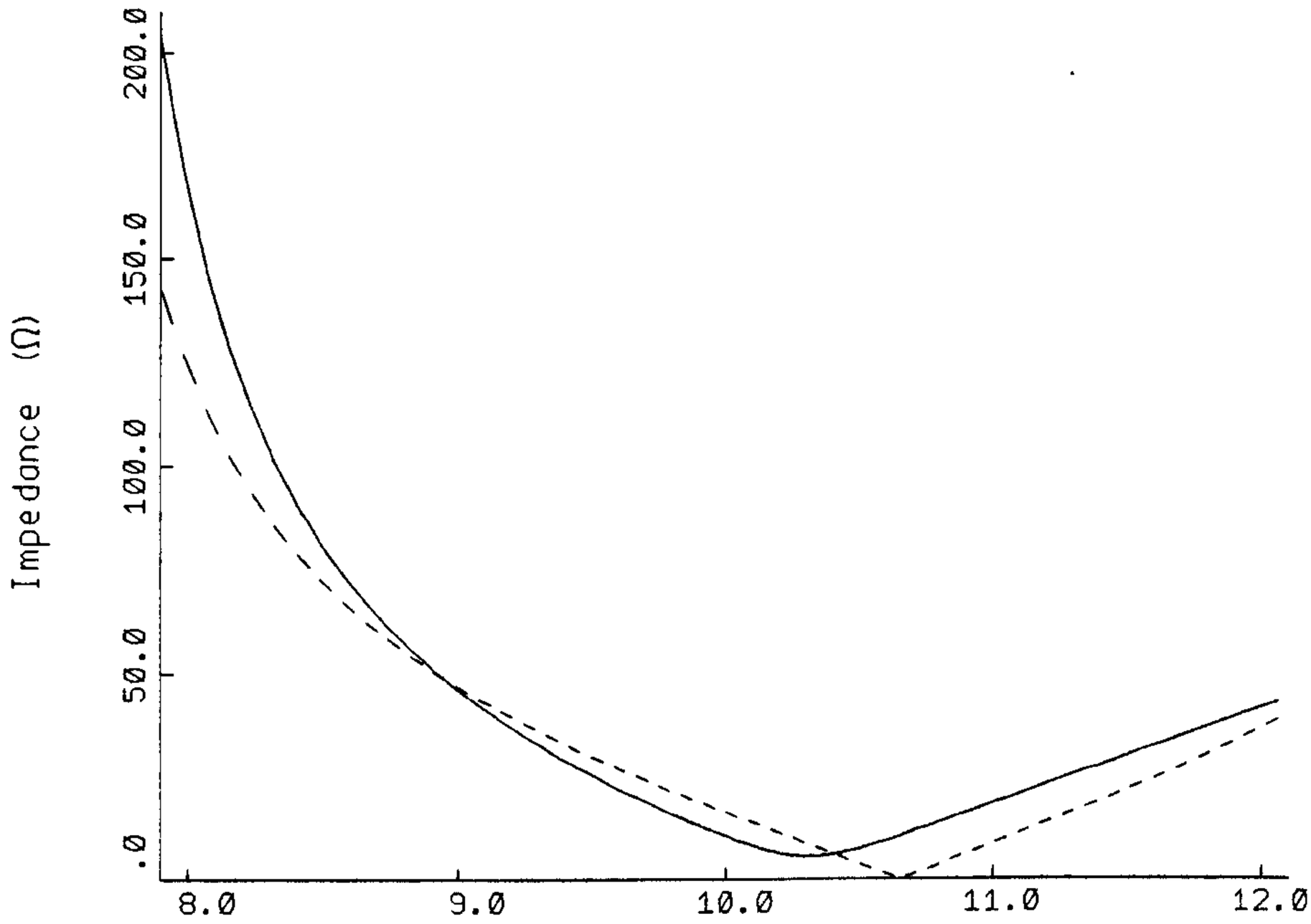

Figure 2.25: Theoretical responses showing the variation of input impedance of an open-circuited stub, 8mm in length, as a function of frequency

from Fig. 2.24, p. 67 that the effect of using the more exact analysis, already justified though practical measurements for assorted coupled lines, is to shift the centre frequency of the response by approximately 350MHz, and to reduce the effective bandwidth of the stub, i.e. the frequency range over which high

input impedance is maintained.

The results for the 6mm stub highlight potential problems with using a simple matching stub. In the present context, a high impedance is one which is high relative to 50Ω, since in the PIN off state the matching stub is shunting the 50Ω of the phase change section. A high input impedance is only obtained for a stub lengths close to $\lambda/2$. This restricts the range of lengths of section A (Fig. 2.1, p. 34) that can be matched in the diode on state, and consequently restricts the magnitude of phase changes that can be accommodated. Limitations of the magnitude of the phase changes that can be obtained is not in itself a problem for the present application, since in a delay line stabilized oscillator, the amplifier in the feed back path can magnify the effects of the phase changes. However, the limited bandwidth of the matching stub will restrict the range over which an oscillator can be switched. If, for example, 300Ω is regarded as a sufficiently high impedance for the present application then the theoretical responses show that the frequency of operation is limited to around 800MHz. These problems would to some extent be solved if the degrees of freedom in the stub design could be extended. It was proposed in section 2.4.2 that this could be achieved by employing some even mode loading at the remote end of the stub. Theoretical responses, showing the effects of even mode loading, are displayed in Fig. 2.26, p. 70, Fig. 2.27, p. 71 and Fig. 2.28, p. 72. In each response X represents the magnitude of the reactive loading as defined in section 2.4.2. Negative values of reactance tend to decrease the stub input impedance, as shown in Fig. 2.28, p. 72, whilst positive values maintain the general shape of the impedance response and produce a shift in the centre frequency. Decreasing the positive reactance from infinity to 50Ω produces a frequency shift of approximately 1GHz, whilst maintaining a high input impedance and an effective bandwidth of 800MHz. Thus it would appear worthwhile using even mode loading in order to increase the possible range of phase changes.

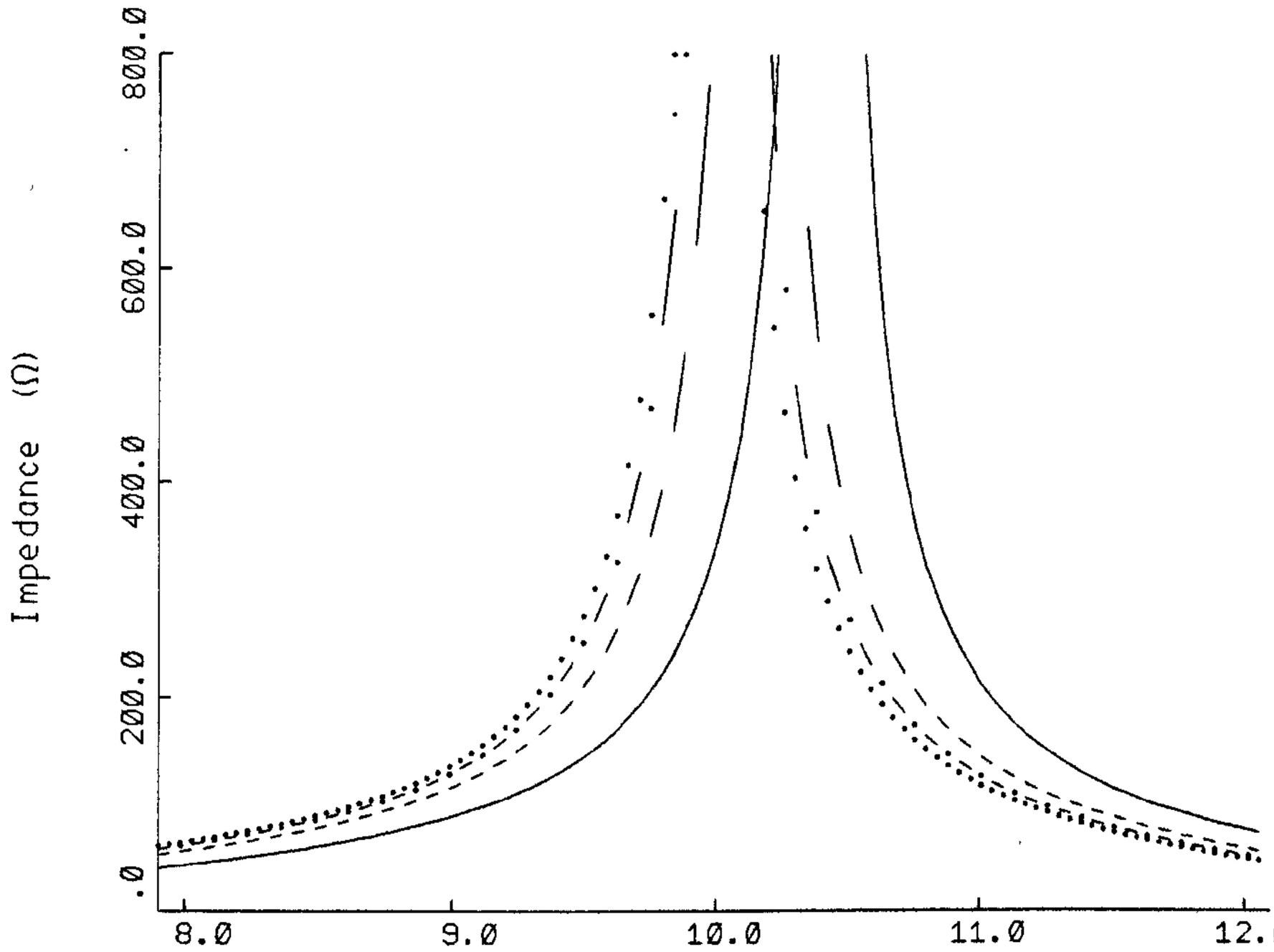

Figure 2.26: **Theoretical responses showing the effect on the input impedance of an open-circuited stub of applying even mode loading (stub length =6mm) (X=100Ω, 200Ω, 300Ω, 400Ω)**

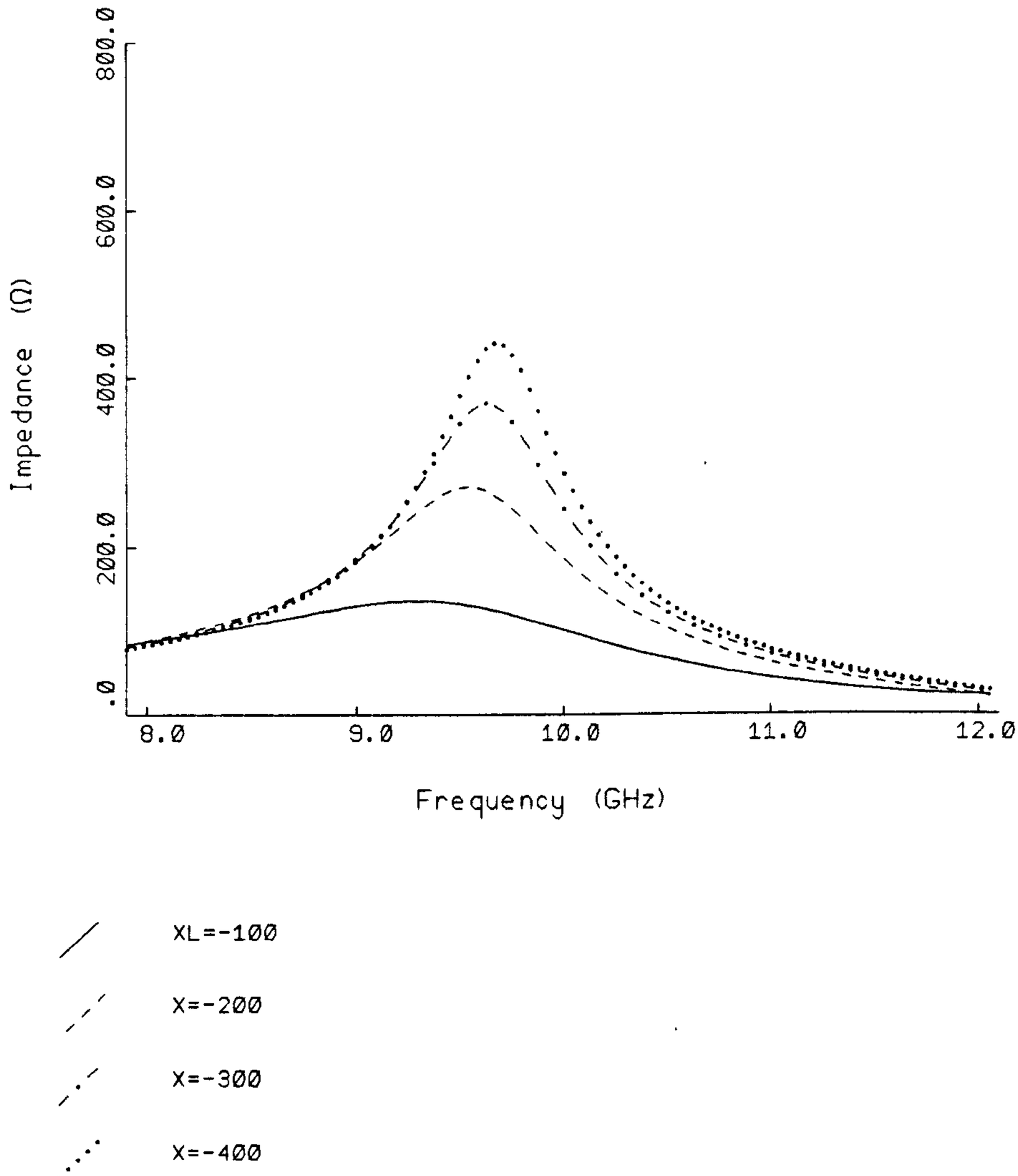

Figure 2.27: **Theoretical responses showing the effect on the input impedance of an open-circuited stub of applying even mode loading (stub length =6mm) (X=-100Ω, -200Ω, -300Ω, -400Ω)**

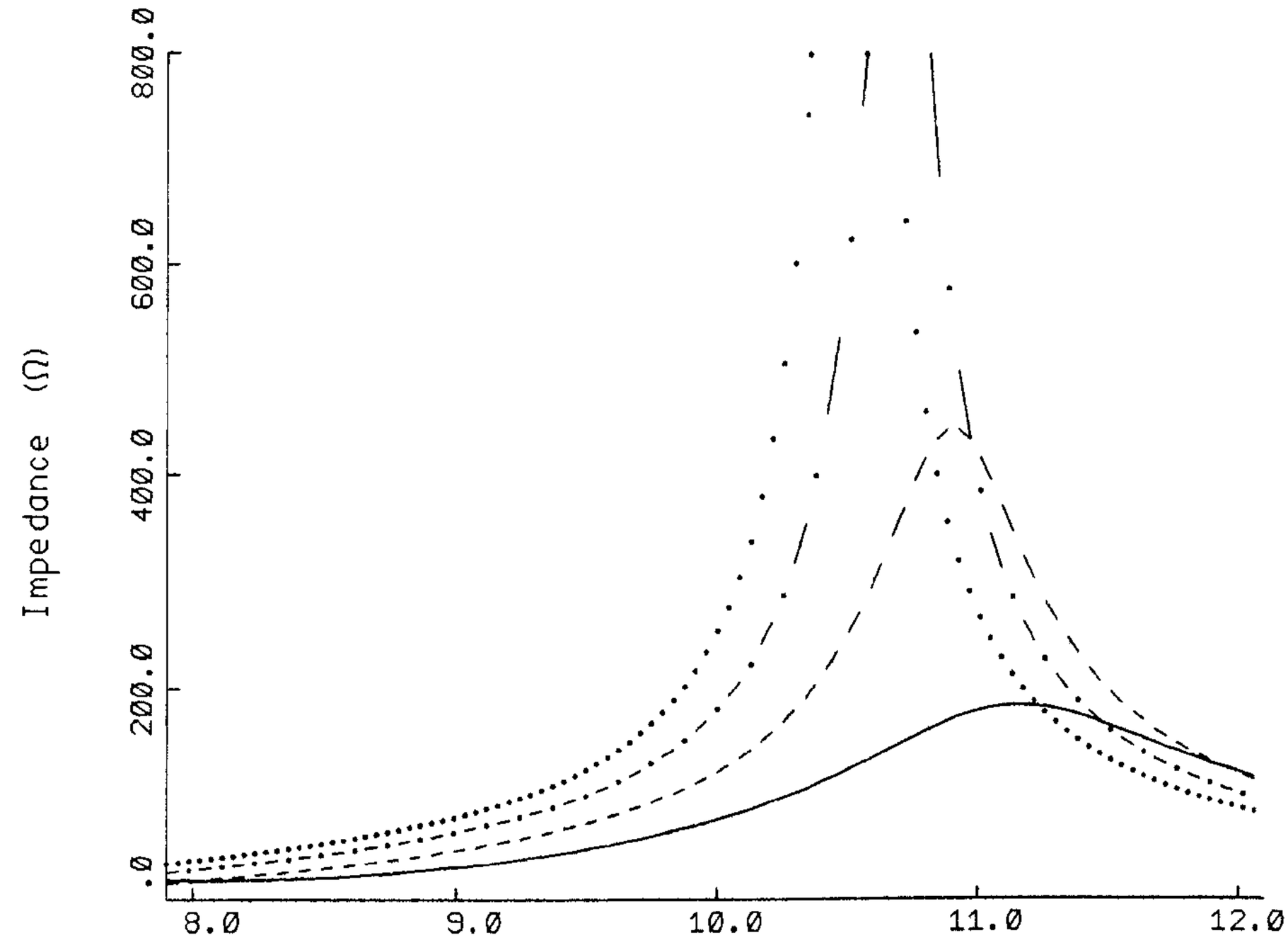

Figure 2.28: **Theoretical responses showing the effect on the input impedance of an open-circuited stub of applying even mode loading (stub length =6mm) (X=0Ω, 25Ω, 50Ω, 75Ω)**

2.9.3 DC breaks

In order to establish the validity of the model proposed in section 2.5.3 to represent the excess phase in microstrip DC blocks, two representative circuits were fabricated on RT/duroid, having a thickness of $635\mu m$ and a relative permittivity of 10.4, and tested over the frequency range 8-12GHz. The breaks were built into lines having a standard characteristic impedance of 50Ω. Fig. 2.29, below gives the calculated element values of the equivalent

	L	C_1	C_2	C_3
	pH	pF	pF	pF
Finger break	74	0.0015	0.0018	0.020
Zigzag slit	44	0.0030	0.0030	0.024

Figure 2.29: **Table of values of discontinuity equivalent circuit elements**

circuit of Fig. 2.11, p. 52 for the two circuits investigated. Converting the values from Fig. 2.29, above into the appropriate equivalent line lengths gave total additional line lengths of $140\mu m$ and $200\mu m$ to represent the discontinuities of the finger break and zigzag slit respectively. The measured and calculated excess phases are compared in Fig. 2.30, p. 74 and Fig. 2.31, p. 75. The figures include the essential dimensional data for the two DC break configurations. In each case the graph A is the calculated excess phase neglecting the end corrections and graph B the calculated excess phase including the end correction in the form of the above specified additional line lengths. It is evident from the results that there is good agreement between the measured excess phase and those computed theoretically with appropriate end corrections. It should be noted that the finger break has a smaller excess phase than the zigzag slit, although as explained in section 2.5 the zigzag arrangement is the preferred geometry for the present application.

In addition to having precise information about the transmission phase through the DC break it is also important that the device should be well matched, since reflections in the coupled line section could alter both the match and transmission phase of the whole structure. Fig. 2.32, p. 76 shows the insertion loss for three DC break configurations, namely the finger break, the zigzag slit and the slanting slit. It can be seen that all three exhibit a

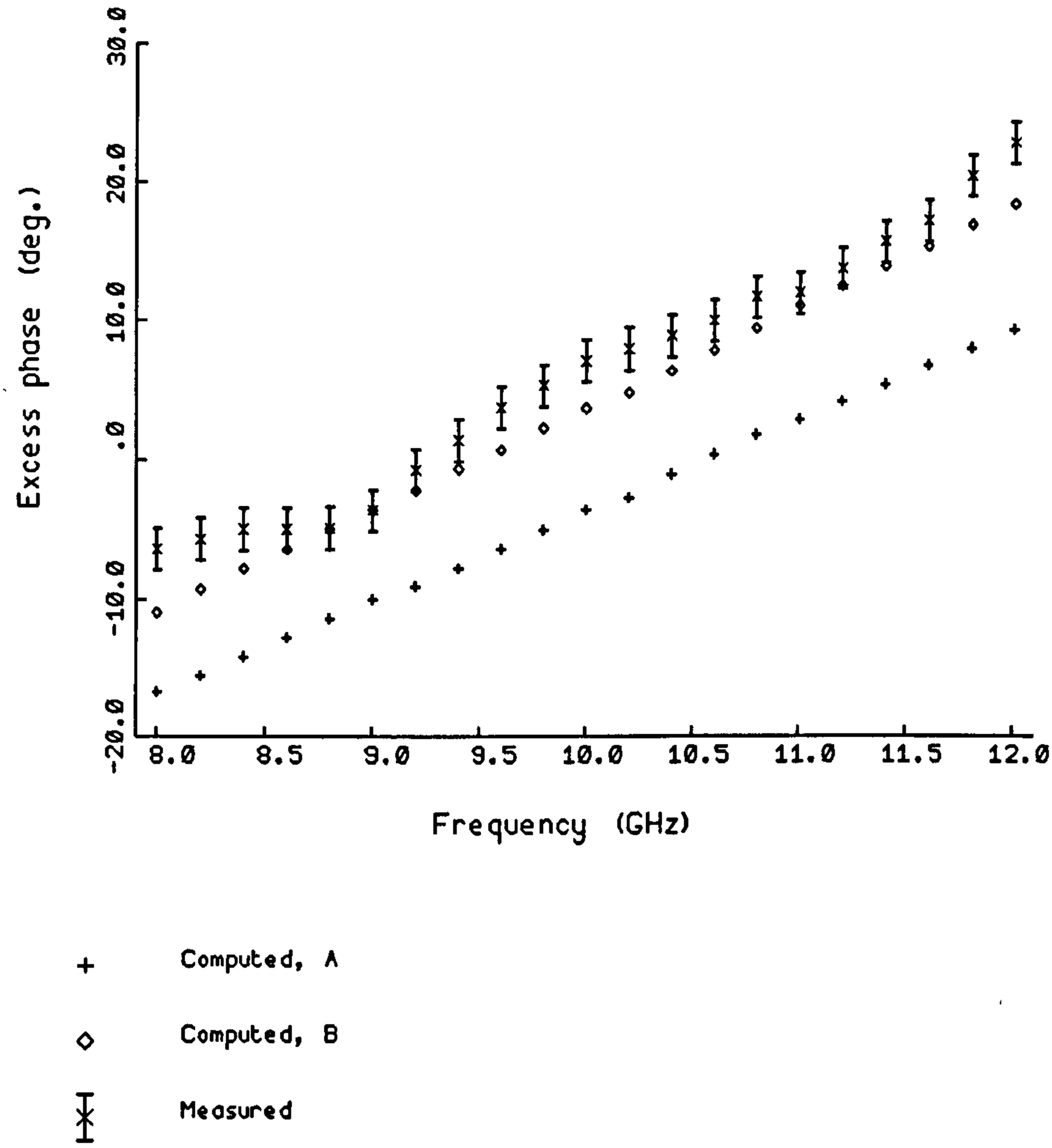

Figure 2.30: Comparison of measured and theoretical excess phase for a microstrip finger break: finger length=3.06mm; finger width=180μm; finger gap=30μm

reasonably small insertion loss in the vicinity of 10GHz, which is the design centre frequency. The insertion loss is primarily due to mismatch and, as would be expected, the finger break structure has the lowest loss since the use of fingers enables a near optimum match to be obtained. The zigzag slit

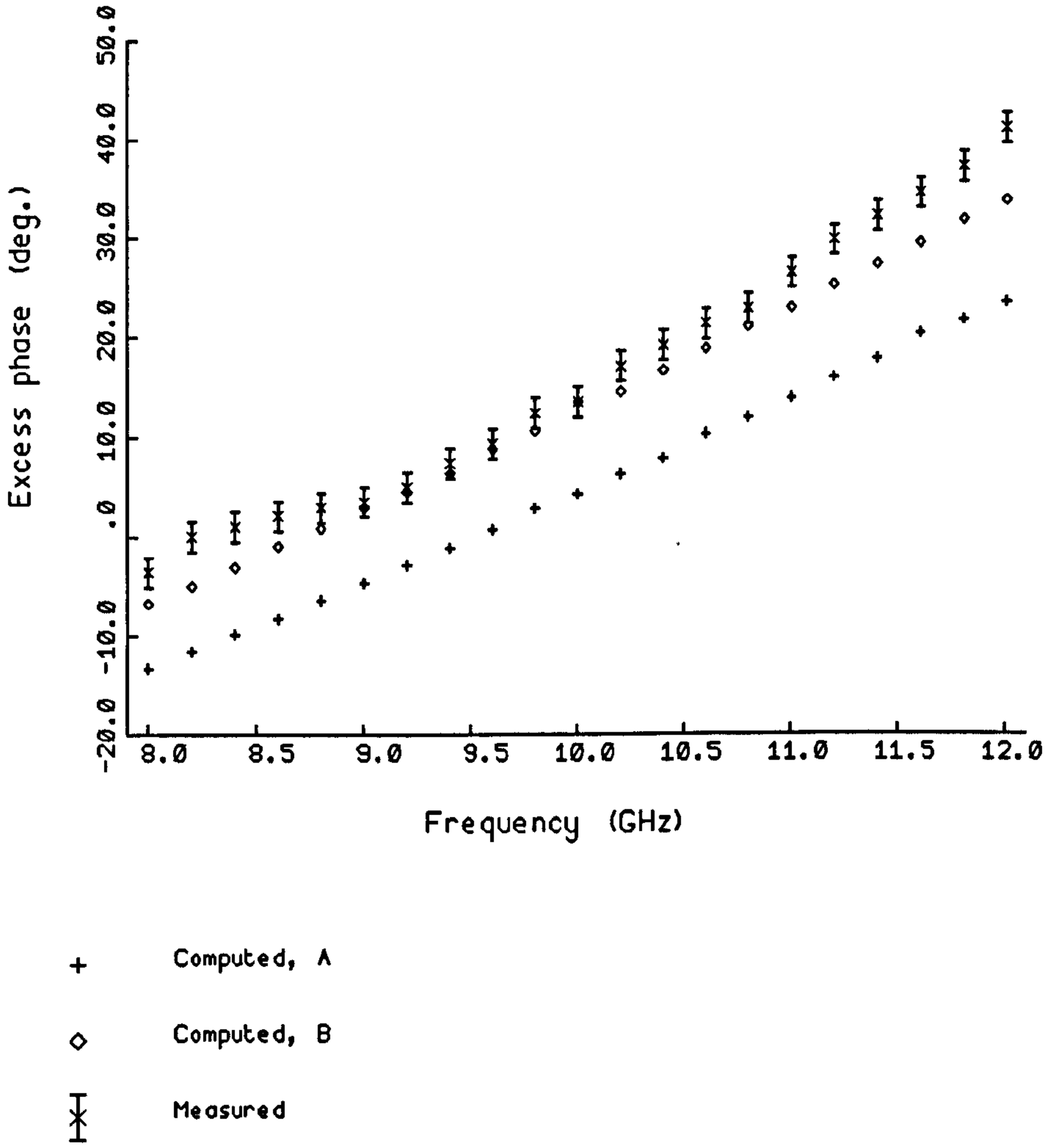

Figure 2.31: **Comparison of measured and theoretical excess phase for a microstrip zigzag break: length of break=3.51mm; gap between coupled lines=70μm**

and the diagonal slit show a similar loss, but for the reasons already discussed the zigzag slit is preferable for inclusion in the coupled line section.

Using the information obtained about the excess phase it is possible to precisely account for the presence of the DC break in the single PIN diode

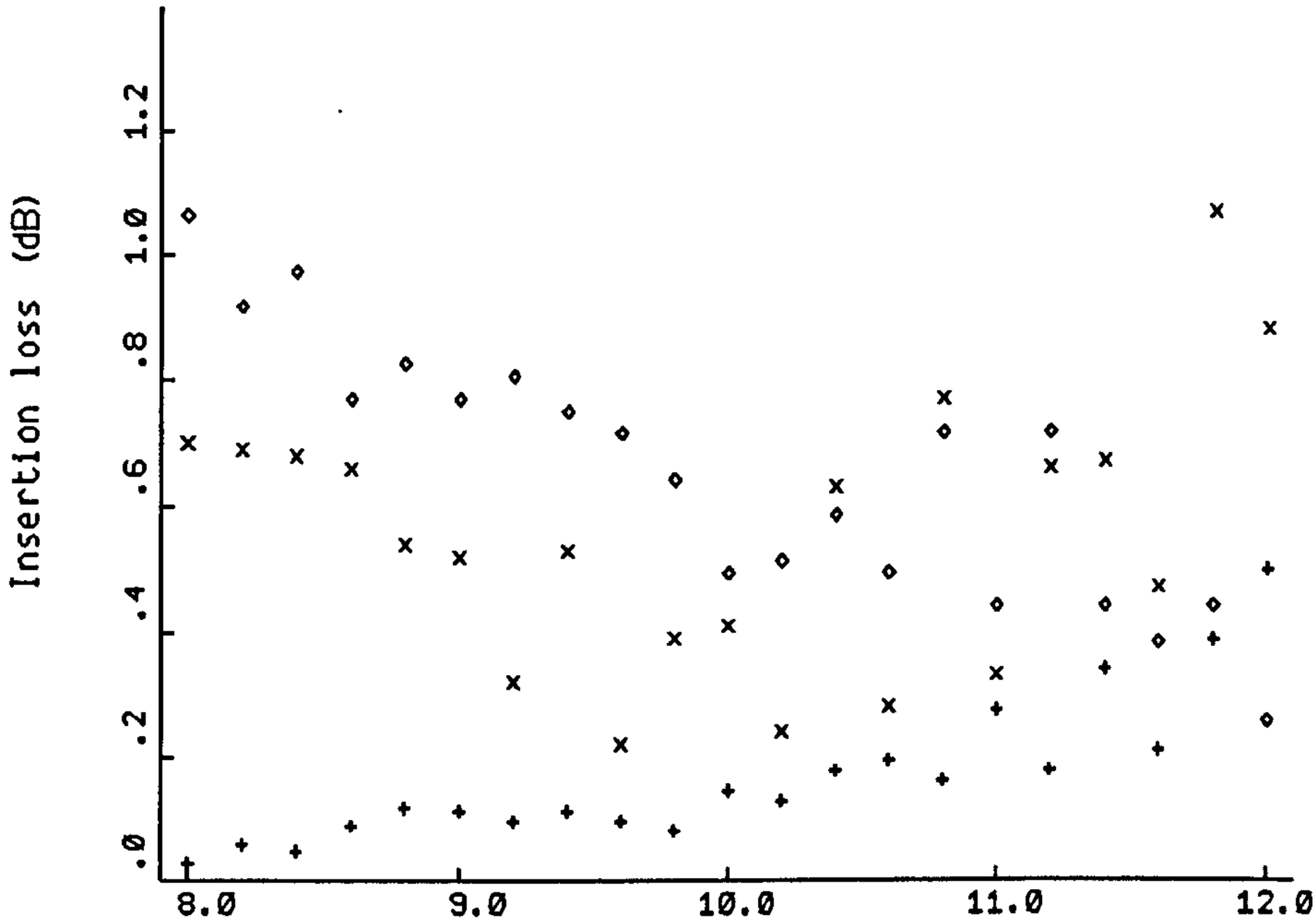

Figure 2.32: **Insertion loss of DC breaks**

phase shifter. In order to include the effects of both the transmission phase and the mismatch due to the break, it was modelled in the final design as a two-port network, represented by the appropriate ABCD matrix, and included in the coupled line analysis.

2.9.4 Microstrip gap

The need for an accurate model for the microstrip gap across which the PIN diode is mounted was discussed in section 2.6. The only expressions available to the circuit designer are those referred to in section 2.6, namely those due to GARG AND BAHL [19]. These expressions, reproduced in appendix A.3, and which are widely quoted in modern microstrip textbooks and designer handbooks, such as EDWARDS [33], were found to contain significant errors. In order to establish the magnitude of the errors, the expressions were evaluated and compared with the original values of BENEDEK AND SILVESTER [18], for a range of microstrip geometries using $\epsilon_r = 2.5$. The results are plotted in Fig. 2.33, p. 78 and Fig. 2.34, p. 79. These plots show that whilst there is reasonable agreement for the odd mode capacitance, the even mode capacitance predicted from the GARG AND BAHL [19] expressions is significantly different from the results of the original theory given in BENEDEK AND SILVESTER [18]. It can also be seen that the GARG AND BAHL [19] expressions are not continuous at s/w=0.3, which is the boundary value for the two sets of expressions for m_e and k_e, which are defined in equations A.47 through A.50 in Appendix A3. Fig. 2.35, p. 80 shows the effect of applying a scaling factor to the C_e/w values obtained from the appropriate equations in appendix A.3. Although the scaling provides a much closer agreement with the results of BENEDEK AND SILVESTER [18], the discontinuity at s/w=0.3 remains and the curve fit is still not good. Errors of the same magnitude as those presented here have also been shown to exist at other, higher values of permittivity. It appears that in order to obtain the 7 per cent accuracy quoted by GARG AND BAHL [19], a significant change in the form of the even mode expression is required. In a comment on the accuracy of these expressions FOOKS AND ZAKAREVICIUS [22] make a misleading statement which implies that they have been supported by the experimental work of OZMEHMET [23]. The latter's work on a simpler gap capacitance model uses the results of BENEDEK AND SILVESTER [18] to verify their measurements and makes no reference to GARG AND BAHL [19].

Fig. 2.36, p. 81 and Fig. 2.37, p. 82 show the practical effect of using the GARG AND BAHL [19] expressions, rather than the theory of BENEDEK AND SILVESTER [18], to calculate the insertion loss of a microstrip gap.

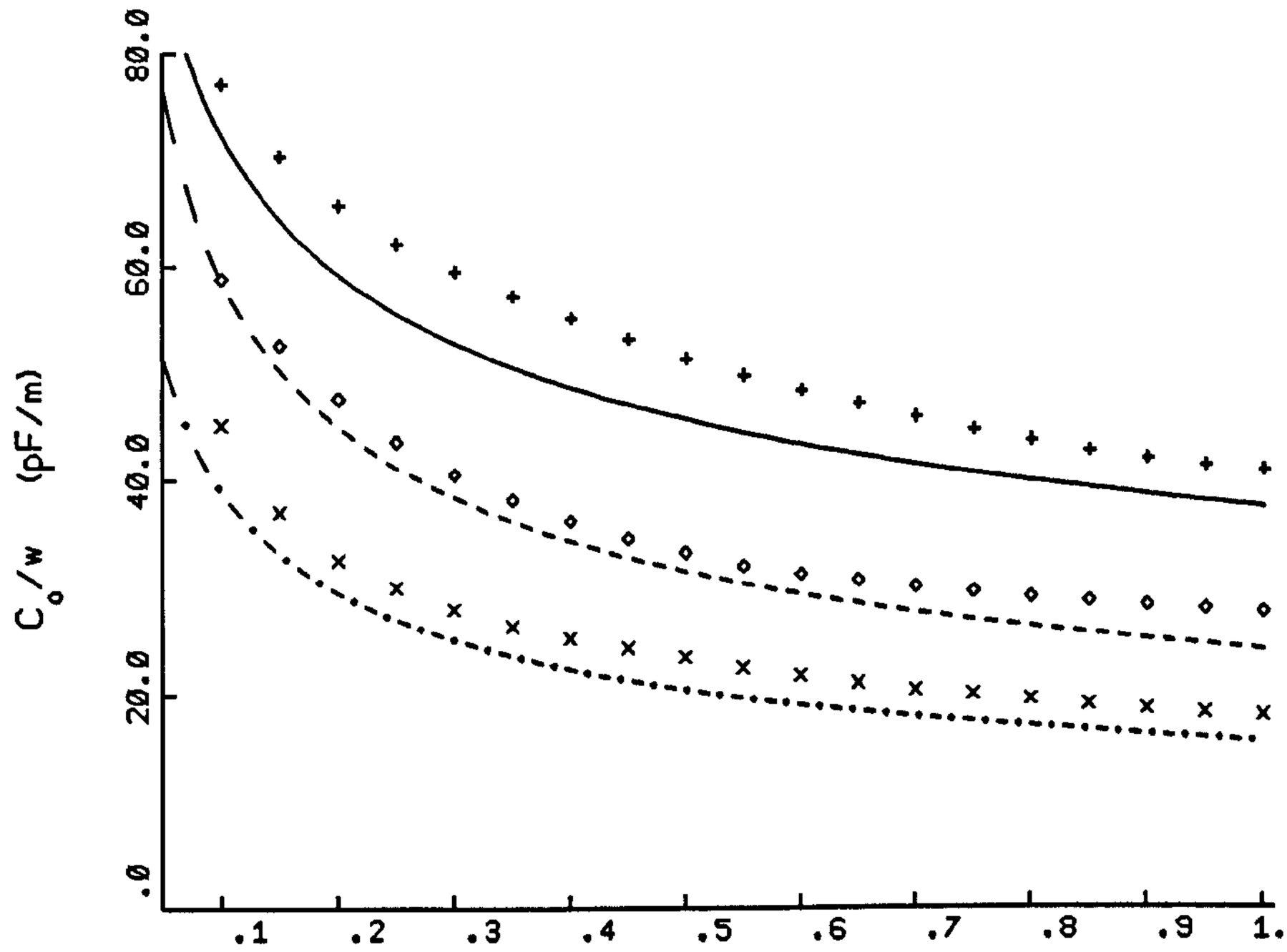

——— Garg & Bahl: w/h = 0.5

- - - - Garg & Bahl: w/h = 1.0

-·-·- Garg & Bahl: w/h = 2.0

\+ Benedek & Silvester: w/h = 0.5

◇ Benedek & Silvester: w/h = 1.0

× Benedek & Silvester: w/h = 2.0

Figure 2.33: **Comparison of odd mode capacitances, $\epsilon_r = 2.5$**

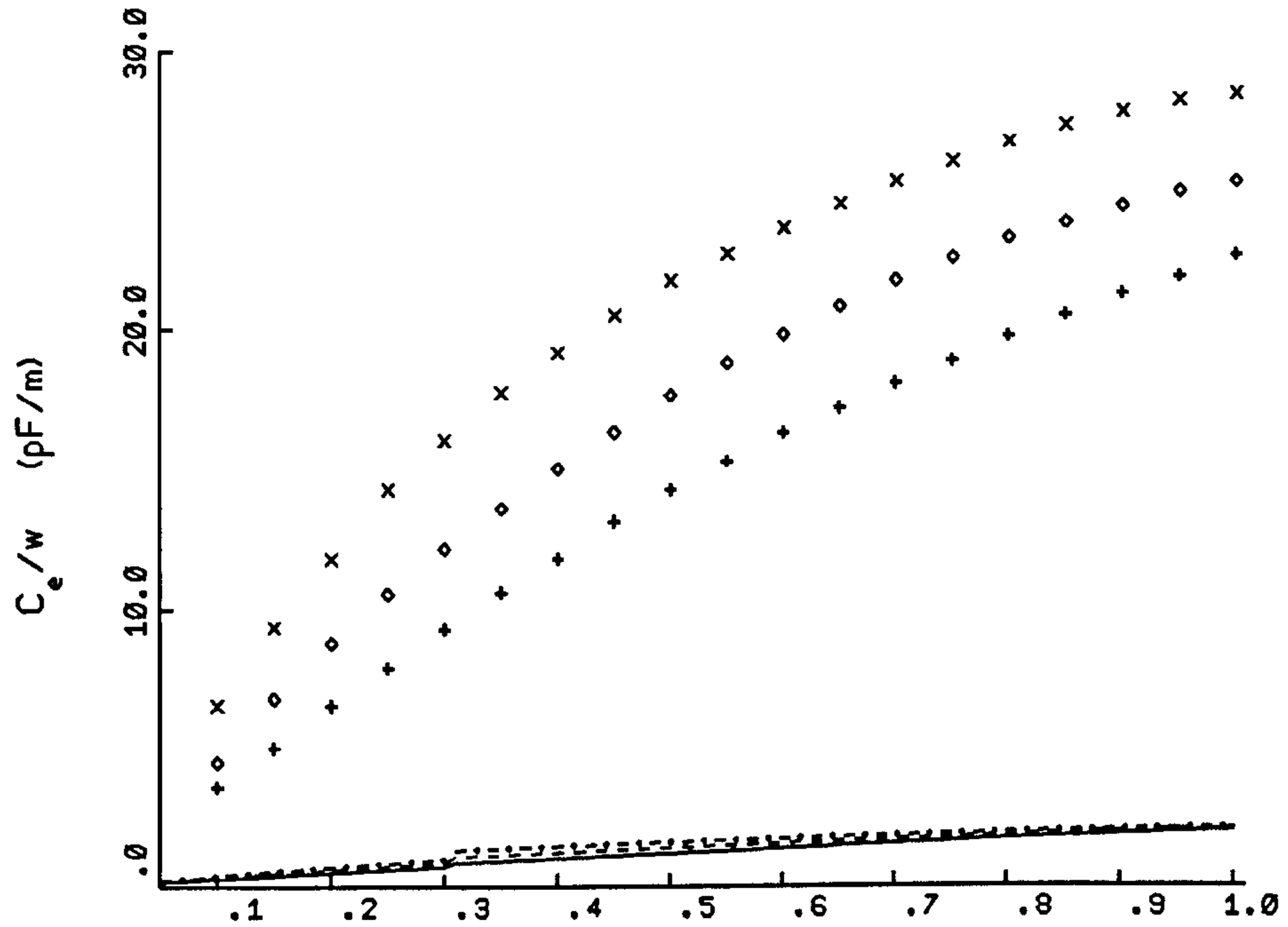

——— Garg & Bahl: w/h = 0.5

- - - - Garg & Bahl: w/h = 1.0

-·-·- Garg & Bahl: w/h = 2.0

\+ Benedek & Silvester: w/h = 0.5

◇ Benedek & Silvester: w/h = 1.0

× Benedek & Silvester: w/h = 2.0

Figure 2.34: **Comparison of even mode capacitances, $\epsilon_r = 2.5$**

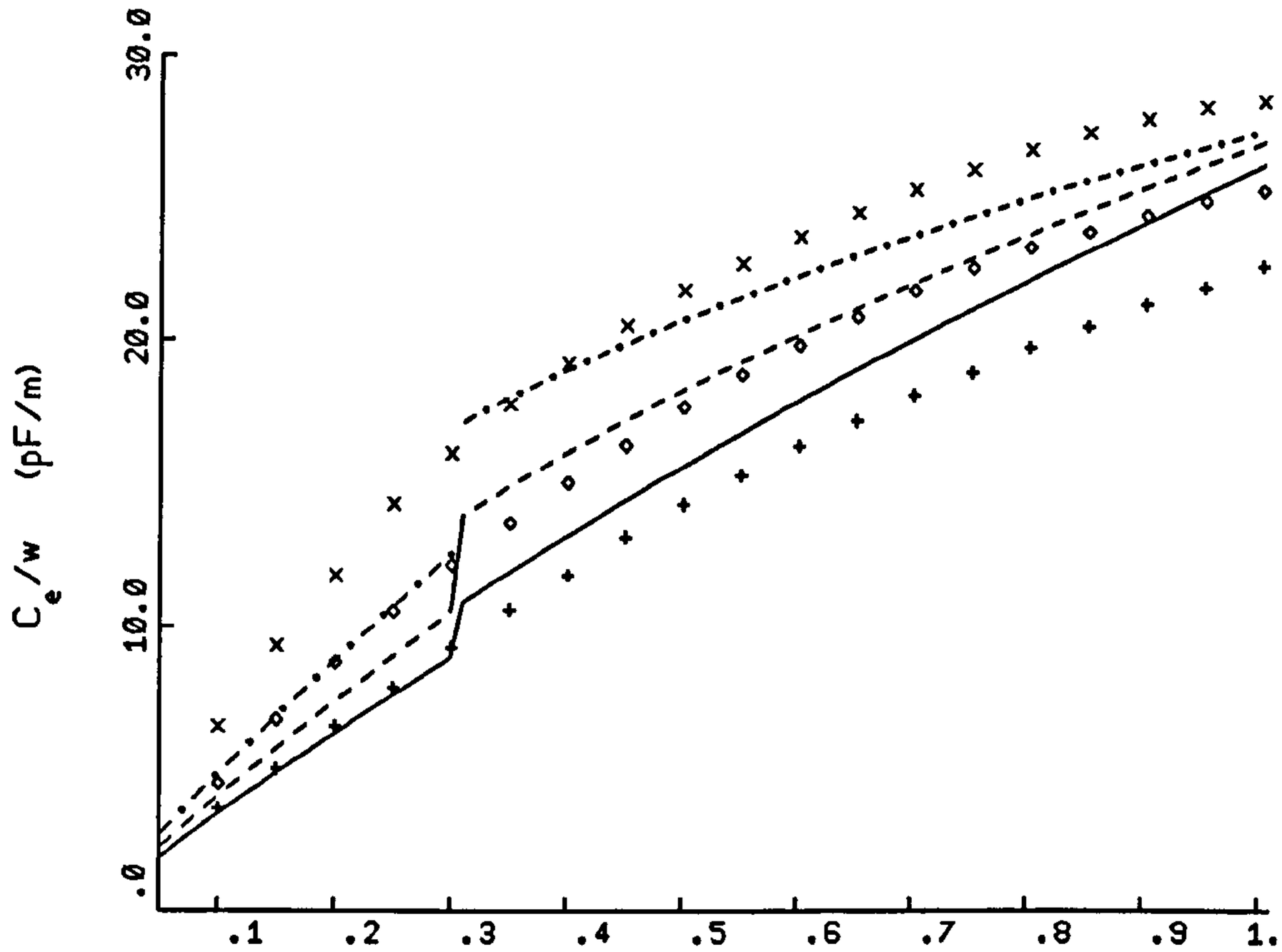

——— Garg & Bahl: w/h = 0.5

- - - - Garg & Bahl: w/h = 1.0

-·-·- Garg & Bahl: w/h = 2.0

\+ Benedek & Silvester: w/h = 0.5

◊ Benedek & Silvester: w/h = 1.0

× Benedek & Silvester: w/h = 2.0

Figure 2.35: Even mode capacitances, showing effect of modifying the Garg and Bahl expressions by a factor of 13, $\epsilon_r = 2.5$

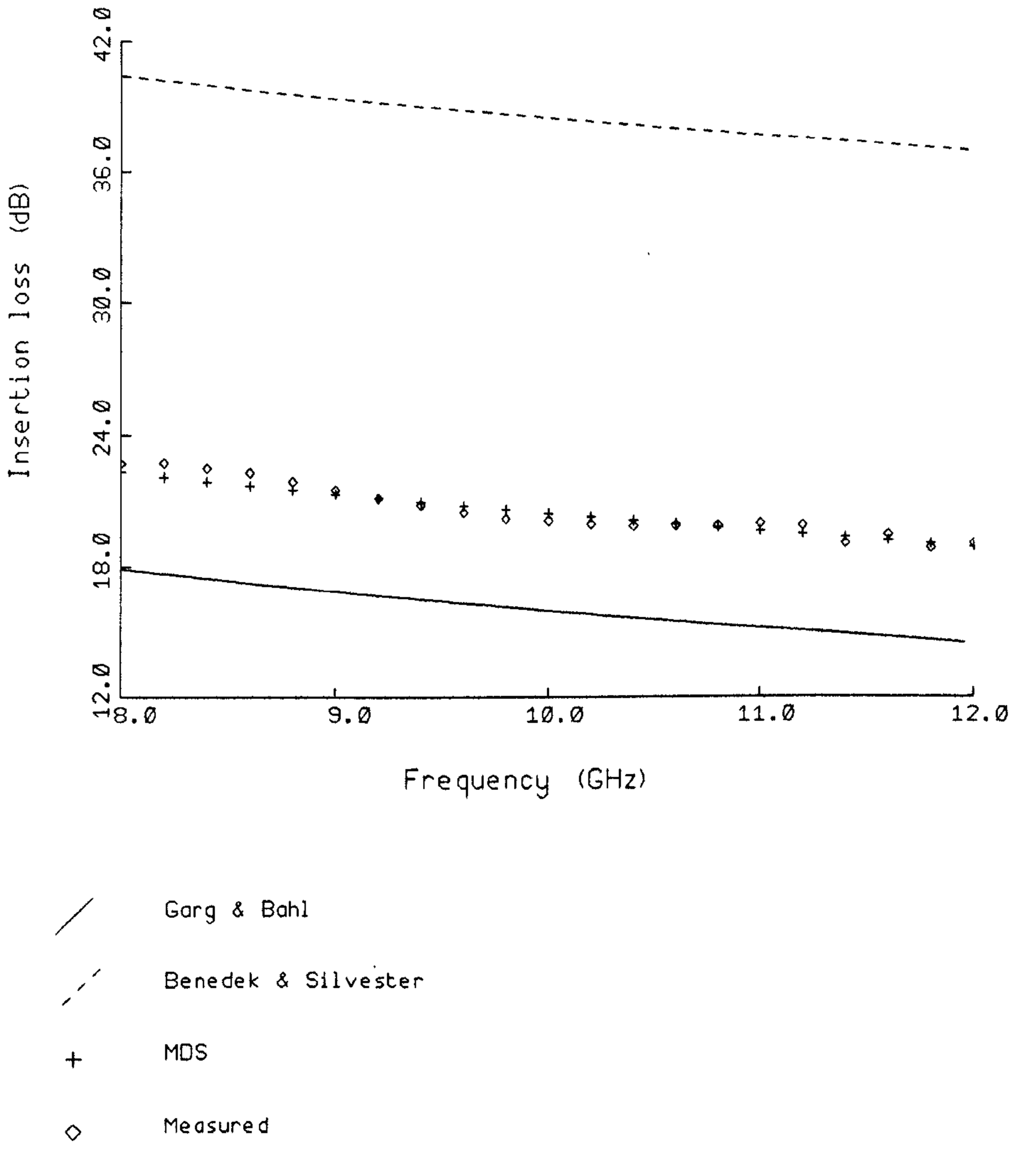

Figure 2.36: **Insertion loss of a microstrip gap (ϵ_r =10.4, w/h=1, s/w=0.4)**

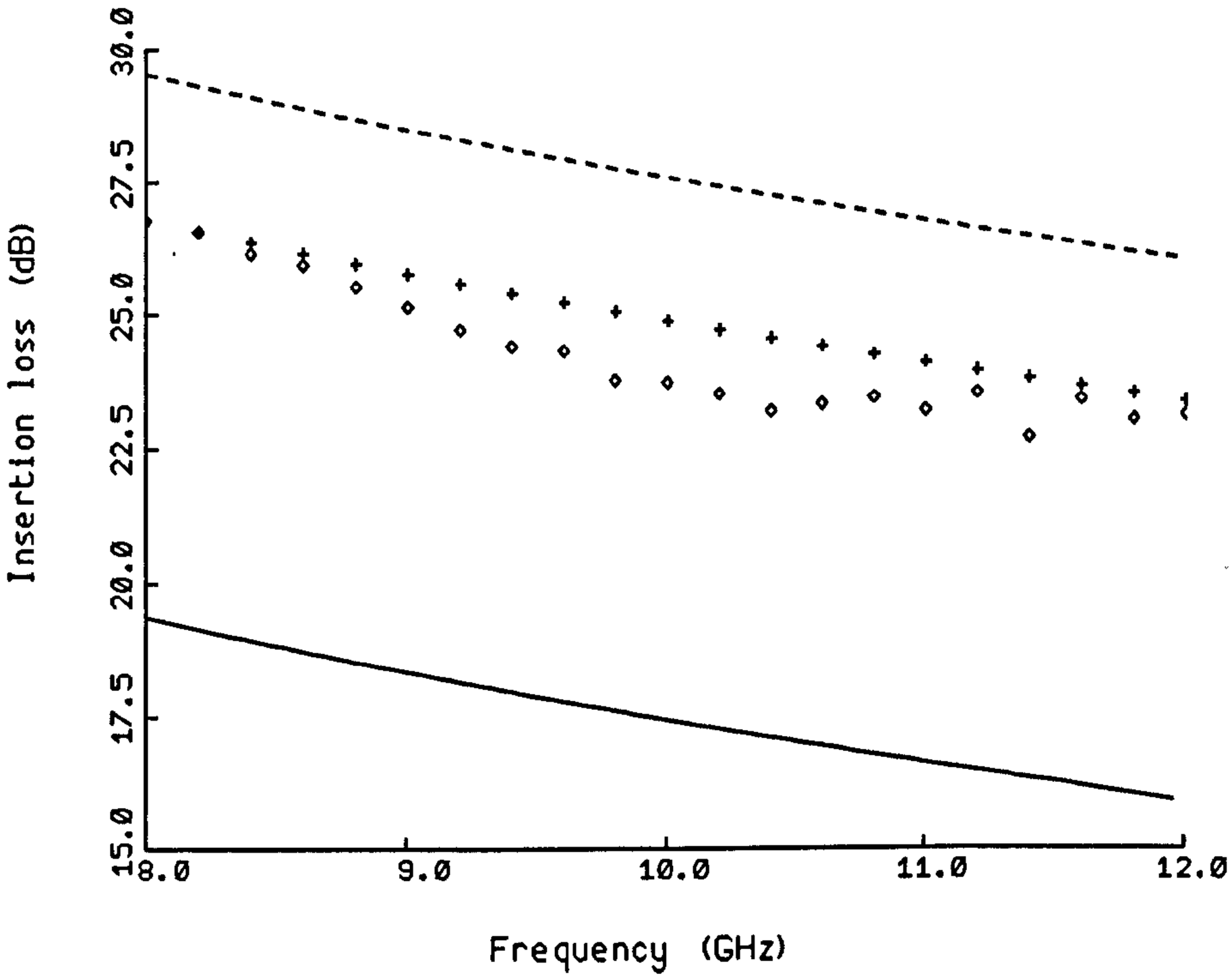

——— Garg & Bahl

- - - - Benedek & Silvester

\+ MDS

◊ Measured

Figure 2.37: **Insertion loss of a microstrip gap (ϵ_r =10.4, w/h=1, s/w=1)**

The figures include simulation data from MDS[1] and measured results. Both figures show very good agreement between measured data and that obtained from MDS over the frequency range 8-12GHz. It can be seen that the practical insertion loss data have values between those obtained through use of the GARG AND BAHL [19] expressions and those predicted from BENEDEK AND SILVESTER [18]. The cyclic variation in the measured data at the top end of the band was attributed to mismatches in the measurement system causing multiple reflections, and is not of particular significance here. However, the results clearly show that a significant error can arise from using the GARG AND BAHL [19] expressions. In Fig. 2.36, p. 81, with s/w=0.4, the error is of the order of 2dB and this increases to 7dB in Fig. 2.37, p. 82, with s/w=1.0. This increase is to be expected from consideration of Fig. 2.34, p. 79, where it is shown that the major source of error is in the even mode capacitance, which has a greater effect on the insertion loss as the gap size increases.

It is worth noting that, in addition to the effects on insertion loss, the use of the incorrect expressions could lead to potentially more serious problems associated with the correct prediction of circuit resonances when an active device is mounted across a microstrip gap. In the present work, the expressions due to GARG AND BAHL [19] will be used, but with the scaling factor of 13 applied to the even mode capacitance.

2.9.5 PIN diode

Finally, in examining the detailed behaviour of the elements constituting the single PIN diode phase shifter, it was necessary to establish an accurate model for the PIN diode in the on and off states, since transmission through the diode had a direct effect on the overall performance of the phase shifter.

Using the standard equivalent circuit for a beam-lead PIN diode, given in Fig. 2.12, p. 53, together with the microstrip gap model discussed in the previous section the insertion phase and loss through a series mounted diode were computed and compared with measured data. The results are shown in Fig. 2.38, p. 84 and Fig. 2.39, p. 85 for the HP 5082-3900 beam-lead PIN diode, and in Fig. 2.40, p. 86 and Fig. 2.41, p. 87 for the HP HPND-4001

[1]MDS™ refers to Microwave Design Software from Hewlett Packard

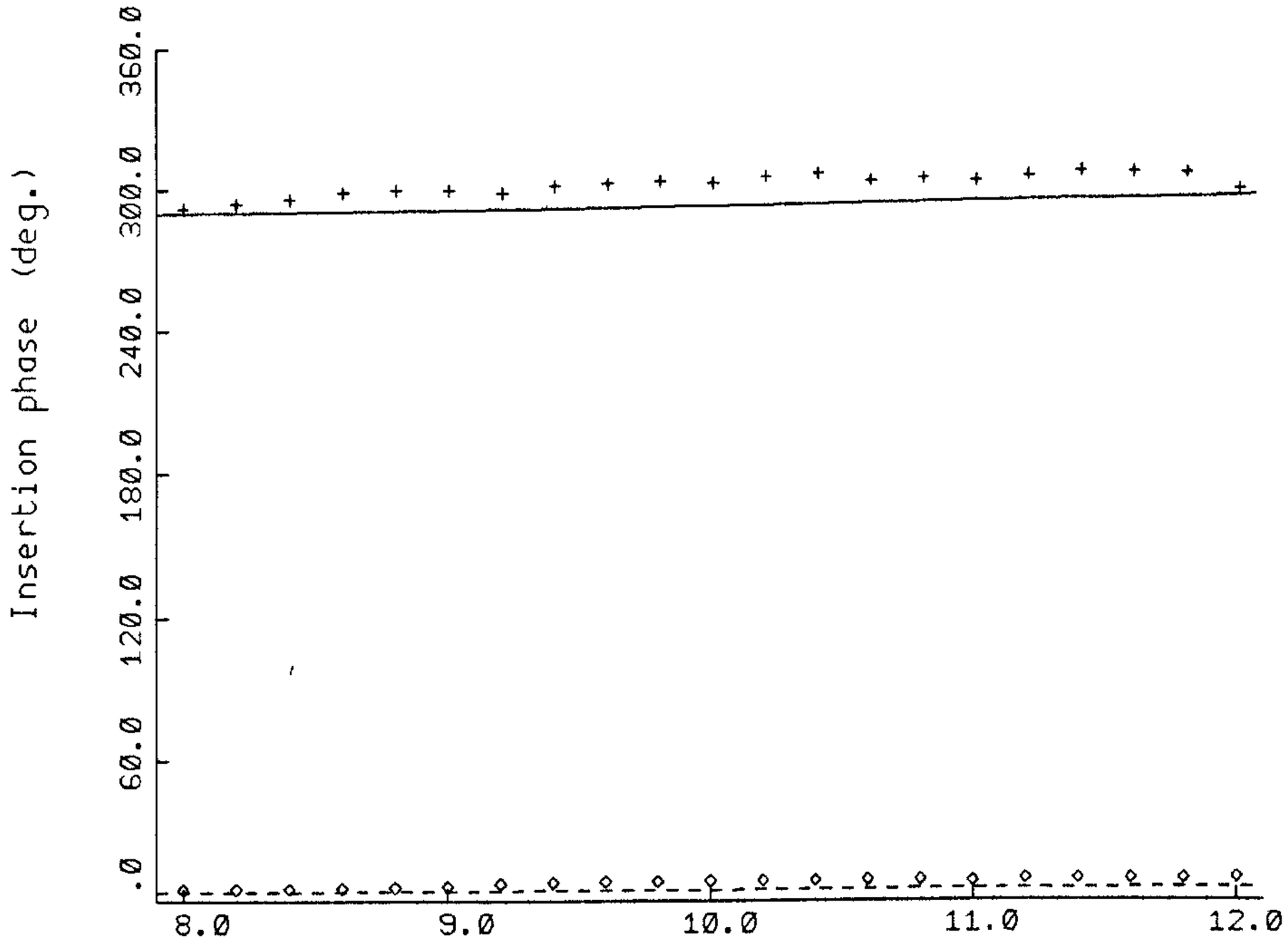

Figure 2.38: **Phase change through HP 5082-3900 PIN diode**

PIN diode. The results in Fig. 2.38, above and Fig. 2.39, p. 85 show very good agreement between the theoretical and measured data. This validates the use of the modified gap capacitance model and, incidentally, shows that no modification to the gap series capacitance value is needed to account for

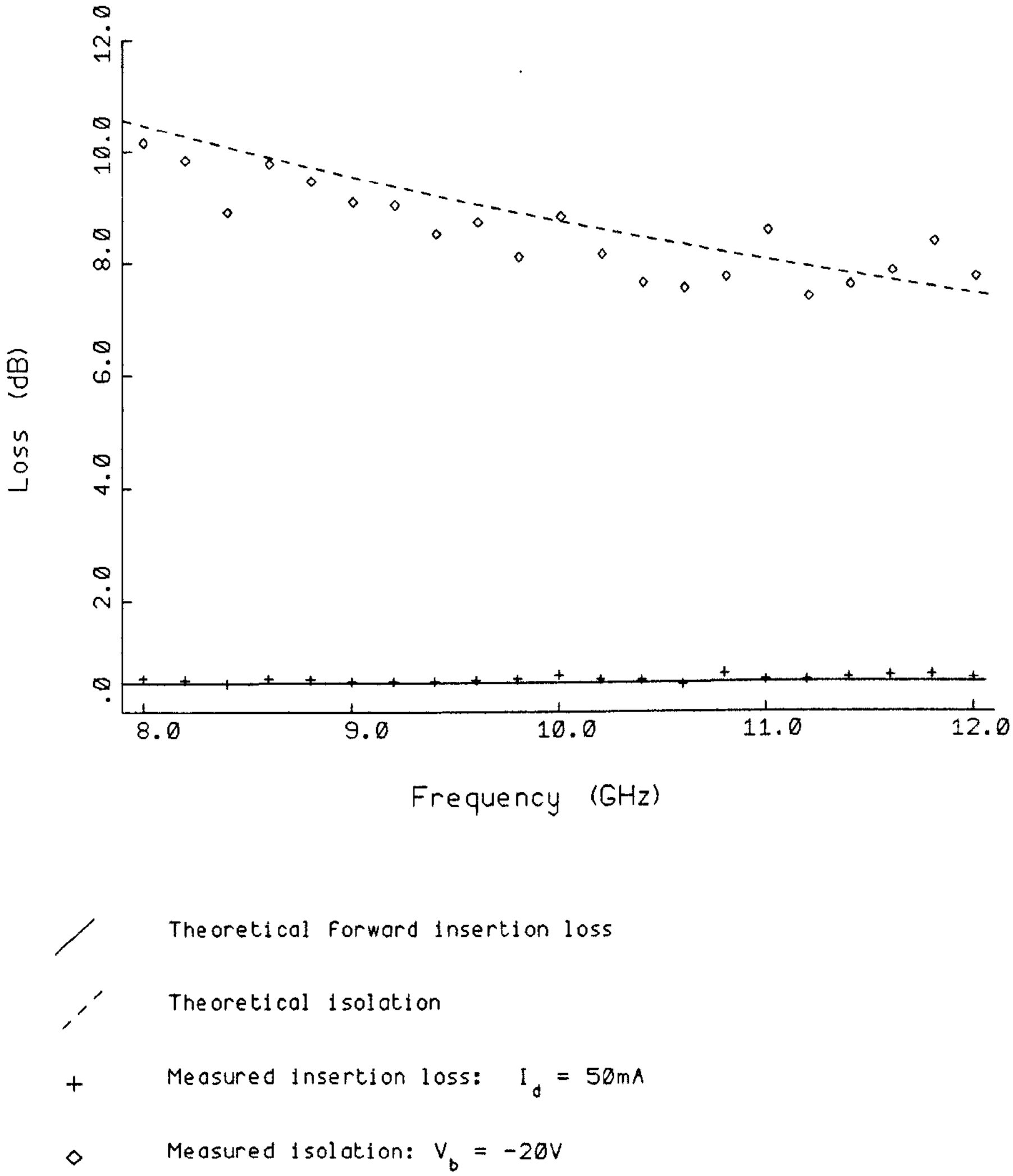

Figure 2.39: **Insertion loss through HP 5082-3900 PIN diode**

the diode being in the odd mode field. Fig. 2.40, p. 86 and Fig. 2.41, p. 87 show results for the alternative PIN diode, which exhibited lower loss, but at the expense of worse isolation. The results for the second diode also show good agreement between the theoretical and measured data, apart from the

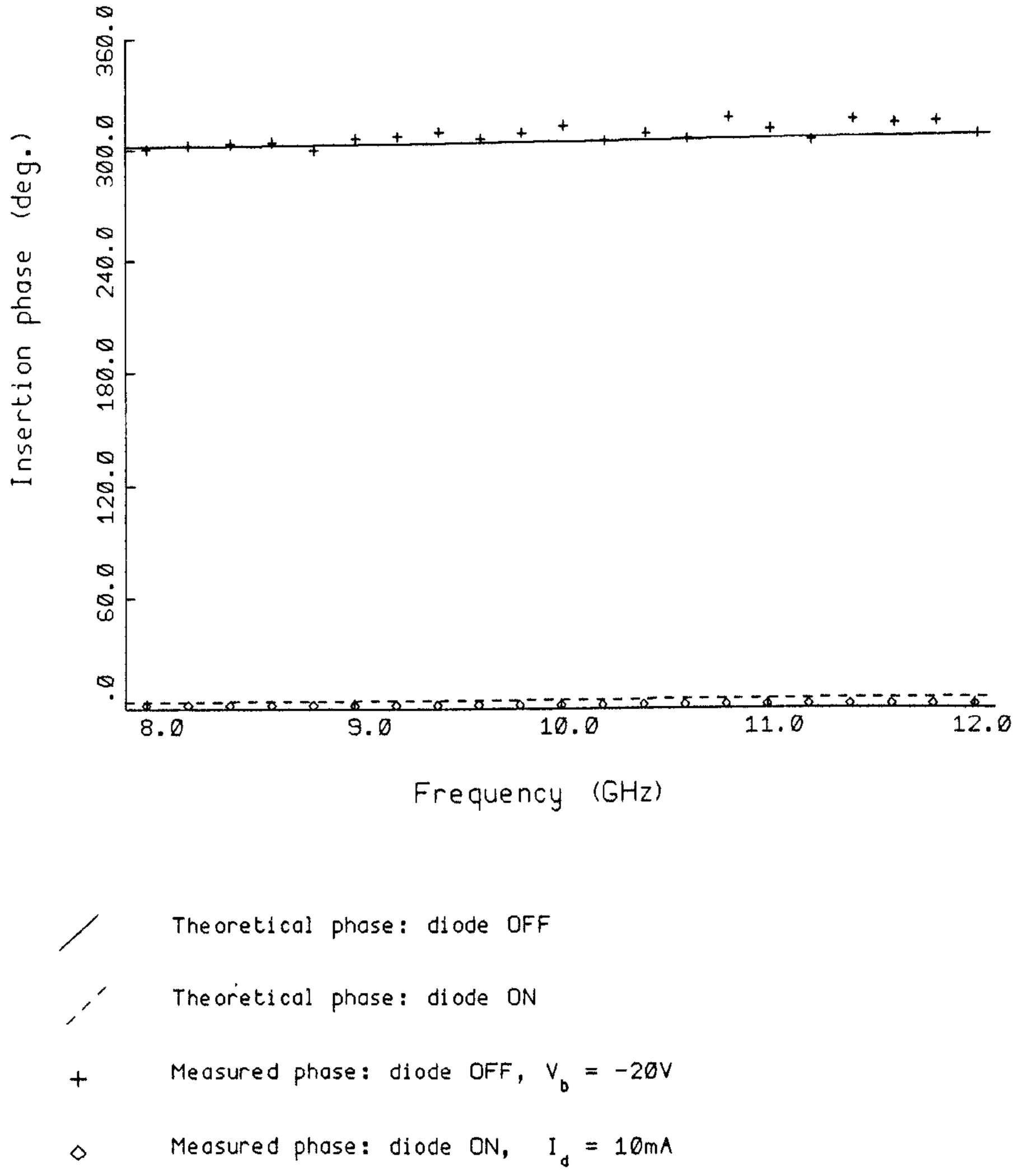

Figure 2.40: **Phase change through HP HPND-4001 PIN diode**

isolation. The measured isolation was worse than predicted, possibly due to the simplified model not allowing for the additional fringing capacitance due to the closer spacing of the diode electrodes which results from the low-loss design.

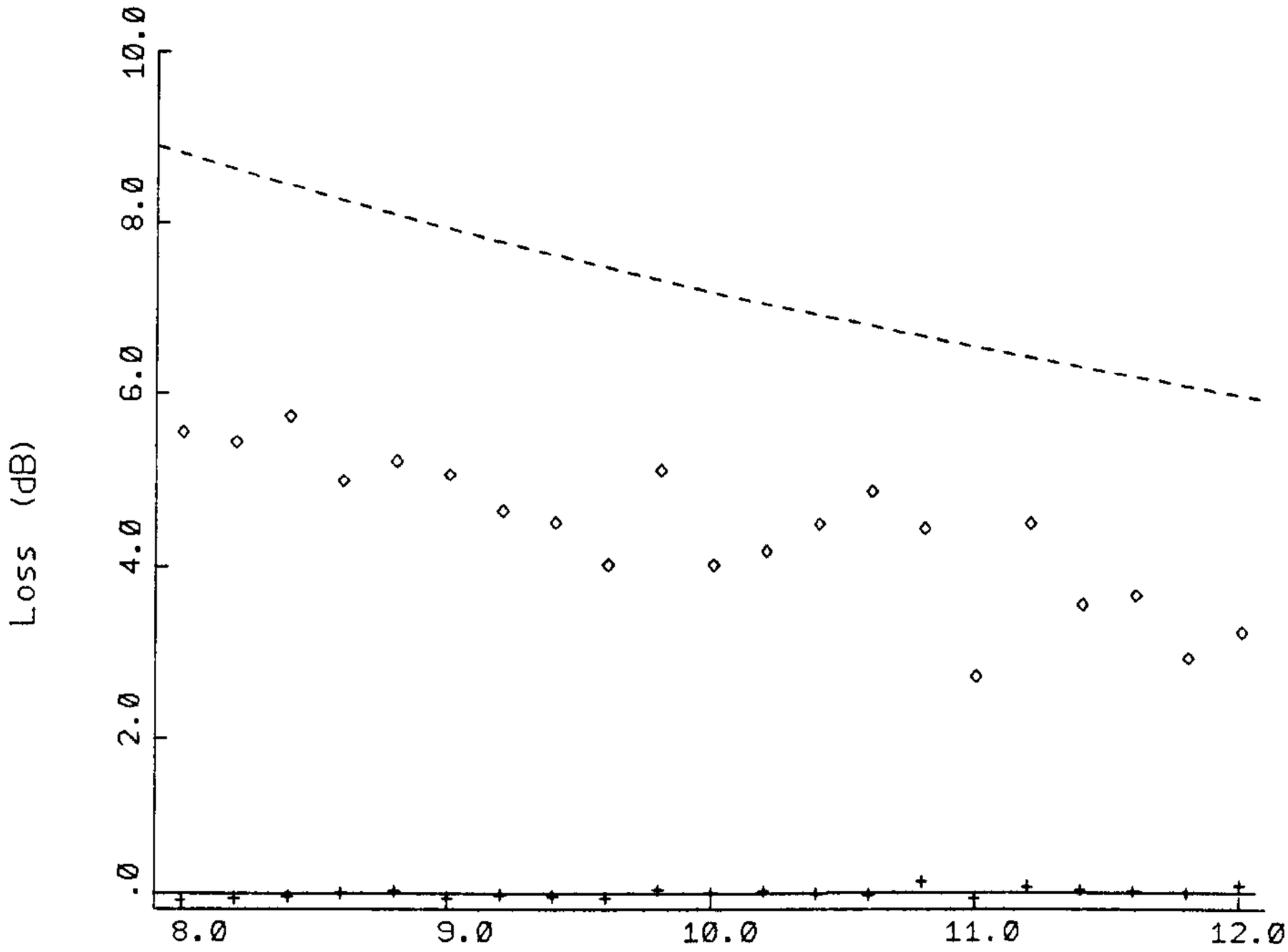

Figure 2.41: **Insertion loss through HP HPND-4001 PIN diode**

It is well known that series mounted PIN diodes have poor isolation, particularly if they have been designed to have low insertion loss. In the present design of phase shifter, good isolation is more important than low insertion loss. The insertion loss and phase change with diode in the on state

can easily be incorporated into the phase shifter design. It is less easy to analyse the situation where the diode is nominally off, and most of the signal propagates though the coupled lines, but there is a small leakage through the diode. This leads to an unnecessarily complicated situation whereby a lumped component is bridging a distributed line, and it is not obvious how the equivalent circuit should be drawn. Therefore, in subsequent designs the HP 5082-3990 PIN diode was used as the active element.

2.9.6 Single PIN diode phase shifters

Theoretical and measured data are compared in Fig. 2.42, p. 89 and Fig. 2.43, p. 90 for a 10GHz single bit phase shifter, without even mode loading on the matching stub. The standard deviation of the measured phase over the frequency range 9-11GHz was 5.1°. The change in insertion loss ($\leq$ 0.5dB) was higher than desirable, but could be reduced by improving the matching with the diode in the on state. The computed switched phase change exhibits some nonlinearity, but this could be reduced by optimisation of the circuit parameters. Fig. 2.44, p. 91 and Fig. 2.45, p. 92 show the results for a single PIN diode phase changer with even mode loading on the matching stub. The even mode loading appears to improve the match of the device, as shown by a reduction in the insertion loss change between states, and to produce a somewhat more linear phase characteristic. As with the device without the matching stub loading, the useful bandwidth appears to be of the order of 1GHz.

In the results presented, the phase changes were deliberately designed to be small, because only small changes in phase were required in the delay-line stabilization circuit. The reason being that large changes of phase would significantly alter the frequency discriminator characteristic of the circuit. Thus the phase changes measured were small changes about 360°. This latter value resulting from the need to include $\lambda/4$ DC breaks in the coupled line section which primarily determined the phase change. However, since only small phase changes are needed, one possible simplification of the single PIN diode phase changer would be to omit the matching stub. Under these conditions, with the diode off, the phase change would be set by the coupled line length, l_c, as before. With the diode on the main line would be

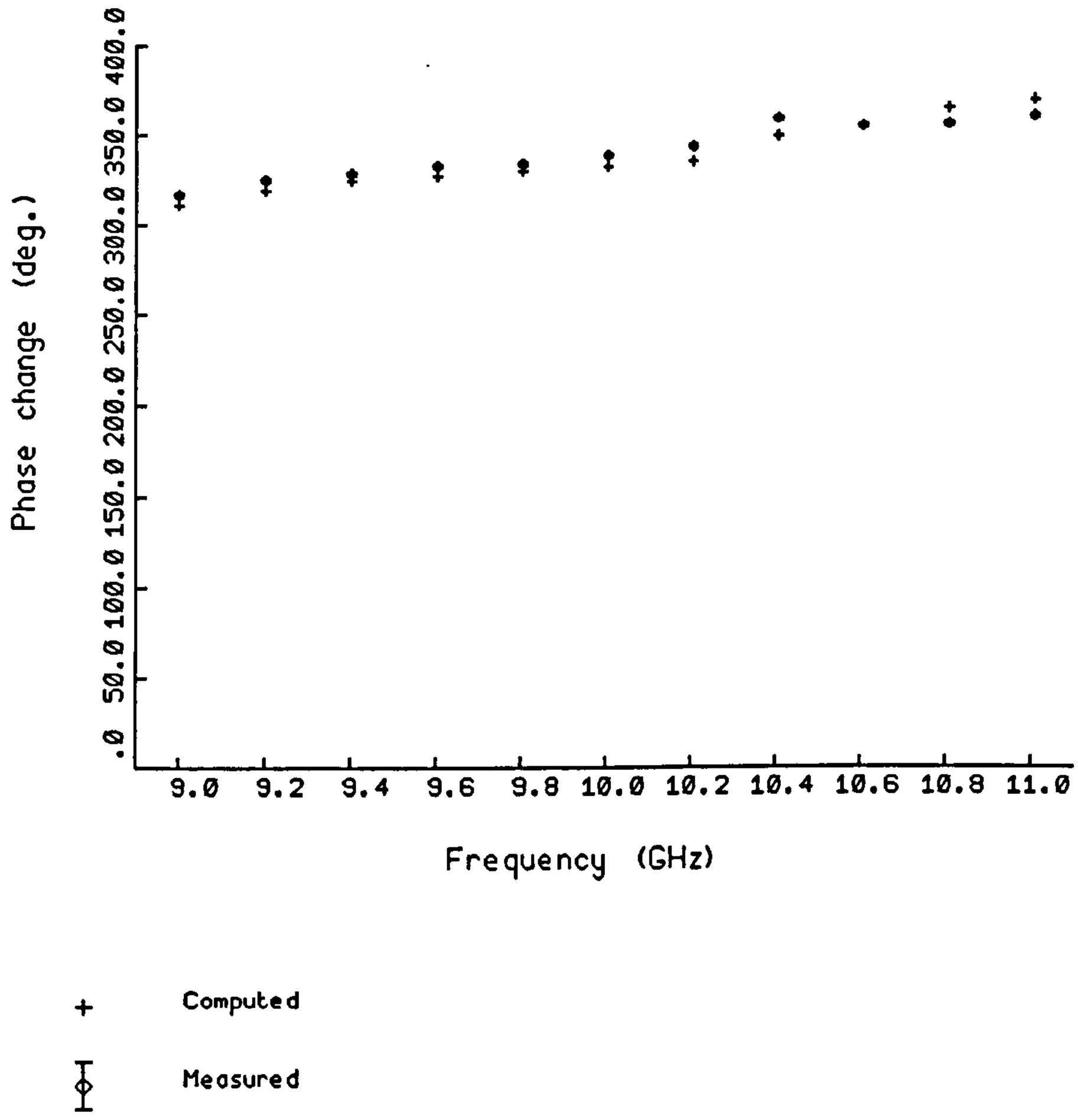

Figure 2.42: **Comparison of measured and theoretical phase data for a single-bit phase shifter**

shunted by a stub, supporting the even mode, of length l_c. Since this length would necessarily be close to $\lambda/2$ the stub, whose remote end is an effective open-circuit, would always shunt the main line with a high impedance and hence have minimal effect on the transmitted signal. Fig. 2.46, p. 93 and Fig. 2.47, p. 94 show the effect of omitting the matching stub. Three sets

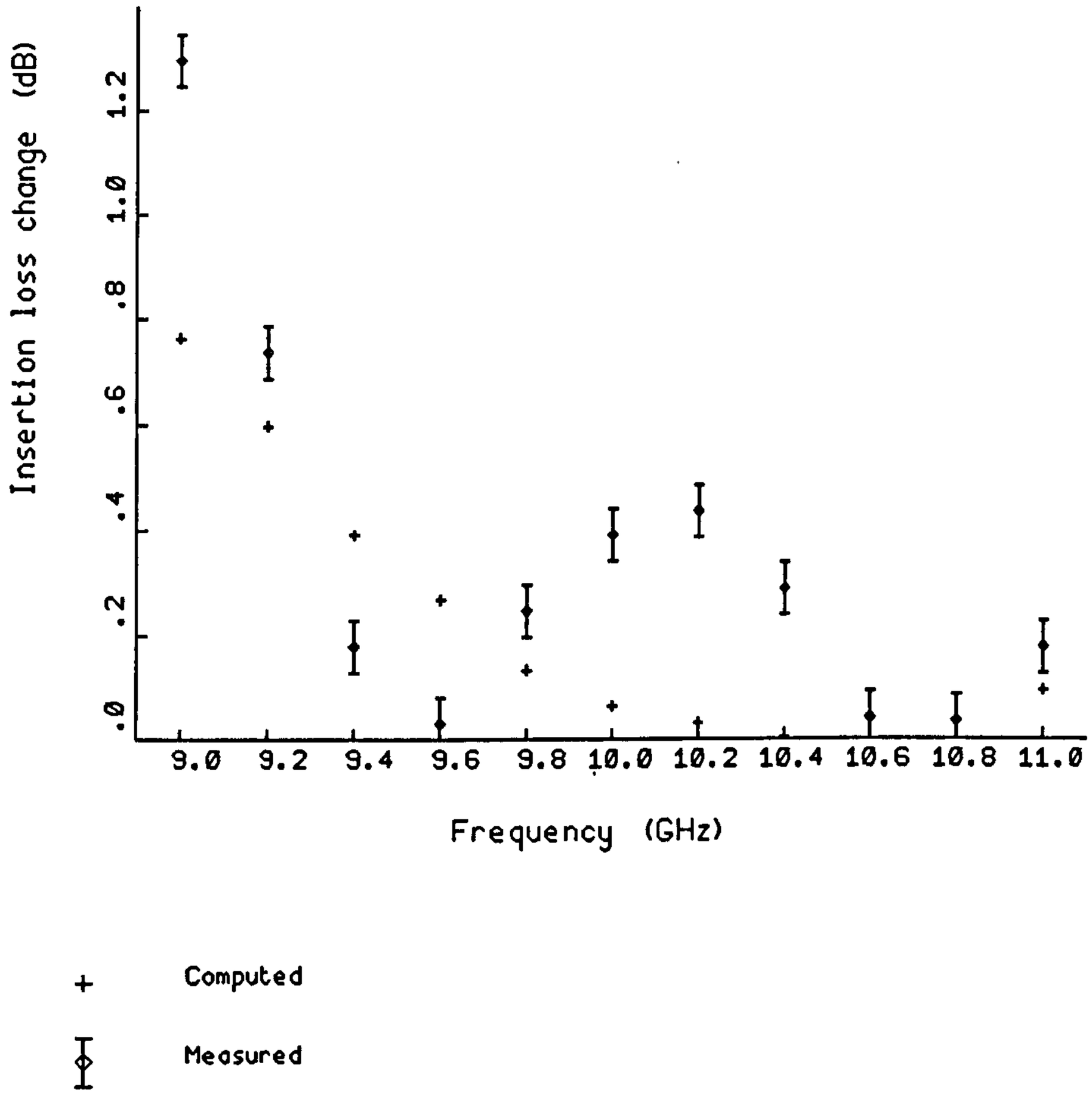

Figure 2.43: Comparison of measured and theoretical loss data for a single-bit phase shifter

of measured values are shown in these figures, representing three couplers of slightly different lengths. It can be seen that significant phase changes are obtained, and that the change in insertion loss between states is reasonably small. Thus it would appear that the omission of the matching stub is a practical proposition for small phase changes and narrow bandwidths.

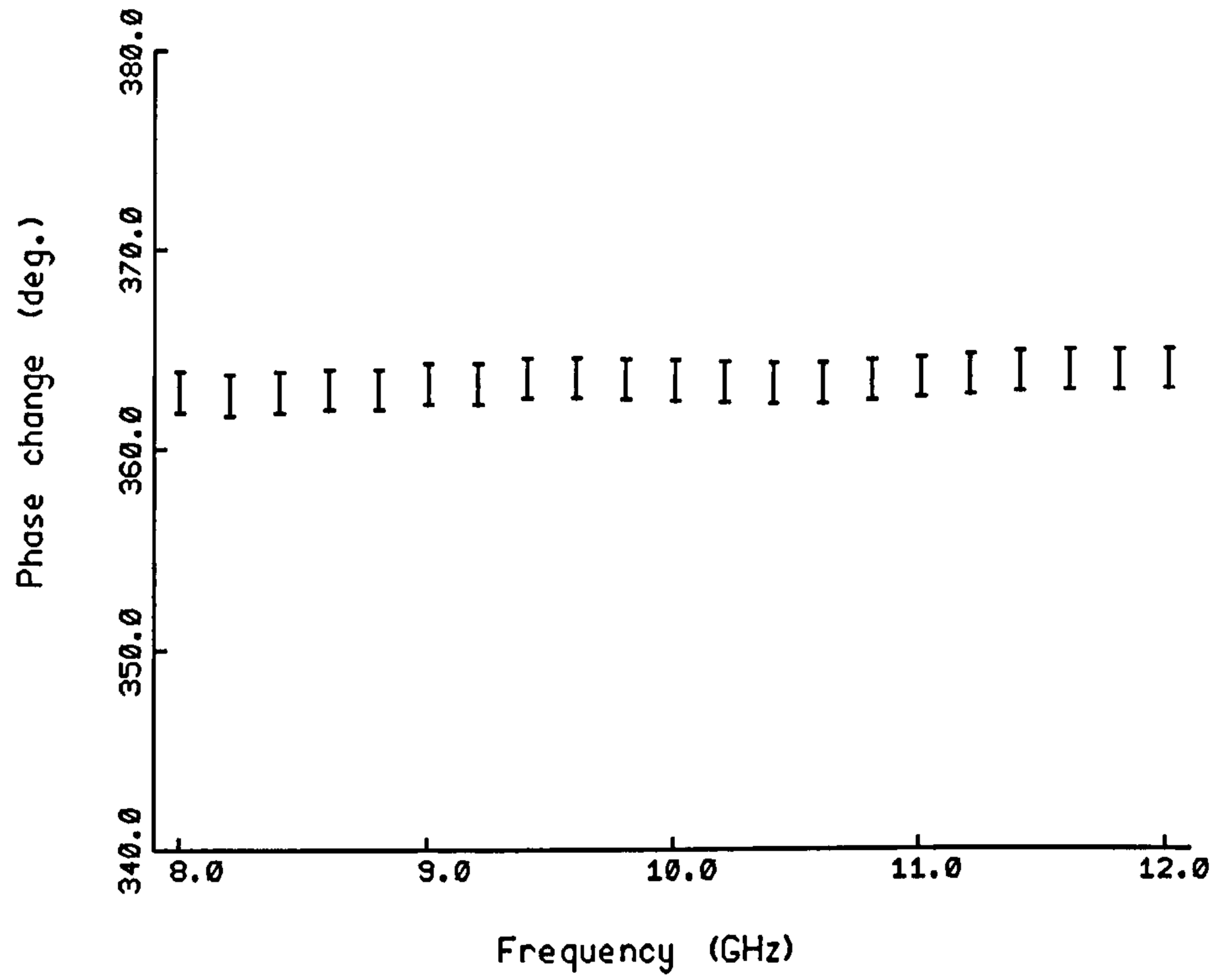

Figure 2.44: Measured phase response for a single-bit phase shifter with even mode loading

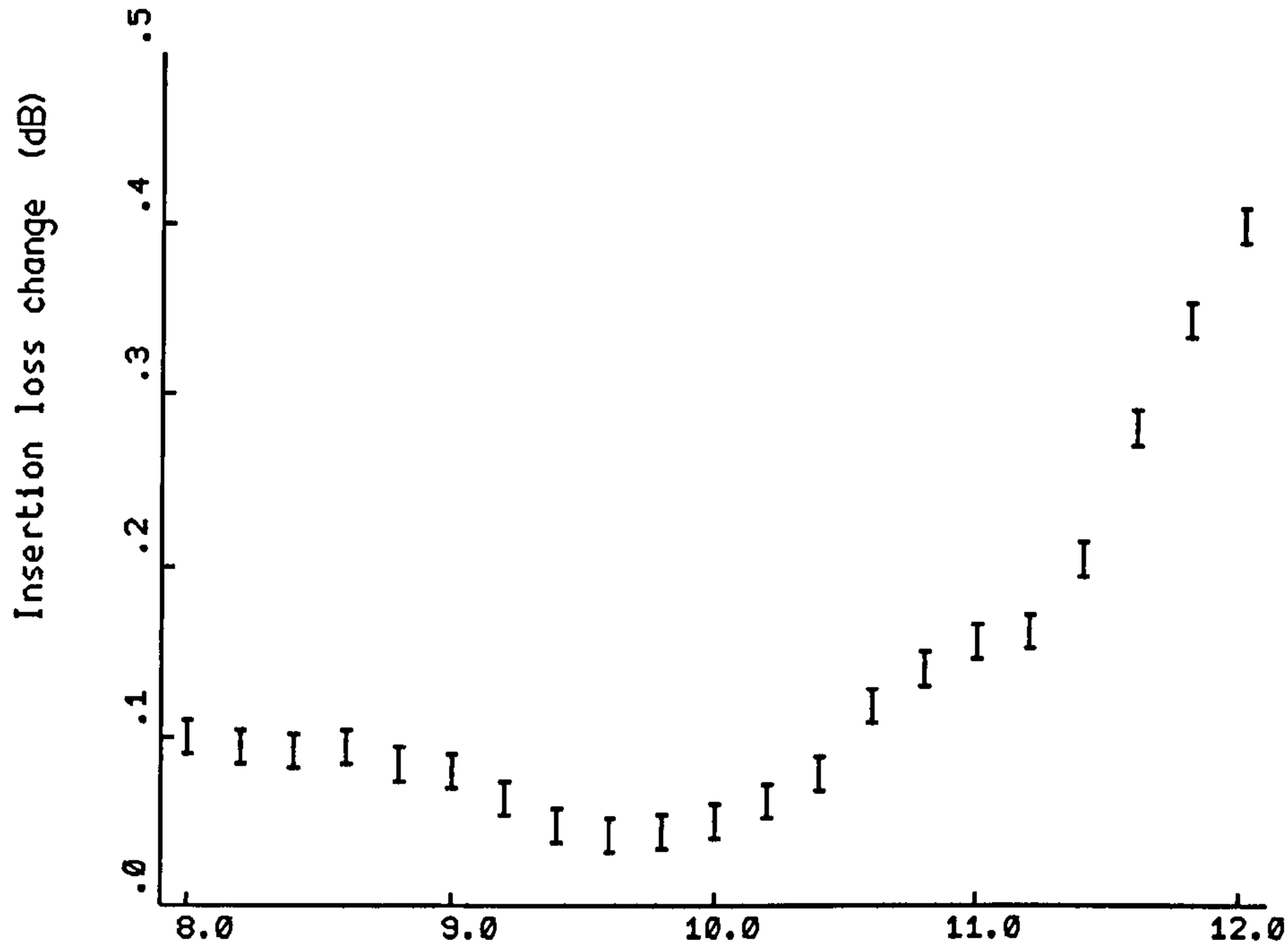

Figure 2.45: Measured insertion loss change for a single-bit phase shifter with even mode loading

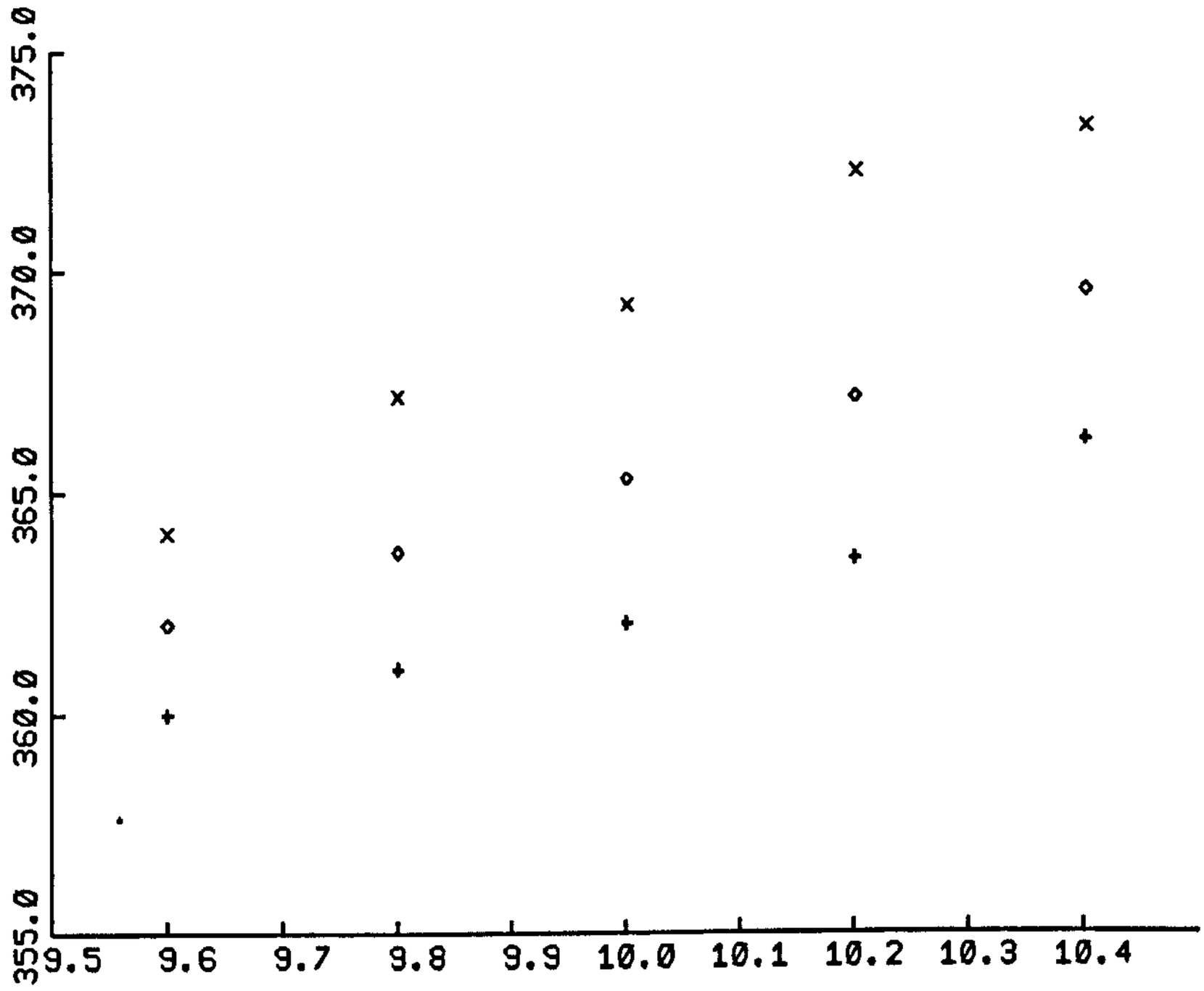

Figure 2.46: **Measured phase data for single PIN diode (SPD) phase shifters with no matching stub**

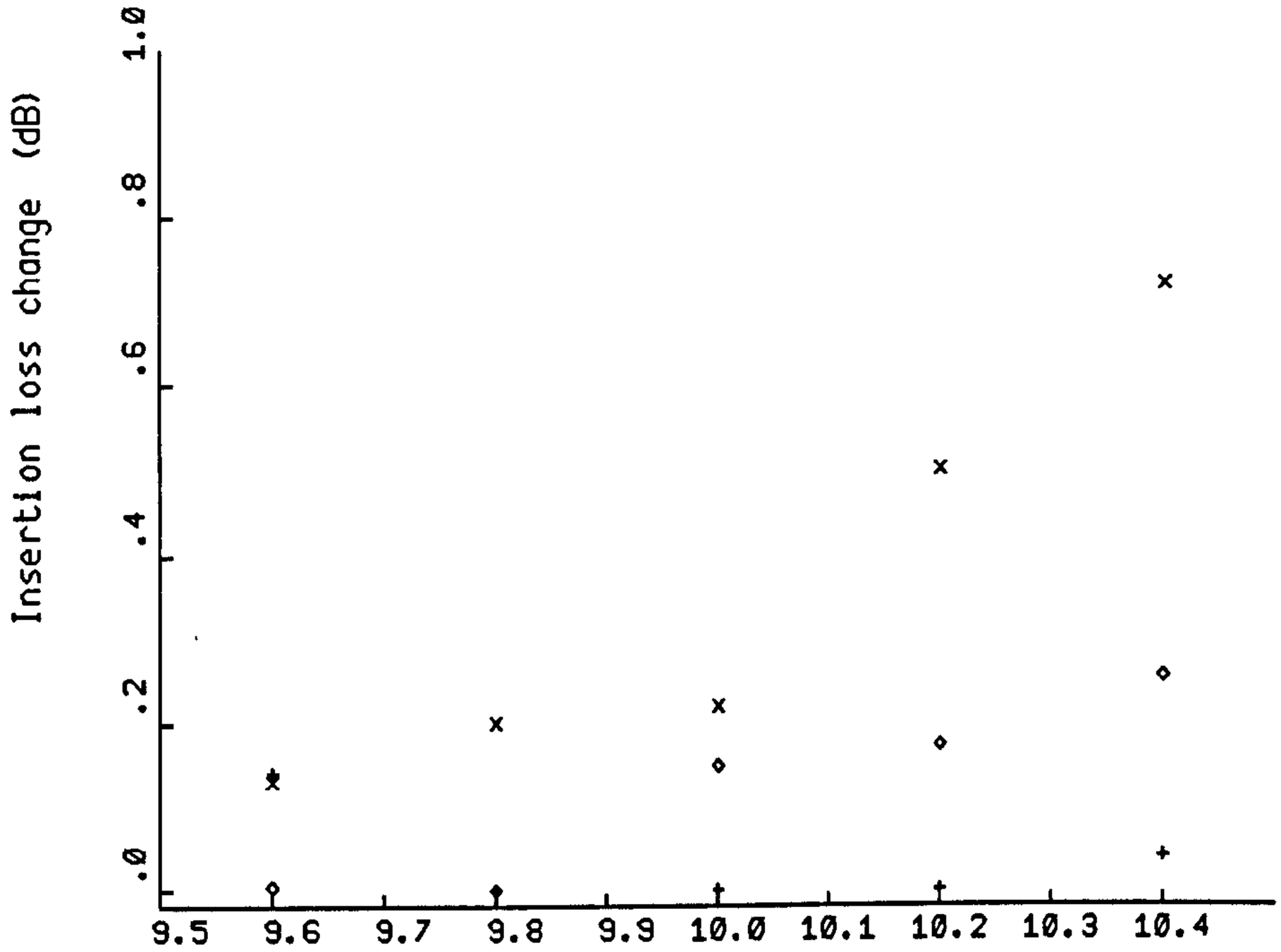

Figure 2.47: Measured insertion loss data for SPD phase shifters with no matching stub

2.10 Conclusions

It has been shown that an exact analysis method is needed to satisfactorily predict the performance of coupled-line phase shifters and, moreover, that the device exhibits a significant mismatch under certain conditions. A comparison between measured and theoretical data shows that the new exact theory, in terms of the independent odd and even mode velocities, provides a better prediction of the nonlinear phase responses which are observed in practice. Useful information has also been obtained on the effective length of the coupler which should be employed in practical designs.

Microstrip DC breaks have been shown to exhibit significant excess phase. Moreover, end effects have been shown to contribute significantly to the total excess phase. An equivalent circuit has been deduced to represent the discontinuities associated with microstrip DC breaks which yields good agreement between experimental and measured values of phase. The agreement has been shown to hold for two microstrip DC blocks of slightly different geometry.

A serious source of error in commonly quoted expressions for the capacitance values in microstrip gap equivalent circuits has been identified. Some indication of the magnitude of the error, together with the effect on practical circuit design has been established.

A novel microstrip phase shifter has been developed, using a single PIN diode, which yields good agreement between measured and theoretical data at X-band. The performance compares well with that of other published devices using a greater number of switching elements. The device appears attractive for the development of compact, multi-bit phase shifters in either hybrid or monolithic microwave integrated circuits.

Chapter 3

Three Port Ring Discriminator

3.1 Summary

A new design of microstrip discriminator is presented which is based on a three-port ring. The new circuit structure has been rigorously analysed and the theoretical results compared with measured data over the X-band frequency range.

Various test circuits, using both circular and rectangular ring geometries, have been designed and evaluated. The test circuits were designed with a centre frequency of 10GHz and were fabricated on RT/duroid 6010.

The effects which microstrip discontinuities have on the discriminator performance have also been considered. The discontinuity of particular importance for the three-port ring is the T-junction and its effect was investigated by making appropriate allowances in the design, based on published discontinuity data, and by introducing compensating circuitry.

3.2 Introduction

The structure and behaviour of conventional microwave delay-line discriminators was discussed in chapter 1. Included in that discussion was a microstrip discriminator, shown in Fig. 1.3, p. 26, which employed two four-port hybrid rings. However this arrangement suffers from two principal disadvantages: (i) it occupies a significant substrate area because of the necessity of having two hybrid rings, and (ii) the match of the input and output ports are quite

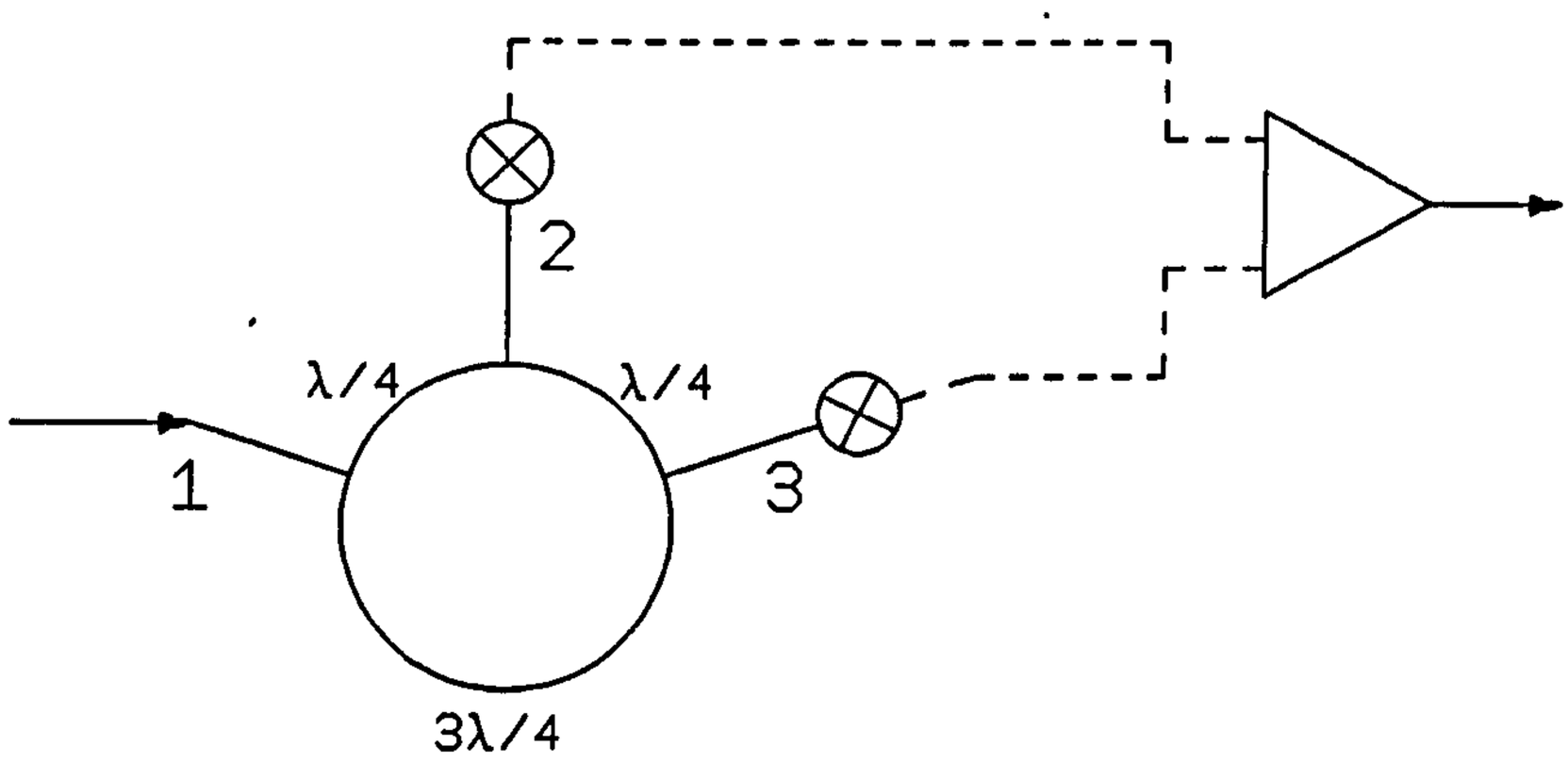

Figure 3.1: **Three-port ring discriminator**

frequency sensitive because of the presence of a number of frequency sensitive sections. The three-port ring arrangement proposed in this chapter, and shown connected as a discriminator in Fig. 3.1, above, overcomes the problem of size by combining the signal splitting and delay-line functions in a single ring. Whilst the new arrangement would still exhibit a frequency-dependent match at the input and output ports, this should be less than for the dual hybrid ring approach, because of the simplicity of the structure.

The three-port ring thus provides a simple, compact discriminator whose size advantage could be significant in microstrip circuit layouts, particularly for microwave integrated circuit applications.

3.3 Circuit operation and design

The fundamental operation of the three-port ring as a frequency discriminator may be deduced from consideration of the electrical lengths separating the three ports. In Fig. 3.1, above, the port separations are shown at the

design (centre) frequency. Clearly, at this frequency a signal applied at port 1 will give equal outputs at ports 2 and 3. If the frequency is increased, the waves travelling in opposite directions around the ring will tend to move into phase at port 2 and out of phase at port 3, by virtue of the quarter-wavelength spacing between ports 2 and 3. Conversely, if the frequency is decreased the waves will move into phase at port 3 and out of phase at port 2. Thus, feeding the detected signals at ports 2 and 3 into a differential amplifier will yield a frequency discriminator response at the amplifier output, with the response centred on the design frequency.

Whilst the design of the three-port ring is constrained by the need to have a quarter-wave spacing between the output ports to maintain the discriminator function, there are two degrees of freedom in the design which enable the best input match to be chosen. Firstly, the ring impedance Z_r may be chosen independently of the discriminator requirements. Secondly, an additional length of line, x, may be inserted between ports 1 and 2 and between ports 1 and 3, without violating the conditions for frequency discrimination. The theory presented in the next section enables optimum values of Z_r and x to be chosen. However, it should be noted that there will always be a mismatch at the input of the circuit since there is a general theorem which states that a passive, lossless three-port network can never be simultaneously matched at all ports. The design strategy should therefore be to match the output ports to the detector diodes, to prevent unwanted reflections entering the ring, and to accept a degree of mismatch at the input. In practice this mismatch would not present a problem, since in the proposed stabilization system the discriminator is in the feedback path to the oscillator, rather than in the main output power line and, moreover, could be preceded by an isolator.

3.4 Theory

The theoretical investigation of the behaviour of the three-port ring was based on a static analysis which involved first reducing the ring to two equivalent circuits. This approach, whereby the ring is reduced to two equivalent two-port networks by considering odd and even excitation of the ring is an application of the method normally used for the analysis of four-port hy-

brid rings. PON [26] and ZARBEL [25] describe the basis of the method, as applied to hybrid rings, in some detail. However, the method requires a plane of symmetry to be established though the circuit in order that the four-port structure can be split into two equivalent two-port networks. Unlike the four-port hybrid ring the three-port structure being considered here requires the plane of symmetry to be taken through one of the ports. This does not present any difficulty providing that appropriate modifications are made to the impedance of that port in the equivalent circuits. Alternatively, a dummy fourth port can be introduced, thus avoiding the need to split one of the ports with the plane of symmetry, and a solution sought which makes the signal at the dummy port zero. Such a technique would be required if the original three-port structure were asymmetric, whence the dummy port could be used to create geometric symmetry. Both methods are described in the following sections.

3.4.1 Odd and even circuit analysis

The basic three-port ring discriminator is shown in Fig. 3.2, p. 100. It can be observed that there is geometric symmetry about the line AA'. Consequently if in-phase waves of equal amplitude are applied to ports 1 and 3 the electric field in the ring will be even about AA'. Under this condition the ring may be split along the line AA' and the split ends represented by open circuits. This leads to the two-port equivalent circuit shown in (a) of Fig. 3.3, p. 101.

Similarly, when anti-phase waves of equal amplitude are applied to ports 1 and 3, the electric field is odd about the line AA'. Again, if the circuit is split along the line AA', the split ends can be represented by short circuits as shown in (b) of Fig. 3.3, p. 101.

A particular solution for the three-port ring may therefore be found by adding any linear combination of the even and odd field solutions, assuming of course that equal amplitude waves are applied in each case so that the net result is an input at a single port. The final solution is most conveniently expressed in terms of S-parameters.

To obtain the reflection and transmission coefficients for the equivalent circuit shown in (a) of Fig. 3.3, p. 101, the ABCD parameters are first found,

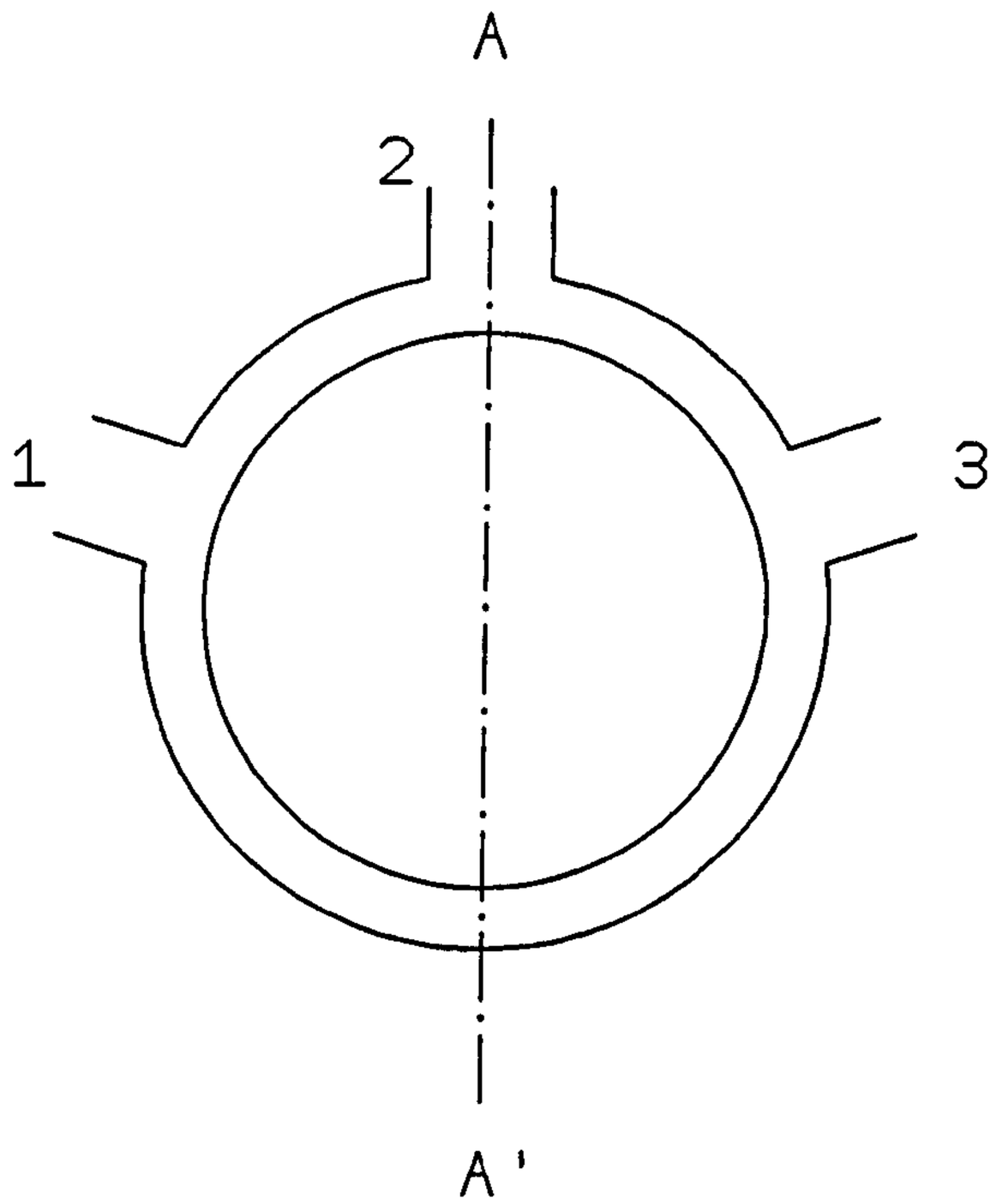

Figure 3.2: **Basic microstrip three-port ring structure.**

these parameters being the most convenient for analysing cascaded elements in series.

The circuit of (a) in Fig. 3.3, p. 101 may be redrawn as shown in Fig. 3.4, p. 102. It has been assumed that each of the ports is terminated in Z_o, which is equal to the characteristic impedance of the port lines. Port 2 is terminated in $2Z_o$ to represent the effect of splitting the circuit through this port. The value of Y_1 in Fig. 3.4, p. 102 is given by

$$Y_1 = jY_r tan\left(\beta\frac{3\lambda}{8}\right) \tag{3.1}$$

where Y_r if the characteristic admittance of the ring and λ is the wavelength in the ring at the design frequency. The A matrix of the cascaded combination between ports 1 and 2 is

$$\begin{bmatrix} A_e & B_e \\ C_e & D_e \end{bmatrix} = \begin{bmatrix} 1 & 0 \\ Y_1 & 1 \end{bmatrix} \begin{bmatrix} cos\left(\beta\frac{\lambda}{4}\right) & jZ_r sin\left(\beta\frac{\lambda}{4}\right) \\ jY_r sin\left(\beta\frac{\lambda}{4}\right) & cos\left(\beta\frac{\lambda}{4}\right) \end{bmatrix} \tag{3.2}$$

From standard two-port network theory, the transmission coefficient is then

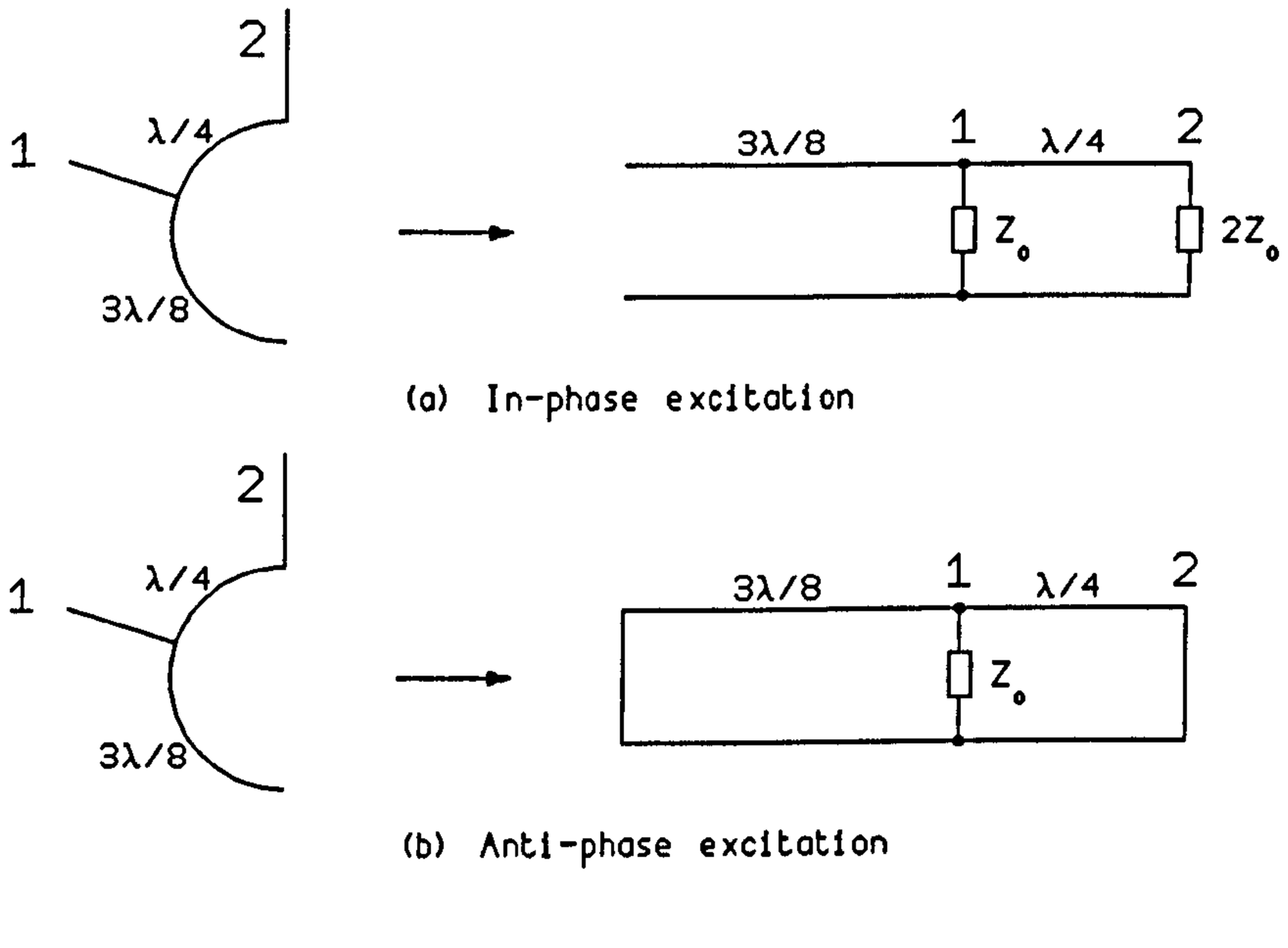

Figure 3.3: **Three-port ring equivalent circuits**

given from

$$T_{21e} = \frac{1}{A_e + \frac{B_e}{2Z_o} + C_e Z_o + \frac{D_e}{2}} \tag{3.3}$$

and the reflection coefficient at port 1 from

$$T_{11e} = \frac{Y_o - Y_{te}}{Y_o + Y_{te}} \tag{3.4}$$

where

$$Y_{te} = Y_1 + Y_2 \tag{3.5}$$

and

$$Y_2 = Y_r \frac{Z_r cos\left(\beta\frac{\lambda}{4}\right) + j2Z_o sin\left(\beta\frac{\lambda}{4}\right)}{2z_o cos\left(\beta\frac{\lambda}{4}\right) + jZ_r sin\left(\beta\frac{\lambda}{4}\right)} \tag{3.6}$$

Having found expressions for the reflection and transmission coefficients for the even field produced by in-phase excitation of the ring, we need to fol-

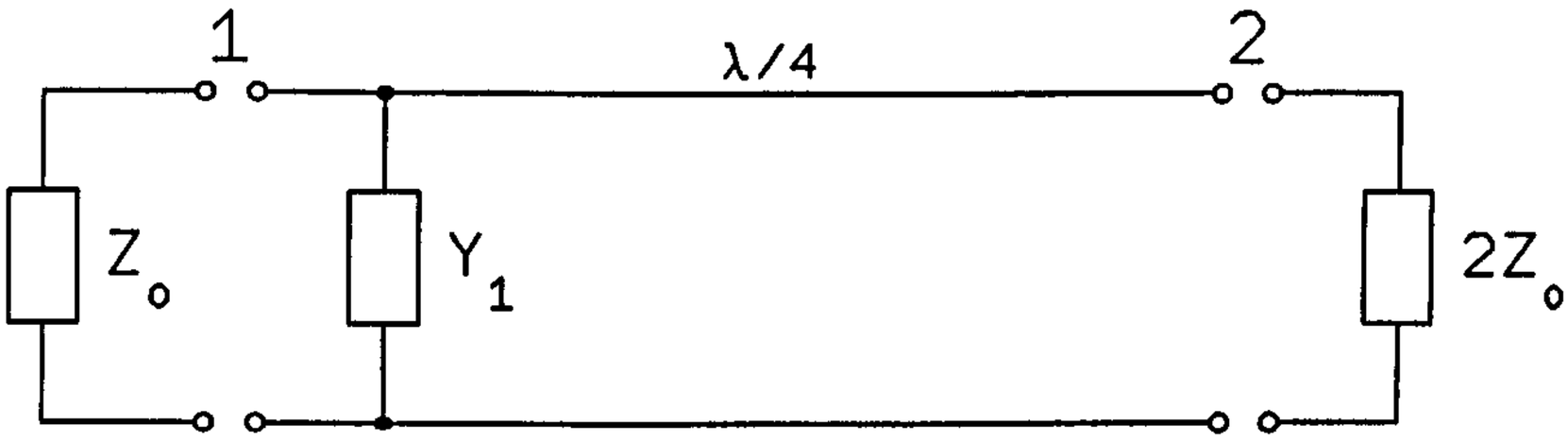

Figure 3.4: **Even field equivalent circuit redrawn in a conventional two-port network format**

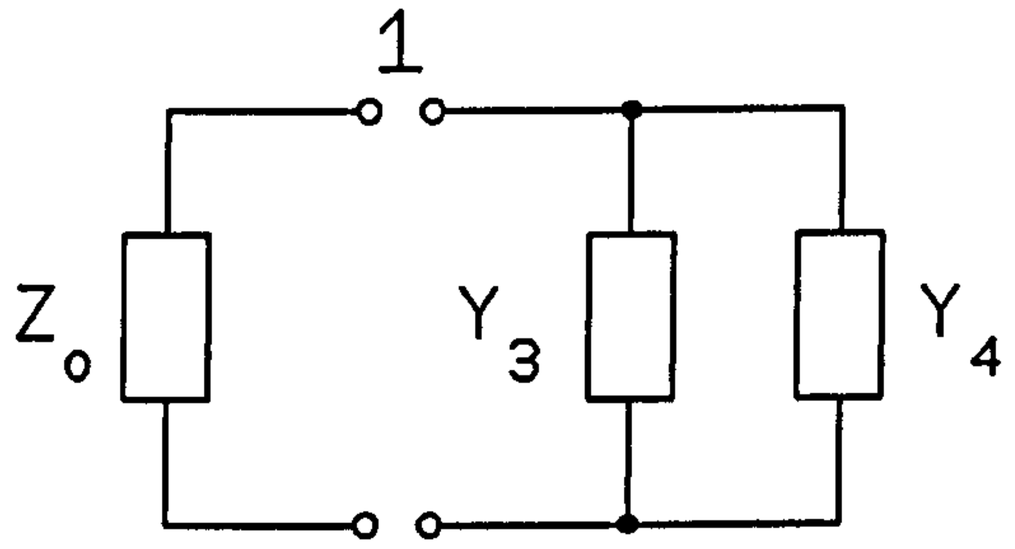

Figure 3.5: **Equivalent circuit for anti-phase excitation, redrawn as a one-port network**

low a similar analysis for the case of anti-phase excitation. Considering the equivalent circuit shown in Fig. 3.3, p. 101 for anti-phase excitation, it can be seen that there is zero transmission between ports 1 and 2 for this situation. Therefore the only parameter required is the reflection coefficient. The equivalent circuit shown in (b) of Fig. 3.3, p. 101 may therefore be simplified to that shown in Fig. 3.5, above. In this figure,

$$Y_3 = -jY_r cot\left(\beta\frac{3\lambda}{8}\right) \tag{3.7}$$

and

$$Y_4 = -jY_r cot\left(\beta\frac{3\lambda}{4}\right) \tag{3.8}$$

The reflection coefficient for anti-phase excitation then follows directly as

$$T_{11o} = \frac{Y_o - Y_{to}}{Y_o + Y_{to}} \tag{3.9}$$

where

$$Y_{to} = Y_3 + Y_4. \tag{3.10}$$

The complete solution for the three-port ring is now obtained by summing the solutions for in-phase and anti-phase excitations. If the input waves producing these excitations are considered to have unit amplitude, then the summation will represent a ring with a single input, of twice unit amplitude, at port 1. The final solution, in terms of S-parameters will be

$$S_{11} = \frac{T_{11e} + T_{11o}}{2} \tag{3.11}$$

$$S_{21} = \frac{T_{21e} + T_{21o}}{2} \tag{3.12}$$

$$S_{31} = \frac{T_{33e} + T_{33o}}{2} \tag{3.13}$$

$$= \frac{T_{11e} - T_{11o}}{2} \tag{3.14}$$

It should be noted that prior to the summation of the transmission and reflection coefficients in 3.11 through 3.14, the coefficients could not be written directly in terms of S-parameters, the reason being that not all of the ports in the relevant equivalent circuits were terminated in the same reference impedance, which is necessary to satisfy the basic S-parameter definitions. This situation arose because the plane of symmetry was taken though one port, whose impedance was, in consequence, doubled in the equivalent circuit. Once the solutions for the in-phase and anti-phase excitations are added, all of the ports have their nominal Z_o terminations and the S-parameter specification is valid.

The ring circuit which has been analysed so far is the basic structure involving the minimum port spacings. Clearly additional multiples of the ring wavelength may be added between any of the ports without altering the discriminator function, or the matching conditions at the centre frequency. Inserting additional wavelengths gives the circuit greater flexibility in that the

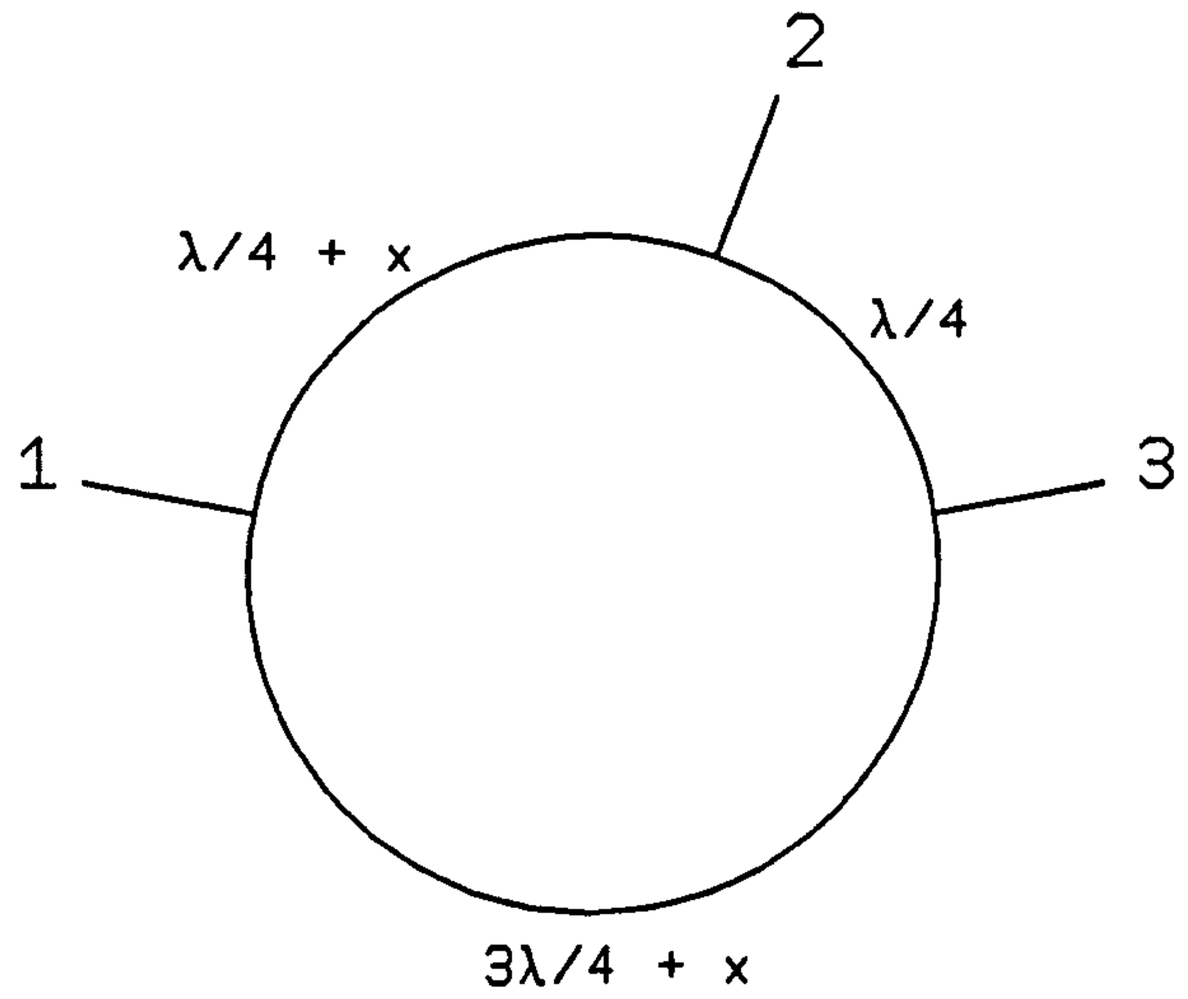

Figure 3.6: **Modified three-port ring**

sensitivity of the discriminator response can be altered and space provided in the ring to insert additional components such as switched phase shifters. The required modification to the theory is straightforward and merely involves adding $m\lambda_o$ to the appropriate trigonometric arguments, where λ_o is the ring wavelength at the centre frequency and m is the integer number of wavelengths that have been added. Of more interest however, is the effect of adding arbitrary lengths into the ring. Adding such a length between ports 1 and 3, for example, would have the effect of displacing the discriminator response in frequency and generating an offset voltage at the original centre frequency. This would also change the relative position of the input port in the ring and, intuitively it will change the impedance and match of this port. However, the addition of some arbitrary length will make the circuit asymmetric and require some modifications to the analysis.

3.4.2 Modified even and odd field analysis

A modified three-port ring, in which an arbitrary path length, x, has been added is shown in Fig. 3.6, above. In order to apply the same general method of analysis that has been used so far a dummy port is introduced, and a solution sought which makes the output at the dummy port zero. The configuration is shown in Fig. 3.7, p. 105, where port 4 is the dummy port.

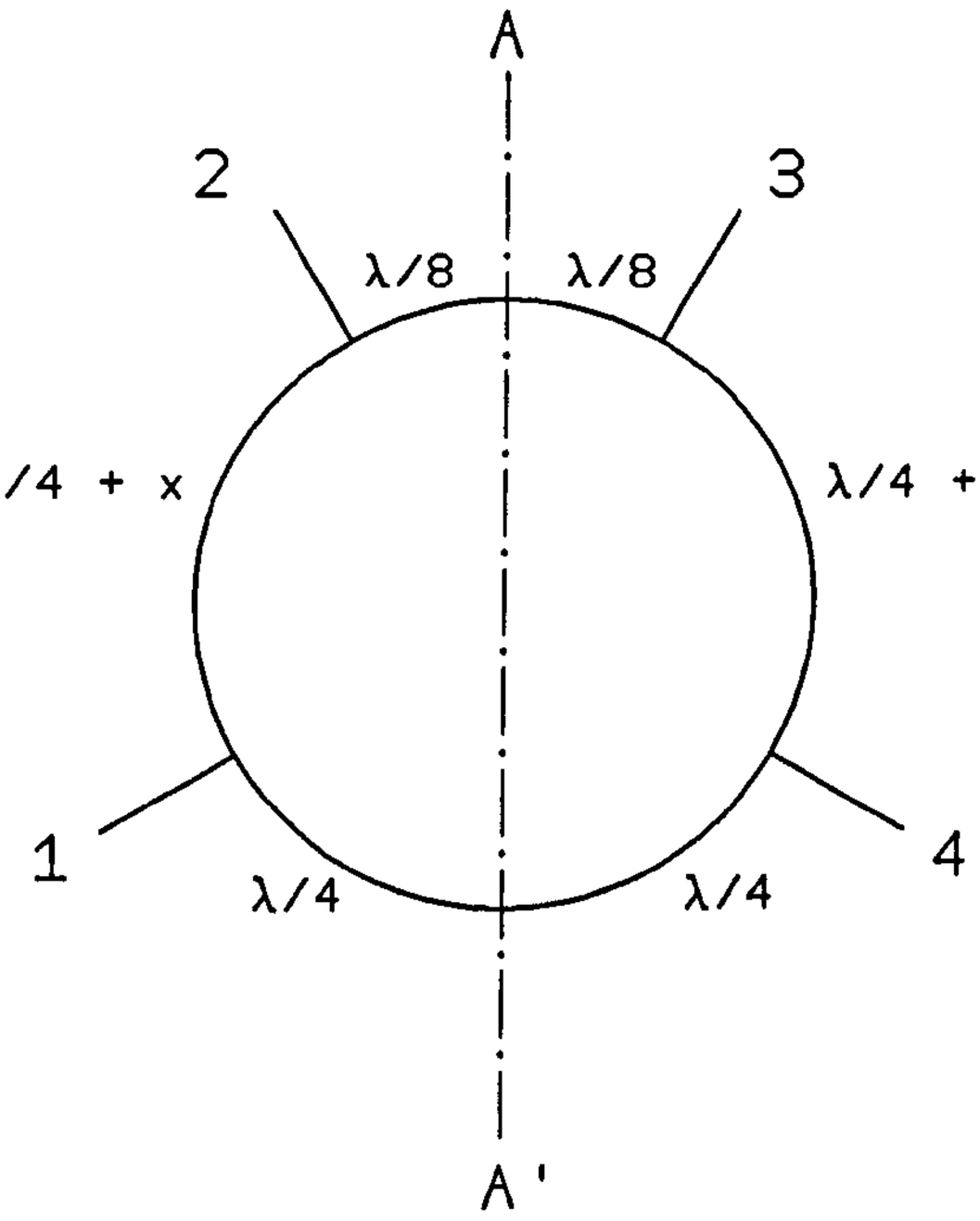

Figure 3.7: **Introduction of dummy port**

The position of this port is chosen so that a convenient plane of symmetry, AA', can be established.

The analysis proceeds in a similar way to that of the previous section. Even excitation is achieved by applying in-phase waves of unit amplitude at ports 1 and 4, and odd excitation by applying anti-phase waves of unit amplitude at the same ports. The equivalent circuits which represent the two conditions are shown in Fig. 3.8, p. 106. The circuit shown in (a) of Fig. 3.8, p. 106 may be redrawn in a conventional two-port network format as shown in Fig. 3.9, p. 106 and where

$$Y_{1e} = jY_r tan\left(\beta\frac{\lambda}{8}\right) \tag{3.15}$$

$$Y_{2e} = jY_r tan\left(\beta\frac{\lambda}{4}\right) \tag{3.16}$$

The two port network consists of a number of units in cascade and the overall

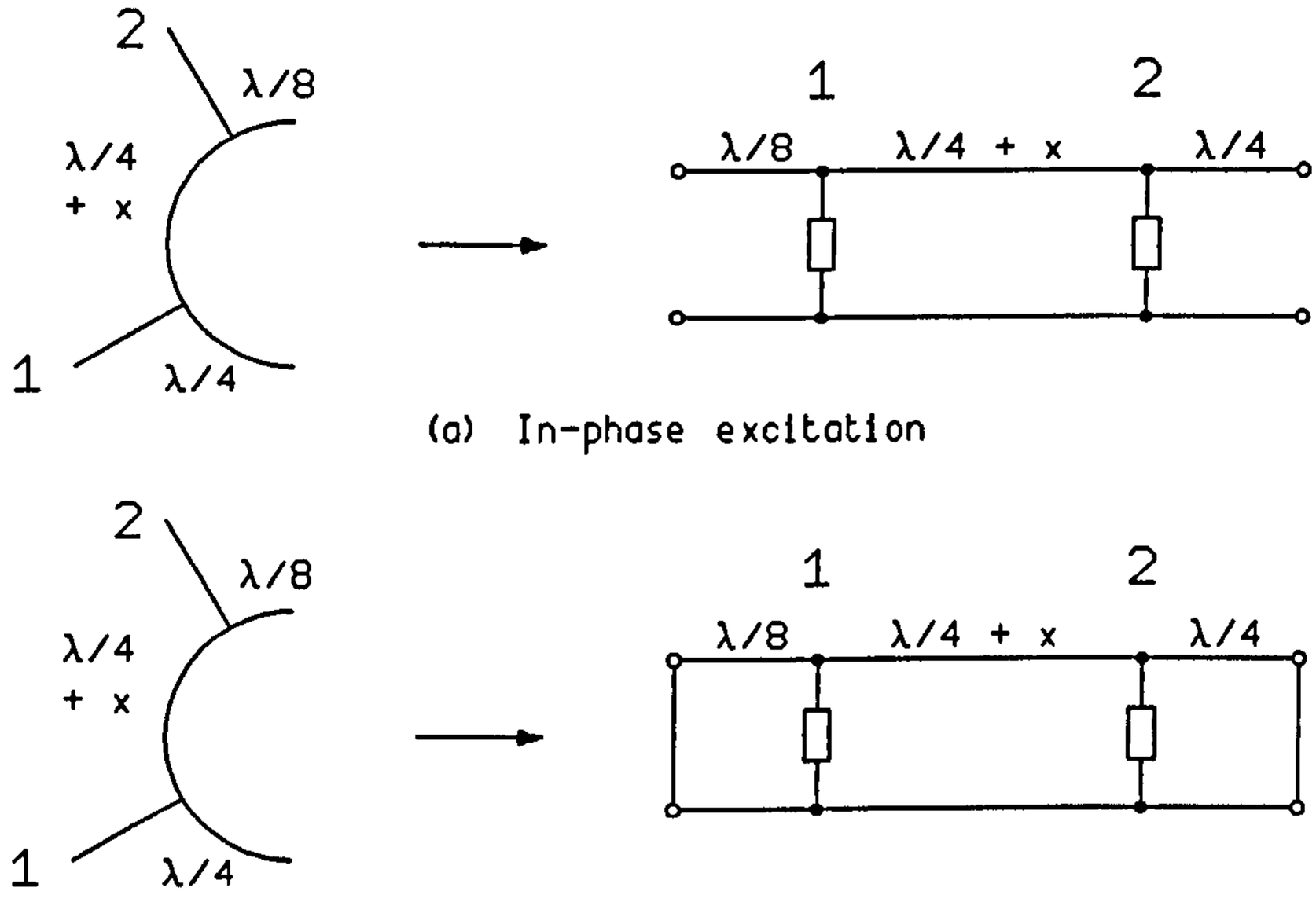

Figure 3.8: **Equivalent circuits for ring with dummy port**

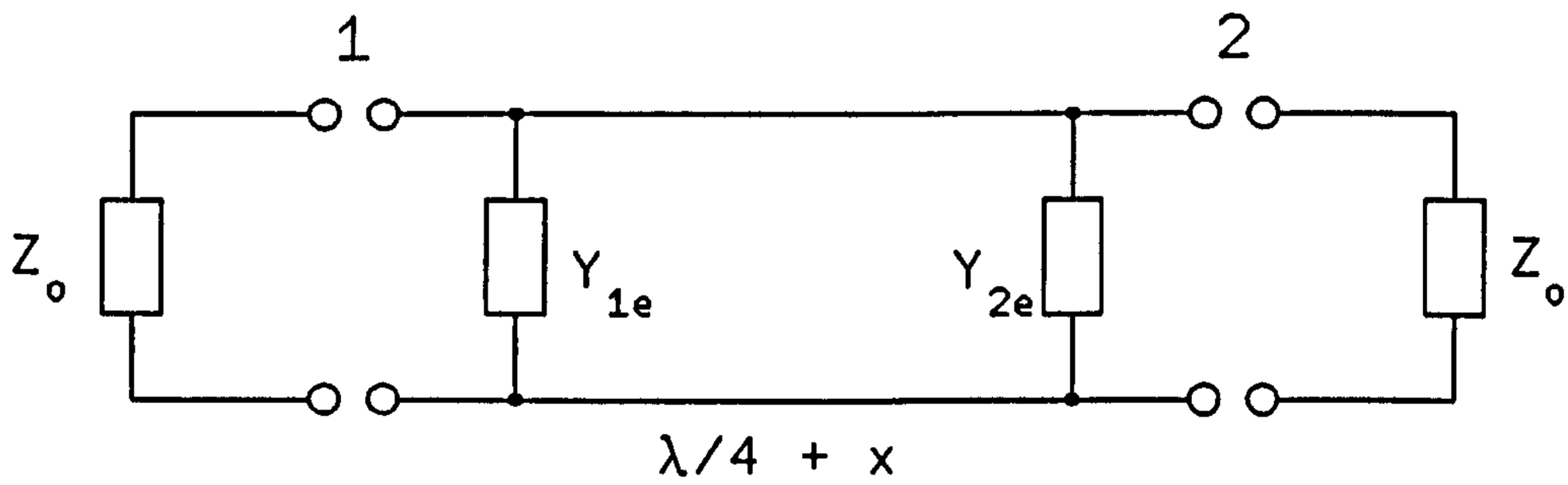

Figure 3.9: **Equivalent two-port representation of in-phase excitation of ring with dummy port**

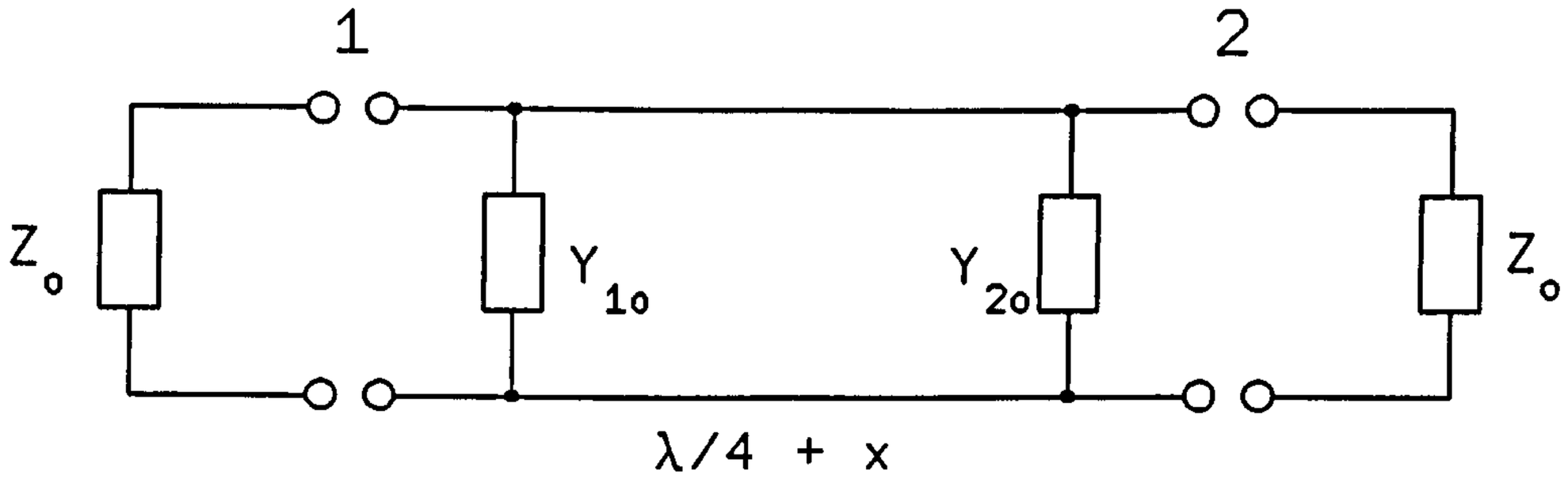

Figure 3.10: **Equivalent two-port representation of anti-phase excitation of ring with dummy port**

performance can be represented in terms of an ABCD matrix where

$$\begin{bmatrix} A_e & B_e \\ C_e & D_e \end{bmatrix} = \begin{bmatrix} 1 & 0 \\ Y_{1e} & 1 \end{bmatrix} \begin{bmatrix} cos\beta\left(\frac{\lambda}{4}+x\right) & Z_r sin\beta\left(\frac{\lambda}{4}+x\right) \\ Y_o sin\beta\left(\frac{\lambda}{4}+x\right) & cos\beta\left(\frac{\lambda}{4}+x\right) \end{bmatrix} \begin{bmatrix} 1 & 0 \\ Y_{2e} & 1 \end{bmatrix} \tag{3.17}$$

Since the two-port network is connected between source and load impedances of Z_o, the ABCD matrix may be converted directly to S-parameter notation using

$$\begin{bmatrix} S_{11e} & S_{12e} \\ S_{21e} & S_{22e} \end{bmatrix} = \begin{bmatrix} \frac{A_e+B_e-C_e-D_e}{\Delta_e} & \frac{2(A_eD_e-B_eC_e)}{\Delta_e} \\ \frac{2}{\Delta_e} & \frac{-A_e+B_e-C_e+D_e}{\Delta_e} \end{bmatrix} \tag{3.18}$$

The equivalent two-port network for anti-phase excitation is shown in Fig. 3.10, above and where

$$Y_{1o} = jY_r cot\left(\beta\frac{\lambda}{8}\right) \tag{3.19}$$

$$Y_{2o} = jY_r cot\left(\beta\frac{\lambda}{4}\right) \tag{3.20}$$

The ABCD matrix then follows as

$$\begin{bmatrix} A_o & B_o \\ C_o & D_o \end{bmatrix} = \begin{bmatrix} 1 & 0 \\ Y_{1o} & 1 \end{bmatrix} \begin{bmatrix} cos\beta\left(\frac{\lambda}{4}+x\right) & Z_r sin\beta\left(\frac{\lambda}{4}+x\right) \\ Y_o sin\beta\left(\frac{\lambda}{4}+x\right) & cos\beta\left(\frac{\lambda}{4}+x\right) \end{bmatrix} \begin{bmatrix} 1 & 0 \\ Y_{2o} & 1 \end{bmatrix} \tag{3.21}$$

from which the S-matrix is obtained using the same form of transformation given in 3.18. The even and odd field solutions may be added to give the following result which represents a single input, of unit amplitude, at port 1.

$$S_{11} = \frac{S_{11e} + S_{11o}}{2} \tag{3.22}$$

$$S_{21} = \frac{S_{21e} + S_{21o}}{2} \tag{3.23}$$

$$S_{31} = \frac{S_{33e} + S_{33o}}{2} \tag{3.24}$$

$$= \frac{S_{11e} + S_{11o}}{2} \tag{3.25}$$

$$S_{44} = \frac{S_{44e} - S_{44o}}{2} \tag{3.26}$$

$$= \frac{S_{11e} - S_{11o}}{2} \tag{3.27}$$

Using these equations an optimum value of x can be found, consistent with the requirement that S_{44} should be zero. The equations will be used in a subsequent section to compare measured data with theoretical predictions.

3.5 Design information

3.5.1 Discriminator specification

The discriminator circuits were designed to have a centre frequency of 10GHz and input and output port impedances of 50Ω.

3.5.2 Microstrip data

The test circuits were fabricated on RT/duroid having a substrate thickness of 635μm and a relative permittivity of 10.4. The conducting tracks were copper and had a thickness of 4.5μm.

3.5.3 T-junction discontinuity data

A well established equivalent circuit exits for the microstrip T-junction discontinuity and this is shown in Fig. 3.11, p. 109. The circuit shows how the reference planes are displaced from the geometric centre of the junction and the shunt capacitance which exists at the centre. However, there is some

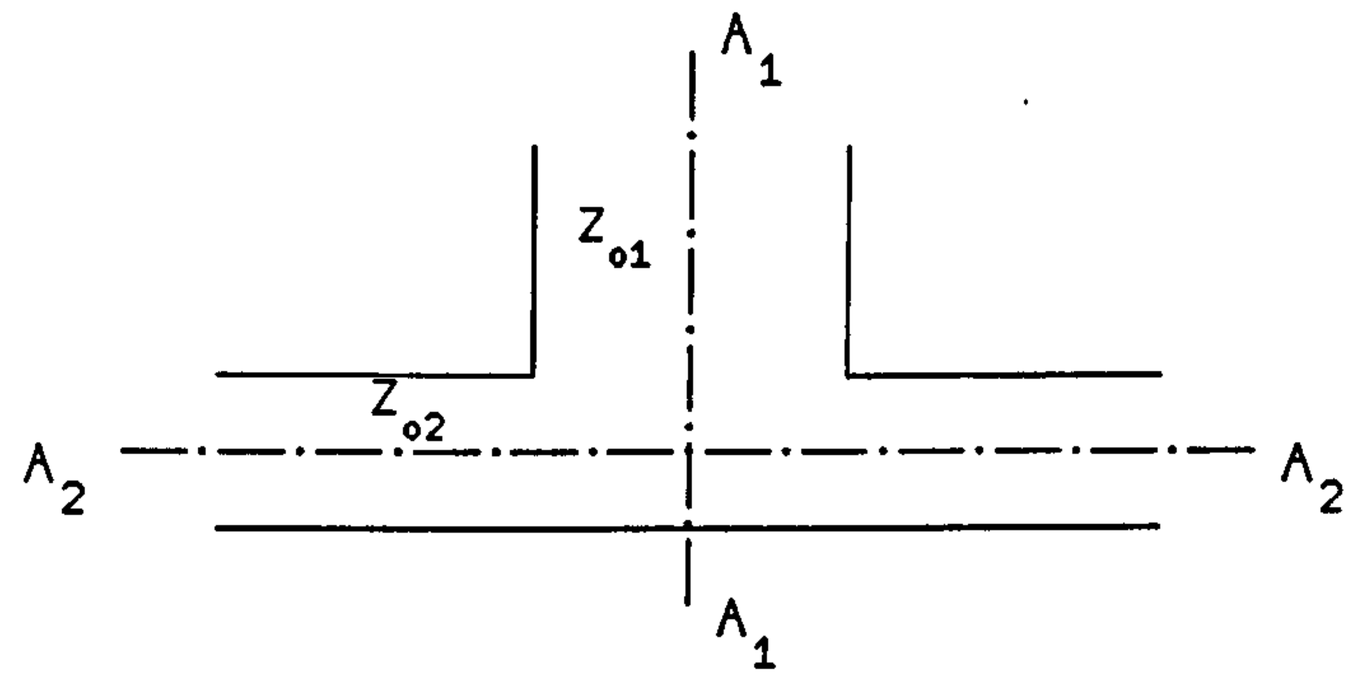

(a) Geometry of T-junction

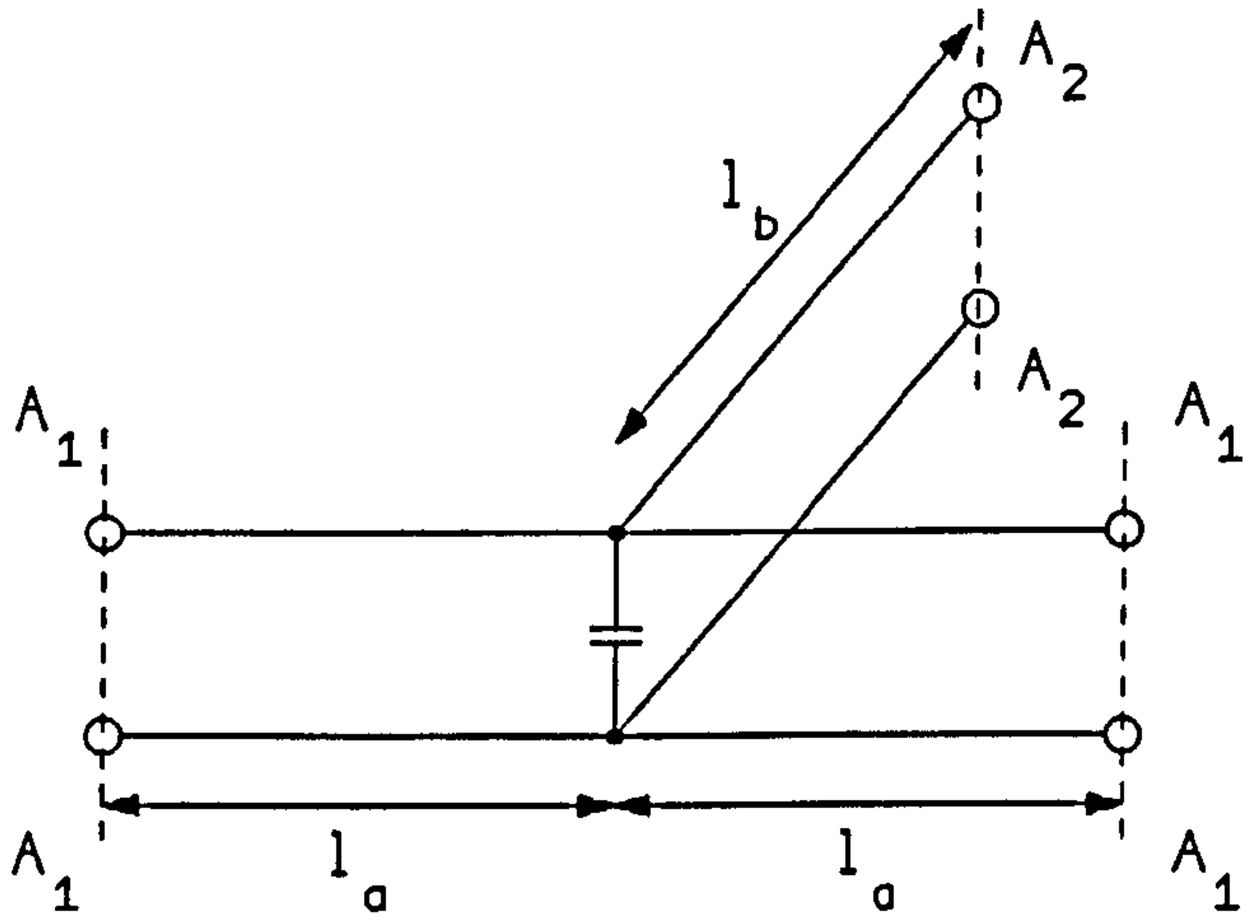

(b) Equivalent circuit of T-juntion

Figure 3.11: **Microstrip T-junction**

disagreement between authors about the values of the equivalent line lengths shown in (b) of this figure. The following tables give results from two sources,

	Thomson-Easter	Hammerstad and Bekkadal
l_a	$65\mu m$	$116\mu m$
l_b	$244\mu m$	$548\mu m$

Figure 3.12: **Table of discontinuity data:$Z_{o1} = 50\Omega$, $Z_{o2} = 70\Omega$**

	Thomson-Easter	Hammerstad and Bekkadal
l_a	$38\mu m$	$82\mu m$
l_b	$174\mu m$	$577\mu m$

Figure 3.13: **Table of discontinuity data:$Z_{o1} = 50\Omega$, $Z_{o2} = 50\Omega$**

namely, the design equations of HAMMERSTAD AND BEKKADAL [16] and the results of THOMSON AND GOPINATH [27] and EASTER ET AL [28]. In the latter case the authors' results are for slightly different microstrip parameters to those used here and some interpolation has been applied. DYDYK [30] proposed a compensation arrangement for microstrip T- junctions using short matching sections of transmission line to achieve a desired minimum mismatch for the junction. In general, the compensated junction has the geometry shown in Fig. 3.14, p. 111. Applying Dydyk's technique to a symmetrical T-junction with $Z_{o1} = 50\Omega$ and $Z_{o2} = 70\Omega$ gave the following results at 10GHz for the substrate previously specified. (The significance of the Z_{o2} value will be discussed later.)

If the minimum voltage standing wave ratio (VSWR) required is 1.05, then

$$Z_w = 49.9\Omega$$
$$\theta_w = 0.05mm$$
$$Z_z = 71.5\Omega$$
$$\theta_z = 0.301mm$$

Z_w is so close to the port impedance of 50Ω that its effect can be neglected. The value of θ_z is of the same order as the width of port 1, so that the effect of applying the compensation is to produce a wide, shallow slit as shown in Fig. 3.15, p. 111.

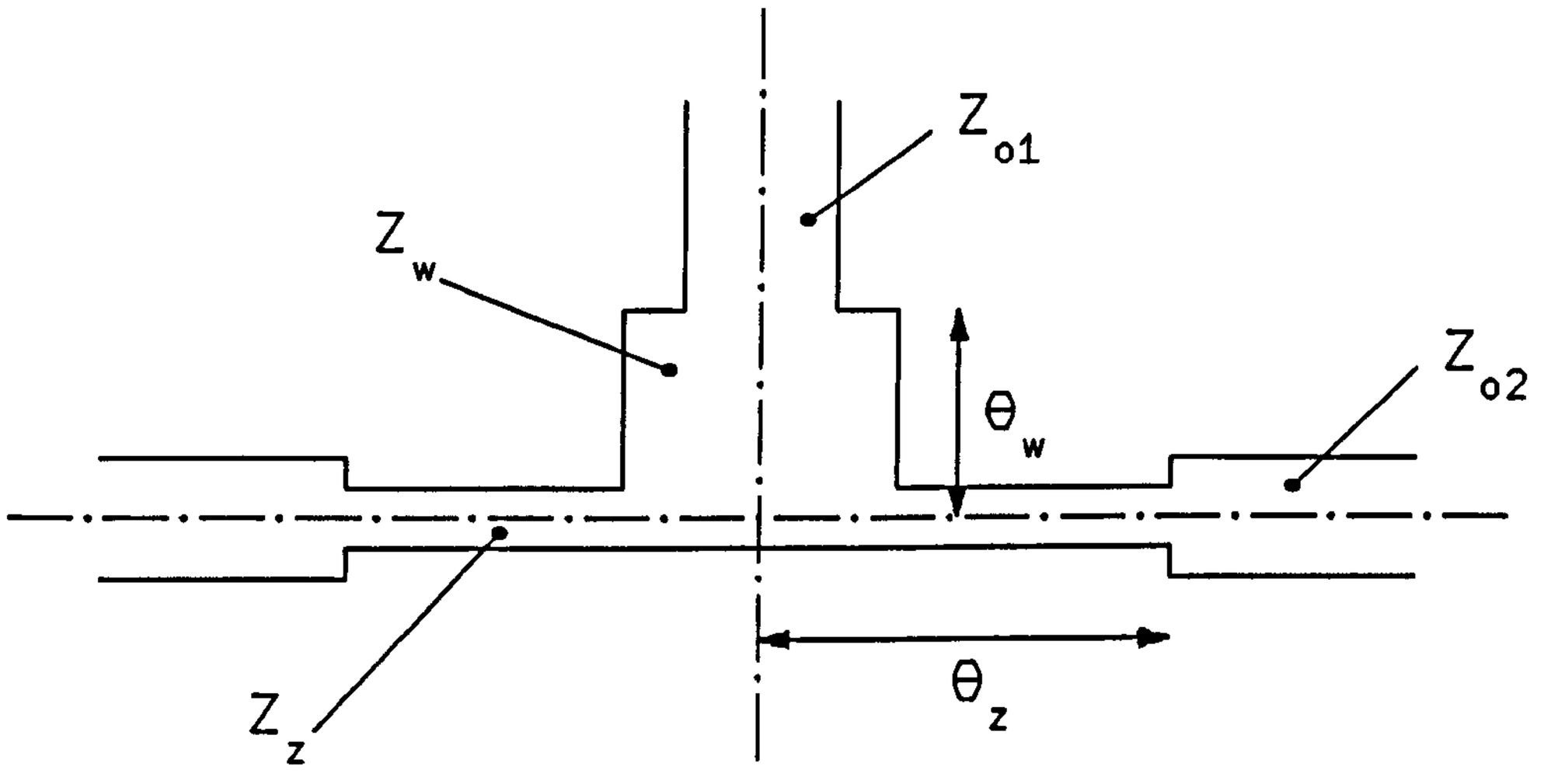

Figure 3.14: **Compensated microstrip T-junction (Dydyk method)**

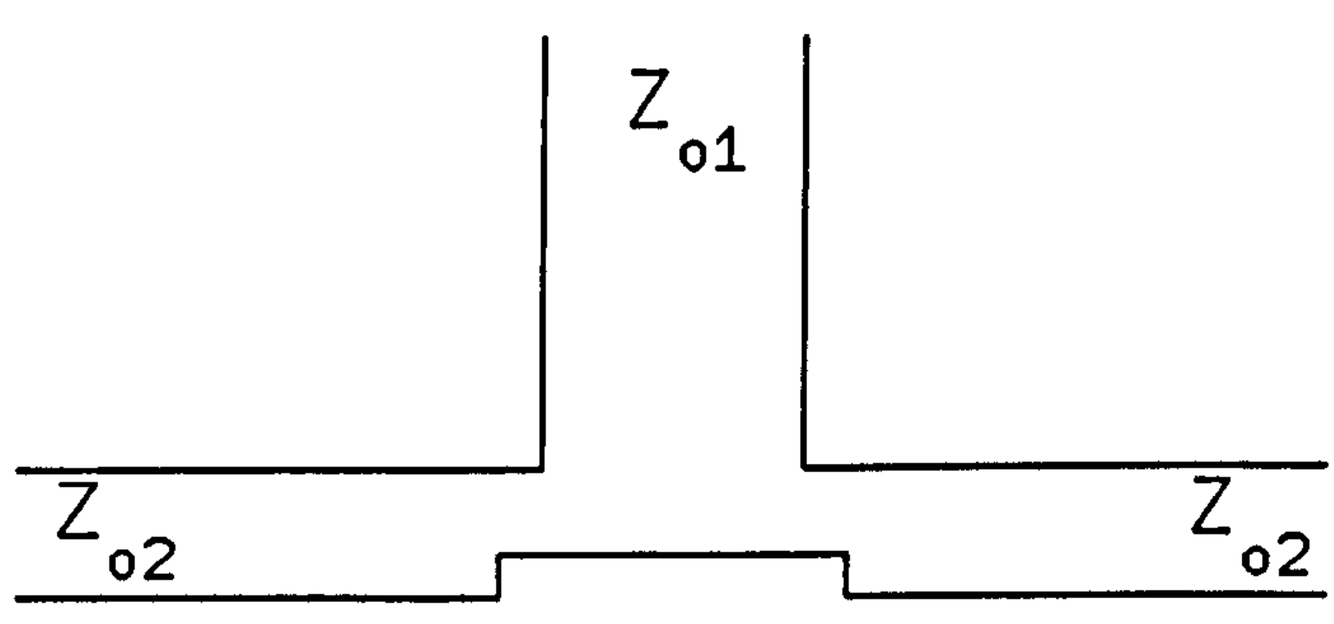

Figure 3.15: **Geometry of compensated microstrip T-junction**

3.5.4 T-junction compensation (Stub method)

It was seen in Fig. 3.11, p. 109 that the microstrip T-junction can be represented in terms of a shunt capacitance at its geometric centre. This capacitance can be matched out by using an open-circuit stub to provide a shunt inductance, having the same susceptance as the junction capacitance.

For a T-junction with $Z_{o1} = 50\Omega$ and $Z_{o2} = 70\Omega$ the value of the capacitive susceptance at the junction is, from the expressions of HAMMERSTAD AND BEKKADAL [16], 2.68mS at 10GIIz. The stub could be attached to the junctions shown in Fig. 3.16, p. 112. In order to minimise the discontinuity at the point of attachment of the stub, the stub should have a relatively

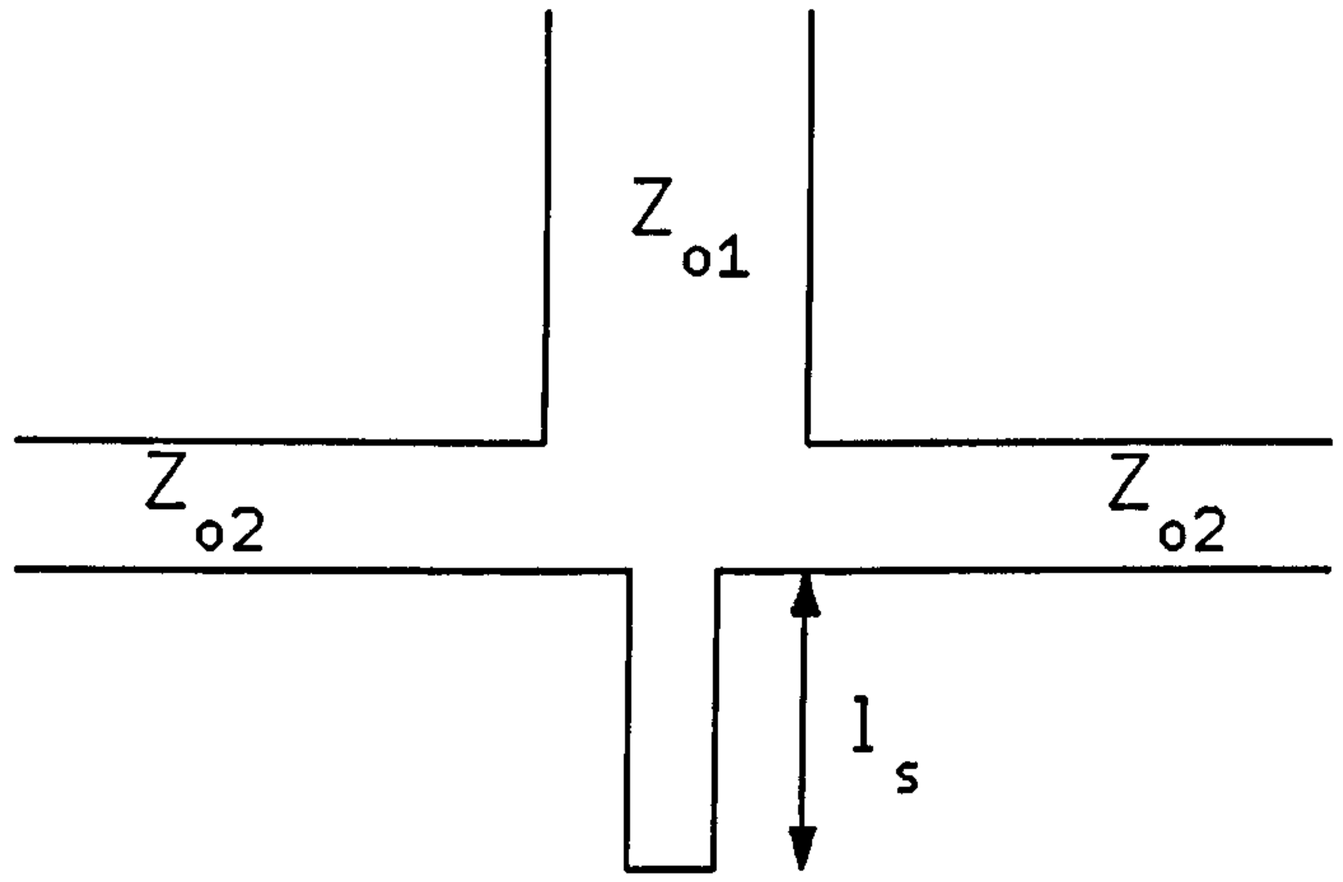

Figure 3.16: **T-junction compensation using a microstrip stub**

high impedance. For a stub of characteristic impedance 80Ω, the required normalised input susceptance is -0.2144. This needs a stub of length 0.467λ, or 5.57mm at 10GHz. The actual stub length will be less than this value, due to the open-end fringing effect. Standard open-end discontinuity theory from HAMMERSTAD AND BEKKADAL [16] gives the equivalent end-effect length as 140μm. Thus the required matching stub length is 5.43mm.

3.5.5 Single-stub tuner (SST) design

It has already been established that the three-port ring cannot be simultaneously matched at all three ports. One method of achieving a match at the input port, port 1, would be to include a single-stub tuner in the feed line to this port, as shown in Fig. 3.17, p. 113. Applying the previous theory to achieve a minimum mismatch at port 1 gives an input reflection coefficient at this port of $0.334/-72°$. Standard SST theory then gives the following nominal tuner dimensions: $d = 0.248\lambda$ and $l_s = 0.098\lambda$. Modifying these dimensions to account for the T-junction and open-end discontinuity effects gives the following dimensions at 10GHz: d=2.55mm and $l_s = 1.10mm$. The distances are specified to the geometric centres of the junctions involved.

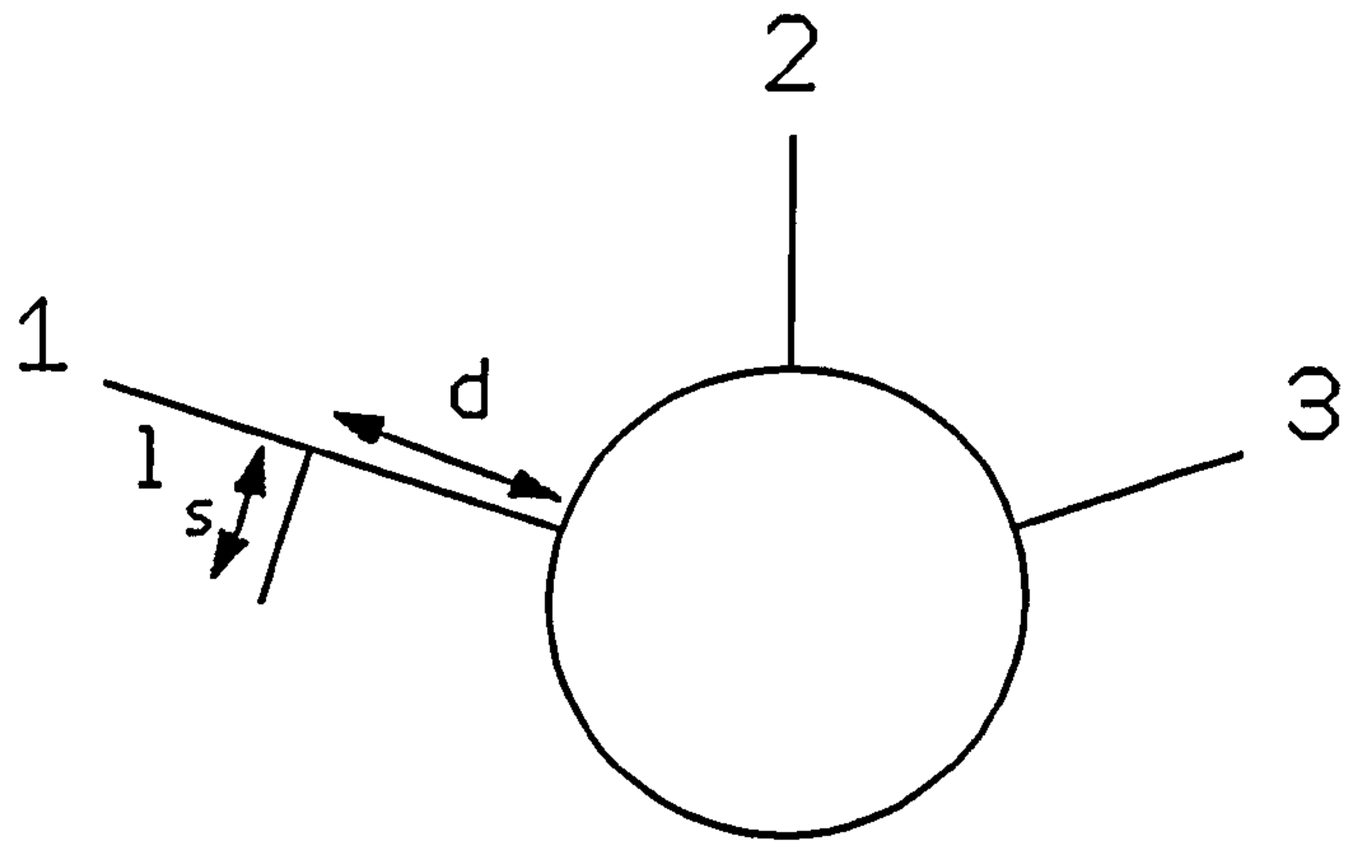

Figure 3.17: **Input matching using a single-stub tuner**

3.6 Catalogue of test circuits

This section provides a catalogue giving full dimensional data of all the test circuits used to investigate various aspects of the three port ring. All of the test circuits were fabricated on RT/duroid 6010 which had the following parameters:

$$\text{substrate thickness} = 635\mu m$$
$$\text{substrate relative permittivity} = 10.4$$
$$\text{copper thickness} = 4.5\mu m \text{ (0.125oz)}$$

The substrate used was supplied with copper electro-deposited on both sides and a conventional photoresist/wet-etching process was used to fabricate the circuits. In the table attached to each circuit diagram in the following catalogue, data are given for the nominal (design) circuit dimensions and the dimensions after etching. The differences are due to mask image spreading and undercutting in the etching process. However, the differences are small and introduce a negligible percentage error.

The tables provide all of the critical dimensions for each circuit. Unless otherwise stated the port impedances were 50Ω (corresponding to a track width of $584\mu m$) and the ring impedance 70Ω (corresponding to a track width of $253\mu m$). The port spacings are specified between geometric centres and the circular ring radii as mean distances.

CIRCUIT: *CCT3.1*		DIMENSIONS	
		Design	Fabricated
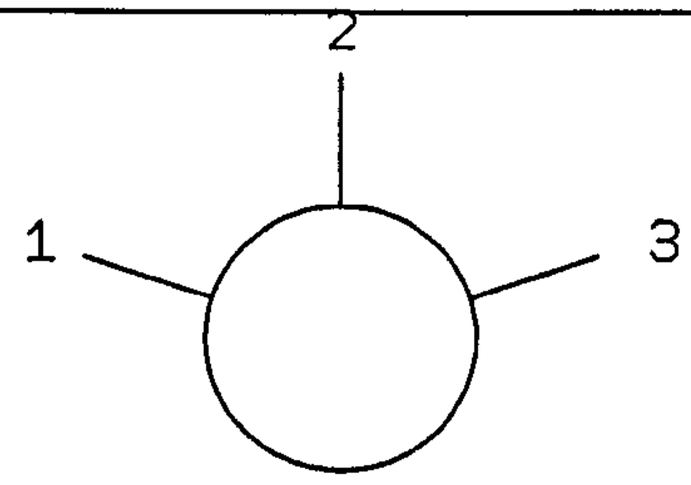	I.rad.	2174μm	2195μm
	O.rad.	2428μm	2415μm
	$1 \rightarrow 2$	2895μm	2909μm
	$2 \rightarrow 3$	2895μm	2909μm
$1 \rightarrow 2 = 2 \rightarrow 3 = \frac{\lambda}{4}$ $\quad 1 \rightarrow 3 = \frac{3\lambda}{4}$			
Notes: Circular three port ring used to investigate the basic three-port ring with nominal port spacings. I.rad. & O.rad. = ring inner & outer radii.			

CIRCUIT: *CCT3.2*		DIMENSIONS	
		Design	Fabricated
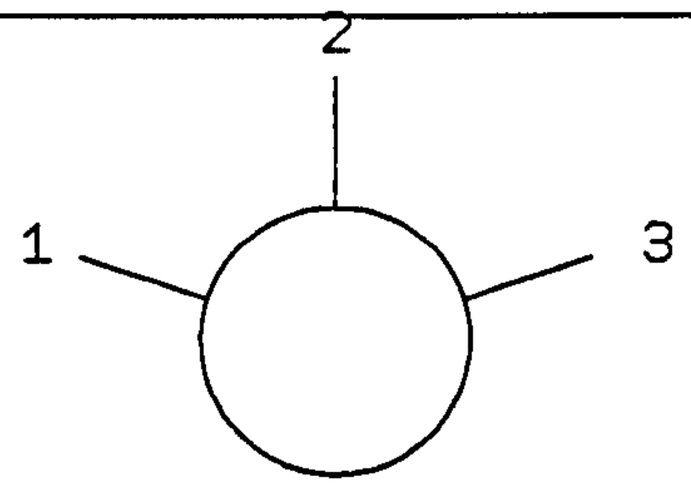	I.rad.	2144μm	2155μm
	O.rad.	22368μm	2376μm
	$1 \rightarrow 2$	2765μm	2770μm
	$2 \rightarrow 3$	2765μm	2776μm
$1 \rightarrow 2 = 2 \rightarrow 3 = \frac{\lambda}{4}$ $\quad 1 \rightarrow 3 = \frac{3\lambda}{4}$			
Notes: As CCT3.1 but with port spacings modified (reduced) to compensate for T-junction discontinuities using interpolated Thomson-Easter data.			

CIRCUIT: *CCT3.3*		DIMENSIONS	
		Design	Fabricated
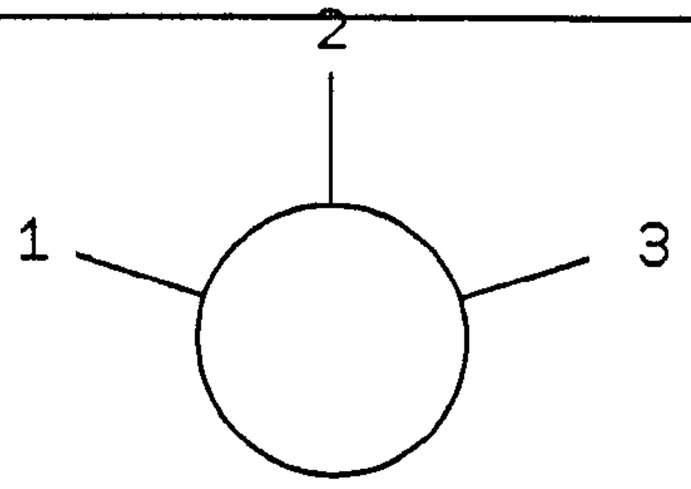	I.rad.	2050μm	2075μm
	O.rad.	2304μm	2295μm
	$1 \rightarrow 2$	2663μm	2643μm
	$2 \rightarrow 3$	2663μm	2648μm
$1 \rightarrow 2 = 2 \rightarrow 3 = \frac{\lambda}{4}$ $\quad 1 \rightarrow 3 = \frac{3\lambda}{4}$			
Notes: As CCT3.1 but with port spacings modified (reduced) to compensate for T-junction discontinuities using Hammerstad-Bekkadal theory.			

CIRCUIT: *CCT3.4*	DIMENSIONS		
		Design	Fabricated
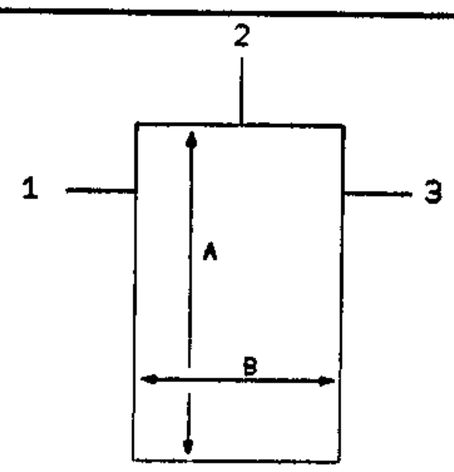 $1 \rightarrow 2 = 2 \rightarrow 3 = \frac{\lambda}{4}$ $1 \rightarrow 3 = \frac{3\lambda}{4}$	A	$4000\mu m$	$4007\mu m$
	B	$3000\mu m$	$3004\mu m$
	b	$188\mu m$	$182\mu m$
	$1 \rightarrow 2$	$2702\mu m$	$2716\mu m$
	$2 \rightarrow 3$	$2702\mu m$	$2707\mu m$
Notes: As CCT3.2 but in rectangular format. To compare rectangular and circular ring performances. Corner chamfer (b=0.6w) modifies mean length around each corner by $-63\mu m$ (EASTER ET AL [28])			

CIRCUIT: *CCT3.5*	DIMENSIONS		
		Design	Fabricated
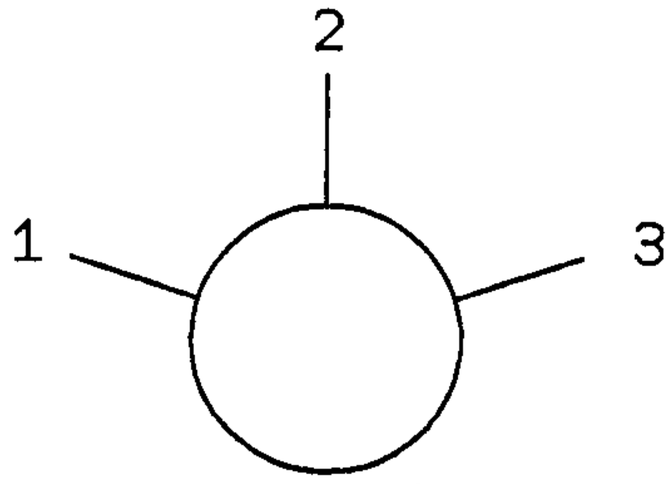 $1 \rightarrow 2 = 2 \rightarrow 3 = \frac{\lambda}{4}$ $1 \rightarrow 3 = \frac{11\lambda}{4}$	I.rad.	$5801\mu m$	$5839\mu m$
	O.rad.	$6055\mu m$	$6087\mu m$
	$1 \rightarrow 2$	$2765\mu m$	$2785\mu m$
	$2 \rightarrow 3$	$2765\mu m$	$2804\mu m$
Notes: Circular three port ring used to investigate the effect of including an additional 2λ between ports 1 and 3.			

CIRCUIT: *CCT3.6*	DIMENSIONS		
		Design	Fabricated
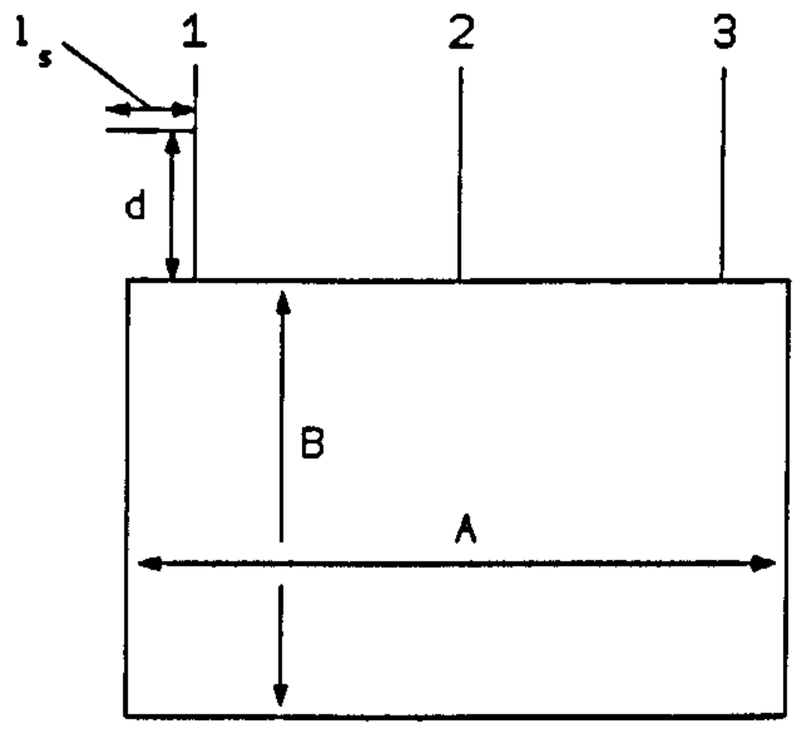 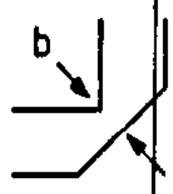 $1 \rightarrow 2 = 2 \rightarrow 3 = \frac{\lambda}{4}$ $1 \rightarrow 3 = \frac{11\lambda}{4}$	A	11068μm	11149μm
	B	7402μm	7454μm
	$1 \rightarrow 2$	2765μm	2778μm
	$2 \rightarrow 3$	2765μm	2774μm
	l_s	1100μm	1090μm
	d	2550μm	2550μm
	b	188μm	182μm
Notes: Large rectangular ring with matching stub on input port. Port spacings modified as in CCT3.2. Stub dimensions compensated for T-junction discontinuity and open-end-effect. Ring corners chamfered and dimensions modified as in CCT3.4.			

CIRCUIT: *CCT3.7*	DIMENSIONS		
		Design	Fabricated
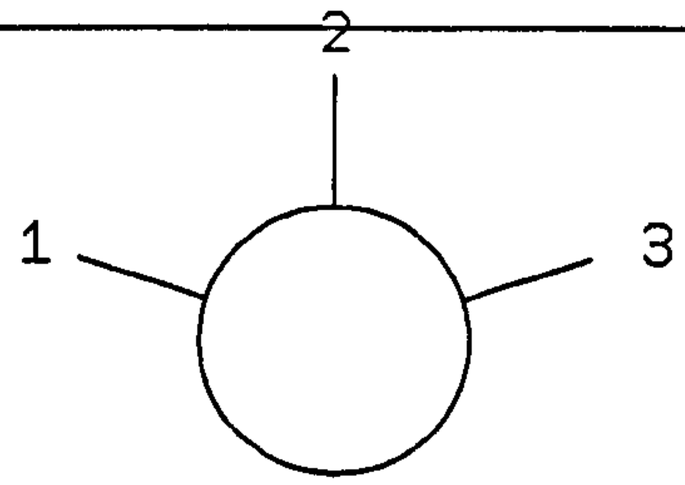 $1 \rightarrow 2 = 2 \rightarrow 3 = \frac{\lambda}{4}$ $1 \rightarrow 3 = \frac{7\lambda}{4}$	I.rad.	3985μm	3975μm
	O.rad.	4276μm	4275μm
	$1 \rightarrow 2$	2876μm	2942μm
	$2 \rightarrow 3$	2876μm	2933μm
Notes: Medium size three-port ring to be used in conjunction with CCT3.8 to investigate effect of applying DYDYK [30] compensation - characteristic impedance of ring is 62.5Ω.			

CIRCUIT: *CCT3.8*	DIMENSIONS		
		Design	Fabricated
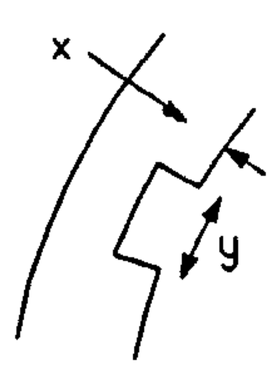 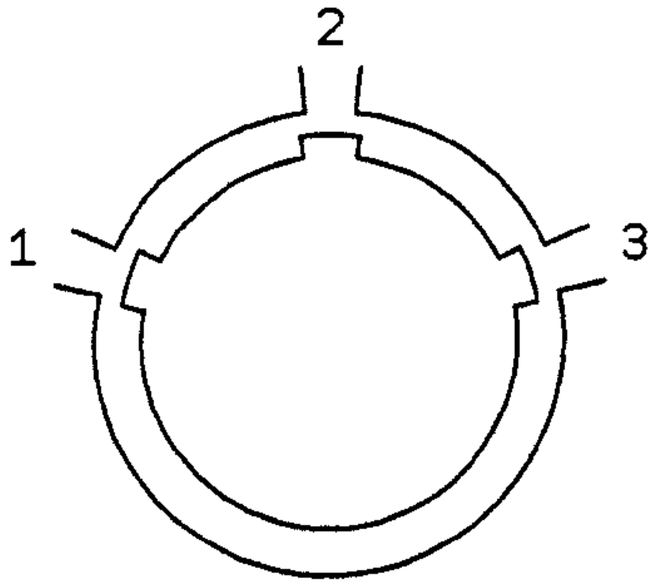 $1 \rightarrow 2 = 2 \rightarrow 3 = \frac{\lambda}{4}$ $1 \rightarrow 3 = \frac{7\lambda}{4}$	I.rad. O.rad. $1 \rightarrow 2$ $2 \rightarrow 3$ x y	$3985\mu m$ $4276\mu m$ $2876\mu m$ $2876\mu m$ $85\mu m$ $602\mu m$	$3975\mu m$ $4275\mu m$ $2942\mu m$ $2933\mu m$ $77\mu m$ $578\mu m$
Notes: Circuit dimensions same as for CCT3.7, but with T-junctions modified according to DYDYK [30] theory. Circuit designed to give a minimum input VSWR of1.05.			

CIRCUIT: *CCT3.9*	DIMENSIONS		
		Design	Fabricated
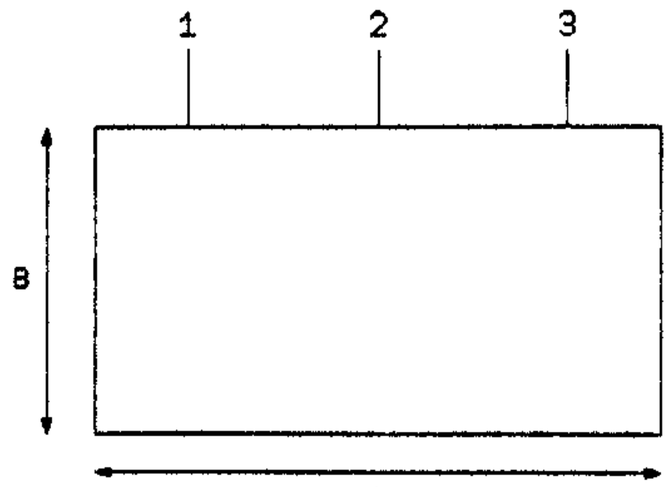 $1 \rightarrow 2 = 2 \rightarrow 3 \stackrel{A}{=} \frac{\lambda}{4}$ $1 \rightarrow 3 = \frac{11\lambda}{4}$	A B $1 \rightarrow 2$ $2 \rightarrow 3$	$11200\mu m$ $7500\mu m$ $2895\mu m$ $2895\mu m$	$11160\mu m$ $7481\mu m$ $2918\mu m$ $2921\mu m$
Notes: Large rectangular ring to be used in conjunction with CCT3.10 to investigate effect of stub matching each T-junction to compensate for junction shunt capacitance. Corners chamfered/compensated as in CCT3.4.			

CIRCUIT: *CCT3.10*	DIMENSIONS		
		Design	Fabricated
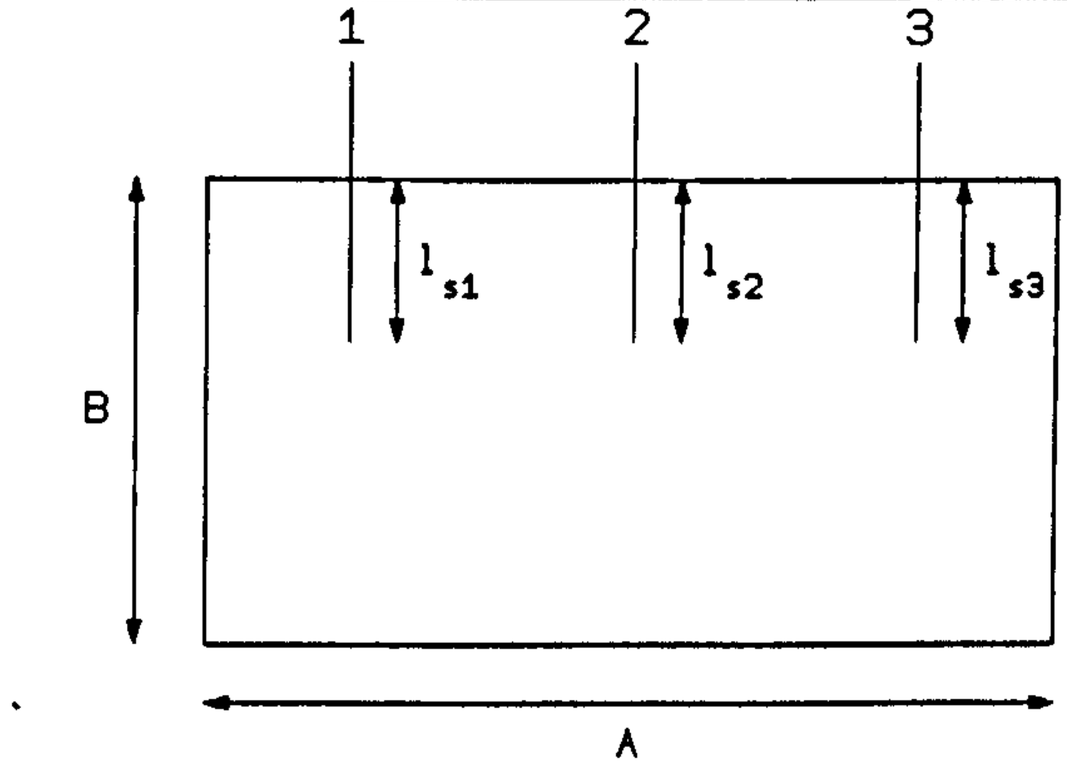 $1 \rightarrow 2 = 2 \rightarrow 3 = \frac{\lambda}{4}$ $1 \rightarrow 3 = \frac{11\lambda}{4}$	A	11200μm	11160μm
	B	7500μm	7481μm
	$1 \rightarrow 2$	2895μm	2918μm
	$2 \rightarrow 3$	2895μm	2921μm
	l_{s1}	5430μm	5453μm
	l_{s2}	5430μm	5450μm
	l_{s3}	5430μm	5450μm
Notes: Circuit dimensions as for CCT3.9 but with matching stubs connected to each junction. Stub characteristic impedance designed to be 80Ω to give a narrow (178μm wide stub and so minimise stub junction discontinuity. Stub compensated for open-end effect - equivalent to 141μm.			

CIRCUIT: *CCT3.11*	DIMENSIONS		
		Design	Fabricated
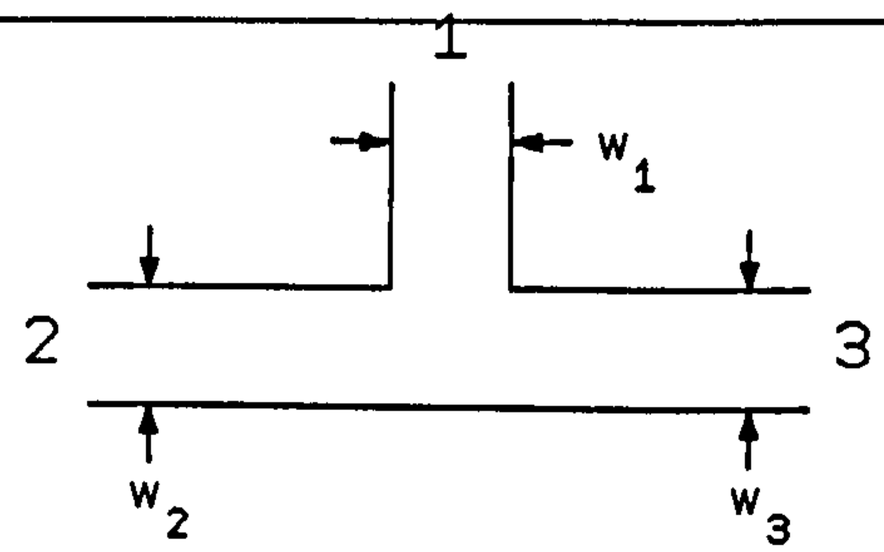	w_1	584μm	594μm
	w_2	584μm	598μm
	w_3	584μm	598μm
Notes: T-junction formed from 50Ω microstrip lines. To be used in conjunction with CCT3.12 and CCT3.13 to investigate the influence of stub position when stub matching a microstrip T-junction			

CIRCUIT: *CCT3.12*	DIMENSIONS		
		Design	Fabricated
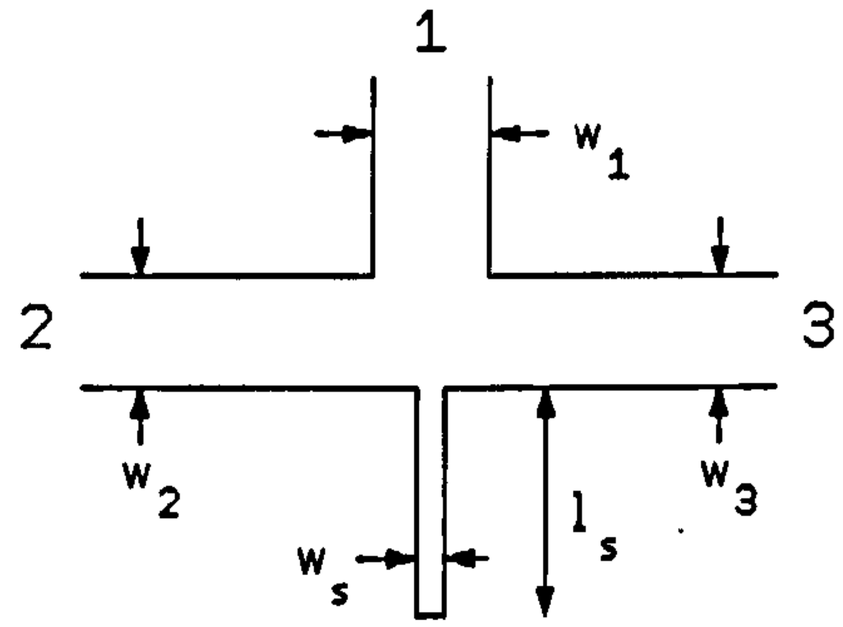	w_1	$584\mu m$	$594\mu m$
	w_2	$584\mu m$	$598\mu m$
	w_3	$584\mu m$	$598\mu m$
	l_s	$5430\mu m$	$5450\mu m$
	w_s	$178\mu m$	$190\mu m$

CIRCUIT: *CCT3.13*	DIMENSIONS		
		Design	Fabricated
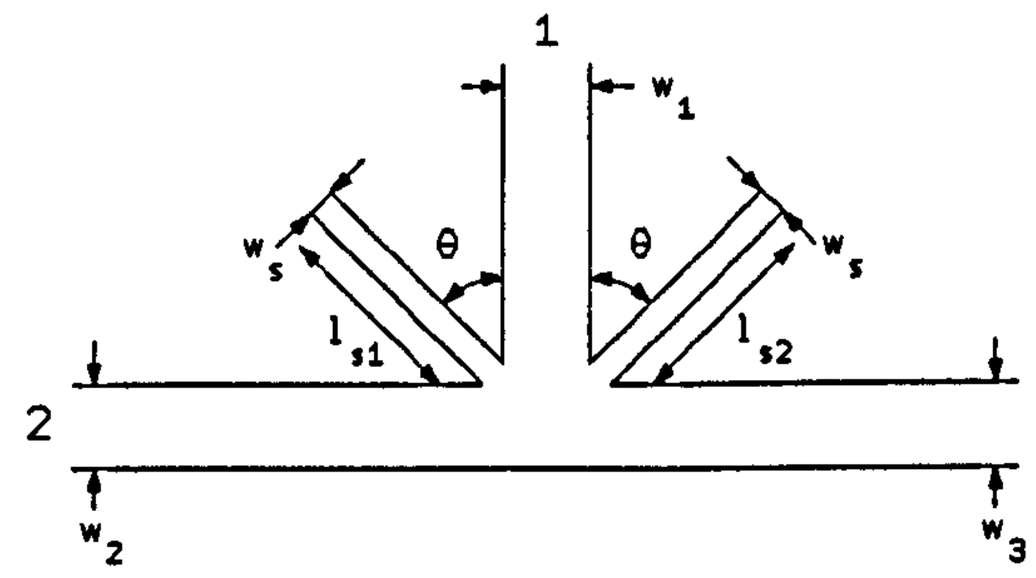	w_1	$584\mu m$	$594\mu m$
	w_2	$584\mu m$	$598\mu m$
	w_3	$584\mu m$	$598\mu m$
	l_{s1}	$5608\mu m$	$5589\mu m$
	l_{s2}	$5608\mu m$	$5619\mu m$
	w_s	$178\mu m$	$174\mu m$
	θ	$45°$	

Notes: Matching stubs positioned in re-entrant corners of T-junction. Sub lengths designed on basis that the two stubs effectively act in parallel to cancel the shunt capacitance of the T-junction.

3.7 Measurement conditions

3.7.1 Equipment

Measured data were obtained using an HP 8410 Network Analyser. The practical discriminator responses for the three-port networks were obtained by taking the difference in the magnitudes of the measured values of S_{21} and

S_{31}, thereby eliminating any errors associated with the differential amplifier which would be used to sum the outputs in practice. Reflection coefficients were obtained directly from return loss measurements.

For testing, the microstrip circuits were mounted on a standard OSM[1] test fixture and connections to the tracks made using coaxial-to-microstrip transitions. This is not the ideal method of mounting because the measurements then include errors associated with the assembly onto the jig of the coaxial-to-microstrip transition. However, this method is necessary in order to make three simultaneous connections to the circuit, which precludes the use of a Wiltron jig.

3.7.2 Compensation for coaxial-to-microstrip transitions

Measurements of reflection coefficient using the jig described in the previous section involve de-embedding the circuit from the test fixture, i.e. transferring the measurement at the face of the coaxial connector through the connector to the port of the three-port ring. This transfer requires a knowledge of the reflection and transmission coefficients of the launcher. It is well known that coaxial-to-microstrip launchers are a source of mismatch and, furthermore, that they exhibit some excess phase associated with the coaxial-microstrip field discontinuity. The excess phase in this type of launcher, together with the techniques for its measurement are given in CHAPMAN AND AITCHISON [31] and GOURLEY AND CHAPMAN [32].

The launchers used for the measurements here were Omni-Spectra Type 14107A, for which the manufacturer quotes a maximum VSWR of 1.1 at 10GHz. It is reasonable to assume that the mismatch occurs primarily at the launcher tab/microstrip interface and therefore by transforming the measured reflection coefficient to this plane, superposition can be applied to obtain the unknown (three-port ring) reflection coefficient. It will be assumed that only first order reflections are significant, since the mismatch of the launcher is relatively small. A more exact result could be obtained summing the effects of the multiple reflections between the launcher and the ring, using convergent series theory. But since all the terms of this series will necessarily involve at least third order products of the launcher and ring reflection

[1]OSM^{TM} is the trade-mark of Omni Spectra Inc

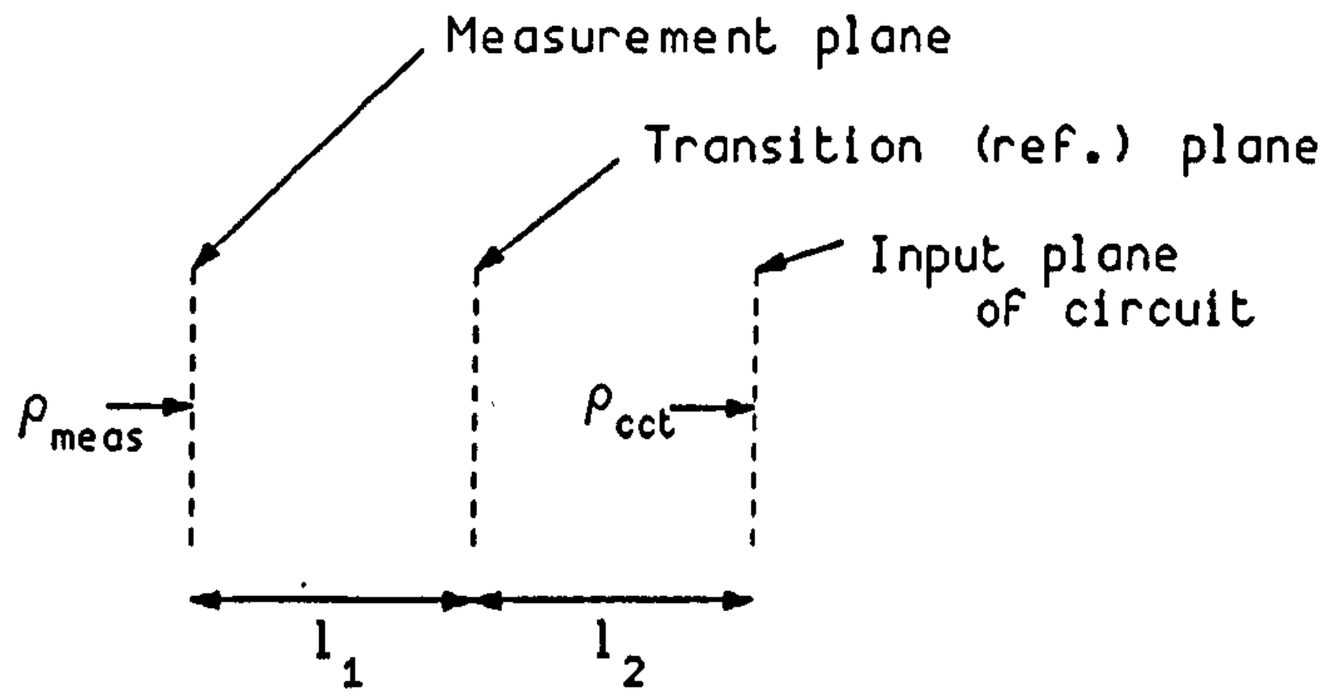

where l_1 = length of launcher
l_2 = length representing excess phase of launcher
ρ_{meas} = measured reflection coefficient
ρ_{cct} = reflection coefficient of microstrip circuit

Figure 3.18: **Coaxial-to-microstrip launcher compensation**

coefficients, the effects will be negligible.

Fig. 3.18, above shows the disposition of the reference planes for the de-embedding procedure. If it is assumed that the reflection coefficient of the launcher is negligible then the measured reflection coefficient, ρ_{meas}, is related to the reflection coefficient of the ring, ρ_{cct}, by

$$\rho_{cct} = \rho_{meas} \frac{1}{L^2} e^{2(\beta_1 l_1 + \phi_e)} \tag{3.28}$$

where

β_1 = phase propagation constant for launcher
ϕ_e = excess phase due to launcher
L = launcher transmission loss factor

the other parameters being defined in Fig. 3.18, above. The values of β_1 and l_1 can be found directly from measurements on the launcher, together with a

knowledge of the relative permittivity of the dielectric in the coaxial portion of the launcher. In practice, these two parameters may need to be split into two, to represent the air and dielectric filled portions of the launcher. The value of excess phase is not normally provided by the manufacturer and has to be measured. In the present work, the excess phase of the launchers being used was measured using the technique described in GOURLEY AND CHAPMAN [32].

3.8 Results and discussion

For convenience, this section is divided into two sections, the first dealing with some of the theoretical aspects of the three-port ring, and the second with comparisons between theory and measured data.

3.8.1 Comments on theoretical results

The theoretical discriminator response plotted in Fig. 3.19, p. 124 shows some asymmetry about the centre (design) frequency. This asymmetry does not impose any serious limitations on the use of the device in discriminator circuits, since a differential amplifier would normally be used to combine the detected signals from the two output ports of the ring and appropriate compensation could be applied. It can be observed from Fig. 3.19, p. 124 that the response is quasi-linear over a 20% bandwidth centred on the design frequency, which compares well with other microwave discriminator arrangements. The sensitivity of the characteristic, i.e. the rate of change of output signal with frequency, would be expected to increase with the size of the ring. This is verified by the theoretical responses shown in Fig. 3.20, p. 125. This figure also shows the cyclic variation of output level with frequency, which would be expected since the output is proportional to the cosine of the effective delay introduced between ports 1 and 3. It also follows therefore that increasing the sensitivity will decrease the useful bandwidth of the circuit. As discussed in the introduction, it is intended that a switched phase shifter be introduced into the delay line discriminator, so as to provide offset voltages for controlling the frequency of an oscillator. In the three-port ring the effective delay path is that between ports 1 and 3. Fig. 3.20, p. 125 shows the

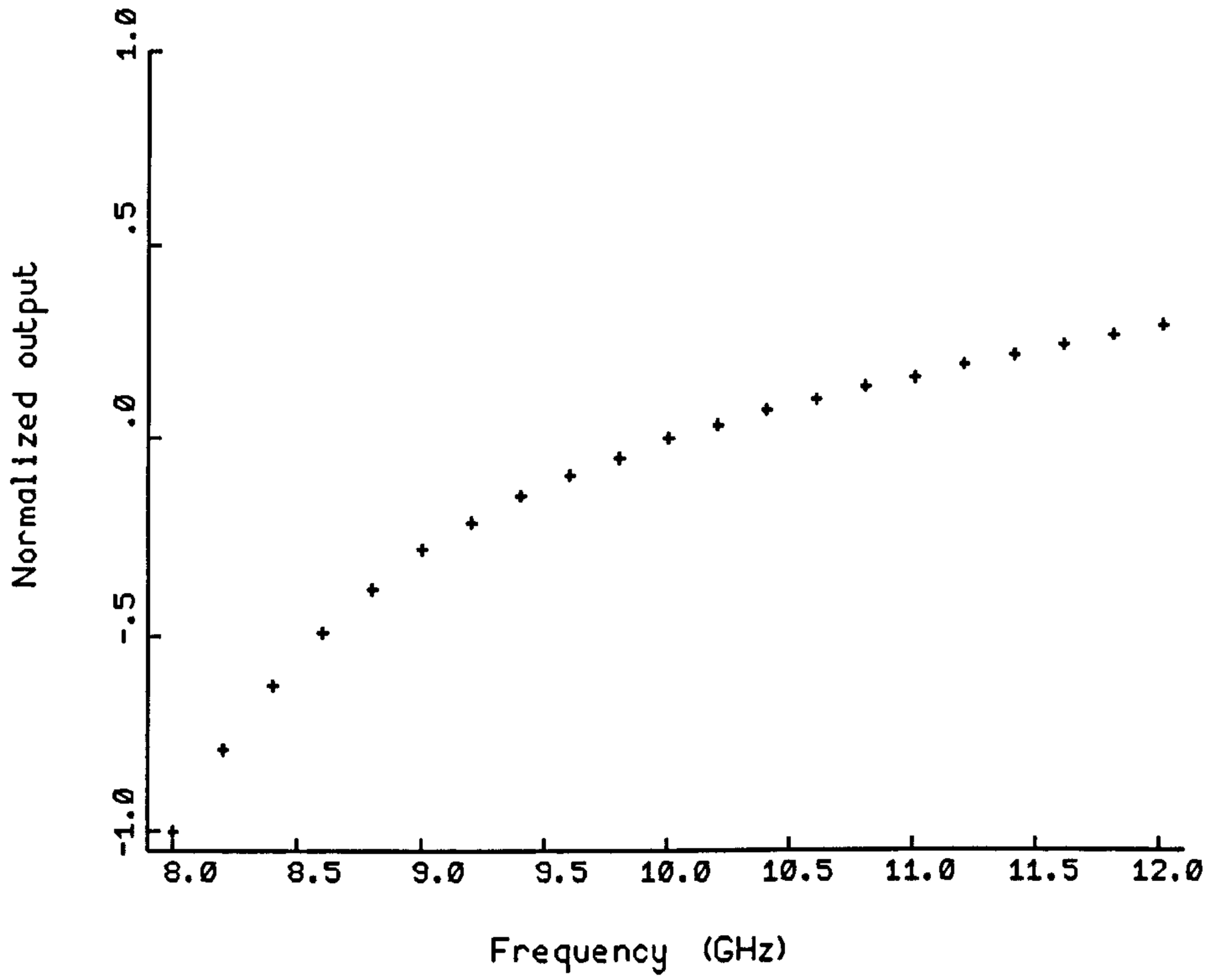

Figure 3.19: **Theoretical discriminator response for a three-port ring with normal port spacings of $\lambda/4$, $\lambda/4$ and $3\lambda/4$.**

effect of introducing 10° phase changes between ports 1 and 3. It can be seen that the discriminator function is maintained as the phase is changed and that an offset voltage is produced at the centre (10GHz) frequency. This offset voltage is proportional to the phase change. Thus by including a switched phase changer, such as the single PIN diode arrangement described in the previous chapter, the three-port ring could be used to control the frequency of an oscillator whilst maintaining low-noise performance. It is worth noting from Fig. 3.20, p. 125 that the non-linearity between the offset voltage and the phase changes, which is apparent at 10GHz, could be removed by applying a positive DC offset in the system. This would provide a more linear and more sensitive variation of output voltage around 10GHz, as well as yielding

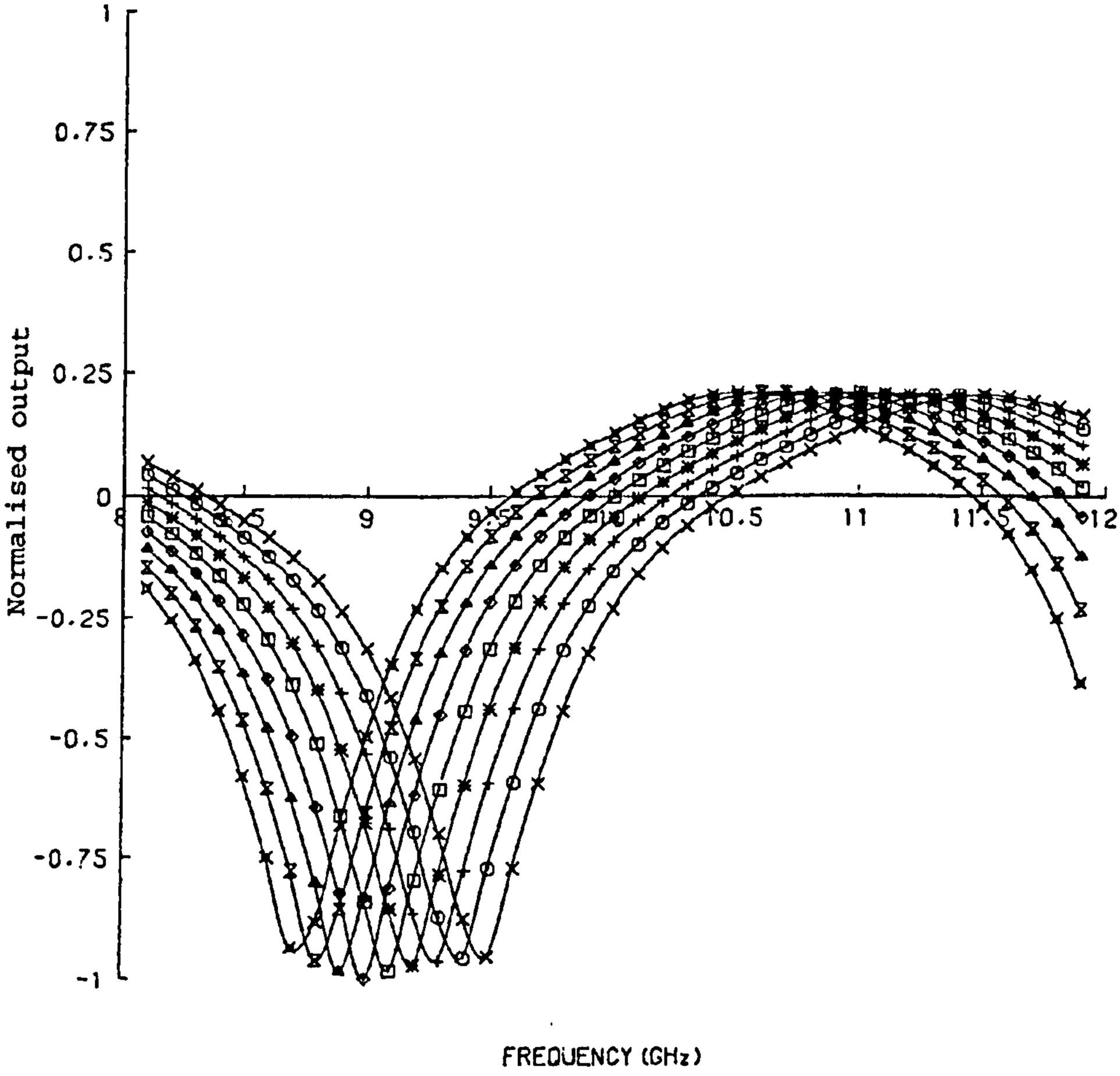

Figure 3.20: **Effect of introducing 10° steps from −40° to +40° into separation of ports 1 and 3 in a three-port ring with nominal port spacings of: $1 \rightarrow 2 = 2 \rightarrow 3 = \frac{\lambda}{4}$ and $1 \rightarrow 3 = \frac{11\lambda}{4}$**

a quasi-linear relationship between the changes in output voltage and the changes in phase.

A three-port ring with port spacings of $\lambda/4$, $\lambda/4$ and $3\lambda/4 + m\lambda$ does not produce an input match at the centre frequency when the output ports are terminated in 50Ω. A computer analysis, based on the previous theory, showed that the optimum value of ring impedance was 70Ω, which gave

an input VSWR of 2 at 10GHz. In order to achieve a perfect match it is necessary to introduce a stub into the input port. The use of a single stub would be expected to make the device relatively narrow-band and this is verified by later results. The inclusion of a matching stub does not alter the status of the device as a three-port network, since there are still only three accessible, dissipative ports. There is no conflict, when seeking conditions to match this device with the three-port network theorem which states that 'a lossless, reciprocal three-port network cannot be simultaneously matched at all three ports'. Reciprocity in this theorem implies that $S_{mn} = S_{nm}$ where m and n denote arbitrary ports in a three-port network. A three-port ring with a matching stub does not exhibit symmetry about the three ports and $S_{mn} \neq S_{nm}$. Consequently a perfect match is theoretically possible without violating the three-port network theorem. Indeed, with the correct separations, a match is theoretically possible in a three-port ring structure which does not include a matching stub. An example of this situation is the conventional four-port hybrid ring in which the isolated port has been removed. Test circuit CCT3.14 shows the conventional hybrid ring layout. If port 1 is the input port, it follows from standard theory that there will be zero output from port 3, which could therefore be removed without altering the circuit conditions. A hybrid ring could thus be converted to a three-port device which is matched at all three ports. Measurements shown in Fig. 3.21, p. 127 support this argument, by showing that there is no significant change in the input match when the isolated port is either open-circuited or removed altogether. Thus, over a limited frequency range, the converted hybrid ring will function as a matched, lossless power splitter and provides an economic alternative to the Wilkinson power splitter, which requires a load to simulate a fourth port with a consequent loss of power. The obvious limitation of the three-port power splitter, compared to the Wilkinson device, is its limited bandwidth.

The conditions, i.e. port spacings, which provide the matched arrangement of the hybrid ring are not consistent with those for obtaining frequency discrimination. The modified theory presented earlier for a three-port ring with the input port (1) in an arbitrary position was developed to enable an optimum position for this port to be found which would provide a simultaneous match on all three ports. It was not straightforward with this theory

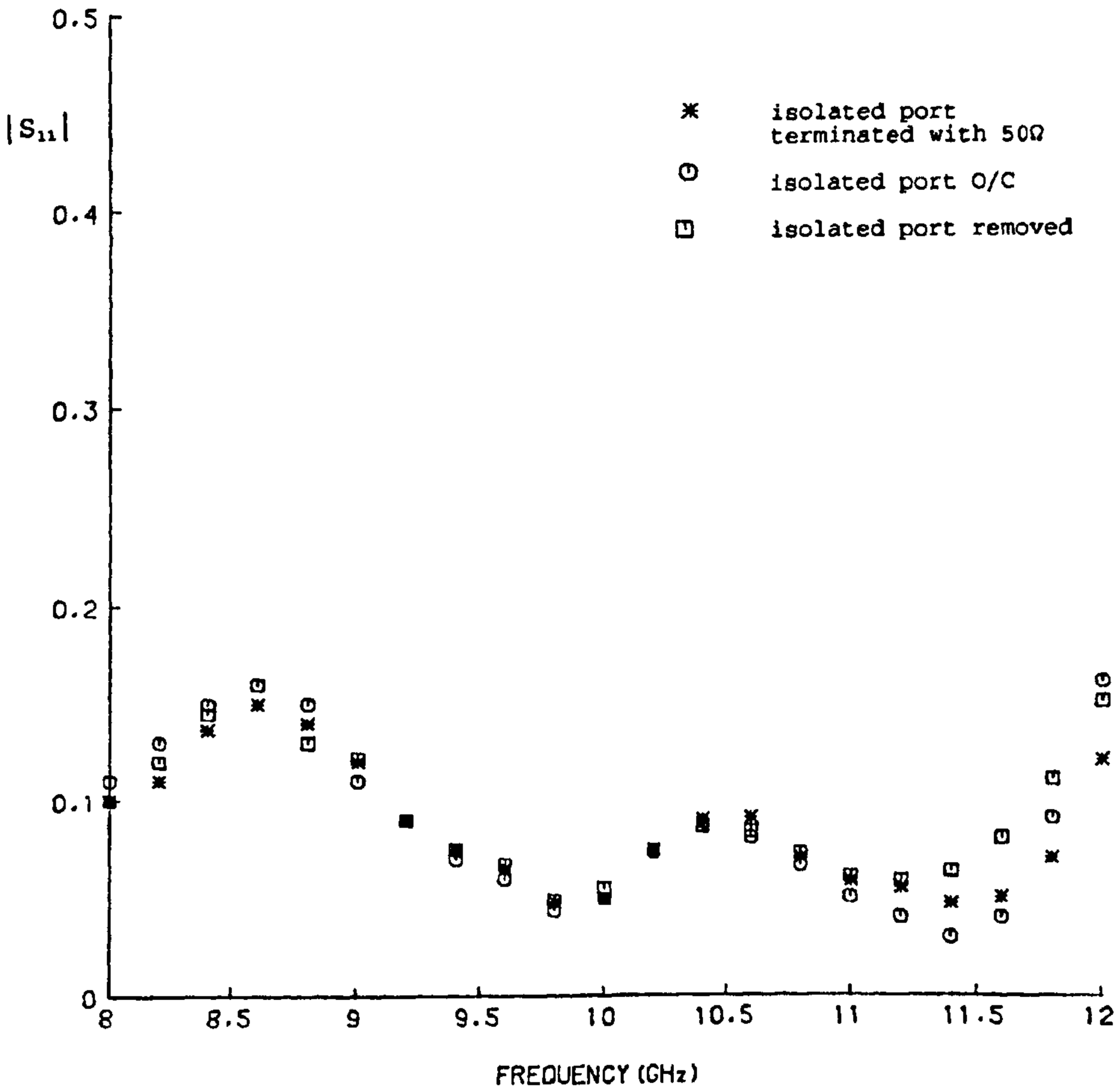

Figure 3.21: **Measured data showing the effect of open-circuiting or removing the 'isolated' port in a conventional four-port hybrid ring.**

to find such a solution which would isolate the dummy fourth port, and it must be concluded that the three-port ring will always exhibit some input mismatch.

A significant difference between the three-port ring discussed in this chapter and the conventional four-port hybrid ring is that reflections which arise at the T-junction discontinuities do not cancel at the input port as they

do in the hybrid ring. Thus the investigation of the three-port circuit requires the effects, characterization and compensation of the T-junctions to be considered. However, there are some problems in performing a theoretical analysis in terms of the reflections due to T-junction discontinuities. The circuit analysis approach which has been adopted in the earlier sections cannot accommodate the effect of multiple reflections in the ring which occur due to the T-junction mismatches. A possible alternative approach would be to consider the propagation of a wavefront around the ring, and to use a convergent series to sum the reflections which occur. This would be a cumbersome method of analysis and is limited by the information available on the T-junctions. Whilst there is a significant amount of information in the literature on the magnitudes of the circuit coefficients describing microstrip T-junctions, such as that given by MEHRAN [29], there is a lack of data on the phase behaviour of these junctions. However, since there are some well established equivalent circuits for this type of junction it should be possible to extend the published data to include the phase responses, and this would seem to be the next logical step in developing the ring theory.

3.8.2 Comparison between measured and theoretical data

The measured discriminator responses shown in Fig. 3.22, p. 129 for small circular rings were unsatisfactory. While the responses exhibit the general trend of the theoretical response a significant distortion, in the form of a knee, was evident in the characteristics in the vicinity of the zero crossing points. Several circuits were measured and all showed the same effect. There are three possible explanations for this distortion: (i) a resonance within the ring whose frequency is dependent upon the port spacing - this would be consistent with the measured responses showing the distortion occurring in the same relative position for the three rings of slightly different sizes; (ii) a peculiarity associated with curvature effects and not allowed for in the theory; (iii) a resonance determined by the whole structure, analogous to resonance in a circular disc. Measurements, Fig. 3.23, p. 130, on a small rectangular ring having the same port spacing as the basic circular ring did not show the same distortion, which suggests that the effect is not caused

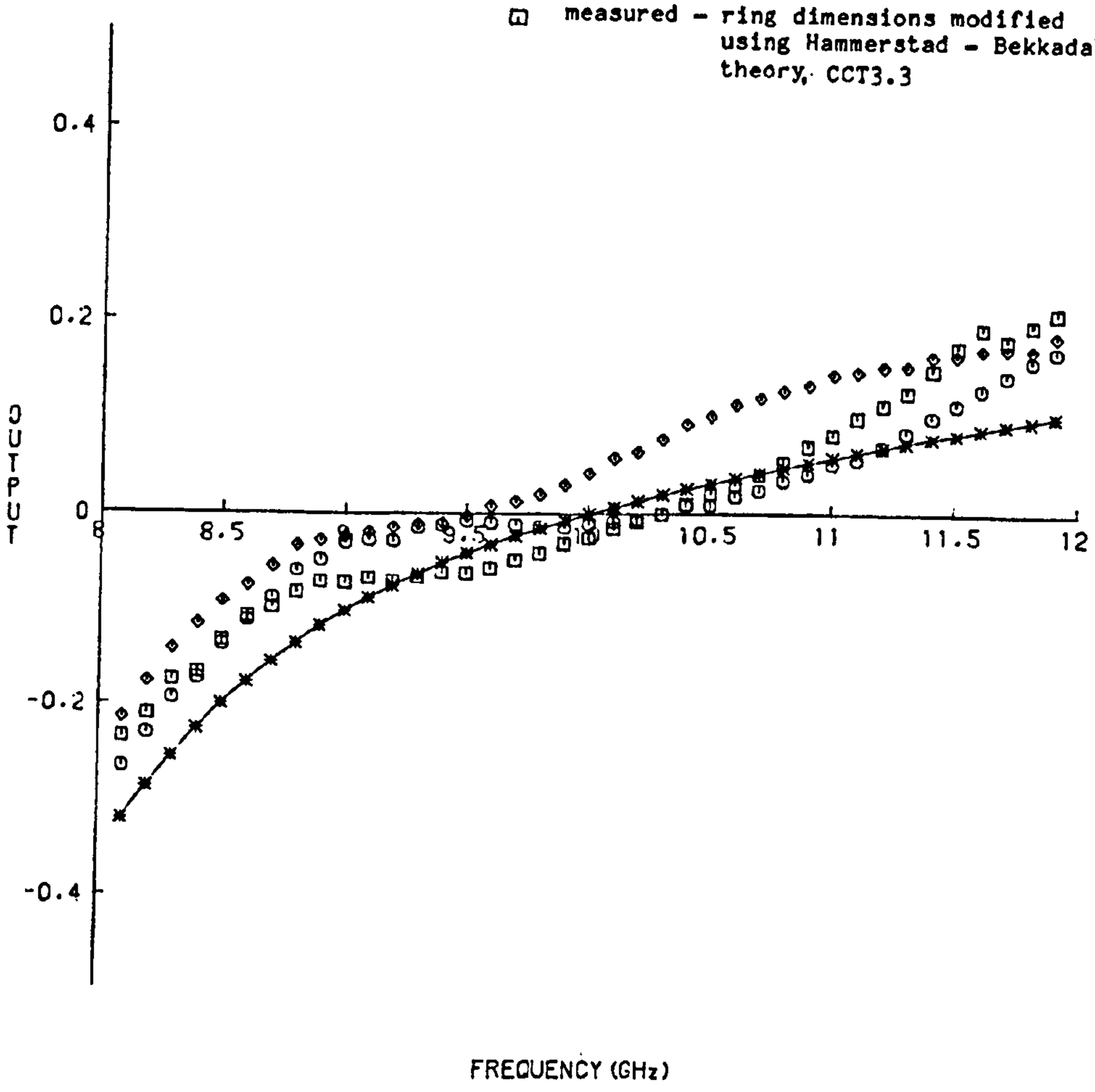

Figure 3.22: Comparison between measured and theoretical data for small circular three-port rings

by non-cancelling reflections producing a resonance associated with the port spacings. This conclusion is further supported by measurements, Fig. 3.24, p. 131, on a larger circular ring where one of the port spacings has been increased by a multiple of λ. In this case the measured results do not show any distortion in the vicinity of the zero crossover. The practical results here show good agreement with the theoretical response, although there is a slight displacement in frequency of the measured data. Similar differences between

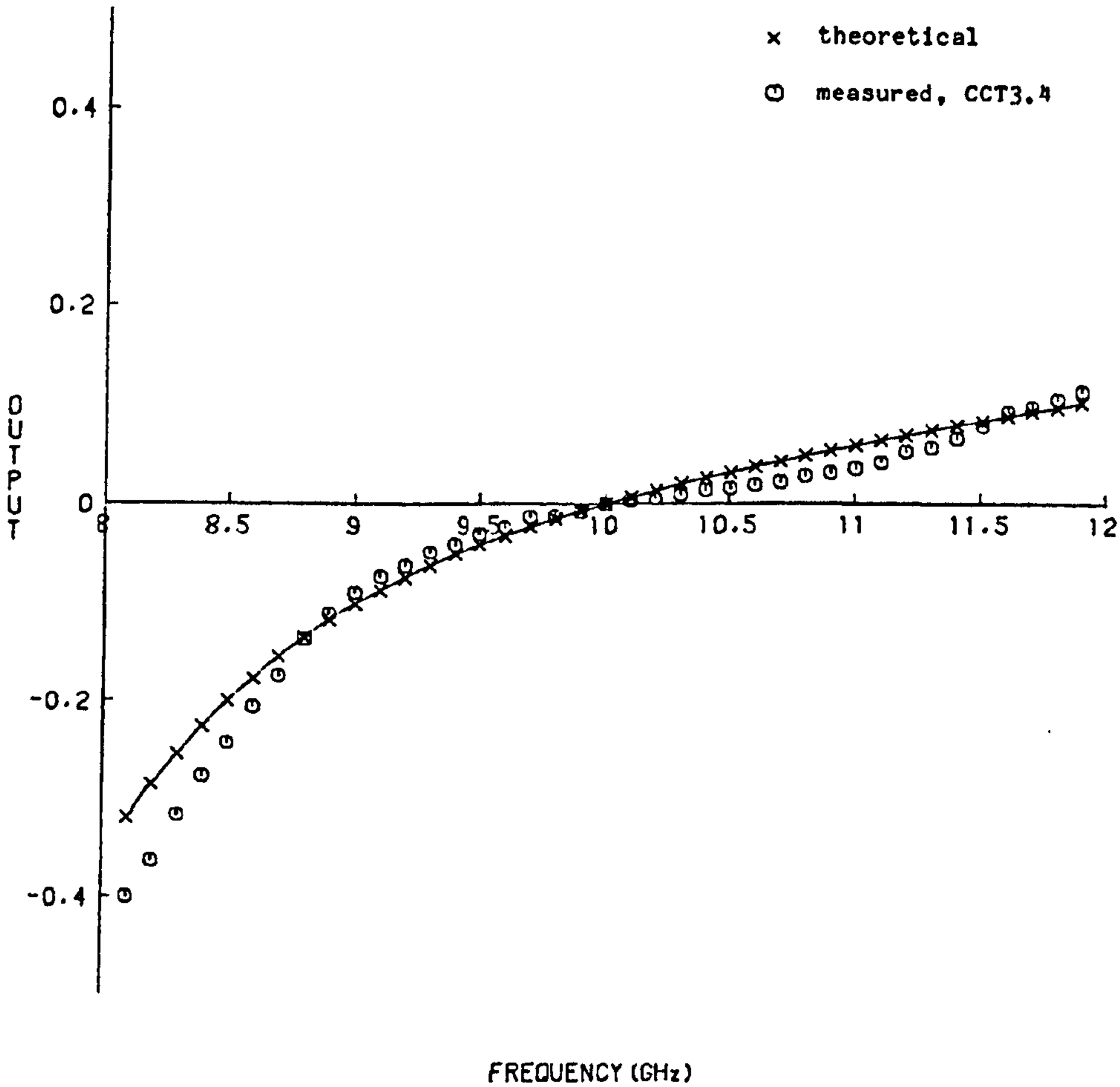

Figure 3.23: **Comparison between measured and theoretical discriminator responses for small rectangular three-port ring**

the performance of the small and large circular three-port ring can be seen in Fig. 3.25, p. 132 and Fig. 3.26, p. 133 where the magnitude of the input match is plotted as a function of frequency. Again, there is relatively good agreement between the measured and theoretical data in the centre of the frequency band for the large ring, but poor agreement for the small ring.

Curvature effects would normally alter the effective relative permittivity of the microstrip ring, which would cause a change in the ring wavelength and

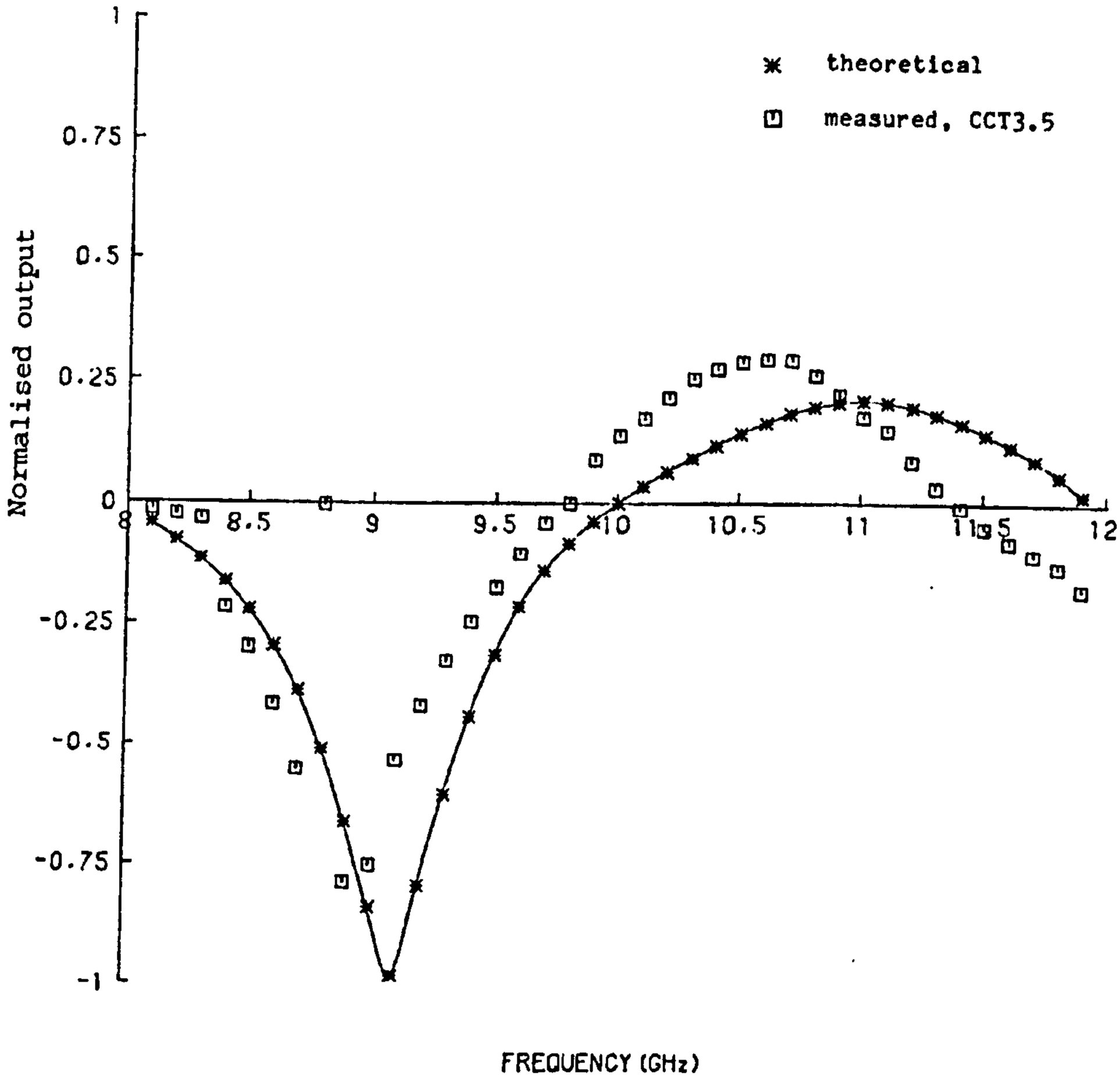

Figure 3.24: Comparison between measured and theoretical discriminator responses for a large circular three-port ring

could account for the measured and theoretical responses being displaced in frequency. OWENS [34] has investigated curvature effects in ring resonators and his results indicate that, for the combinations of track widths and ring diameters used here, the curvature effect is negligible. The most plausible explanation would seem to be that there is a resonance associated with the overall structure of the small rings. This argument is supported by measurements on larger circular rings, which do not show this effect, and where

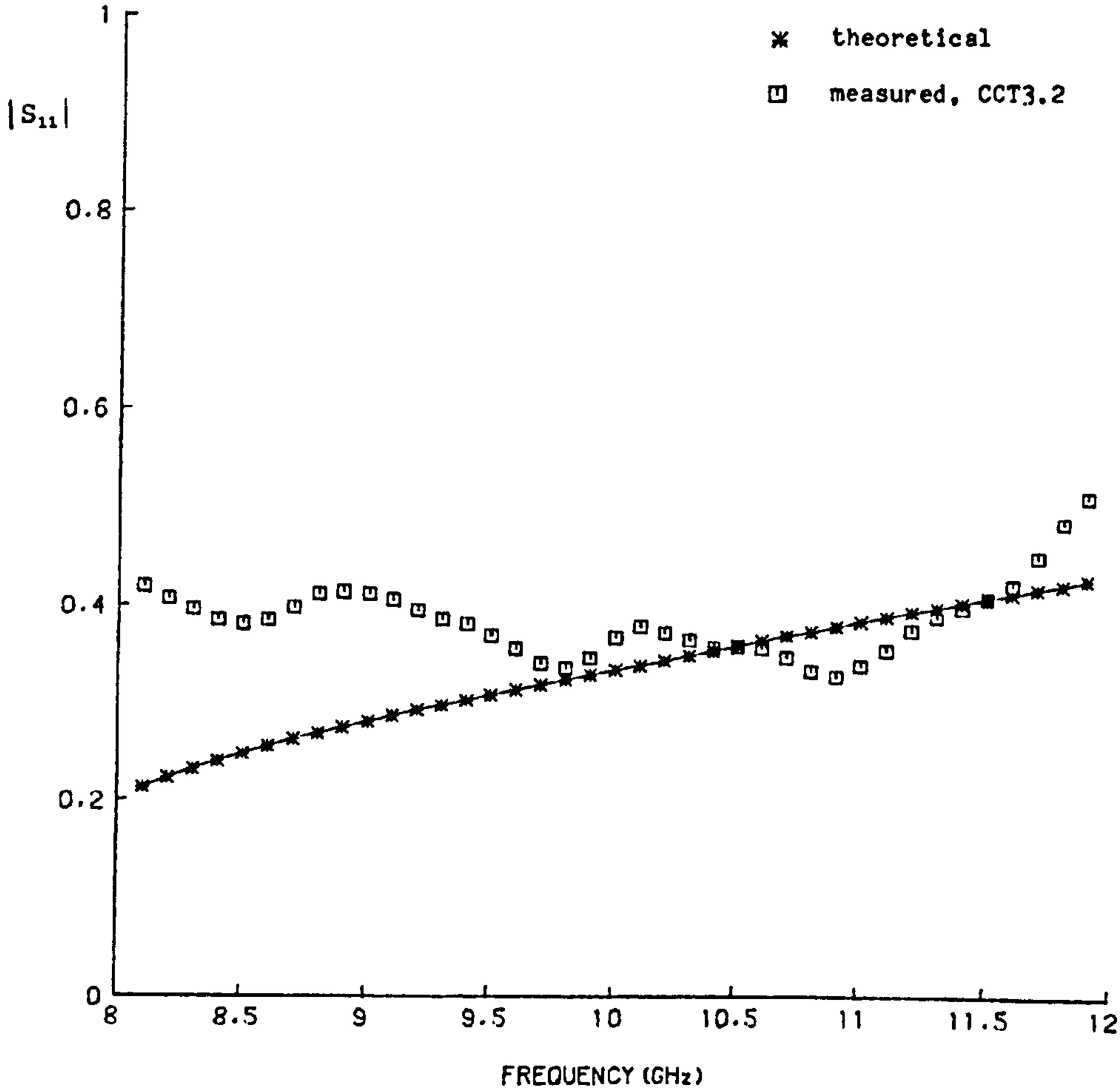

Figure 3.25: **Comparison between measured and theoretical input match for small circular three port ring**

the coupling across the ring would be small. The small rectangular ring tested did not show the effect, but then neither of the principal dimensions was equal to the diameter of the small circular rings. However, the practical significance of this distortion in small circular rings is not serious since the small rectangular version performs satisfactorily, and is the easier shape to fabricate. Indeed, larger rings are potentially more useful in that they give increased discriminator sensitivity and the increased size permits the

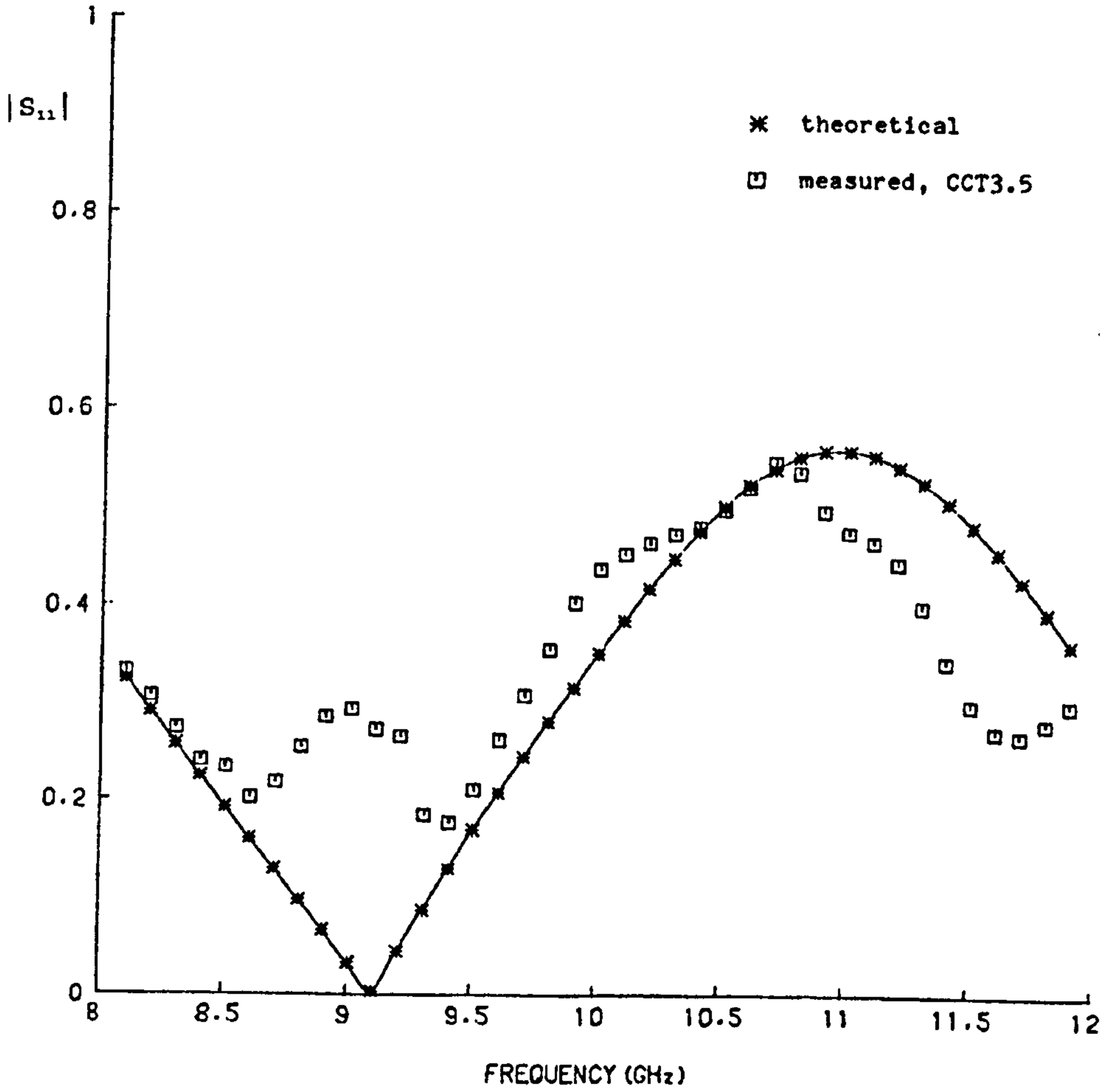

Figure 3.26: **Comparison between measured and theoretical input match for large circular three port ring**

inclusion of switched phase shifters.

The results presented in Fig. 3.22, p. 129 also show how the responses are displaced in frequency due to the port spacings being modified to account for the T-junction discontinuities. It would be expected that a relatively small change in the port spacings would cause a significant displacement of the discriminator zero crossing point. For example, a change of $50\mu m$ in a nominal $\lambda/4$ spacing at 10GHz represents a change in the zero crossing

point of 173MHz. If the working region of the discriminator is to be defined on the frequency axis with reasonable precision it is clearly necessary to establish the exact port separations. This requires an accurate knowledge of the equivalent line lengths associated with the T-junction equivalent circuits. The $50\mu m$ value used in the above example is the order of difference between the equivalent line lengths given by EASTER ET AL [28] and by HAMMERSTAD AND BEKKADAL [16]. Fig. 3.22, p. 129 indicates that Easter's results give the best agreement with theory for the crossing points. The Easter values were subsequently used for rings with better behaved responses and, in general, good agreement between theory and measurement was obtained. In the case of a large rectangular ring it was found that the difference was 0.051GHz, which was close to the limits imposed by experimental error. The observed effects in respect of equivalent line lengths seem to accord with the comments made by EDWARDS [33] who cites a private communication from HALL and JONES who apparently found that the HAMMESTAD AND BEKKADAL [16] semi-empirical expressions gave values for the T-junction equivalent circuits which were too high when compared with their measurements. It was claimed that this error increased with frequency and approached 200 per cent at 17GIIz.

The measured discriminator responses for rectangular rings, Fig. 3.23, p. 130 and Fig. 3.27, p. 135, show good agreement with theory in the centre of the X-band range. Fig. 3.28, p. 136 shows an expanded discriminator response for a large rectangular ring over a 10 per cent central bandwidth. It shows an error of 0.5 per cent in the zero crossing point and there is a standard deviation of 0.02 between the measured and theoretical values. The error of 0.5 per cent in the crossing point would be acceptable for many discriminator applications, although the significance of small errors in the crossing point in the context of the frequency control system being considered in this report will be discussed in a later section. The measured data shows less agreement with theory towards the edge of the band and this may be due to interactions between the expected mismatch of the ring and mismatches due to discontinuities. Fig. 3.29, p. 137, which compares measured and theoretical input reflection coefficients for a small rectangular ring, shows evidence of secondary, frequency selective mismatches through the existence of a ripple in the response. The results, Fig. 3.30, p. 138, for the input match

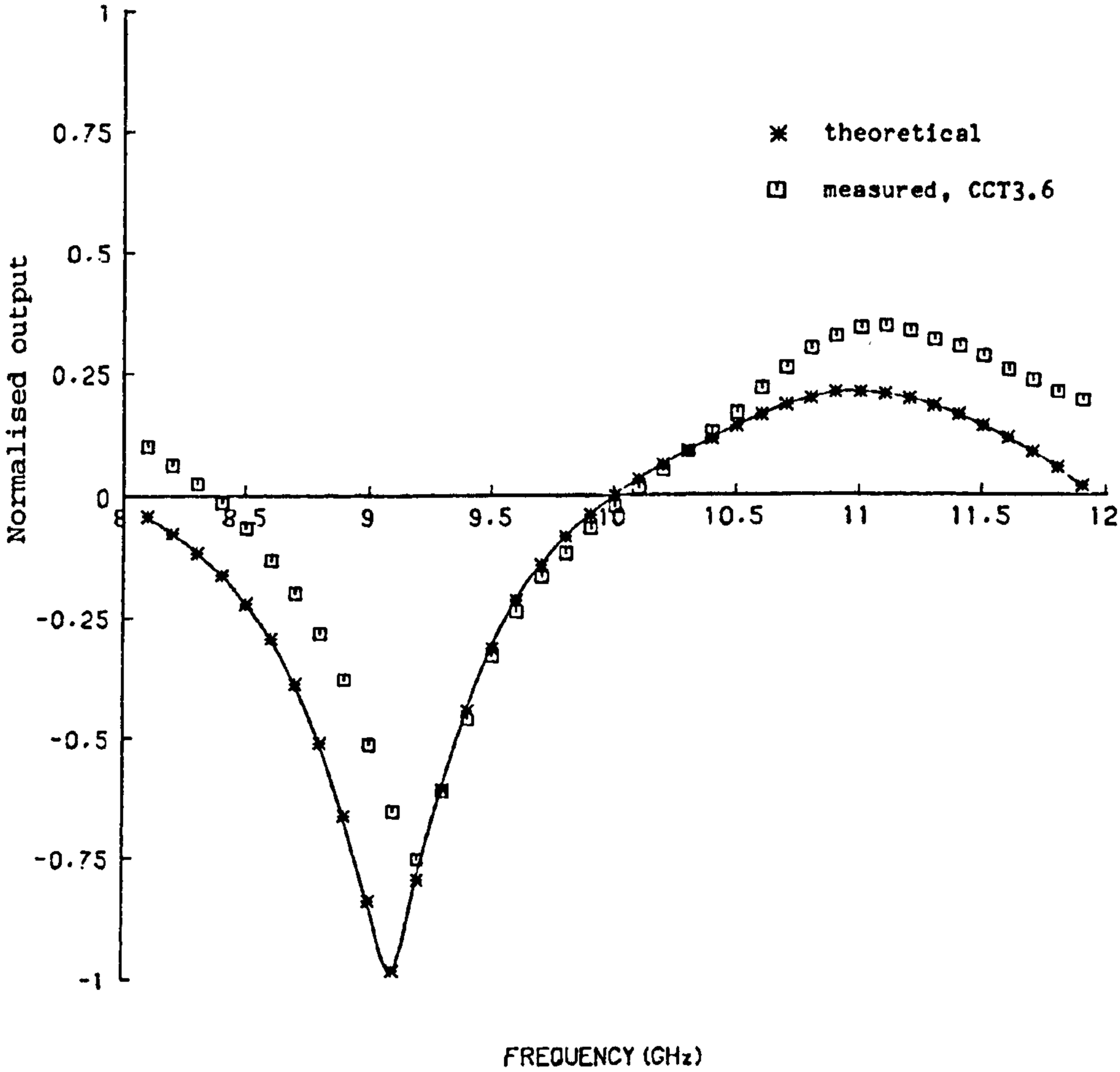

Figure 3.27: Comparison of measured and theoretical discriminator responses for a large rectangular three-port ring with input stub matching

of a large rectangular ring, show reasonable agreement between theory and measurement. A further improvement was obtained, Fig. 3.31, p. 139, by compensating the measured input match data to allow for the OSM coaxial-to-microstrip launcher discussed in an earlier section. The compensation was based on measurements of the launcher's excess phase, shown in Fig. 3.32, p. 140 and the manufacturer's VSWR data.

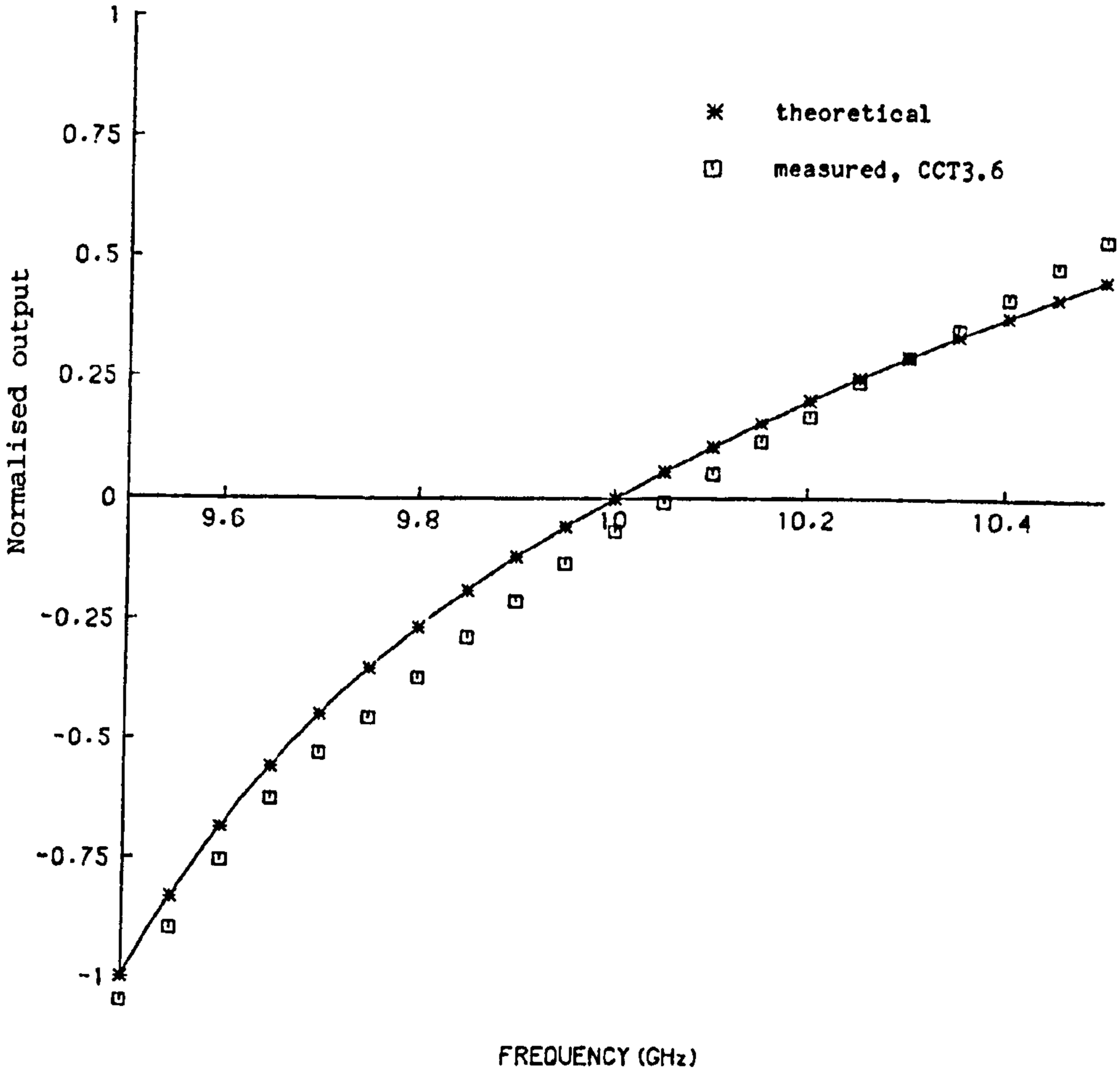

Figure 3.28: **Comparison of measured and theoretical discriminator responses for a large rectangular three-port ring with input stub matching: shows detail of central frequency region (CCT3.6)**

The measured excess phase was in general agreement with the results of GOURLEY AND CHAPMAN [32]. A launcher VSWR of 1.1 was assumed, based on the manufacture's quoted maximum value at 10GHz. This value is obviously a potential source of error and an additional improvement in the results may be obtainable if a measured value of launcher VSWR could be found. A further source of error relating to launcher compensation is

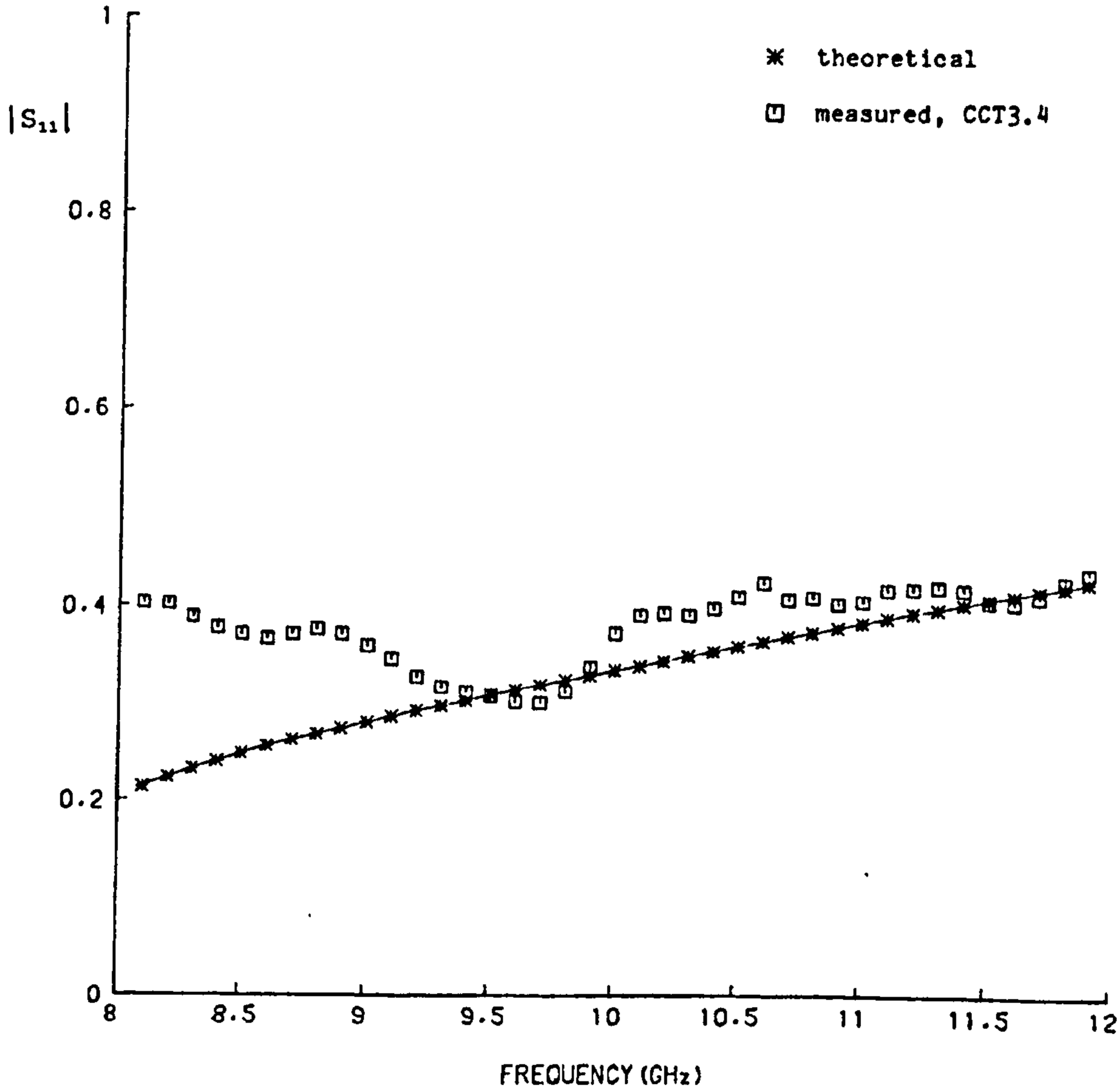

Figure 3.29: **Comparison between theoretical and measured input match for a small rectangular ring**

the reproducibility of the launcher connection. This problem was addressed by GOURLEY AND CHAPMAN [32], but only in respect of connections to Alumina substrates. The problem is considerably accentuated when soft substrates such as RT/duroid are being used. As was mentioned earlier, all of the practical circuits reported here were made on this particular soft substrate. A difficult compromise has to be achieved when assembling tab type launchers on this type of substrate, between obtaining a good electrical con-

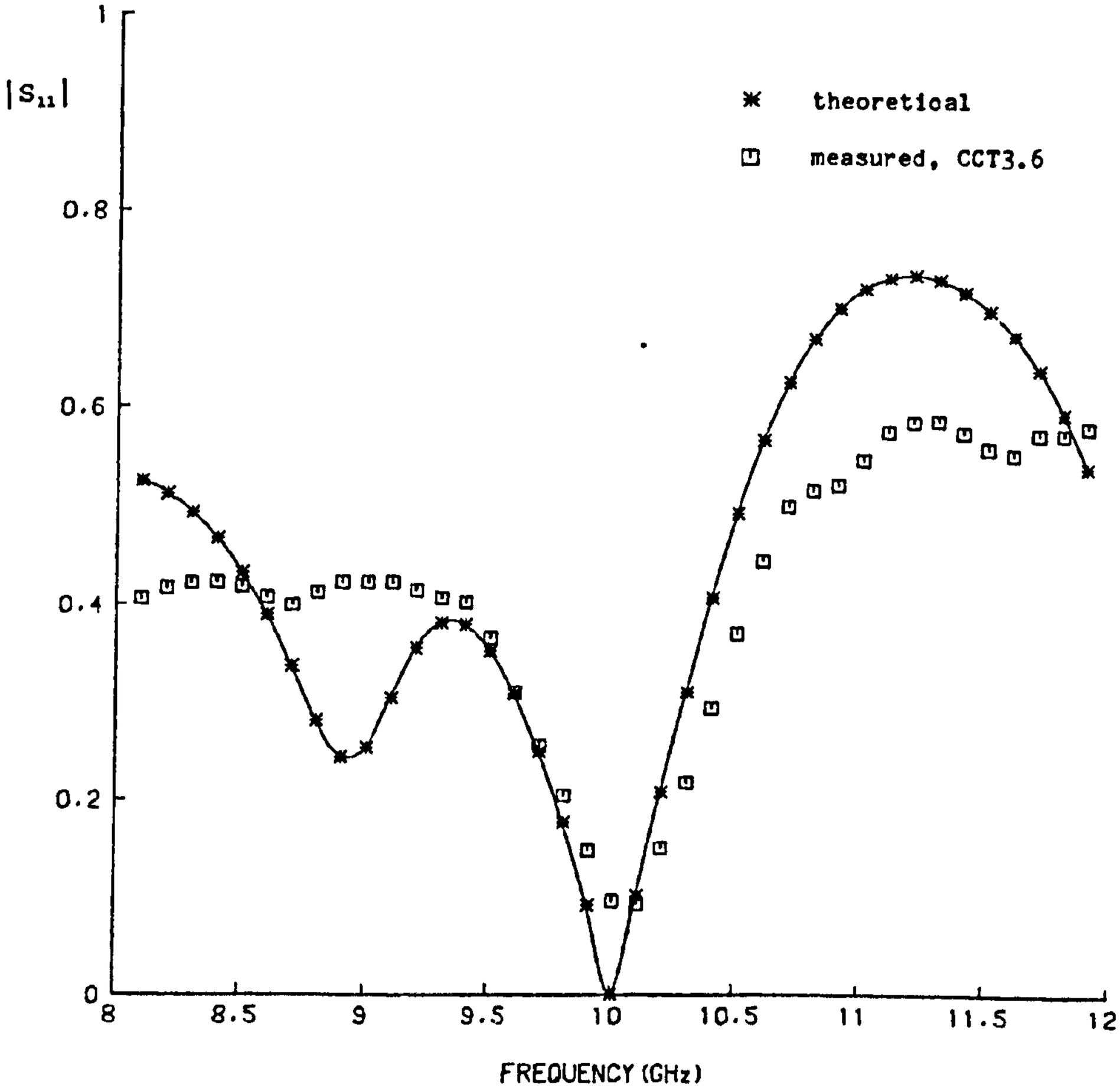

Figure 3.30: **Comparison between theoretical and measured input match for a large rectangular ring**

tact and damaging, or even shearing, the end of the copper microstrip track. Clearly, if the assembly of the launcher on the test circuit is not equivalent, in mechanical terms, to the assembly on the launcher characterization circuit, the method is prone to error. It would be useful to investigate the extent to which track and substrate deformations affect the parameters of the launcher equivalent circuit. In Fig. 3.31, p. 139 it is seen that the compensated data not only improves the best match value, to 0.04, but gives a better overall fit

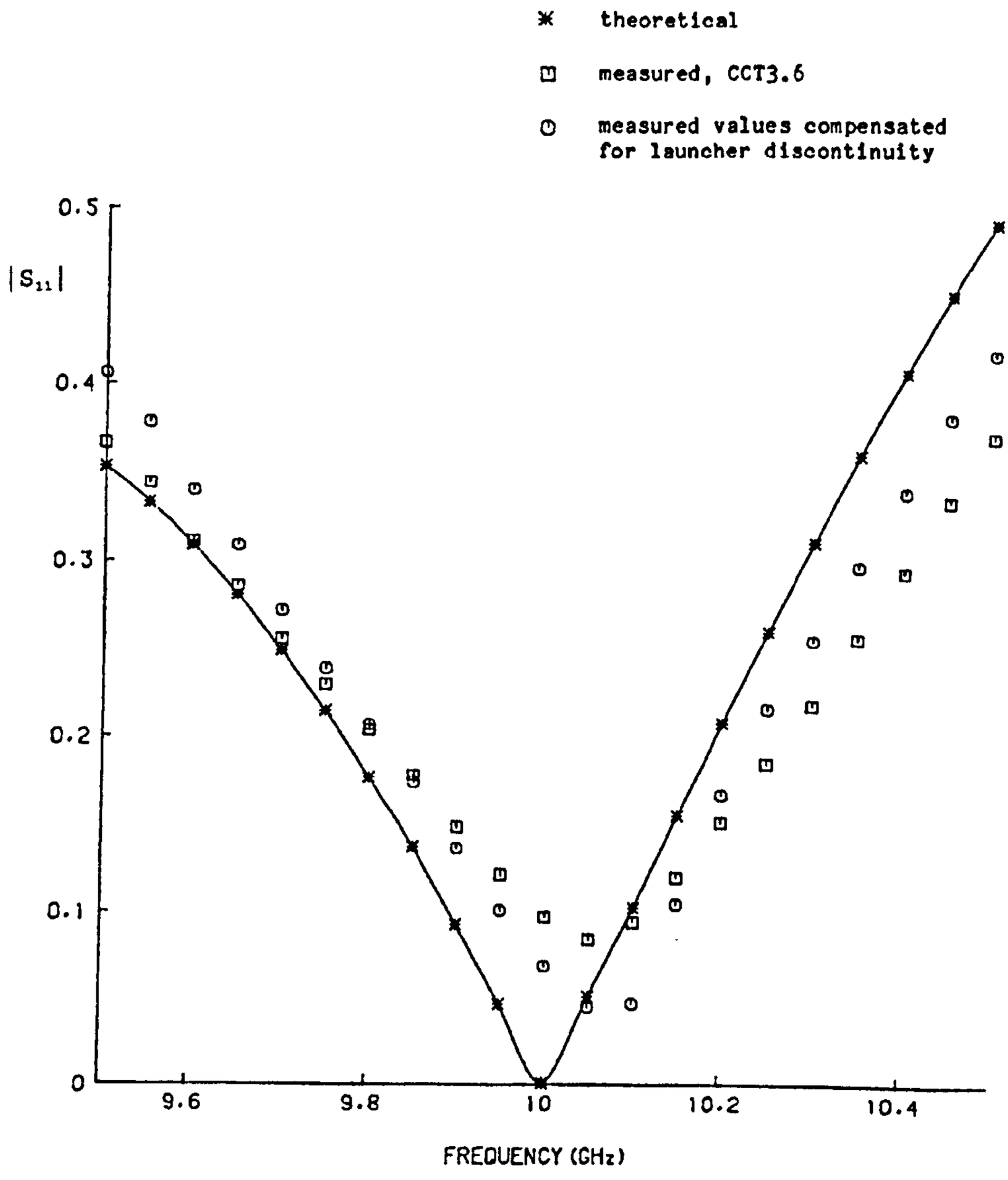

Figure 3.31: Comparison between theoretical and measured input match for a large rectangular ring, showing the effect of compensating for the discontinuity introduced by the launcher in the test jig

to the predicted response, which indicates the usefulness of this compensation technique.

In an attempt to minimise reflections in the ring due to the T-junctions, circuits were tested which included modifications to the microstrip geometry to compensate for the junction discontinuities. Two compensation methods

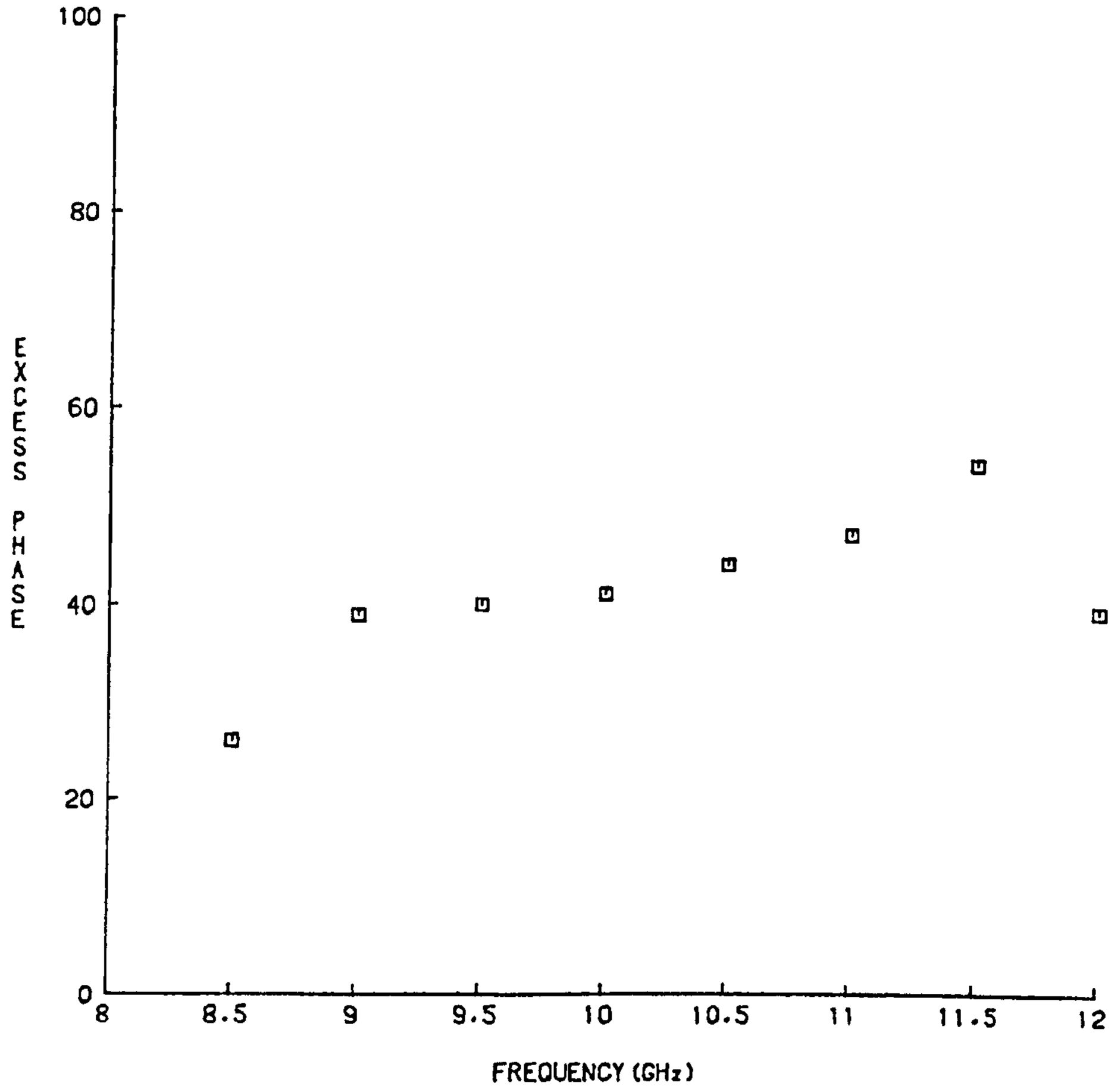

Figure 3.32: Measured excess phase (in degrees) of coaxial-to-microstrip transition (OSM-14107A)

were investigated: firstly, the method described by DYDYK [30] and secondly, simple stub compensation. Fig. 3.33, p. 141 compares the match of a circuit with and without the Dydyk compensation. It can be seen that there is little difference between the two sets of measured data over the central range, although the compensated results gave a marginally better fit to the theoretical response. Towards the edge of the frequency range measured, the compensated circuit showed a greater deviation from the predicted response,

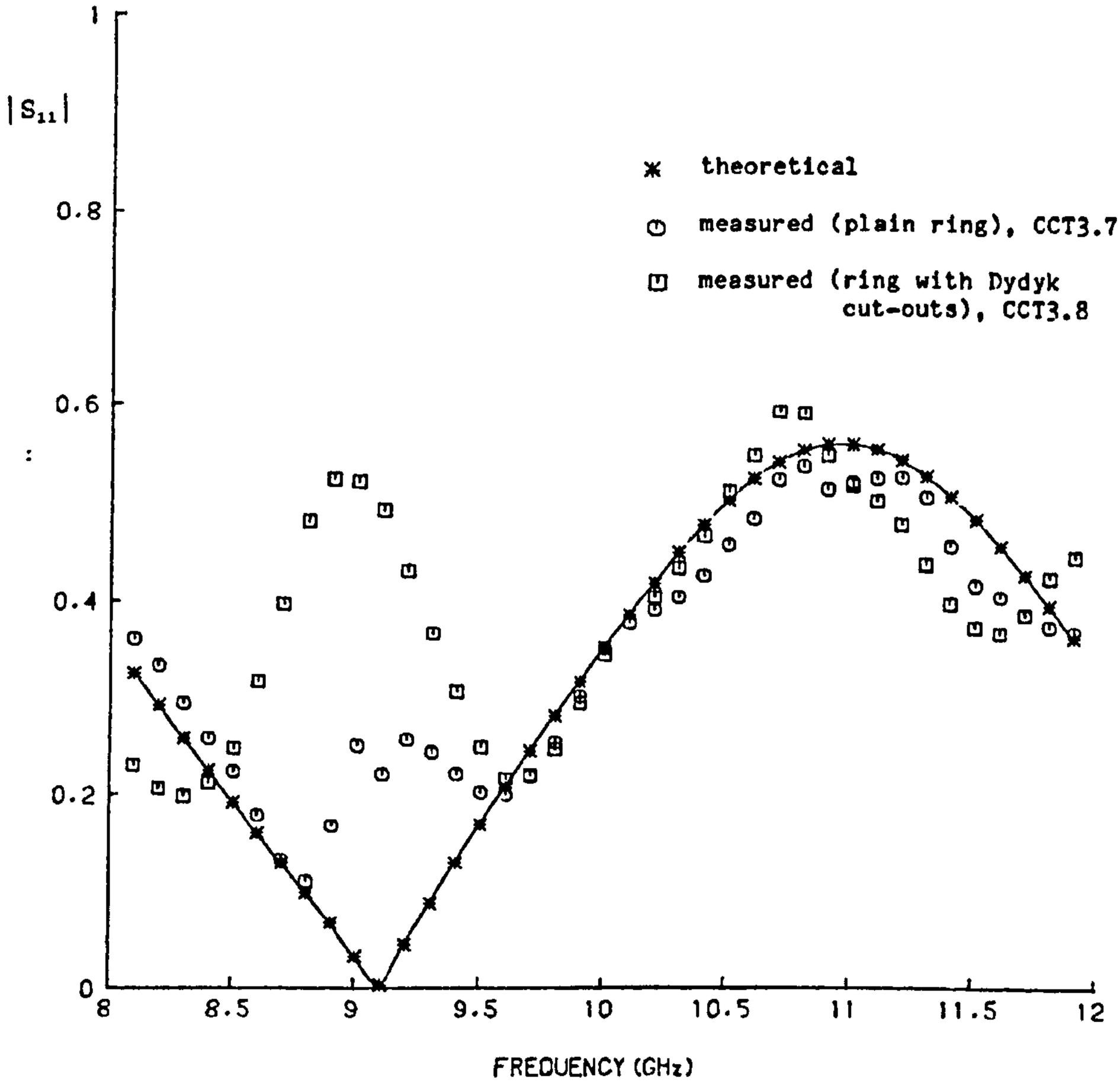

Figure 3.33: Comparison between measured and theoretical input match for a medium size circular three-port ring, showing the effect of introducing T-junction compensation using the Dydyk technique

presumably due to the frequency sensitive nature of the Dydyk modification. Whilst the Dydyk method indicates some slight improvement, the results are not impressive. The reason for this may be related to some aspects of Dydyk's method which seem unsatisfactory. As indicated in the earlier section on compensation techniques, this method changes the geometry of the T-junction by introducing what are effectively short matching sections of line.

Thus the parameters of the original T-junction change when the compensation is applied, making the use of the original design parameters (for the unmodified junction) invalid. This in not taken into account in Dydyk's theory, which seems to require a more extensive analysis involving an iterative procedure. Moreover, Dydyk's paper does not give dimensions, or substrate details, relating to the test circuits for which he quotes results. Thus the test results cannot be confirmed. To achieve the general configuration given in Dydyk's paper for a compensated junction, and reproduced in Fig. 3.14, p. 111, a low permittivity substrate would be required. The extension of the technique to high permittivity materials, with the consequent reduction in substrate wavelength, is questionable as it leads to the somewhat distorted re-entrant shape described earlier. It is unlikely that this is behaving in the intended manner. Dydyk gives results for two circuits which include junction compensation, a single pole, double throw (SPDT) switch and a branch line coupler, which are unconvincing. The SPDT switch results show an insertion loss varying between 1dB and 3dB, between 15.5GHz and 17.5GHz. Such a large variation, together with what seems a higher order of loss for a switch at these frequencies, would tend to swamp the mismatch losses due to the T-junction. It would have been more illuminating, in assessing the effectiveness of the compensation technique, if the results had been presented for the the circuit with and without the junction modification. The branch line coupler also seems a poor choice of circuit to demonstrate the technique, since reflections due to the T-junctions would tend to cancel by virtue of the $\lambda/4$ spacings between the junctions. As with the SPDT switch, the results do not show the improvement due to the modification. EDWARDS [33] and GUPTA ET AL [36] both cite the Dydyk method as a useful technique, although neither author gives any further results or applications. It would seem useful to investigate the validity of the Dydyk method over a wider range of frequency and for substrates of different permittivities.

An alternative compensation technique is possible, using stubs to cancel the junction shunt susceptances in a rectangular three-port ring. The results for the match of the ring, with and without stubs, are shown in Fig. 3.34, p. 143. As with the Dydyk method there was little difference over the central frequency range due to the presence of the stubs, but some difference is evident at the band edges, presumably due to the frequency sensitive nature

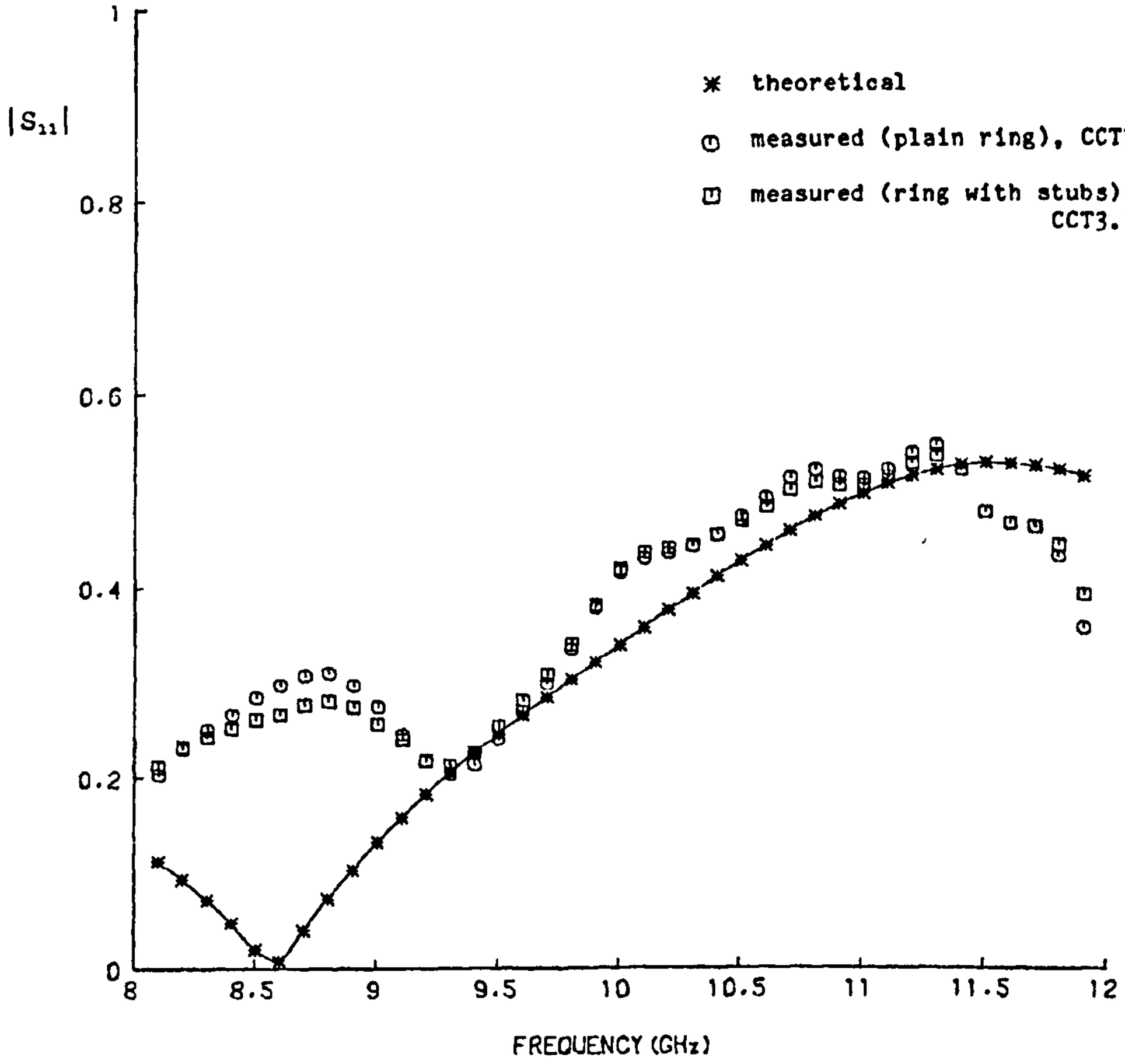

Figure 3.34: **Comparison between measured and theoretical input match for a large rectangular three-port ring, showing the effects of applying stub compensation to each junction**

of the modification. The stub compensation technique is open to the same criticism as the Dydyk method, namely that the presence of the stubs alters the properties and hence the design parameters of the original junction it is intended to compensate. In this case a crossover junction is created. To minimise the effect of the connection discontinuity the stub impedance in the test circuits was made 80Ω, which required a stub width of$178\mu m$, which was

small compared to the other dimensions of the junction, and so should not significantly alter the electromagnetic field pattern in the vicinity of the main junction. AKELLO [35] has presented experimental data for an asymmetric microstrip crossover junction of similar geometry to that produced here by the addition of stubs in the ring. His results indicate that the arrangement can produce a significant capacitance shunt susceptance. However, insufficient data are available to interpolate a precise value appropriate to the dimensions of the junction formed here by the addition of the 80Ω stub. If the correct value of the crossover discontinuity capacitance were known it should be possible to modify the stub length to provide a frequency match.

Since the stubs appeared to have little effect on the performance of the ring, some additional measurements were made on individual, 50Ω – 50Ω compensated T-junctions to establish the effectiveness of the stub technique. It was thought possible that the stub might not be having any significant effect because of its position, on the basis that the junction could produce a standing wave pattern with a minimum opposite the junction arm. This being the position at which the stub was attached. To investigate this, two stubs giving the same total susceptance as the single stub already designed were positioned in the re-entrant corners of the T-junction, where the field is known to be significant and hence where there should be significant interaction with the stub. Fig. 3.35, p. 145 through Fig. 3.37, p. 147 compare the results for the two stub arrangements which have been discussed. They show that for the junction arm (port 1) the two techniques provide a similar improvement at the centre frequency, and give a reflection coefficient of magnitude 0.35. This is close to the ideal junction, which would cause two 50Ω impedances to be presented in parallel to port 1, giving a reflection coefficient of magnitude 0.33. The results show that the crossover stub had little effect on the mismatch in the through arm ports, but some improvement was obtained in the match of these ports using the re-entrant stubs. At 10GHz, for the dual stub arrangement, the magnitudes of S_{22} and S_{33} were 0.21 and 0.24 respectively. Experimental error could reasonably account for the difference in these values. These values would be expected to be significantly different from the ideal value of 0.33 calculated previously, since the junction viewed from the through arm ports is asymmetric. Overall, the re-entrant stubs appear to give the best compensation. However, the method has not been

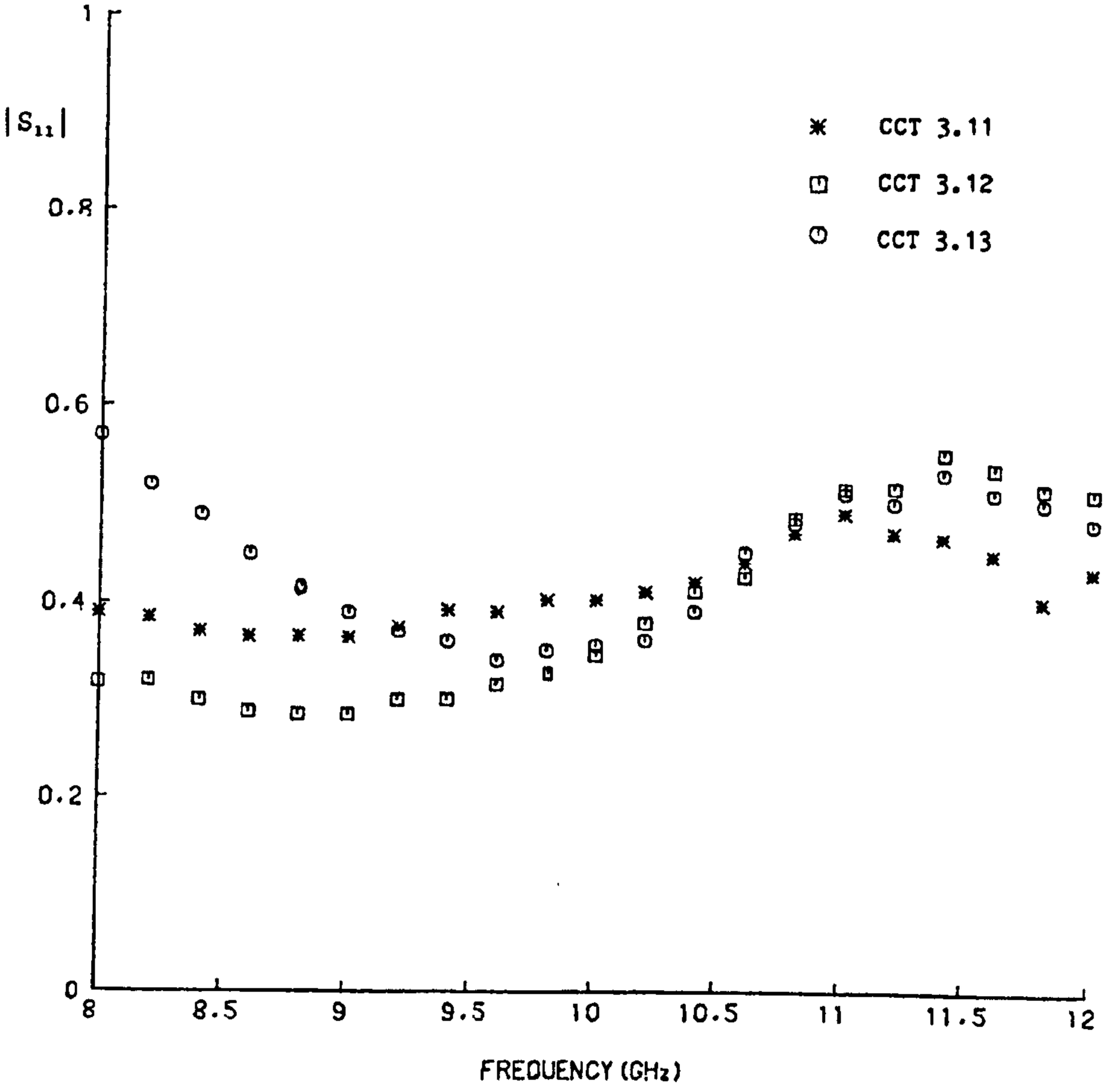

Figure 3.35: Measured data showing effects of different matching stub configurations on the magnitude of S_{11} of a T-junction

discussed in the literature and would seem worthy of further investigation.

Some further measurements were made on single stub matching of a T-junction, to see if a match could be found experimentally by varying the stub length. Effectively this would be experimentally finding the shunt capacitance of the asymmetric crossover discussed earlier. These results are shown in Fig. 3.38, p. 148 and Fig. 3.39, p. 149. It can be seen that a reasonable compromise between a match on the junction arm and a match on the

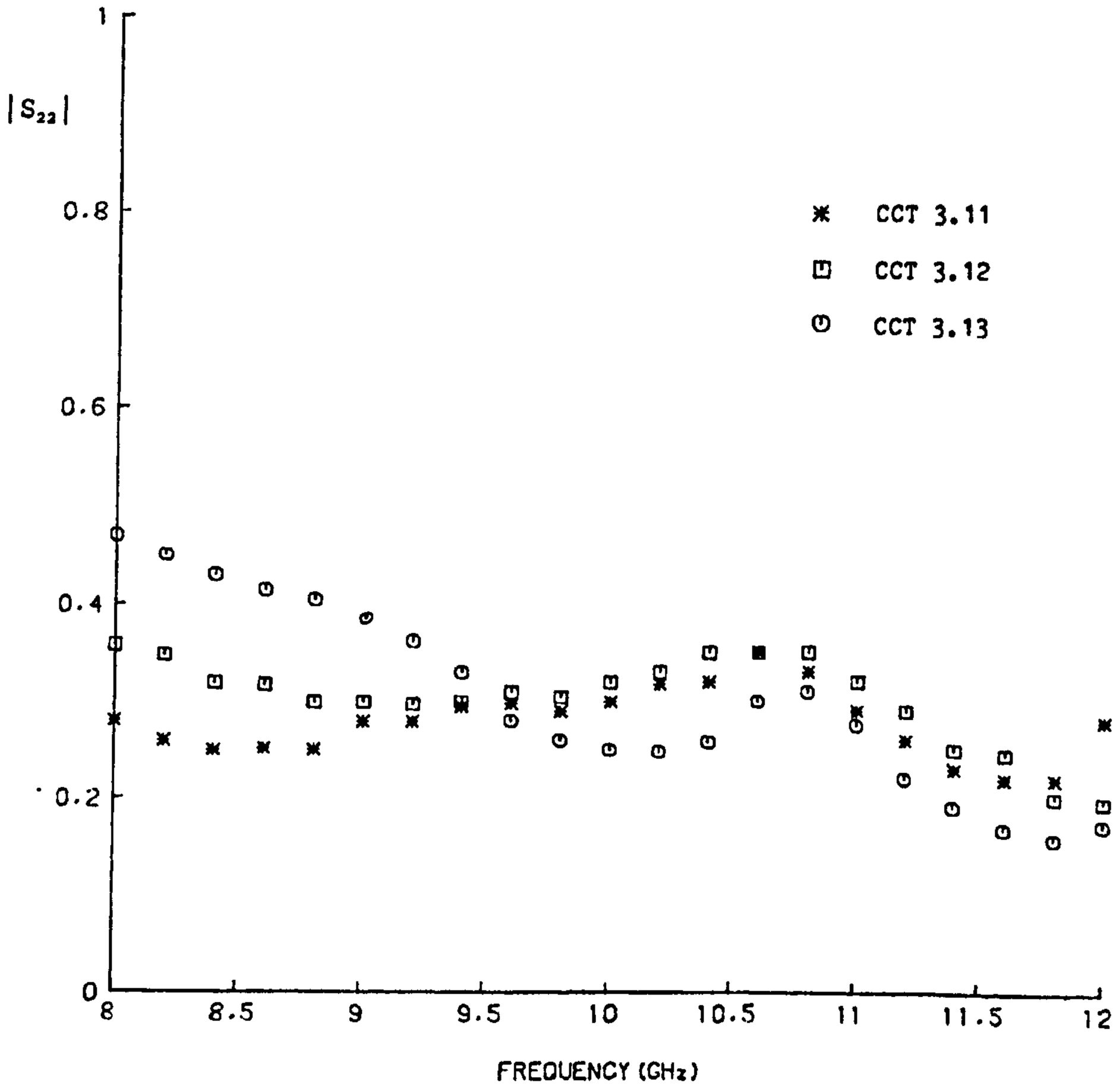

Figure 3.36: **Measured data showing effects of different matching stub configurations on the magnitude of S_{22} of a T-junction**

through arm is obtained with a stub length of 4.30mm. This is not an exact solution since the stub lengths for experimentation were selected arbitrarily, but it does indicate the order of the stub length required, and incidentally the order of the shunt capacitance provided by the crossover junction. The performance overall, with this 'optimum' stub length, is slightly inferior to that provided by the re-entrant stubs.

It is seen that the best stub length is less than the 5.35mm predicted by

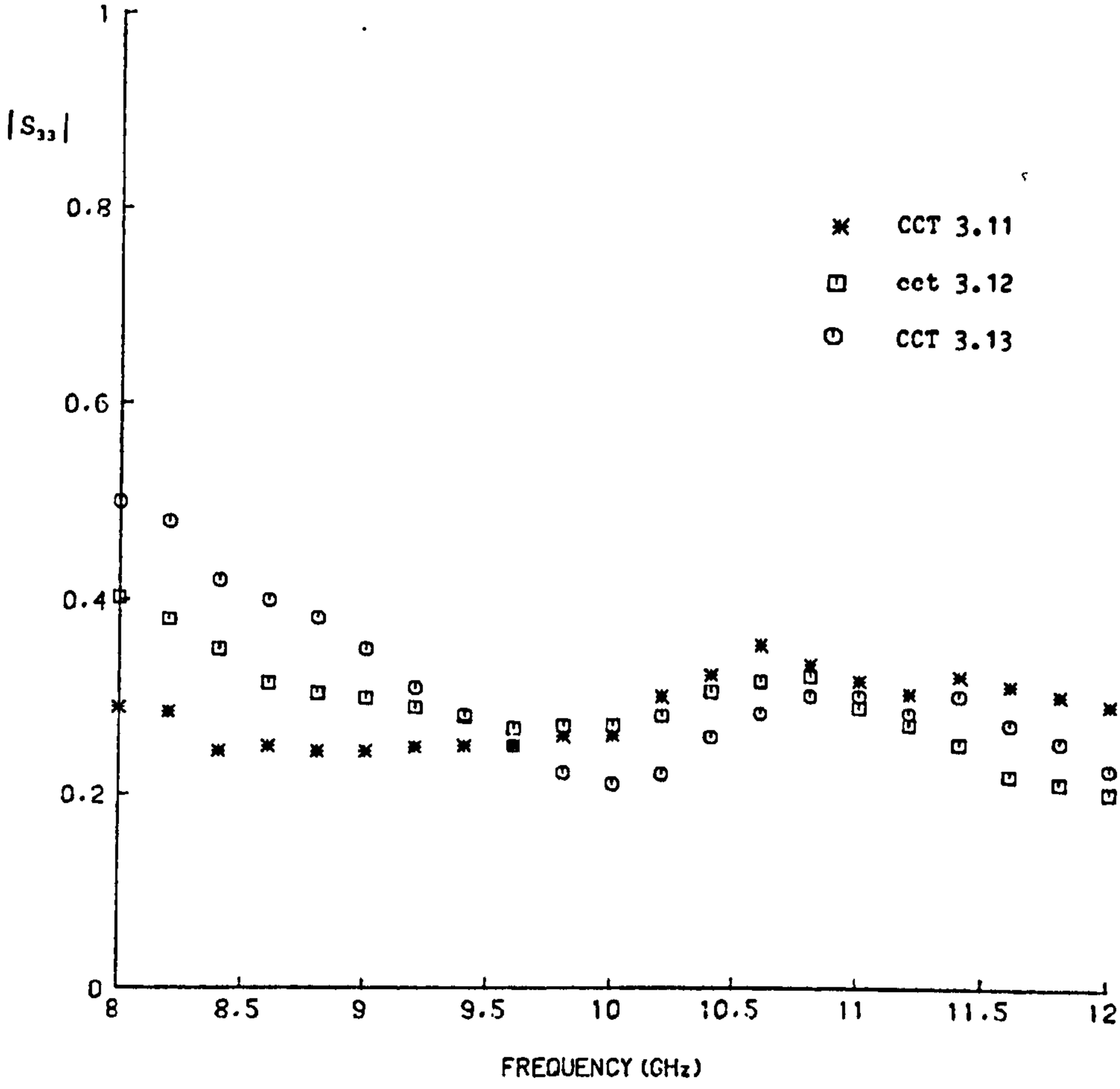

Figure 3.37: Measured data showing effects of different matching stub configurations on the magnitude of S_{33} of a T-junction

applying the theory of HAMMERSTAD AND BEKKADAL [16] to find the shunt discontinuity susceptance of the T-junction. This theory gave a value of $2.17x10^{-3}$S, whereas data from EASTER ET AL [28] gives a value of $1.21x10^{-3}$S which requires a slightly longer length of 5.43mm. It is worth noting that both sources quote reasonably large tolerances for this shunt susceptance, Hammerstad and Bekkadal 5 per cent, and Easter 12 per cent. Therefore it would appear that, even with a very narrow stub, the crossover

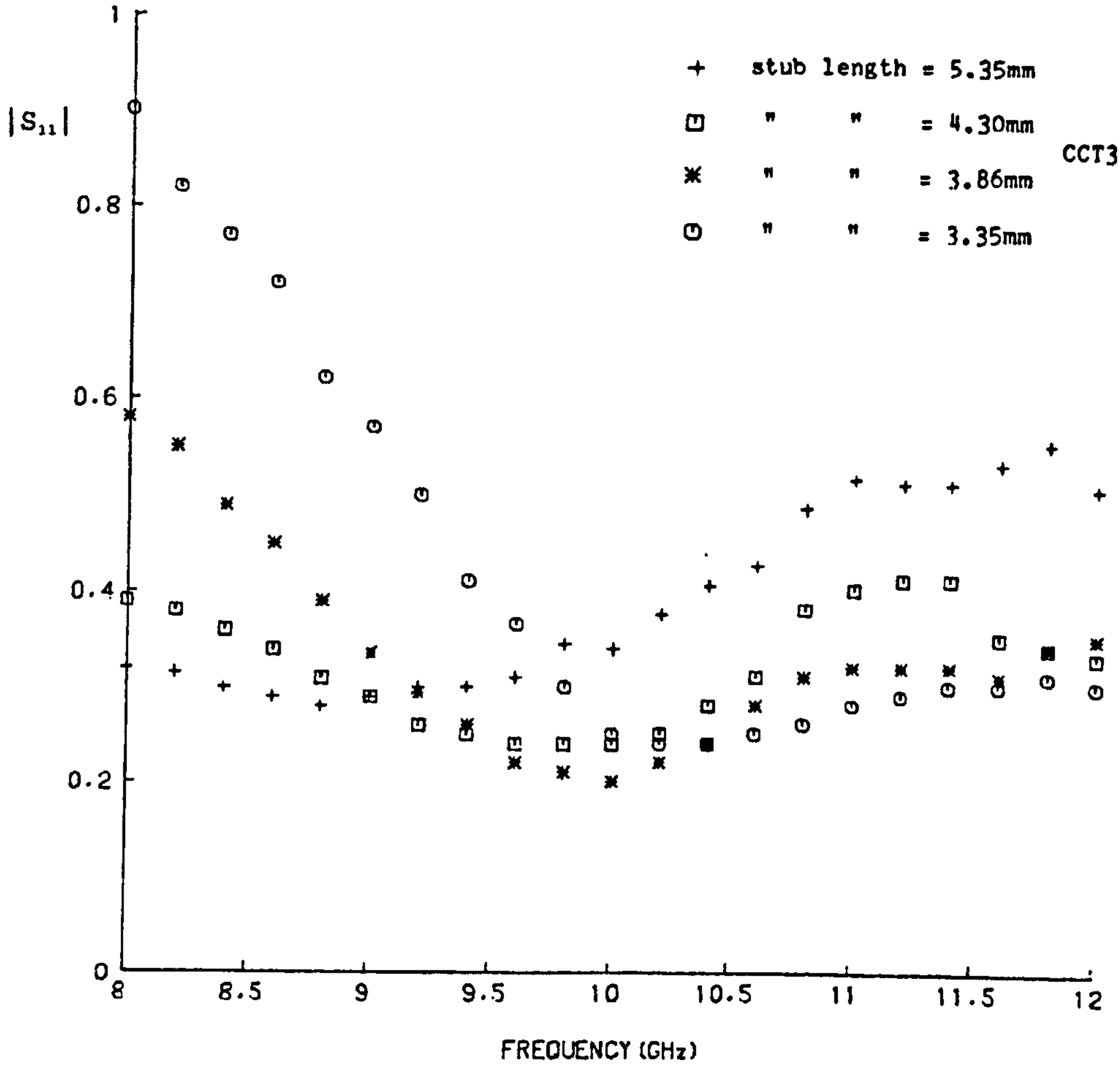

Figure 3.38: **Effect on S_{11} of experimentally varying the length of a single stub used to match a T-junction**

effect cannot be ignored.

3.9 Conclusions

The proposed three-port discriminator structure has been shown to yield useful, predictable results. In addition, it has been show that it is possible to match the device at the centre frequency. Measurements have shown good

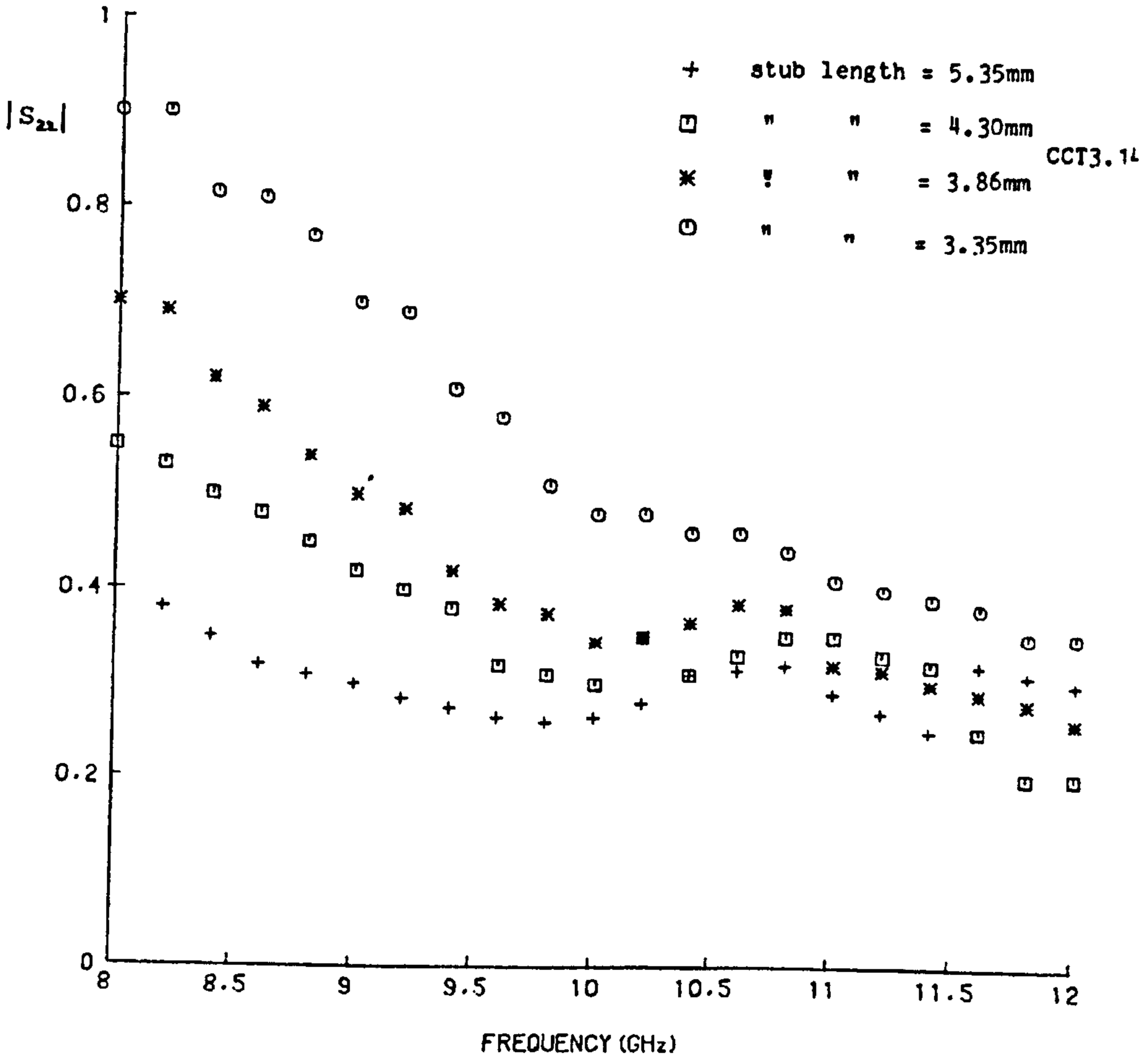

Figure 3.39: **Effect on S_{22} of experimentally varying the length of a single stub used to match a T-junction**

agreement with theory over a 20 per cent bandwidth centred on 10GHz. The

compensation for coaxial-to-microstrip launcher discontinuities in the test jig, making allowance for the excess phase of the launcher, was shown to be a useful technique.

In order to obtain good agreement between measured and theoretical discriminator responses, careful consideration needs to be given to the non-

ideal properties of the microstrip T-junctions in the ring. It was necessary, in the design of the port spacings, to include equivalent line lengths to account for the effective shift in the geometric centres of the junctions due to discontinuity effects. The data from EASTER ET AL [28] for the equivalent line lengths was found to yield better agreement between measured and theoretical results than using the expressions from HAMMERSTAD AND BEKKADAL [16].

Multiple reflections in the ring were identified as a possible source of error, but the analysis is inhibited by the lack of data on phase behaviour of the transmission and reflection coefficients of the microstrip T-junctions.

The DYDYK [30] method of compensation for microstrip T-junctions did not give any observable improvement in performance of the discriminator. Upon closer examination it appears that Dydyk's theory needs to be refined to include the effects of changes in the junction geometry. It also appears that Dydyk's method is limited, both in respect of the frequency range for which it is suitable and the type of substrate on which it can be implemented.

Of the stub compensation methods investigated, it would appear that the use of two re-entrant stubs is the most promising.

Chapter 4

Extended Analysis of Microstrip Ring Circuits

4.1 Summary

A new method of analysis of microstrip ring structures is presented, which offers a number of advantages over the traditional method which was described in the preceding chapter. The odd and even circuit approach discussed in the last chapter is somewhat restrictive in that it can only be applied to circuits where there is geometric, and hence electrical symmetry. There are some circuit components, such as the three-port ring, where this symmetry may not exist. Whilst this problem can be overcome in asymmetric structures by introducing one or more dummy ports to create symmetry, and then seeking solutions using the odd and even circuit analysis which make the signals at these ports zero, the method is cumbersome and time consuming. Furthermore, this method of approach is not particularly amenable to computer analysis.

In this chapter theoretical results are presented which demonstrate the use of the new technique in analysing symmetric and asymmetric three-port ring discriminators. In addition, for the purposes of validation, the method has been applied to the traditional four-port hybrid ring and the results compared to the well-known frequency responses for this component.

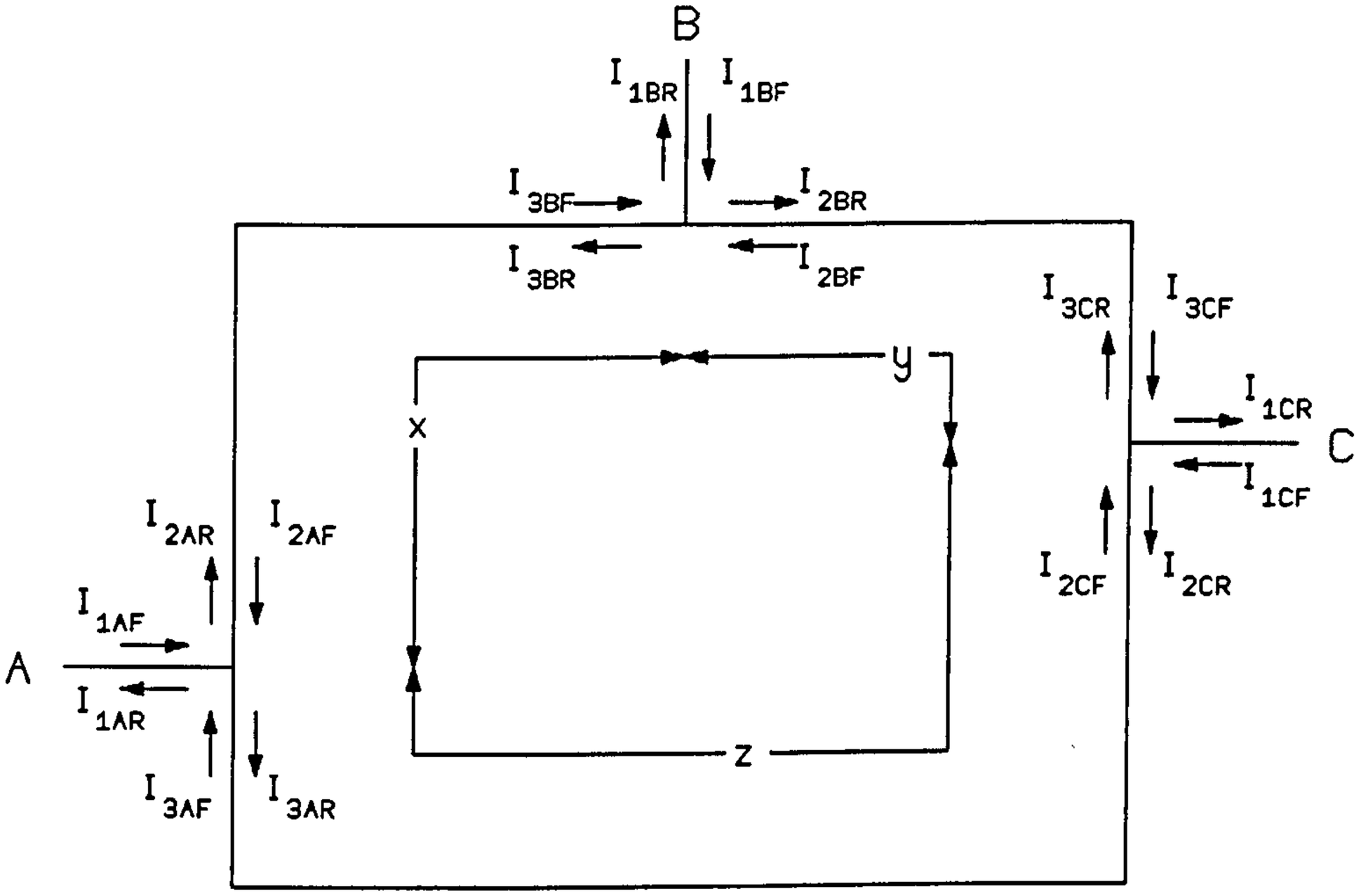

Figure 4.1: **Three-port ring structure, with arbitrary port spacings, showing current nomenclature**

4.2 General method of analysis

The new approach involves summing the currents at each port of the network and then relating the individual currents by the transmission coefficients between and through the various circuit nodes. Thus a set of equations can be generated, from which the ratio of any two input or output currents can be found. Fig. 4.1, above shows a three-port ring, with arbitrary port spacings, labelled with the currents entering and leaving each node. The suffices of the current terms indicate the port (1,2 or3) of each junction (A,B or C) and the direction of current flow, where F represents the incident wave and R the

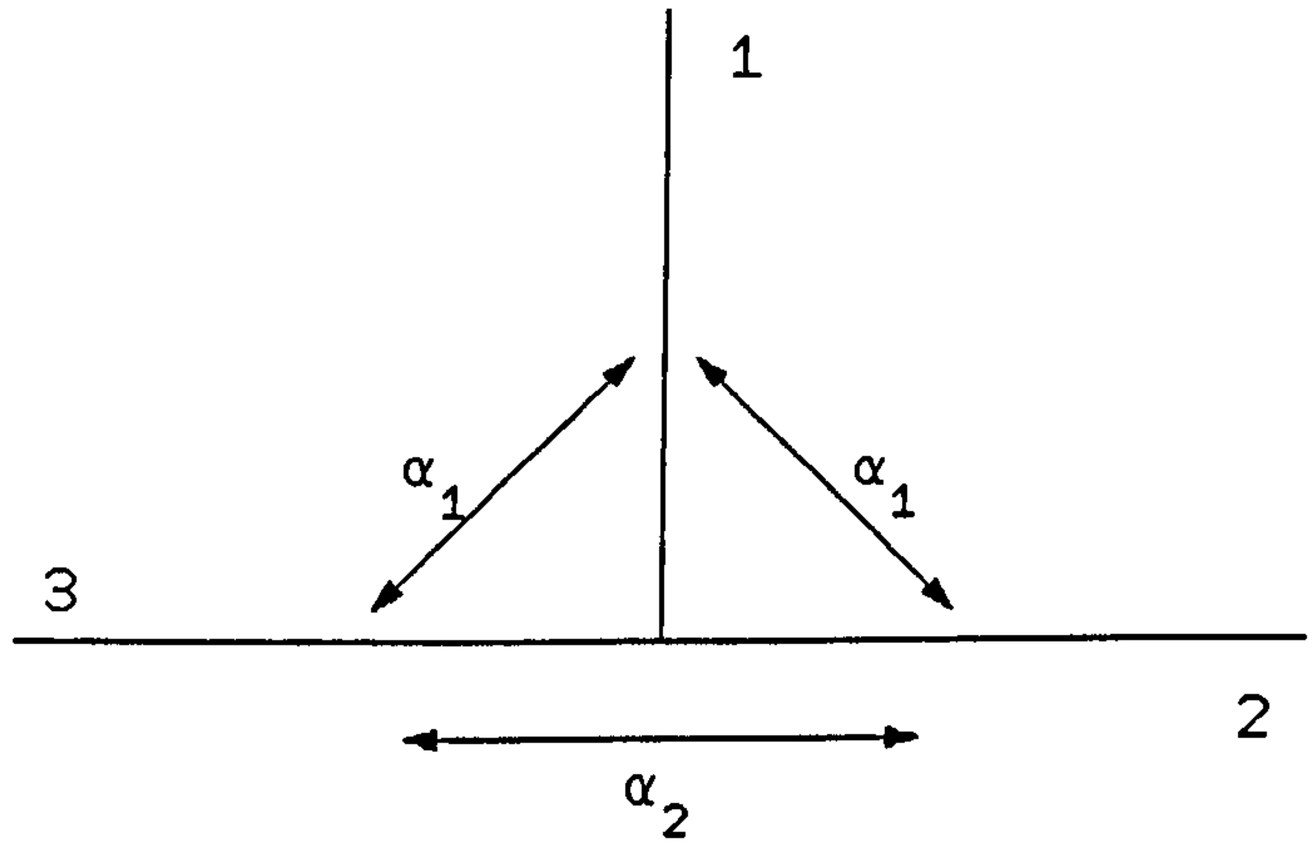

Figure 4.2: Transmission coefficients for each junction

reflected wave. Thus, summing the currents at the three junctions A, B and C gives

$$(I_{1AF} - I_{1AR}) + (I_{2AF} - I_{2AR}) + (I_{3AF} - I_{3AR}) = 0 \qquad (4.1)$$

$$(I_{1BF} - I_{1BR}) + (I_{2BF} - I_{2BR}) + (I_{3BF} - I_{3BR}) = 0 \qquad (4.2)$$

$$(I_{1CF} - I_{1CR}) + (I_{2CF} - I_{2CR}) + (I_{3CF} - I_{3CR}) = 0 \qquad (4.3)$$

The transmission through each symmetrical junction can be represented in terms of the complex transmission coefficients α_1 and α_2 which are defined in Fig. 4.2, above. If it is assumed that ports 2 and 3 of each junction are correctly matched to the ring, and that the reflection coefficient at port 1 of each independent junction is ρ_1, then we have three sets of equations which specify the transmission through the three ports, namely

$$I_{1AR} = \rho_1 I_{1AF} + \alpha_1 I_{2AF} + \alpha_1 I_{3AF} \qquad (4.4)$$

$$I_{2AR} = \alpha_1 I_{1AF} + \alpha_2 I_{3AF} \qquad (4.5)$$

$$I_{3AR} = \alpha_1 I_{1AF} + \alpha_2 I_{2AF} \qquad (4.6)$$

$$I_{1BR} = \rho_1 I_{1BF} + \alpha_1 I_{2BF} + \alpha_1 I_{3BF} \quad (4.7)$$

$$I_{2BR} = \alpha_1 I_{1BF} + \alpha_2 I_{3BF} \quad (4.8)$$

$$I_{3BR} = \alpha_1 I_{1BF} + \alpha_2 I_{2BF} \quad (4.9)$$

$$I_{1CR} = \rho_1 I_{1CF} + \alpha_1 I_{2CF} + \alpha_1 I_{3CF} \quad (4.10)$$

$$I_{2CR} = \alpha_1 I_{1CF} + \alpha_2 I_{3CF} \quad (4.11)$$

$$I_{3CR} = \alpha_1 I_{1CF} + \alpha_2 I_{2CF} \quad (4.12)$$

Finally, we can generate a set of equations to represent propagation between the ports around the ring. Thus we have, in terms of the phase propagation constant, β, for the ring

$$I_{2AF} = I_{3BR} e^{-j\beta x} \quad (4.13)$$

$$I_{3BF} = I_{2AR} e^{-j\beta x} \quad (4.14)$$

$$I_{2BF} = I_{3CR} e^{-j\beta y} \quad (4.15)$$

$$I_{3CF} = I_{2BR} e^{-j\beta y} \quad (4.16)$$

$$I_{2CF} = I_{3AR} e^{-j\beta z} \quad (4.17)$$

$$I_{3CF} = I_{2CR} e^{-j\beta z} \quad (4.18)$$

The set of linear equations, 4.1 through to 4.18, enable the ratio of any two input or output currents to be obtained, either through the use of a standard computer program designed to solve sets of linear equations or through simple successive substitution.

The method does not contain any inherent restrictions, either in the geometry of the ring or in the signal match at the various ports. For example, if we wish to include the effect of mismatch at ports 2 and 3 of each junction then equations of the form of 4.5 and 4.6 can be modified as follows

$$I_{2AR} = \alpha_1 I_{1AF} + \alpha_2 I_{3AF} + \rho_2 I_{2AF} \quad (4.19)$$

$$I_{3AR} = \alpha_1 I_{1AF} + \alpha_2 I_{2AF} + \rho_3 I_{3AF} \quad (4.20)$$

where ρ_2 and ρ_3 are the junction reflection coefficients at ports 2 and 3 respectively. Furthermore, if we wish to consider the effects of a non-uniform ring, i.e. interconnecting the ports with microstrip lines of different geometries, this is simply a matter of using the appropriate values of β in 4.13 through to 4.18, and making the necessary corrections to the reflection coefficient values.

4.3 Three-port ring discriminator

Since the three-port ring discriminator is the ring structure of primary interest for the present work, the equations are developed in more detail to represent this circuit.

For the the basic three-port ring discriminator described in chapter 3, the port spacings are such that, referring to Fig. 4.1, p. 152, $x = y = \lambda/4$ and $z = 3\lambda/4$. Also for a single input to the ring through port A, we have $I_{1BF} = I_{1CF} = 0$, where it is assumed that ports B and C are correctly matched. Then, summing the currents at port B gives

$$-I_{1BR} + I_{2BF} - I_{2BR} + I_{3BF} - I_{3BR} = 0 \tag{4.21}$$

i.e.

$$-I_{1BR}+\alpha_2 I_{3AR}e^{-j4\beta\lambda_o/4}-\alpha_2 I_{2AR}e^{-j\beta\lambda_o/4}+I_{2AR}e^{-j\beta\lambda_o/4}-{\alpha_2}^2 I_{3AR}e^{-j4\beta\lambda_o/4} = 0 \tag{4.22}$$

then putting, for convenience, $\phi = \beta\lambda_o/4$ we have

$$-I_{1BR} + \alpha_2(1-\alpha_2)I_{3AR}e^{-j4\phi} + (1-\alpha_2)I_{2AR}e^{-j\phi} = 0 \tag{4.23}$$

Similarly, summing currents at junction C gives

$$-I_{1CR} + I_{2CF} - I_{2CR} + I_{3CF} - I_{3CR} = 0 \tag{4.24}$$

i.e.

$$-I_{1CR} + I_{3AR}e^{-j3\phi} - {\alpha_2}^2 I_{2AR}e^{-j2\phi} + \alpha_2 I_{2AR}e^{-j2\phi} - \alpha_2 I_{3AR}e^{-j3\phi} = 0 \tag{4.25}$$

hence

$$-I_{1CR} + (1-\alpha_2)I_{3AR}e^{-j3\phi} + \alpha_2(1-\alpha_2)I_{2AR}e^{-j2\phi} = 0 \tag{4.26}$$

At junction A we have

$$I_{3AR} = \alpha_1 I_{1AF} + \alpha_2 I_{2AF} \tag{4.27}$$

$$= \alpha_1 I_{1AF} + {\alpha_2}^3 I_{3AR}e^{-j5\phi} \tag{4.28}$$

giving

$$I_{3AR} = \alpha_1(1-{\alpha_2}^3 e^{-j5\phi})^{-1} I_{1AF} \tag{4.29}$$

Also at junction A

$$I_{2AR} = \alpha_1 I_{1AF} + \alpha_2 I_{3AF} \tag{4.30}$$

$$= \alpha_1 I_{1AF} + \alpha_2{}^3 I_{2AR} e^{-j5\phi} \tag{4.31}$$

giving

$$I_{2AR} = \alpha_1 (1 - \alpha_2{}^3 e^{-j5\phi})^{-1} I_{1AF} \tag{4.32}$$

Substituting from 4.29 and 4.32 into 4.23 gives

$$-I_{1BR}+\alpha_2(1-\alpha_2)\alpha_1(1-\alpha_2^3 e^{-j5\phi})^{-1}e^{-j4\phi}I_{1AF}+(1-\alpha_2)\alpha_1(1-\alpha_2^3 e^{-j5\phi})^{-1}e^{-j\phi}I_{1AF}=0 \tag{4.33}$$

which can be re-arranged to give

$$\frac{I_{1BR}}{I_{1AF}} = \alpha_1(1-\alpha_2)(1-\alpha_2^3 e^{-j5\phi})^{-1}(\alpha_2 e^{-j4\phi} + e^{-j\phi}) \tag{4.34}$$

Substituting from 4.29 and 4.32 into 4.26 gives

$$-I_{1CR}+\alpha_1(1-\alpha_2)(1-\alpha_2^3 e^{-j5\phi})^{-1}e^{-j3\phi}I_{1AF}+\alpha_2(1-\alpha_2)\alpha_1(1-\alpha_2^3 e^{-j5\phi})^{-1}e^{-j2\phi}I_{1AF}=0 \tag{4.35}$$

which can be re-arranged to give

$$\frac{I_{1CR}}{I_{1AF}} = \alpha_1(1-\alpha_2)(1-\alpha_2^3 e^{-j5\phi})^{-1}(e^{-j3\phi} + \alpha_2 e^{-j2\phi}) \tag{4.36}$$

The discriminator function is obtained by taking the difference of the signal magnitudes at the output ports of junctions B and C. Thus the voltage, $V_o(f)$, at the output of the discriminator is given by

$$V_o(f) = k\left(\left|\frac{I_{1CR}}{I_{1AF}}\right| - \left|\frac{I_{1BR}}{I_{1AF}}\right|\right) \tag{4.37}$$

where k is a scalar constant whose magnitude depends on the detector efficiencies and on the transmission and reflection coefficients of the T-junctions in the ring. It should be noted that 4.37 is a function of ϕ and can be used to obtain the frequency response of the ring, since

$$\phi = \beta\lambda_o/4 = \frac{2\pi}{\lambda}\frac{\lambda_o}{4} = \frac{\pi}{2}\frac{f}{f_o} \tag{4.38}$$

where f is the frequency variable and f_o is the centre frequency of the discriminator response.

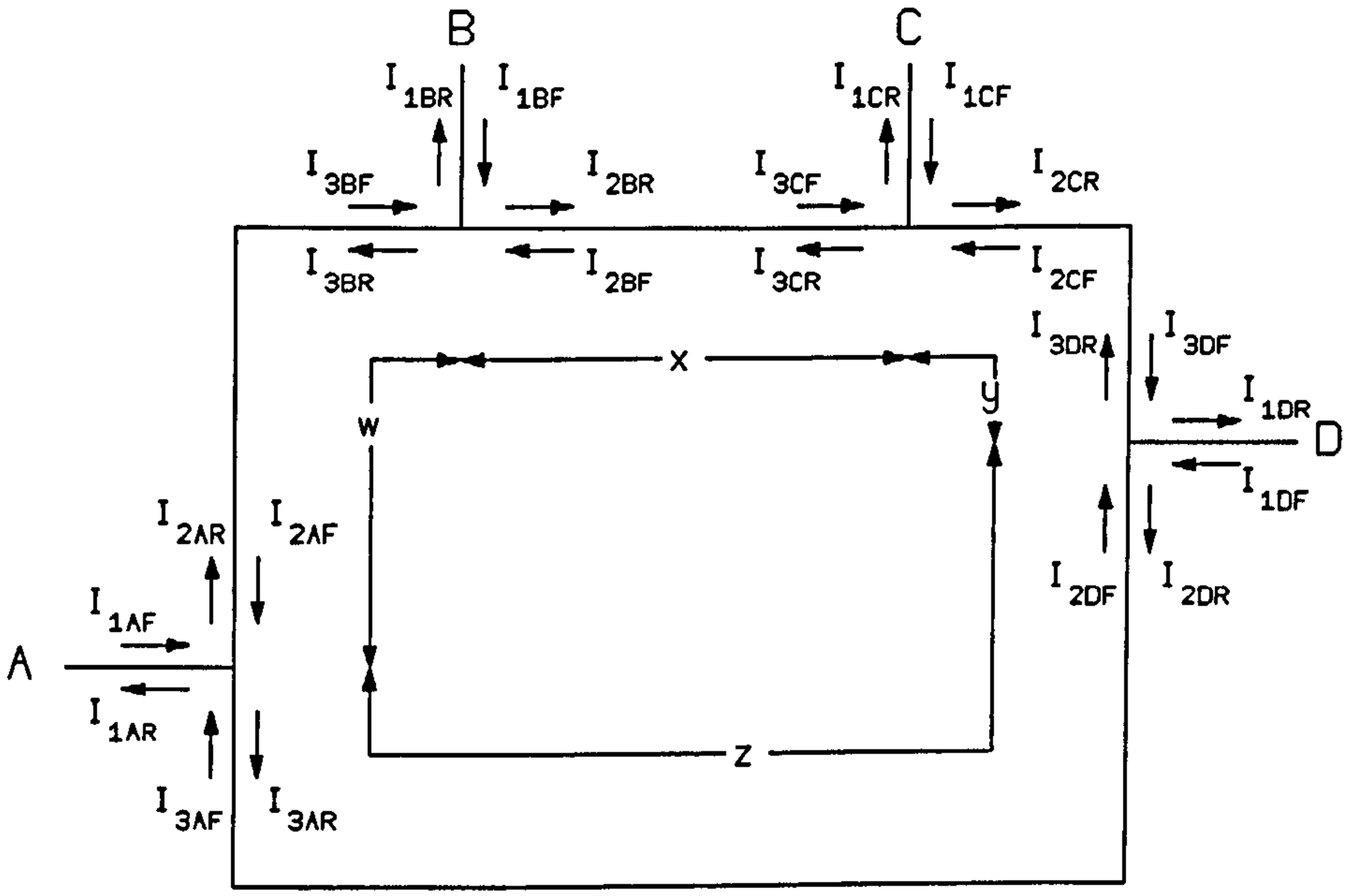

Figure 4.3: **Nomenclature for four-port ring structure**

4.4 Ring structure with two simultaneous feeds

Amongst the advantages of the current summing technique is the ability to easily deal with situations where there are several feed points to a ring structure. Fig. 4.3, above shows a 4-port ring structure, where A and B are the input ports, and C and D the output ports. The port separations w,x and z are arbitrary, but to maintain a discriminator response we need $y = \lambda_o/4$. Since C and D are output ports, I_{1CF} and I_{1DF} will be zero.

Summing the currents at junction C

$$-I_{1CR} + I_{2CF} - I_{2CR} + I_{3CF} - I_{3CR} = 0 \tag{4.39}$$

i.e.

$$-I_{1CR} + \alpha_2 I_{3AR} e^{-j\beta(y+z)} - \alpha_2 I_{2BR} e^{-j\beta x} + I_{2BR} e^{-j\beta x} - \alpha_2^2 I_{3AR} e^{-j\beta(y+z)} = 0 \tag{4.40}$$

$$-I_{1CR} + \alpha_2(1-\alpha_2)I_{3AR}e^{-j\beta(y+z)} + (1-\alpha_2)I_{2BR}e^{-j\beta x} = 0 \qquad (4.41)$$

Similarly, summing the currents at junction D, leads to

$$-I_{1DR} + (1-\alpha_2)I_{3AR}e^{-j\beta z} + \alpha_2(1-\alpha_2)I_{2BR}e^{-j\beta(x+y)} = 0 \qquad (4.42)$$

At junction A

$$I_{3AR} = \alpha_1 I_{1AF} + \alpha_2 I_{2AF} \qquad (4.43)$$

$$= \alpha_1 I_{1AF} + \alpha_2 e^{-j\beta w}(\alpha_1 I_{1BF} + \alpha_2 I_{2BF}) \qquad (4.44)$$

leading to

$$I_{3AR} = (\alpha_1 I_{1AF} + \alpha_1\alpha_2 I_{1BF}e^{-j\beta w})(1-\alpha_2^4 e^{-j\beta t})^{-1} \qquad (4.45)$$

where $t = w + x + y + z$. Similarly, considering the transmission through junction B, leads to

$$I_{2BR} = (\alpha_1 I_{1BF} + \alpha_1\alpha_2 I_{1AF}e^{-j\beta w})(1-\alpha_2^4 e^{-j\beta t})^{-1} \qquad (4.46)$$

Substituting from 4.45 and 4.46 into 4.41 we obtain, after straightforward manipulation

$$\frac{I_{1CR}}{I_i} = \alpha_1(1-\alpha_2)\left(e^{-j\beta x} + \alpha_2 e^{-j\beta(y+z)} + \alpha_2 e^{-j\beta(x+w)} + \alpha_2^2 e^{-j\beta(w+y+z)}\right)\xi \qquad (4.47)$$

where

$$\xi = (1-\alpha_1^4 e^{-j\beta t})^{-1} \qquad (4.48)$$

and where it has also been assumed that currents of equal magnitude, $|I_i|$, are applied to the input ports, i.e. $|I_i| = |I_{1AF}| = |I_{1BF}|$.

Similarly, substituting from 4.45 and 4.46 into 4.42 we obtain

$$\frac{I_{1DR}}{I_i} = \alpha_1(1-\alpha_2)\left(e^{-j\beta z} + \alpha_2 e^{-j\beta(x+y)} + \alpha_2 e^{-j\beta(w+z)} + \alpha_2^2 e^{-j\beta(x+y+w)}\right)\xi \qquad (4.49)$$

As before the discriminator function is obtained by taking the difference between the magnitudes of the output signals detected at junctions B and C, i.e.

$$V_o(f) = k\left(\left|\frac{I_{1CR}}{I_i}\right| - \left|\frac{I_{1DR}}{I_i}\right|\right). \qquad (4.50)$$

Using 4.50 the effect of feeding a ring structure simultaneously at any two positions can be found.

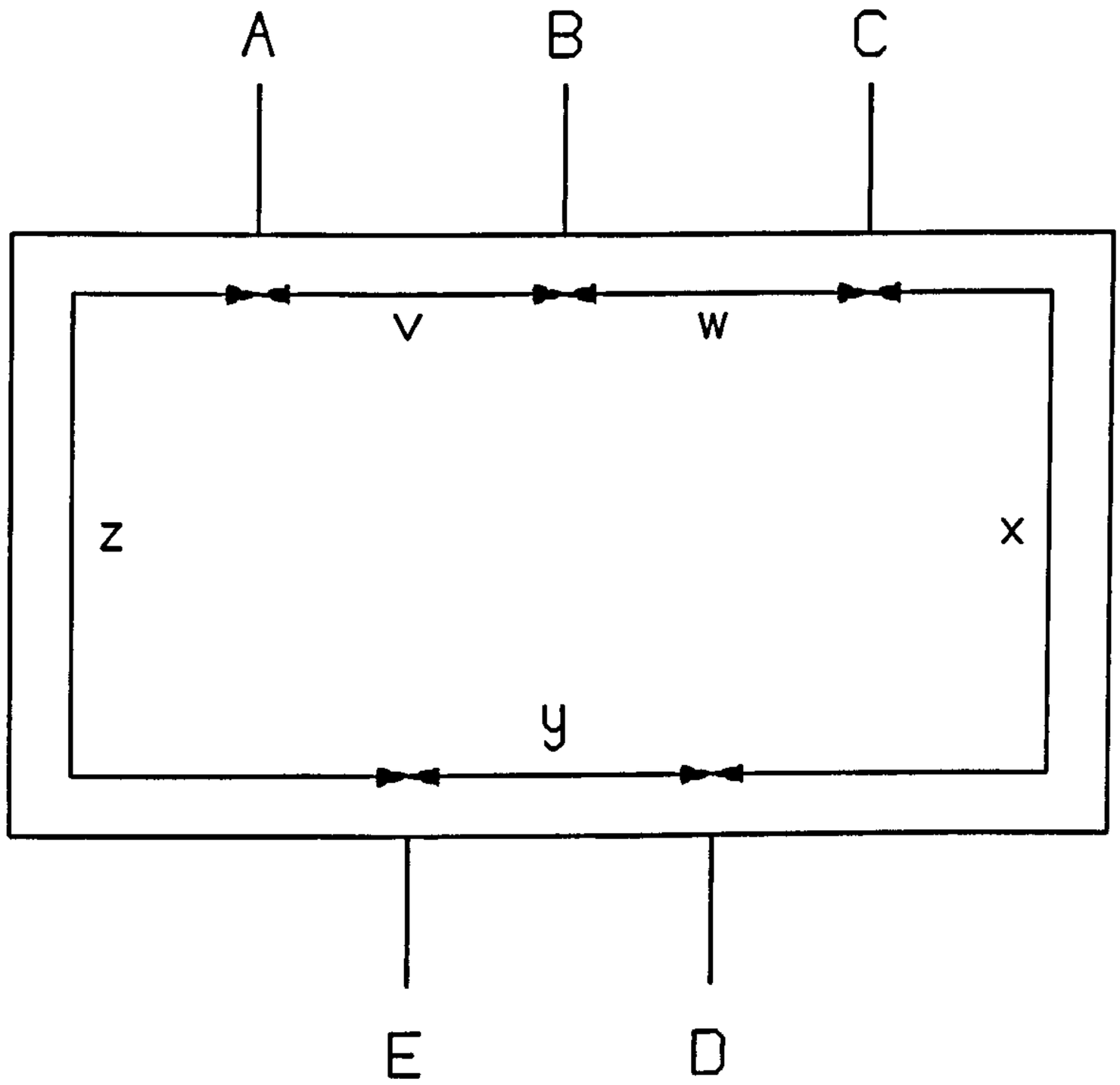

Figure 4.4: **Five-port ring showing nomenclature for junction spacings**

4.5 Ring structure with three simultaneous feeds

The analytical procedure described in the previous section for a dual-fed ring structure can easily be extended to any number of feed ports. A ring with five ports, three of which are to be used as feed ports is shown in Fig. 4.4, above. Only the port spacings are shown in the figure, since the nomenclature for describing the current flow at each junction is identical to that given in Fig. 4.1, p. 152.

Since the analytical procedure for the five-port ring follows directly from that given for the four-port arrangement, only the essential results will be stated here. Assuming that the input signals are applied through junctions A,B and C the currents I_{1DR} and I_{1ER} at the two output ports are obtained

in terms of the input current I_i as

$$\frac{I_{1DR}}{I_i} = (1-\alpha_2)\xi_1(\chi_1+\chi_2) \tag{4.51}$$

and

$$\frac{I_{1ER}}{I_i} = (1-\alpha_2)\xi_1(\chi_1+\chi_4) \tag{4.52}$$

where

$$\chi_1 = (\alpha_1\alpha_2^2 e^{-j\beta v} + \alpha_1\alpha_2^3 e^{-j\beta(v+w)} + \alpha_1\alpha_2)e^{-j\beta(y+z)} \tag{4.53}$$

$$\chi_2 = (\alpha_1 + \alpha_1\alpha_2 e^{-j\beta w} + \alpha_1\alpha_2^2 e^{-j\beta(v+w)})e^{-j\beta x} \tag{4.54}$$

$$\chi_3 = \alpha_1(e^{-j\beta z} + \alpha_2 e^{-j\beta(v+x)} + \alpha_2^2 e^{-j\beta(v+x+w)}) \tag{4.55}$$

$$\chi_4 = \alpha_1\alpha_2(e^{-j\beta(x+y)} + \alpha_2 e^{-j\beta(w+x+y)} + \alpha_2^2 e^{-j\beta(v+w+x+y+z)}) \tag{4.56}$$

$$\xi_1 = (1-\alpha_2^5 e^{-j\beta t_1})^{-1} \tag{4.57}$$

$$t_1 = v+w+x+y+z \tag{4.58}$$

where it has again be assumed that equal magnitude currents are applied at the three input ports.

Having obtained expressions for the output currents, the output voltage from the discriminator is found in the usual way from

$$V_o(f) = k\left(\left|\frac{I_{1DR}}{I_i}\right| - \left|\frac{I_{1ER}}{I_i}\right|\right) \tag{4.59}$$

4.6 Results and discussion

Fig. 4.5, p. 161 shows the simulated frequency response for a simple three-port ring, computed using 4.37. It can be seen that the response has the expected discriminator shape, which demonstrates the validity of the new current summing technique. One of the principal advantages of the new technique is that it makes it possible to easily investigate the effects of asymmetry in the ring. It is of some interest to establish the effect of moving the position of the input port. This will not only change the input impedance to the ring, but should have the effect of displacing the discriminator characteristic in frequency, thereby generating an offset voltage at the design (centre) frequency. The responses obtained by altering the position of the feed port are shown in Fig. 4.6, p. 162, for small spacings, and in Fig. 4.7,

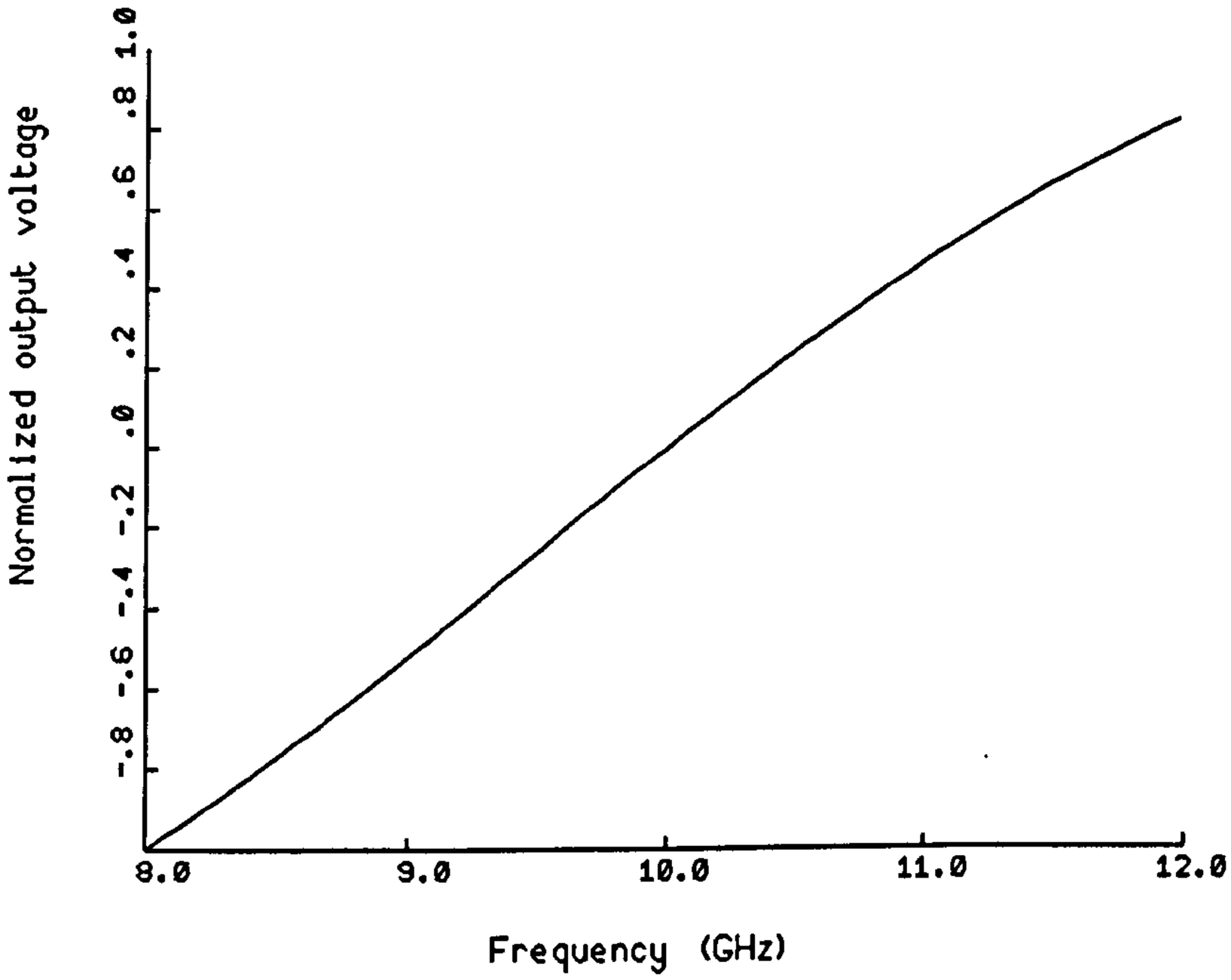

Figure 4.5: **Three-port ring discriminator response**

p. 163 for large spacings. Three responses are shown, each for a different value of δ, which is the displacement of the input port from the original position. The values of δ in Fig. 4.6, p. 162 are expressed as fractions of the wavelength, λ_o, at the nominal centre frequency. (For clarity, δ is defined in Fig. 4.8, p. 164.) In this case the total ring circumference remains unchanged, although the discriminator function will always be obtained providing the spacing between the output ports is $\lambda/4$. It can be seen from the responses in Fig. 4.6, p. 162 that the discriminator function is maintained as the position of port 1 is changed, and more particularly that the linearity in the central region is essentially unchanged. This linearity is significant for the linear control of frequency which is being proposed. This provides some indication of the limits to δ. Comparing the responses in Fig. 4.6, p. 162 and Fig. 4.7, p. 163 it can be seen that the larger spacing is beginning to introduce significant non-linearity. This is only to be expected since the

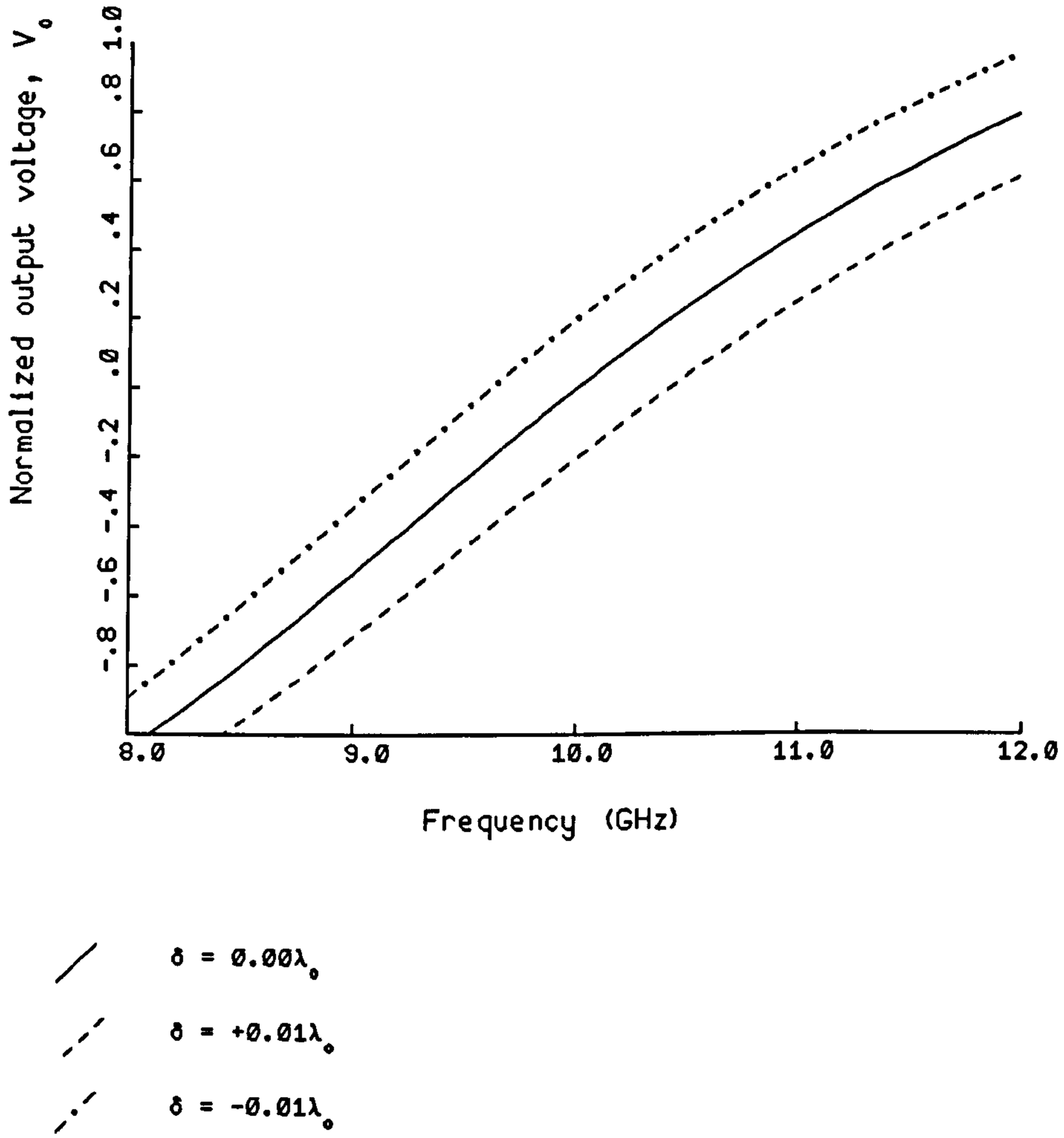

Figure 4.6: **Effect on discriminator responses of changing the position of the input port: small spacing**

discriminator characteristic is formed from part of a cyclic response, and if the input position were moved sufficiently far so as to be symmetric with the output ports, the signals from the latter would be equal and the slope of the response would be zero. It can also be observed from the responses in Fig. 4.6, above and Fig. 4.7, p. 163 that offset voltages are produced as the feed position changes. These offset voltages are plotted as a function of the feed displacement in Fig. 4.9, p. 165. It can be seen that there is an

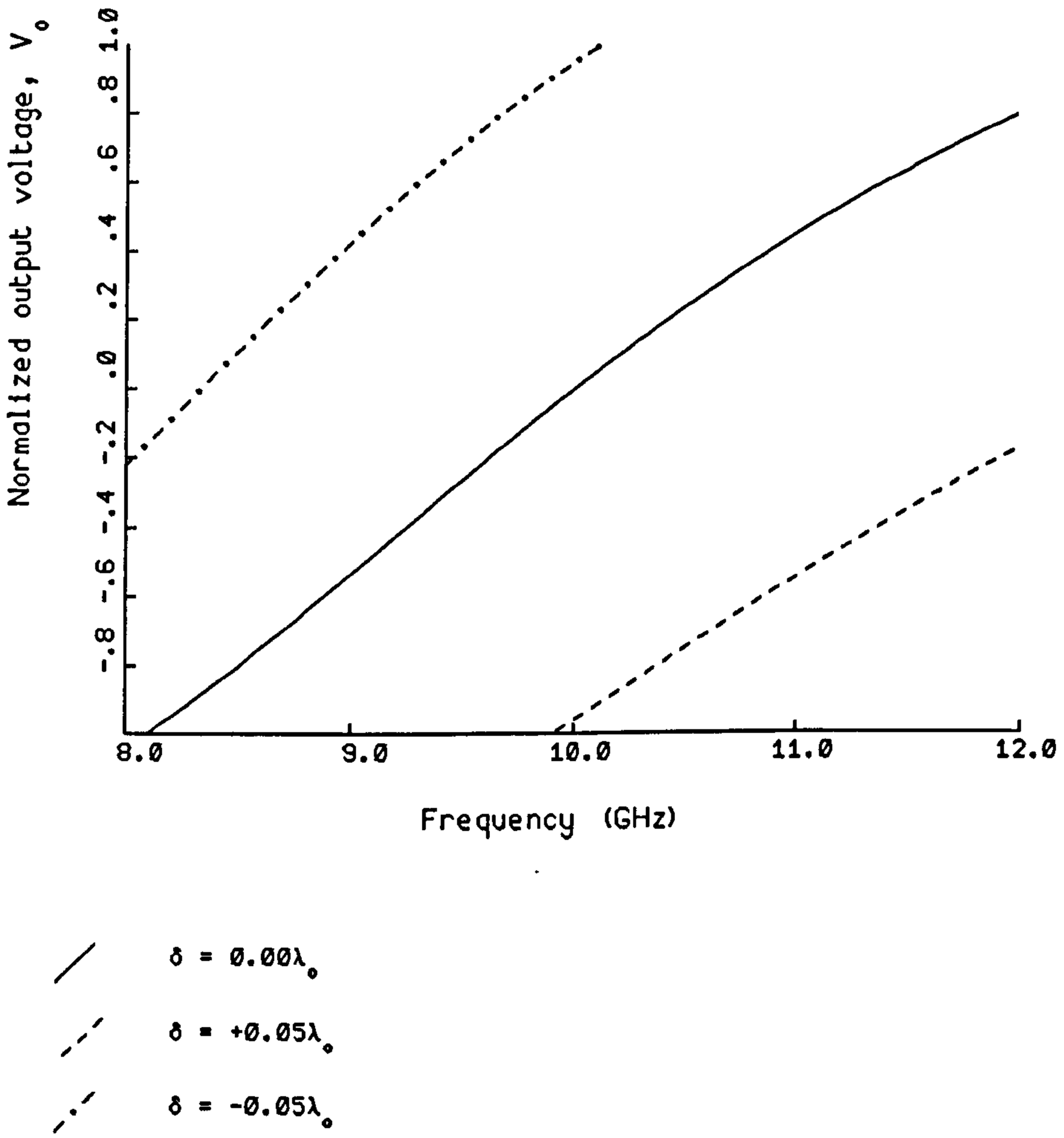

Figure 4.7: **Effect on discriminator responses of changing the position of the input port: large spacing**

approximately linear variation of offset voltage with position, which implies that linear frequency control could be achieved, by using this offset voltage as the feedback signal in the frequency control circuit previously described. If we consider a centre frequency of 10GHz, then the range of port movement ($\pm 0.05\lambda_o$) specified in Fig. 4.9, p. 165 represents a physical range of $\pm 600\mu m$ for a typical microstrip circuit, which indicates that a number of feed attachments, and hence frequency selection points, could be achieved without

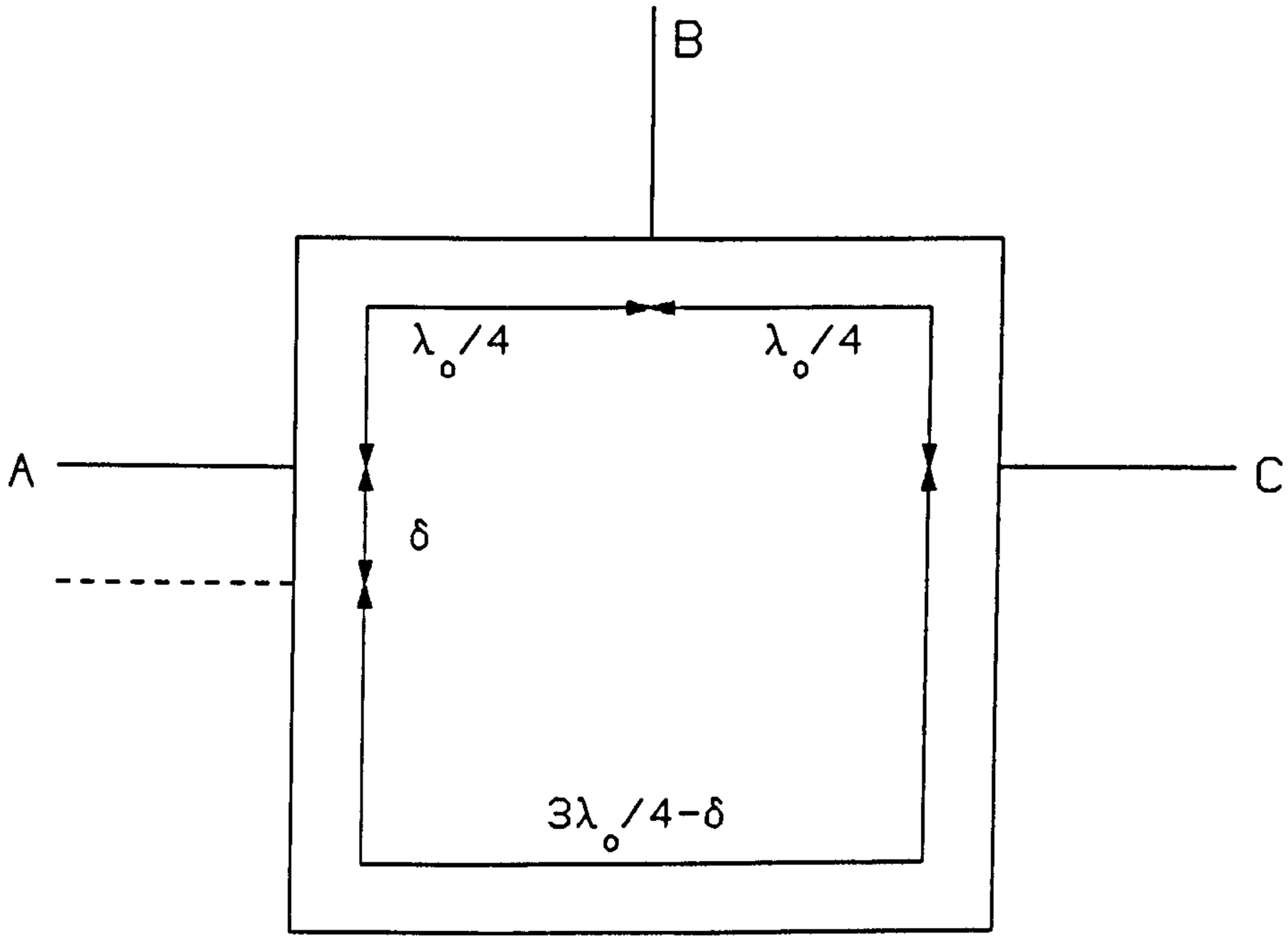

Figure 4.8: **Three-port ring discriminator showing feed offset, δ.**

problems of unwanted coupling in the vicinity of the port-ring junctions.

In Fig. 4.10, p. 166 and Fig. 4.11, p. 167 the effects of using the new theory to investigate the simultaneous excitation of a ring structure at two points are shown. Two interesting features can be seen in these responses. Firstly, the shape and slope of the discriminator responses obtained with a single feed are maintained with the dual feed. Secondly, and more significantly, there is a digital relationship between the offset voltages produced at the centre frequency and the various feed combinations. That is, representing an input signal as the '1' state, the three combinations (01,10,11) possible with two feeds leads to three equi-spaced offset voltages. This means that, not only could the frequency of an oscillator be changed by changing the position of a single feed, but that using a multiple feed system, digital

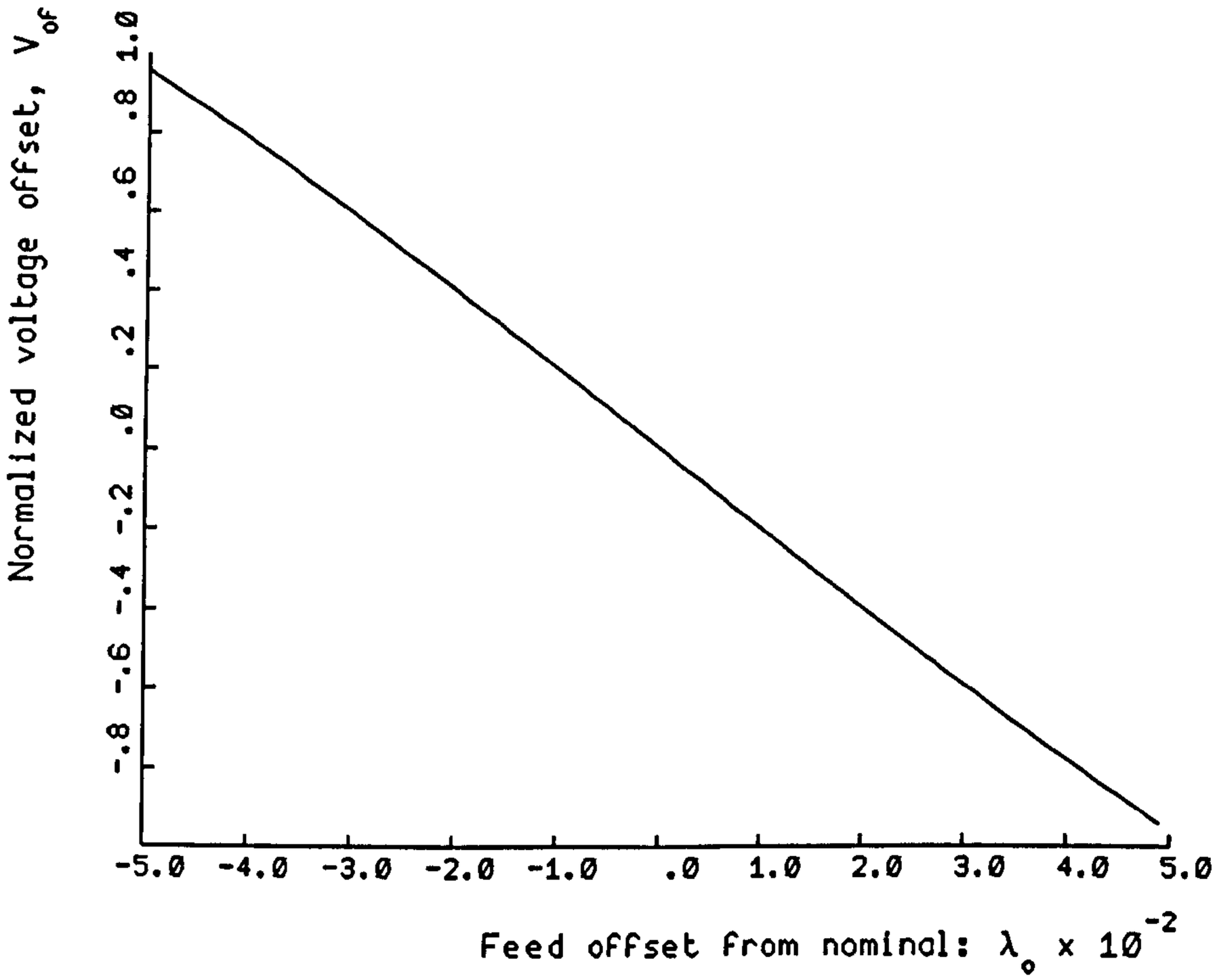

Figure 4.9: **Voltage offset at centre frequency, as a function of the input port position**

control of the oscillator frequency would be possible. In Fig. 4.12, p. 168 and Fig. 4.13, p. 169 the effects of changing the spacing between the input ports of a dual-fed ring are shown. The spacing between the feed ports is δ, which is defined in the same way as for the single port displacements. That is, the sign of δ indicates whether the second feed port is displaced in the clockwise or counter-clockwise direction from the nominal feed port position. The convention adopted here is that positive values of δ indicate a clockwise displacement and negative values a counter clockwise displacement. These responses show that the shape of the discriminator response, together with the linearity of the offset voltage steps, is maintained over a significant range of port separations. The slope of the discriminator response is of the order

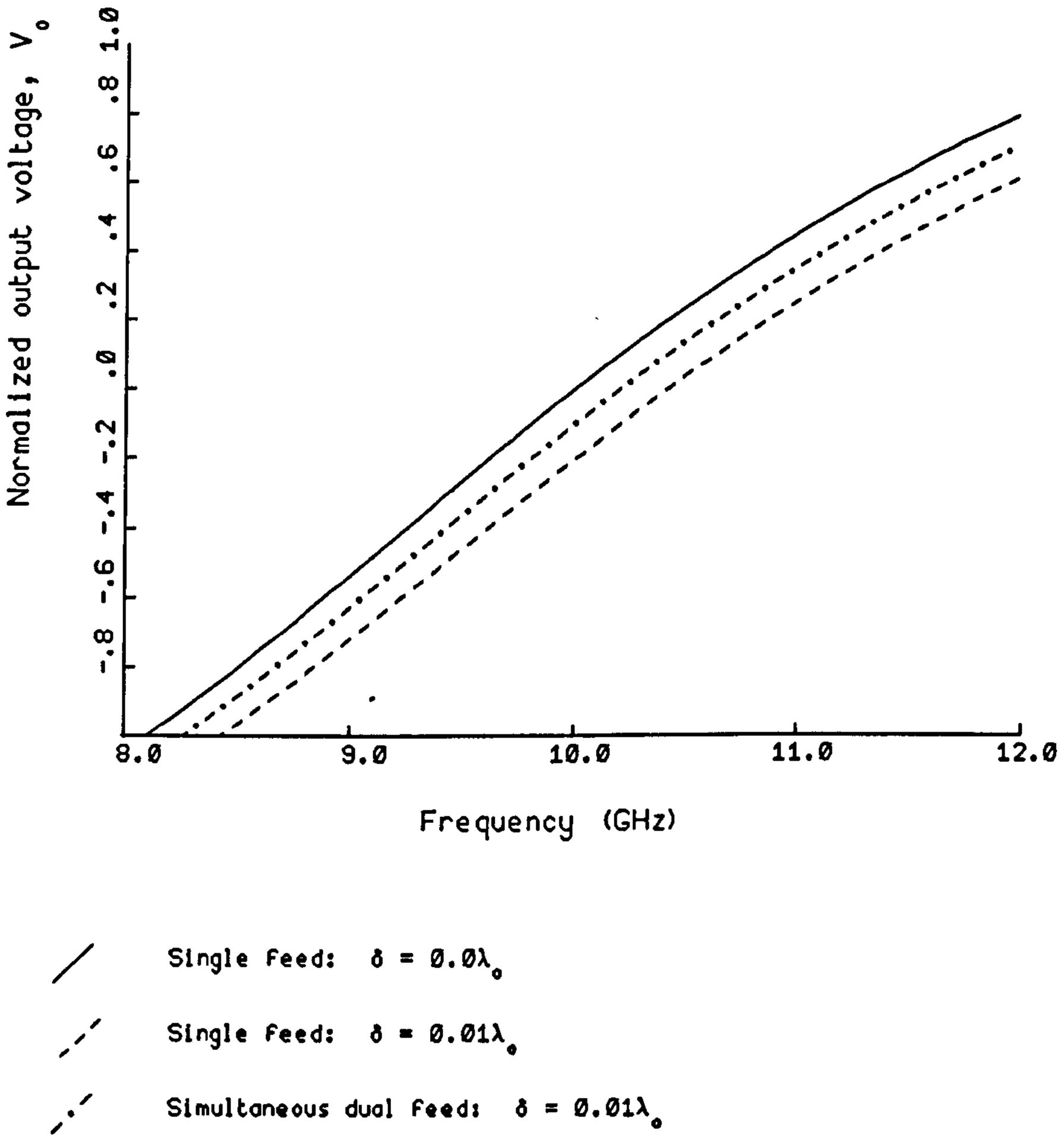

Figure 4.10: **Comparison of discriminator responses using single and dual feeds: small spacing**

of 0.21V/GHz, and this is maintained over a 20 per cent bandwidth for each set of four responses. In Fig. 4.14, p. 170 the offset voltage steps produced by equal changes in the feed separation of dual-fed rings have been plotted in more detail. These exhibit significant nonlinearities, and whilst some compensation could be applied to correct these effects, the results could impose limitations on the frequency range of operation if the circuit was used for digitally controlled frequency selection. In Fig. 4.15, p. 171 the behaviour

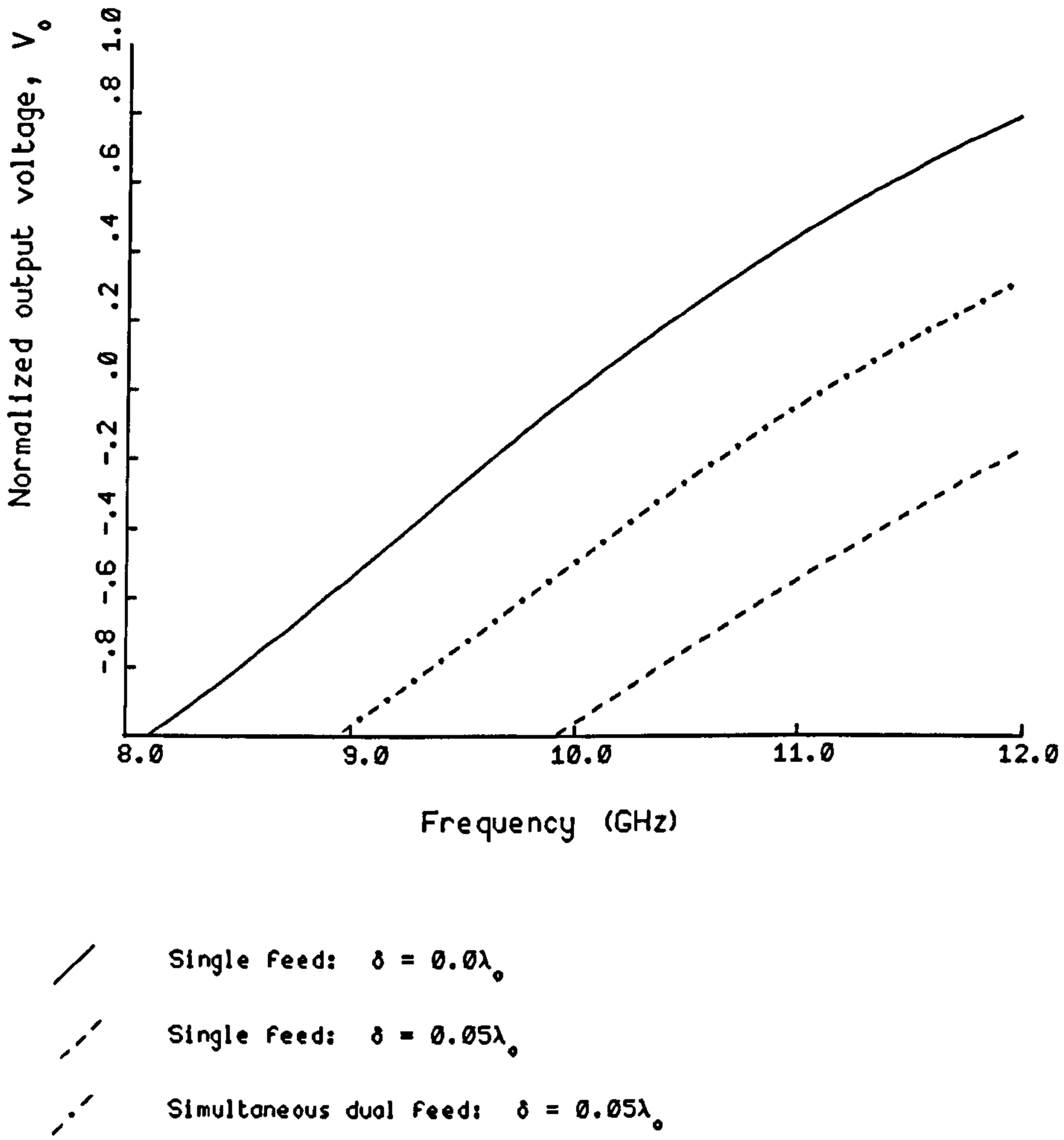

Figure 4.11: **Comparison of discriminator responses using single and dual feeds: large spacing**

of a ring excited simultaneously at three positions is compared with that of a dual fed ring. It can be seen that, whilst the general characteristics are maintained, there are non linear effects associated with the tri-fed structure, largely because of the spread of the ports. This is emphasised more in Fig. 4.16, p. 172, which shows the effect of increasing the port spacings.

However, it is still evident that, providing the spacings between the ports is kept small the concept of digital frequency control using multi-fed rings is

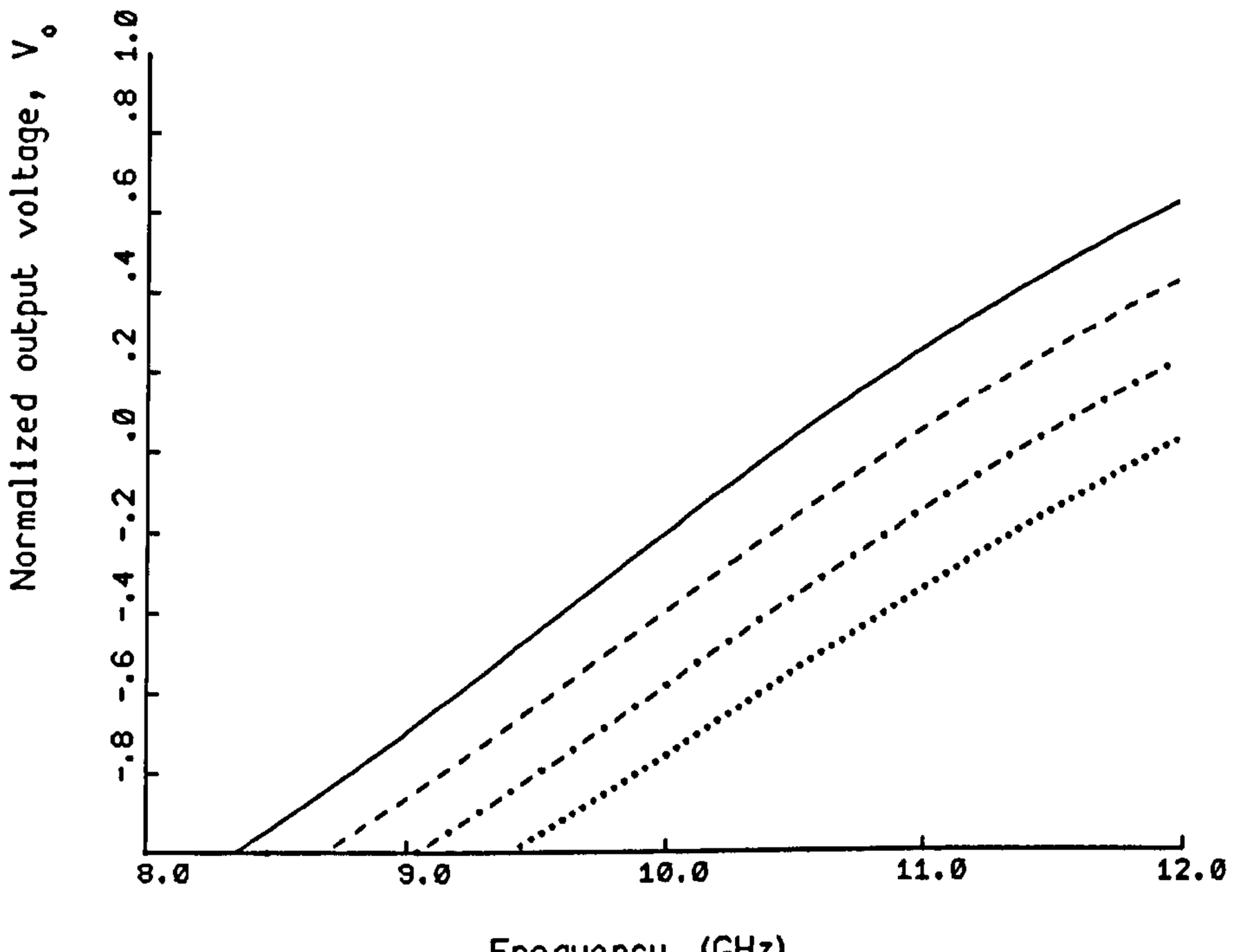

Figure 4.12: **Dual-fed ring with various feed separations: +ve displacement**

viable.

Finally, in Fig. 4.17, p. 173, results are shown for a standard hybrid ring structure, analysed using the new method. These results are presented as

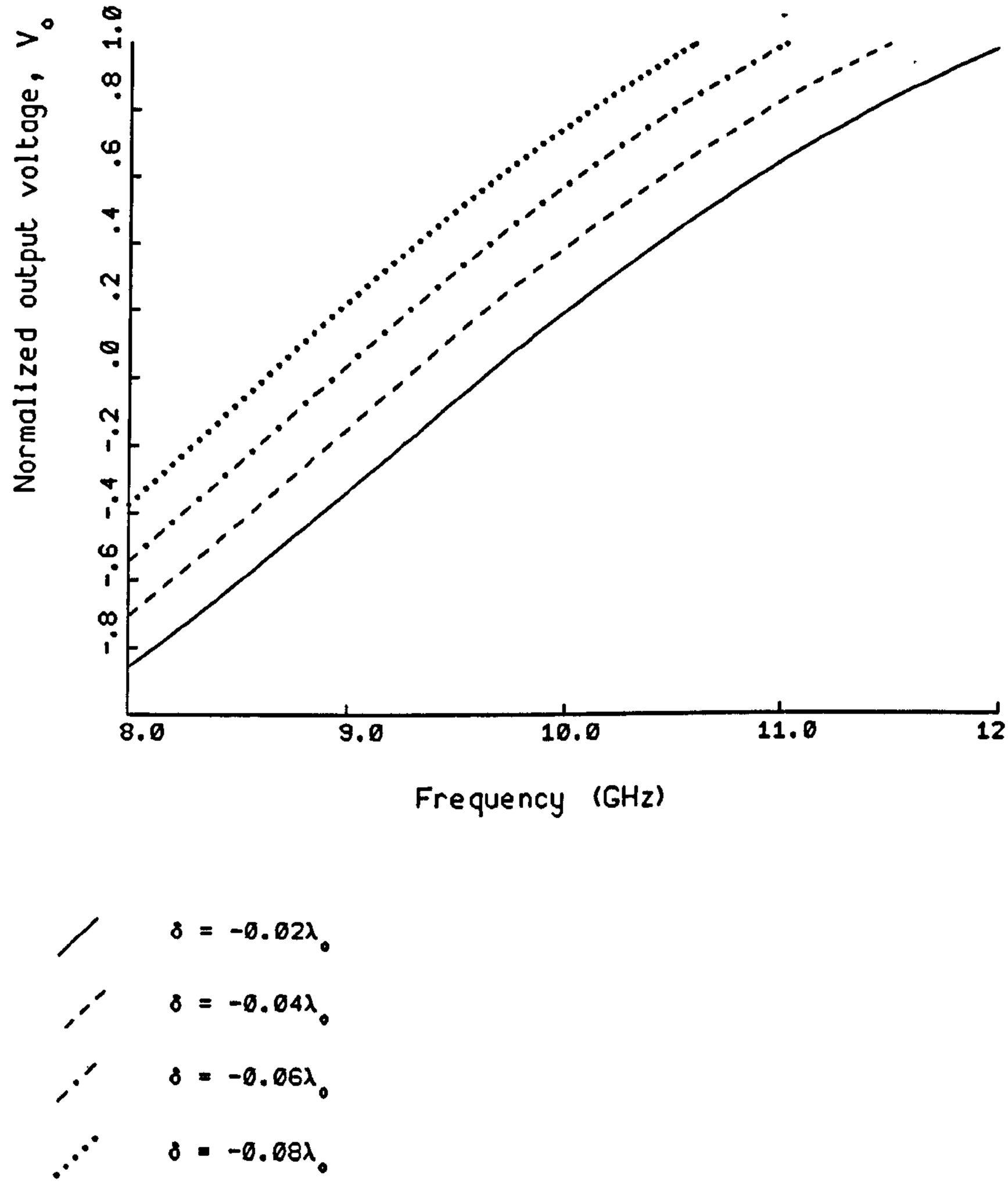

Figure 4.13: **Dual-fed ring with various feed separations: -ve displacement**

further confirmation of the validity of the new method of analysis. The transmission coefficients are as expected, with one isolated port and equal outputs from the remaining two ports. The shapes of the characteristics agree with

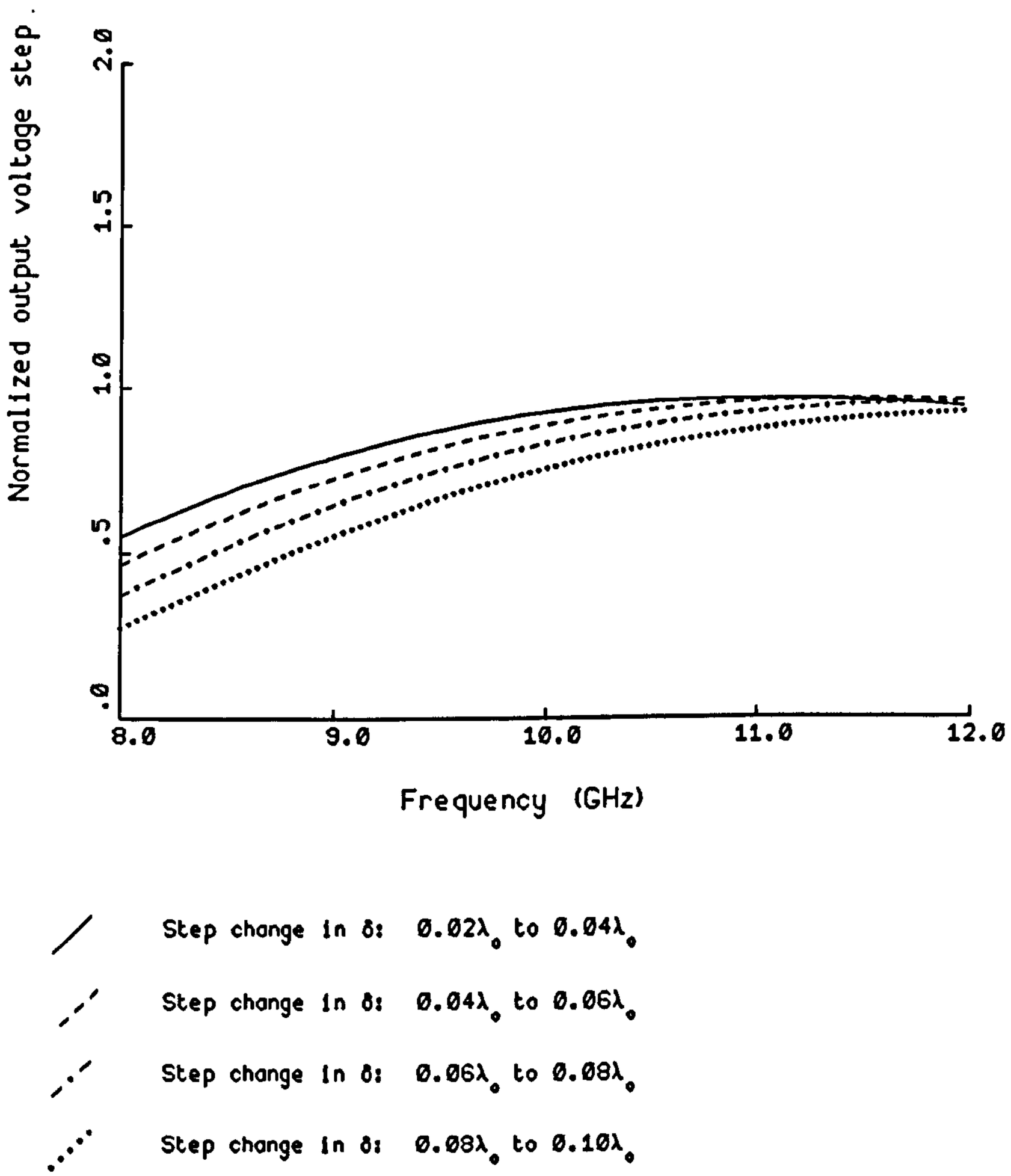

Figure 4.14: **Offset voltages produced by equal steps in feed separation**

those published which are based on the traditional method of analysis using the odd and even circuit approach: examples of these characteristics can be found in PON [26] and ZARBEL [25]. The absolute values of the coefficients are not of primary interest here, since they depend on the coefficients chosen to represent transmission through the T-junctions formed between the ring and the external ports.

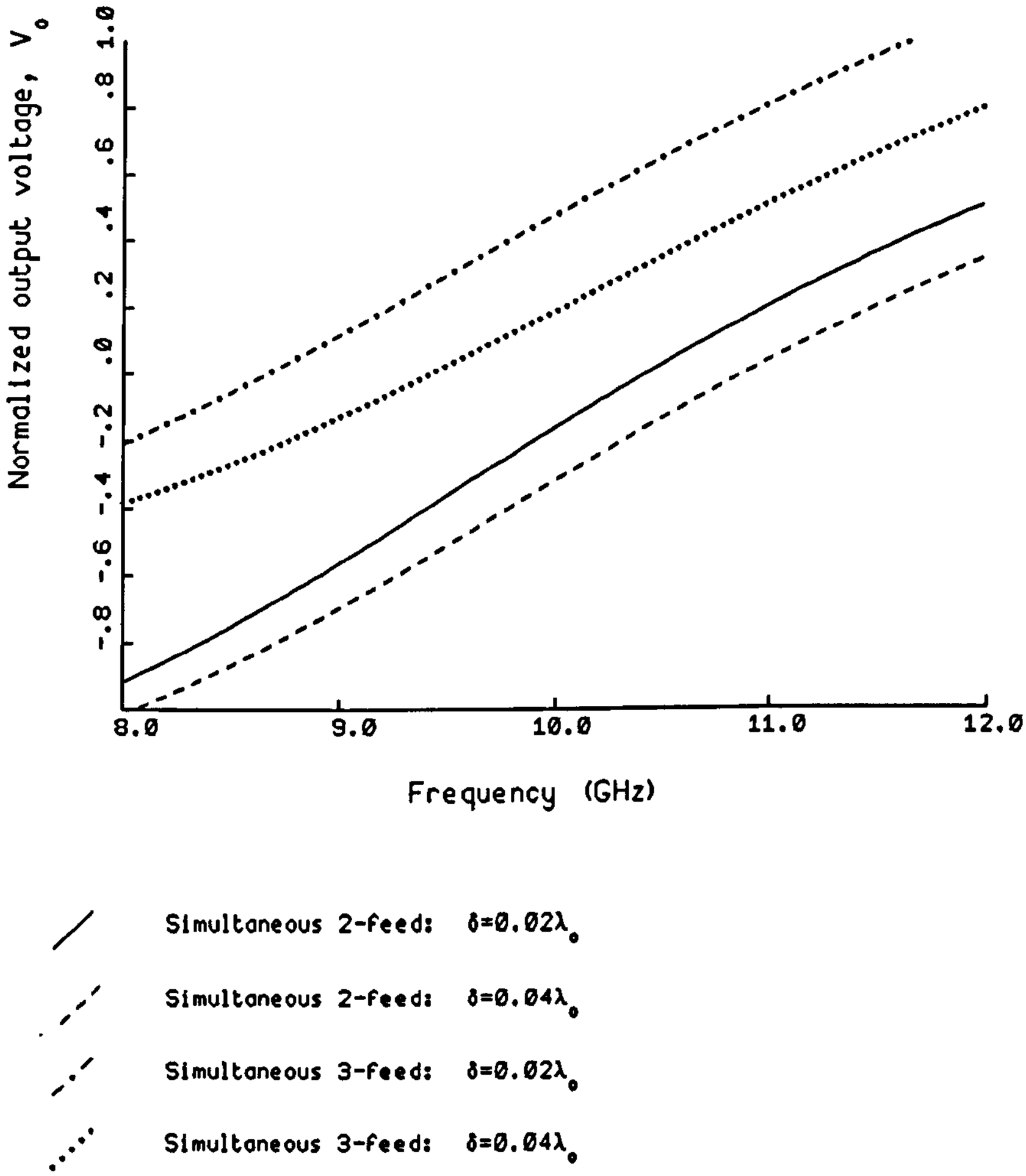

Figure 4.15: **Comparison of discriminator responses with dual-fed and tri-fed rings: small feed spacing**

4.7 Conclusions

A new method of analysis of microstrip ring structures has been developed, and verified through comparison with known circuit behaviour. The method is less restrictive than existing techniques and is particularly suitable for asymmetric networks. Furthermore, using the new analytical procedure a potentially powerful technique for implementing control of a microwave oscillator has been identified, which uses multi-fed rings.

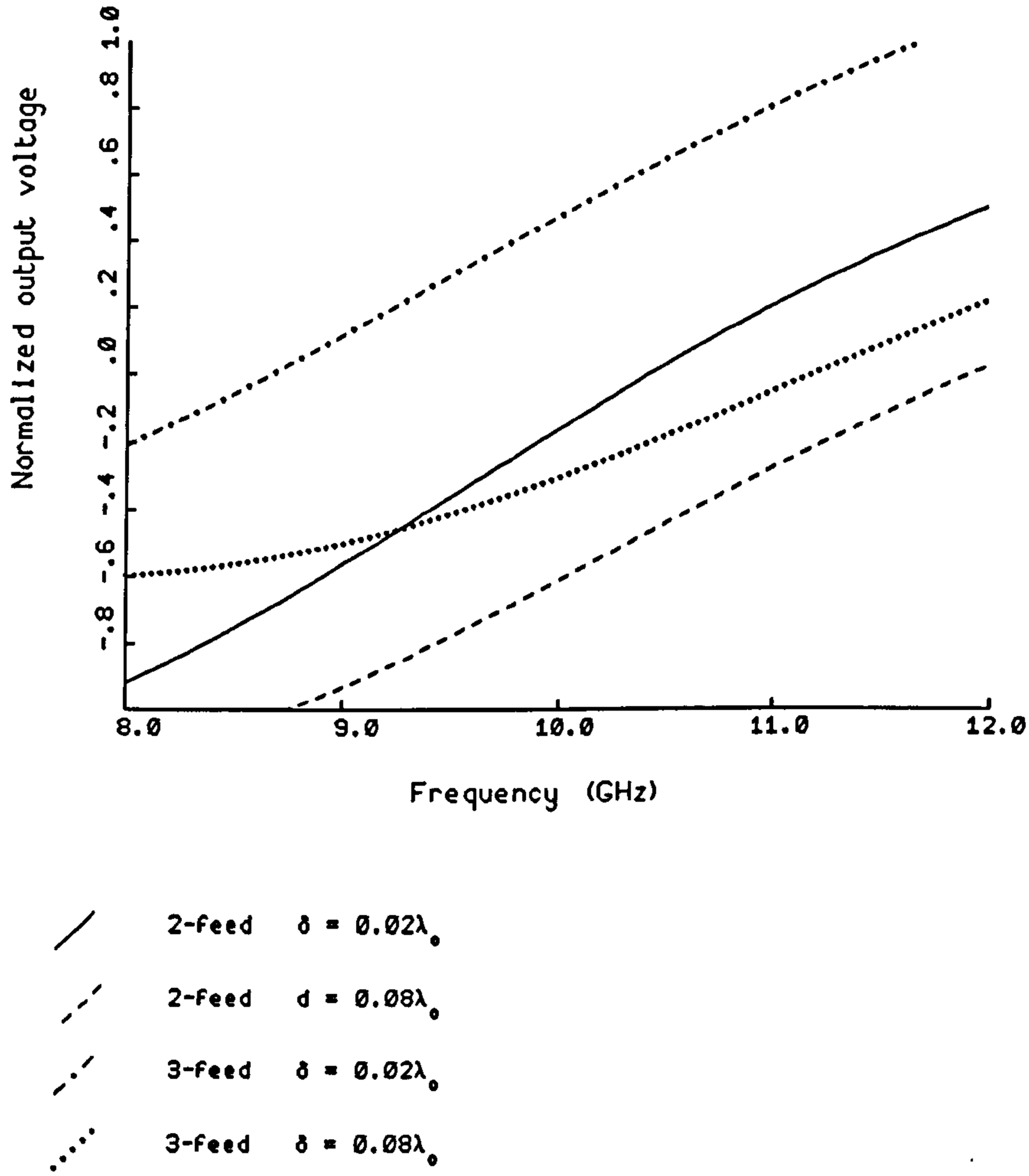

Figure 4.16: **Comparison of discriminator responses with dual-fed and tri-fed rings: large feed spacing**

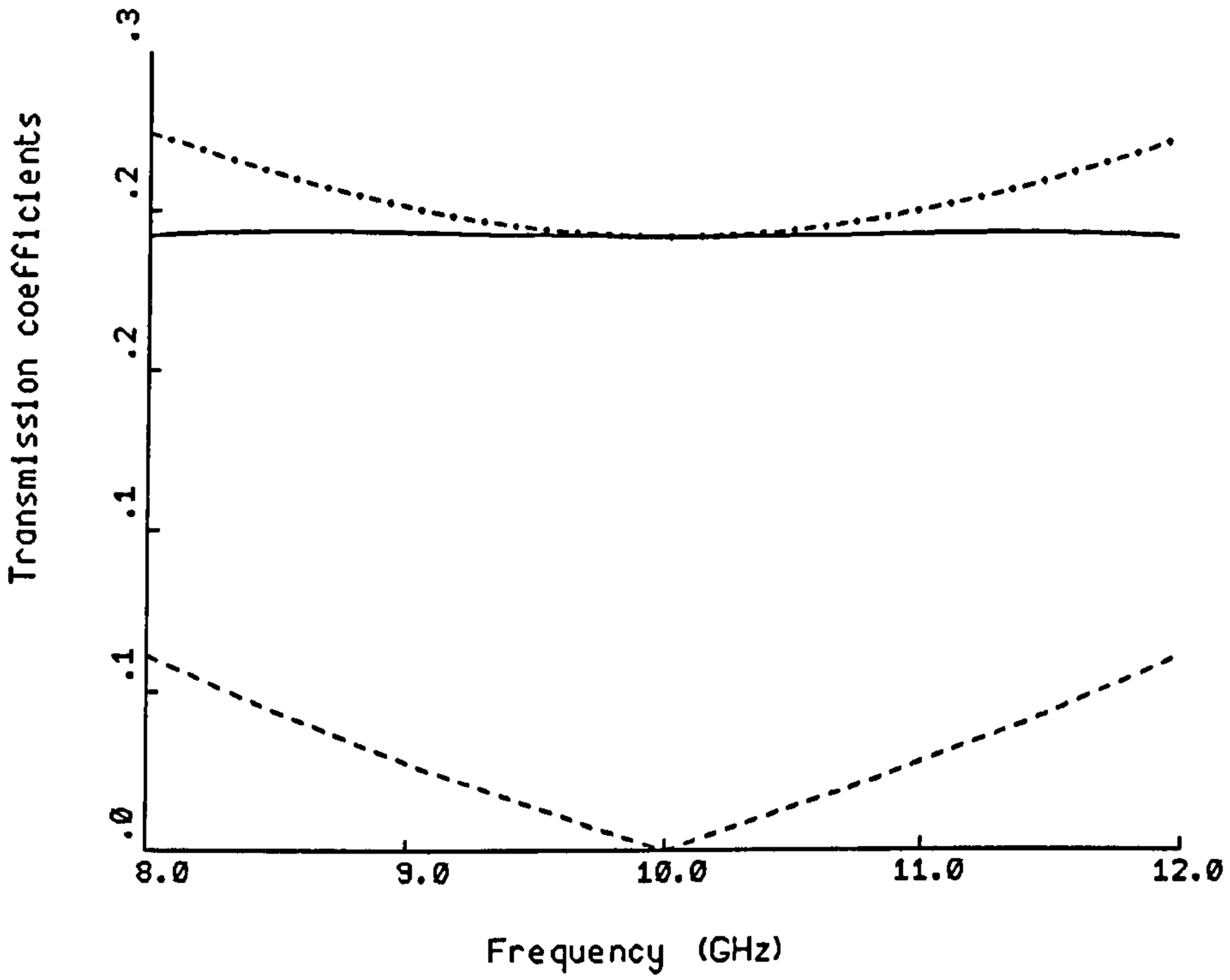

Figure 4.17: **Frequency response of hybrid ring computed using new theory**

Chapter 5

Microwave Oscillator Control using a Single Switched Delay-Line

5.1 Summary

The basic principles of oscillator stabilization and frequency control using delay-line techniques were established in chapter 1. The discussion of these techniques was extended to propose a method of implementation based on existing, well known microstrip components. In chapters 2 and 3 two new microstrip components, namely the single PIN diode phase shifter and three-port ring, were introduced which could perform the required functions of the delay-line technique, but with significant savings in cost and complexity. In this present chapter these new circuit components are combined to provide a simple method of controlling the frequency of a low-noise oscillator.

Measurements from a prototype X-band circuit are presented which confirm the predicted operation. Full circuit details are provided, together with simulations showing the limits of operation.

5.2 Circuit details

A schematic diagram of the circuit investigated is shown in Fig. 5.1, p. 175. The ring dimensions and port spacings were determined through the theory

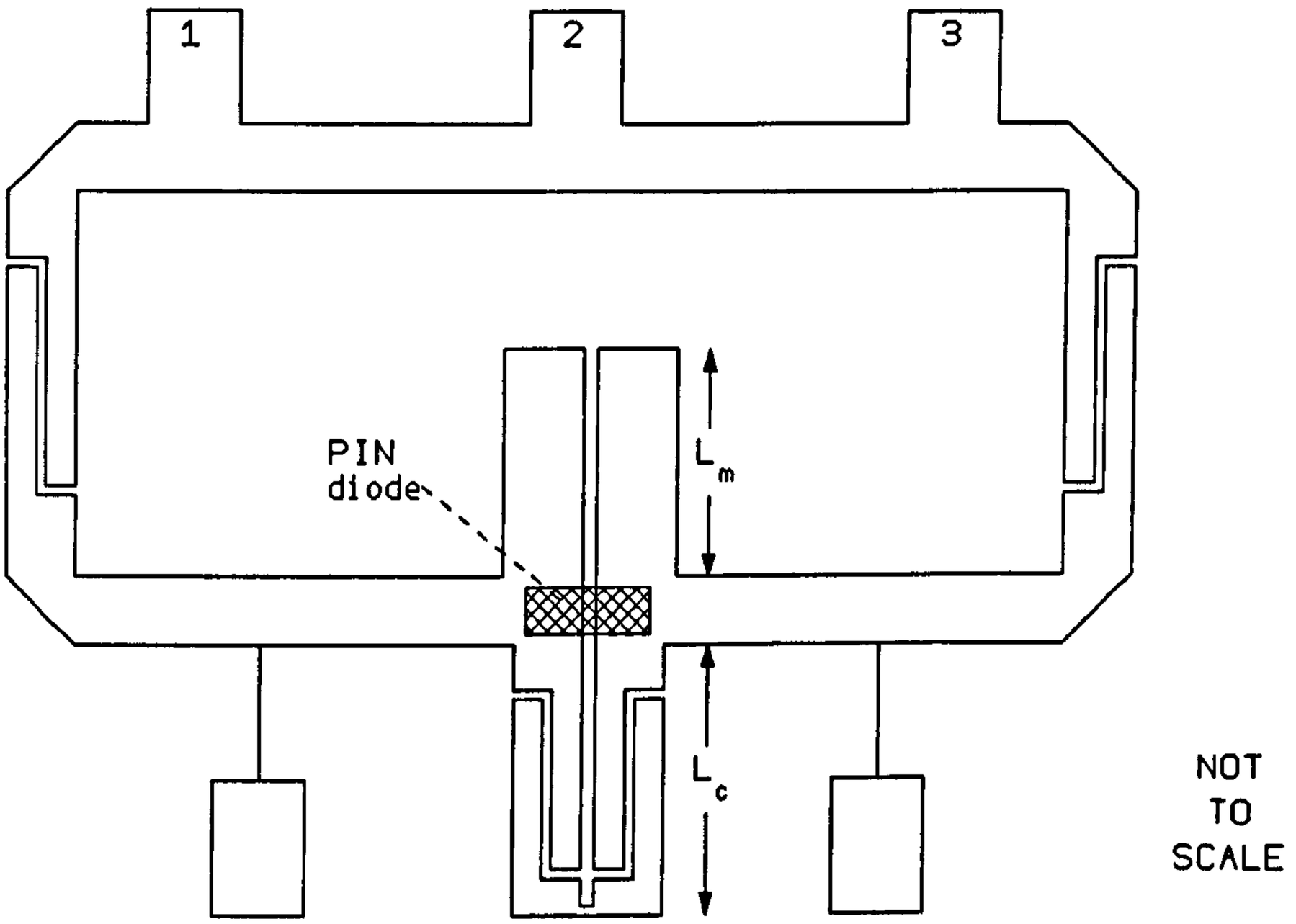

Figure 5.1: **Configuration of a microstrip switched delay-line discriminator**

established in the previous chapters. In the previous chapters, the discussion has been restricted to circular ring structures. However, in order to simplify the mask layout the ring here was made rectangular and appropriate allowances were made in the ring dimensions to allow for the discontinuity due to the chamfered corners. The amount of chamfering on the corners followed the standard recommendation described on pp140-141 of EDWARDS [33], which also gives the equivalent length to be used for the mitred corner. The ring dimensions were calculated to give output port impedances of 50Ω.

The dimensions of the single PIN diode phase shifter were designed to give a switched phase change of 10°, with appropriate allowances being made for the phase changes through the PIN diode in the ON and OFF states. An HP5082-3900 low-loss beam-lead PIN diode was chosen for the active component, mainly because it offered reasonably low insertion loss in the ON state combined with good isolation in the OFF state. As described earlier, the phase shift is primarily determined by the length, l_c, of the coupled line section with the short-circuit termination. Zig-zag slits were incorporated into this section to permit DC biasing of the PIN diode. The DC breaks were included in both sides of the coupled line to maintain the symmetry of the structure and the appropriate transmission phases of these planar breaks, including the excess phase components identified earlier, were included in the calculation of l_c.

Also shown in Fig. 5.1, p. 175 are two conventional bias pads. The lengths were designed to give an effective RF open circuit at the junction with the main ring. An appropriate allowance was made for fringing at the remote end. The width of the narrow section was made as small as the fabrication process would allow, in order to reduce the discontinuity at the junction with the main ring, and the width of the pad was made sufficiently large to permit easy connection of the DC bias leads.

The test circuit was fabricated on RT/duroid 6010, having a substrate thickness of $635\mu m$ and a relative permittivity of 10.4. A summary of the principal dimensions of the circuit is given in Fig. 5.2, p. 177 and a photograph of the circuit is included in appendix B.

5.3 Circuit operation

The oscillator output was applied to port 1 of the circuit shown in Fig. 5.1, p. 175 and a matched pair of coaxial detectors (HP8472A) was connected to ports 2 and 3. The detector outputs were combined in a differential amplifier to yield a discriminator characteristic. A low-pass filter was connected between the differential amplifier output and the frequency control input of the oscillator to suppress any unwanted frequency components generated in the mixer diodes. Switching the PIN diode produced an effective change in the delay path between ports 1 and 3, and produced an offset voltage at the dif-

SINGLE PIN DIODE PHASE SHIFTER:

Coupled line length, l_c = 5.5mm
Coupled line gap = 110μm
Matching stub length, l_m = 5.2mm
Axial length of zig-zag slit = 3.5mm
Width of zig-zag slit = 40μm

RING:

Track width = 310μm
Port spacing (c-c): 1-2 = 3mm
2-3 = 3mm
1-3 = 32mm

DC Break: axial length = 3.1mm
finger width = 250μm
finger spacing = 45μm

Port width = 600μm

BIAS PADS:

Narrow line width = 33μm
Narrow line length = 3.1mm
Wide line width = 1.7mm
Wide line length = 2.8mm

Figure 5.2: **Measured dimensions of the switched delay-line test circuit**

ferential amplifier output. The magnitude of this voltage was proportional to the amount of delay change. This voltage would then cause a step change in the frequency of the oscillator, which would remain stabilized because of the basic discriminator function of the ring. The amount of frequency change, for a given phase change in the ring, could be set by adjusting the sensitivity of the differential amplifier.

5.4 Test conditions

For testing, the microstrip circuit was mounted in a standard Omni Spectra hybrid MIC test fixture, with coaxial-to-microstrip transitions used to couple signals to and from the circuit. The oscillator used for the test was an HP694D sweep oscillator. This was chosen because it offered a convenient VCO facility and a level of phase noise which could conveniently be measured to demonstrate the phase noise reduction provided by the test circuit.

The frequency of the oscillator was observed on an HP8592B spectrum analyser. To measure the phase noise, an HP3561A low frequency dynamic signal analyser was connected to the output of the low-pass filter in the feedback network. The overall test arrangement is shown in Fig. 5.3, p. 179. A continuous averaging function was selected on the HP3561A to provide a display of rms noise.

5.5 Results and discussion

Typical results for the three-port ring incorporating a single PIN diode phase shifter are shown in Fig. 5.4, p. 180, with an example of the close-carrier phase noise response for one of the PIN diode states being given in Fig. 5.5, p. 181.

The results in Fig. 5.4, p. 180 show that a significant frequency step, 30MHz, can be achieved without a significant change in the input match of the ring. Clearly, any change in the return loss between diode states is of particular importance for this type of arrangement, since any mismatch within the ring, due to the switching of the phase shifter element, will cause a change in level at the detector diodes. In these circumstances the offset voltage will be a function of the mismatch in addition to that due to the designed change in phase. The fact that a predictable frequency step can be achieved, with

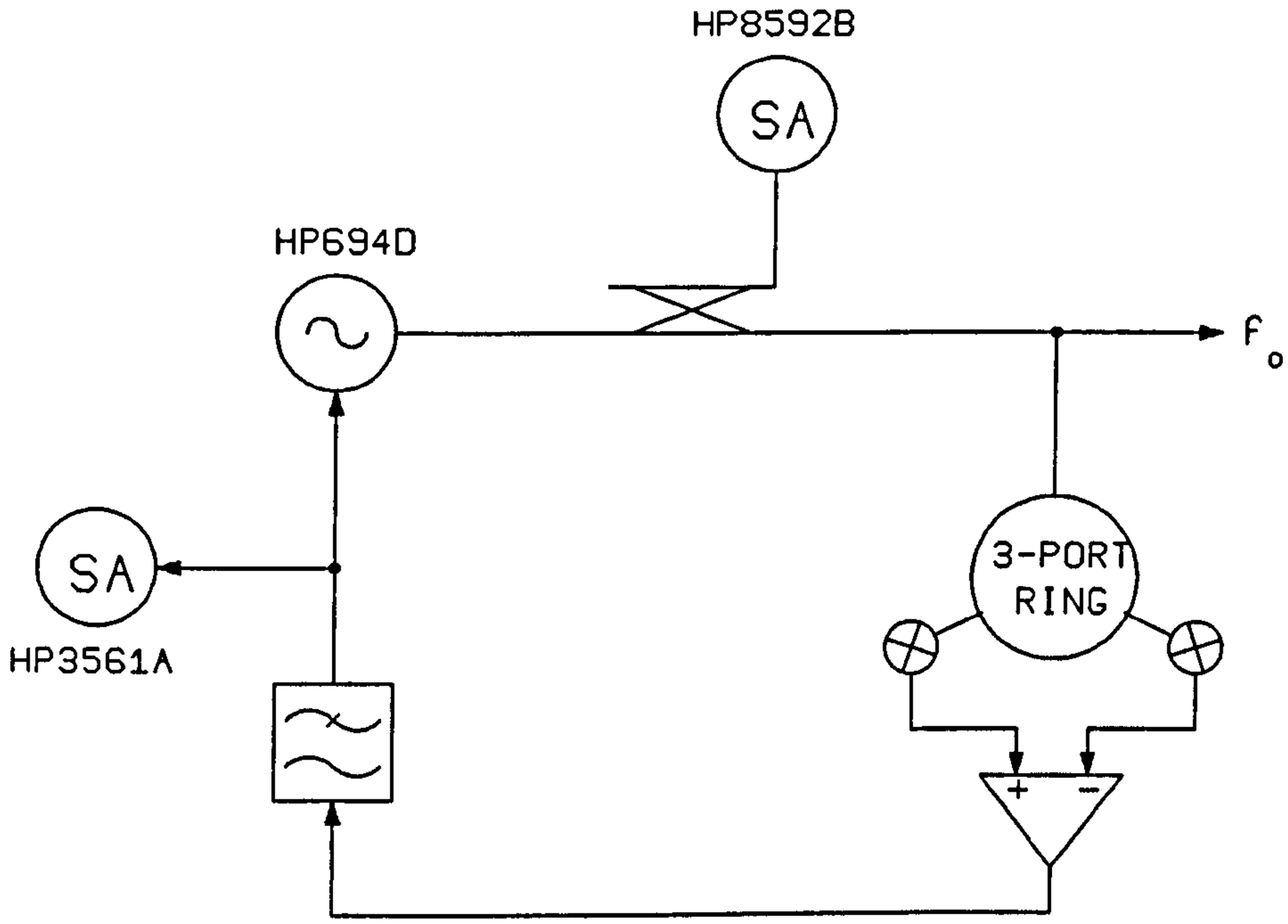

Figure 5.3: **Test system**

only a 0.31dB change in return loss at the external input port indicates that the change in match within the ring is not significant. The absolute value of return loss was of the order of 12dB, although this is less important in the present context than the change in insertion loss which occurs between states.

In order to investigate further the effect of mismatches within the ring, the behaviour of the ring structure, containing an additional mismatched element within the delay path was simulated using MDS. The model for the simulation is shown in Fig. 5.6, p. 182, where the phase shifter is represented by a two port network whose return loss could be varied. This variation was achieved

Carrier frequency	11GHz
Stabilization ratio	6
Switched frequency step	30MHz
Change in input return loss between states	0.31dB
Open-loop phase noise 5kHz off carrier	-75dBc/Hz
Closed-loop phase noise 5kHz off carrier	-91dBc/Hz

Figure 5.4: **Summary of key results**

through adjustment of the ratio of the characteristic impedance of the two-port network relative to that of the ring. For the purpose of this simulation, which was specifically to investigate the effects of reflections within the ring it was assumed that this two port network had zero transmission loss and a transmission phase of 10°. This value of phase change was chosen to be representative of the values that would be used in practice. The results of the simulation are shown in Fig. 5.7, p. 183 and Fig. 5.8, p. 184; each simulation corresponds to a particular value of return loss for the network representing the phase shifter. Three responses are given in each figure: S_{11} is the reflection coefficient at the input port of the ring; S_{21} is the transmission coefficient between port 1 and port 2; S_{31} is the transmission coefficient between port 1 and port 3. Of particular interest is the frequency at which the S_{21} and S_{31} responses intersect, since this represents the centre of the discriminator response. The simulations show that mismatches within the ring have a small effect on the input match of the ring. However, this is not of great practical significance since the ring would not be in the main path

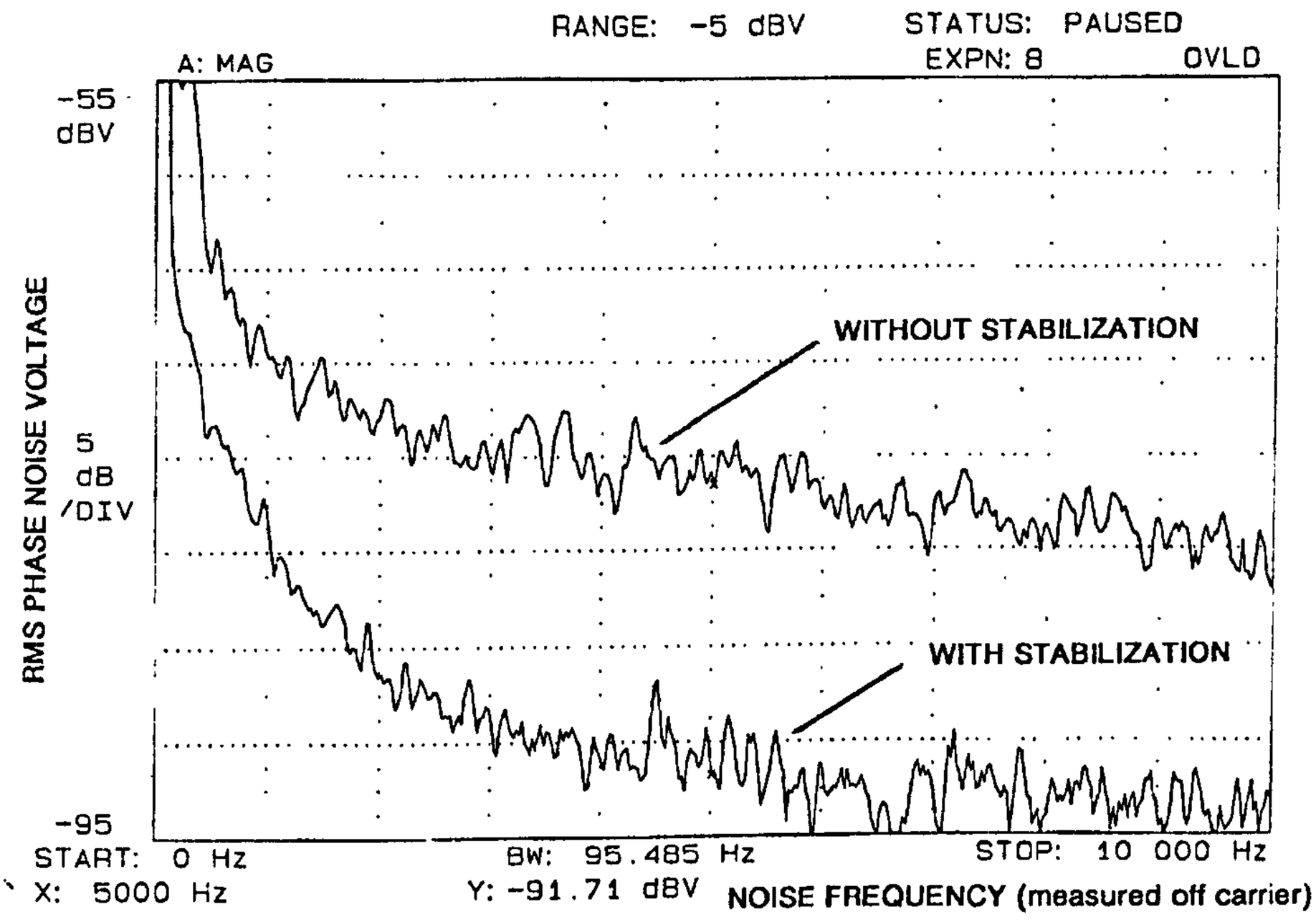

Figure 5.5: **Phase noise responses**

of the oscillator output and could also be preceded by an isolator. It is of more importance that the S_{21} and S_{31} responses are displaced in frequency due to the mismatch within the ring, since this will lead to an error in the differential output from the phase detector. It can be seen from Fig. 5.7, p. 183 and Fig. 5.8, p. 184 that changing the return loss of the component within the ring from 10dB to 20dB caused a shift of 300MHz in the crossing point of the S_{21} and S_{31} responses. Additional simulations were performed to show how the differential output voltage from the ring varied with the return loss of the component in the ring. The results are summarised in Fig. 5.9, p. 184 and indicate that the change in differential output voltage is not significant for phase shifter return loss values greater than 20dB. Results for the single PIN diode phase shifter alone have shown that that it could be designed and fabricated with a return loss better than 20dB over a 10 per cent bandwidth. This indicates that the design approach is valid and that the errors associated with mismatches within the ring can be kept within acceptable limits in practical situations.

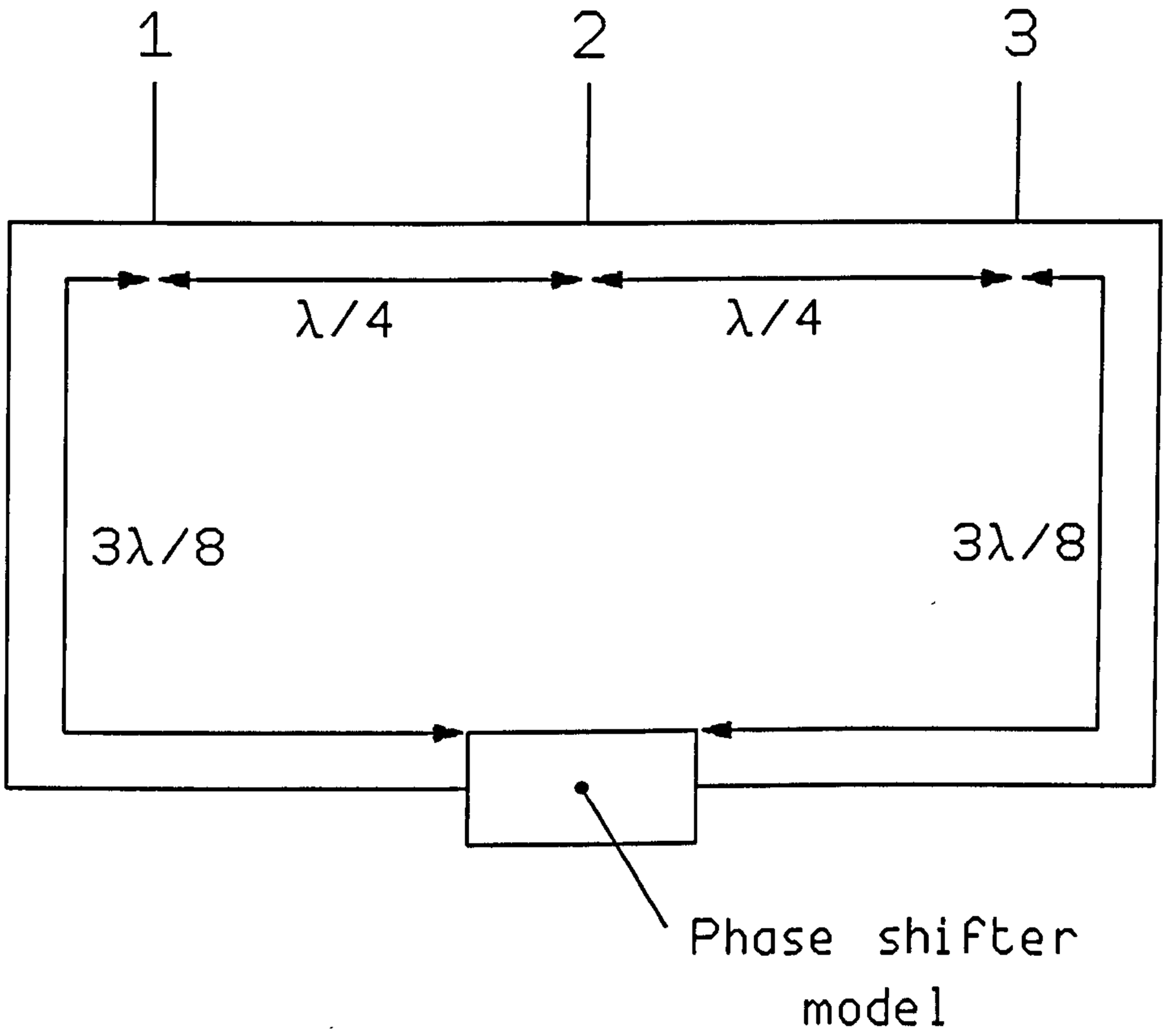

Figure 5.6: **Model used for simulation of three-port ring responses, in order to investigate the effect of mismatches within the ring**

The value of the stabilization ratio given in Fig. 5.4, p. 180, measured as the ratio of the frequency deviations of the oscillator to a DC control stimulus under open and closed loop conditions is a direct function of the sensitivity of the differential amplifier, and can thus be set to any desired value. One implication of this is that the phase change steps introduced into the ring can be comparatively small and still yield an appreciable change in frequency of the VCO.

The bandwidth of the circuit tested was found to be relatively narrow, of the order of ±5 per cent, as expected from the basic theory of the three-port ring. This could be improved by introducing some form of broadband matching in the ring, following the techniques used for broadbanding four-

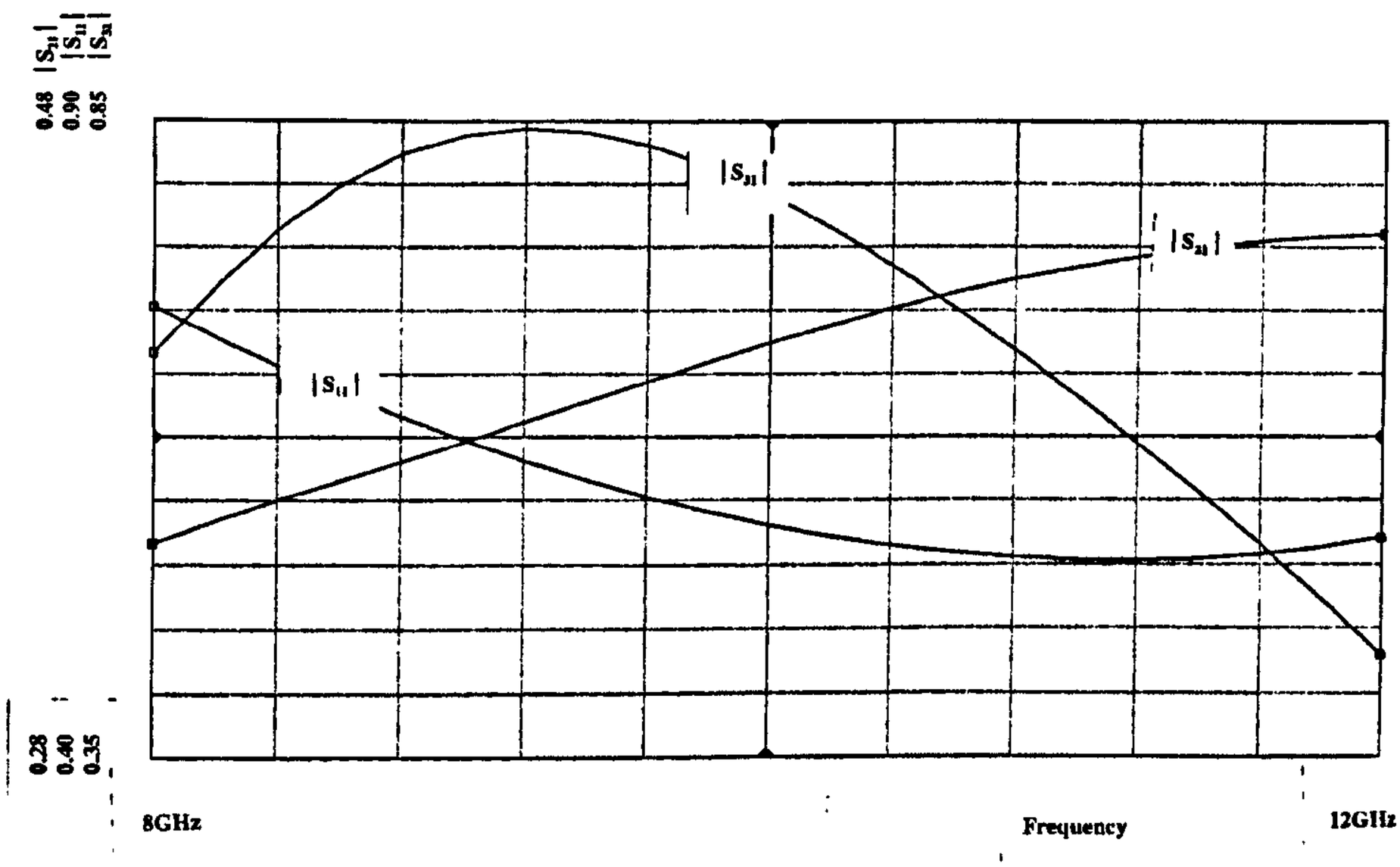

Figure 5.7: **Simulation of three-port ring responses showing effect of a mismatch within the ring: return loss of phase shifter model = 10dB**

port hybrid rings. However, a ±5 per cent bandwidth at 10GHz still yields a usable frequency range of 1GHz, which would be acceptable for a number of applications. Wideband operation could be achieved, still with significant cost benefits, by effectively cascading a number of three-port ring structures, each designed with a different centre frequency.

The phase noise reduction, shown in Fig. 5.5, p. 181, was observed in both diode states. The magnitude of the reduction is a function of the differential amplifier sensitivity, and the variation of the reduction with frequency is determined by the combined frequency response of the differential amplifier and low-pass filter. Two examples of the measured phase noise, expressed in the conventional units of dBc/Hz, are given in the results table in Fig. 5.4, p. 180, using values taken from Fig. 5.5, p. 181. In the latter case the phase noise is left as a relative level, since the absolute value is a function of the particular test oscillator being used and is not of primary interest here.

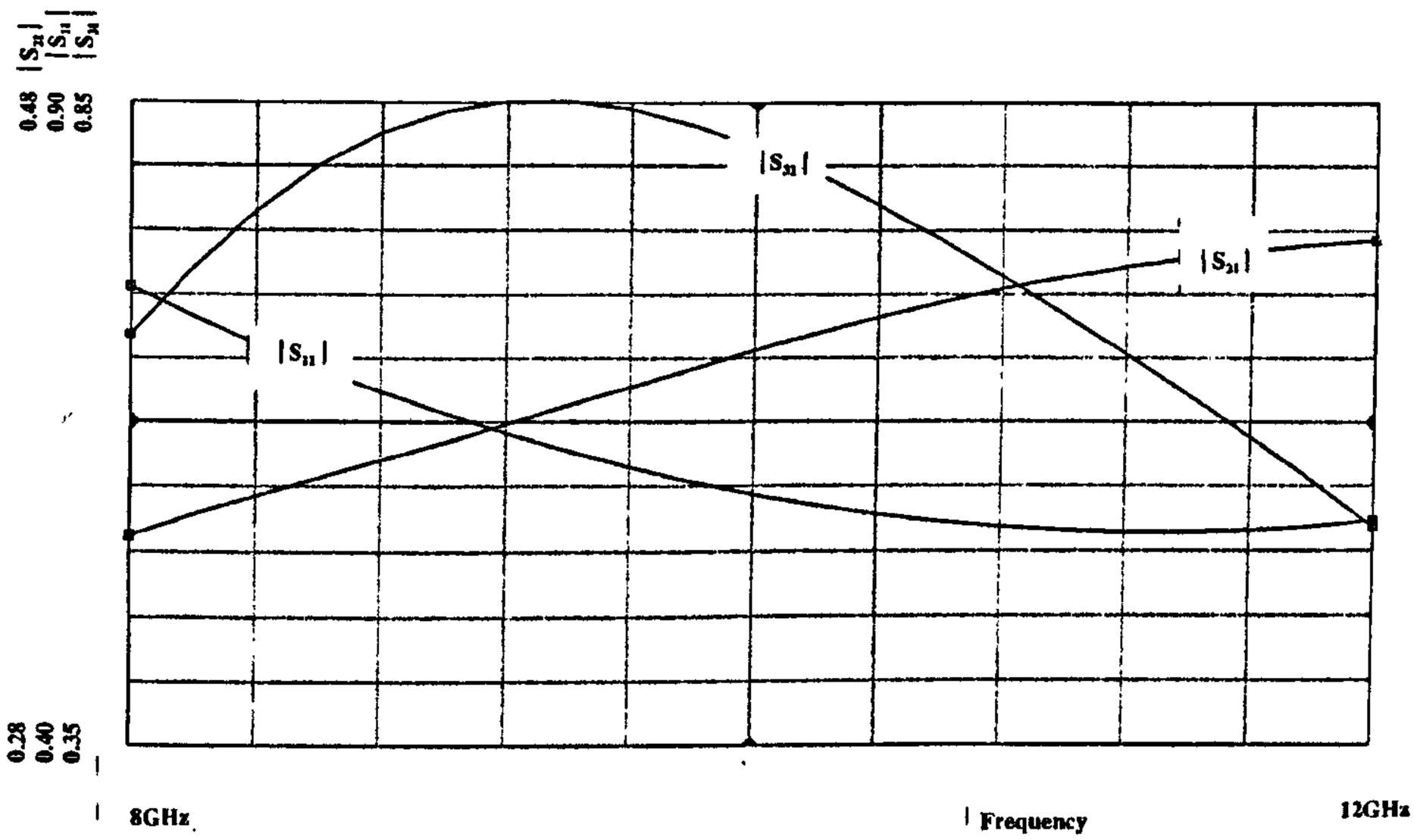

Figure 5.8: **Simulation of three-port ring responses showing effect of a mismatch within the ring: return loss of phase shifter model = 20dB**

RETURN LOSS (dB)	% change in V_o
∞	0
20	0.53
15	3.74
10	16.58

Figure 5.9: **Effect of mismatches within ring on differential output voltage**

5.6 Conclusions

The predicted functions of a delay-line stabilized oscillator, incorporating a frequency selection capability, have been verified through practical X-band measurements on a prototype microstrip circuit. The novel technique, together with the use of new circuit geometries, offers significant potential for the development of digitally controlled microwave oscillators, either in hybrid or monolithic form.

Chapter 6

A Digitally Controlled Microwave Oscillator

6.1 Summary

A new and potentially powerful technique for digitally controlling the frequency of a microwave oscillator is described. The technique makes use of the theory developed in chapter 4 for dual-fed three-port rings.

It was shown in chapter 4 that the discriminator function of the three-port ring could be maintained if the position of the feed port was changed. Furthermore, it was shown that as the input port position was changed an offset voltage was generated at the nominal centre frequency, which exhibited a quasi-linear relationship with the change in position. The theory was extended to show that a dual-feed ring could produce three, equi-spaced offset voltages corresponding to the three possible feed combinations i.e. two single feeds and one dual feed.

In this chapter results are presented for two three-port ring microstrip circuits which show how these offset voltages can be used to control the frequency of an X-band oscillator.

6.2 Multi-feed three-port ring

The circuit arrangement of an oscillator whose frequency is controlled by a three-port ring with four input feed positions is shown in Fig. 6.1, p. 187. The

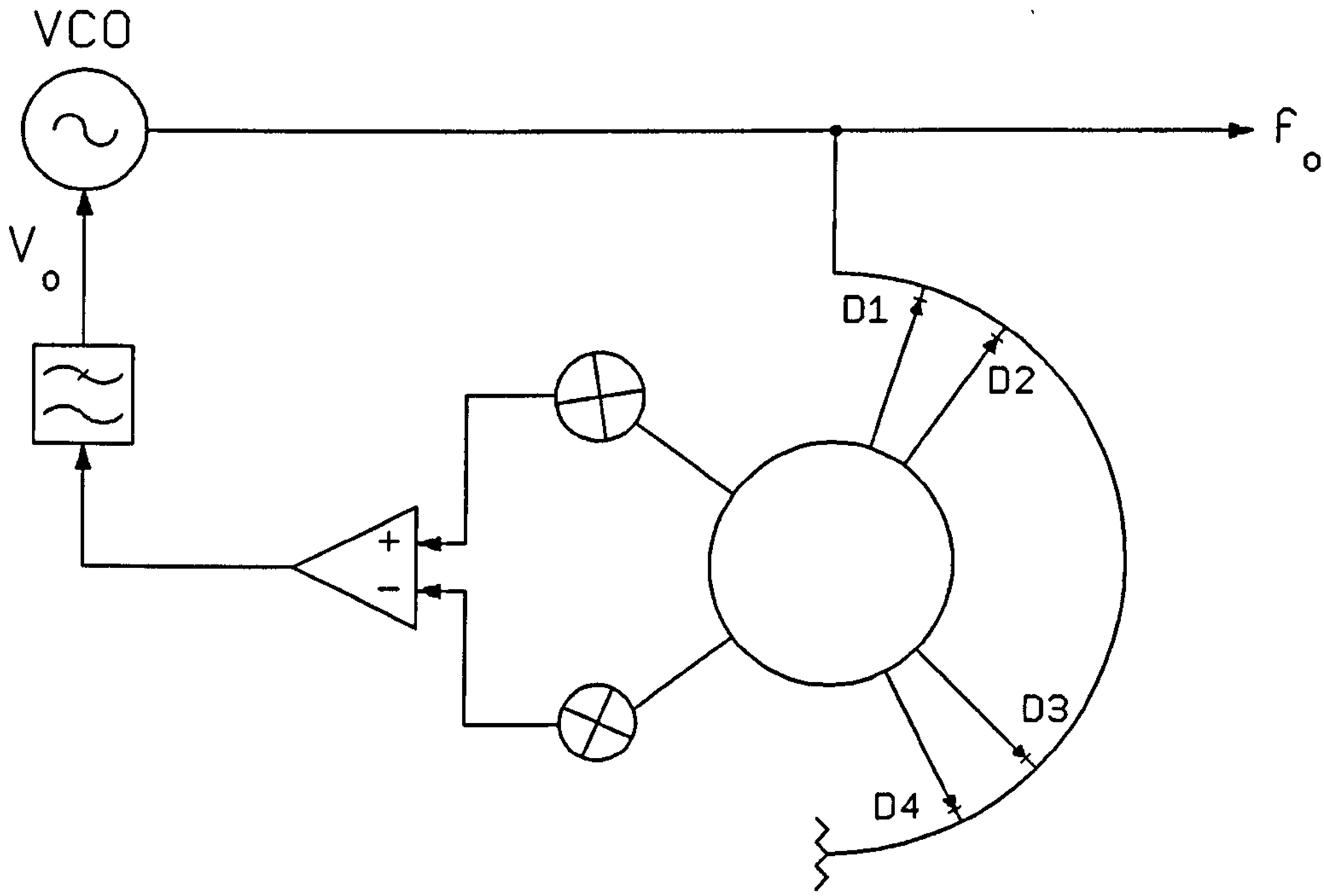

Figure 6.1: **Frequency control circuit with multi-feed three-port ring**

diodes D1, D2, D3 and D4 determine the point at which the three- port ring discriminator is fed. In order to avoid unwanted coupling between closely spaced feed lines, diodes D1 and D2 provide inputs to one side of the ring and D3 and D4 inputs to the opposite side. It should be noted that changing the feed position from one side of the ring to the other causes a change in polarity at the output of the differential amplifier. This means that there must be a simultaneous switching of the output voltage polarity if the feed position is switched between opposite sides of the ring. The voltage output from the differential amplifier was fed through a low-pass filter to control the frequency of the VCO in the usual manner.

A photograph of the actual 10GHz microstrip test circuit is shown in appendix B. The circuit was fabricated on RT/duroid substrate having a

thickness of $635\mu m$ and a relative permittivity of 10.4. Low-loss, beam-lead diodes (HP5082-3900) were used as the switching elements. The track dimensions were designed to provide output impedances of 50Ω, so as to match the input impedances of a matched pair of coaxial detectors (HP8472A) which were externally connected to the microstrip circuit. Three chip capacitors were mounted in the main line from the oscillator, so as to permit independent biasing of the four PIN diodes. The DC control to the centre two diodes was provided through conventional microstrip pads. The outer PIN diodes were biased off-circuit using standard coaxial bias-tees. One crucial element in the design was the length of the feed lines connecting each diode to the ring. These lengths were made $\lambda_s/2$, where λ_s is the substrate wavelength, so as to reflect a high shunt impedance across the ring with the diode in the off state. For testing, the circuit was mounted in a conventional Omni-Spectra test fixture, and connected to external devices through coaxial-to-microstrip transitions.

6.3 Dual-feed three port ring

Fig. 6.2, p. 189 shows the circuit arrangement of an oscillator controlled by a dual-fed three-port ring. Since the control circuit is an extension of the three-port ring principle introduced in chapter 3, the ring circuit will be referred to using this nomenclature, although in the present case the ring has four active ports when both diodes are in the ON state. The operation of the circuit follows directly from the theory which was established in chapter4. The two diodes, D1 and D2, allow the ring to be fed at two different positions, either independently or simultaneously. Thus three offset voltages are possible, which permit the selection of three equi-spaced frequencies. The configuration of the feed connections to the ring is somewhat different to that used for the multi-feed ring described in the previous section. An arrangement was chosen for the dual-feed such that with both diodes biased in the ON state, the two feed connections would supply equal power to the ring.

A photograph of the actual microstrip test circuit is shown in appendix B. The circuit was fabricated on RT/duroid having a substrate of relative permittivity 10.4 and thickness $635\mu m$. Surface mount, low-loss, beam-lead PIN diodes (HP5082-3900) were used as the switching elements. The ring dimen-

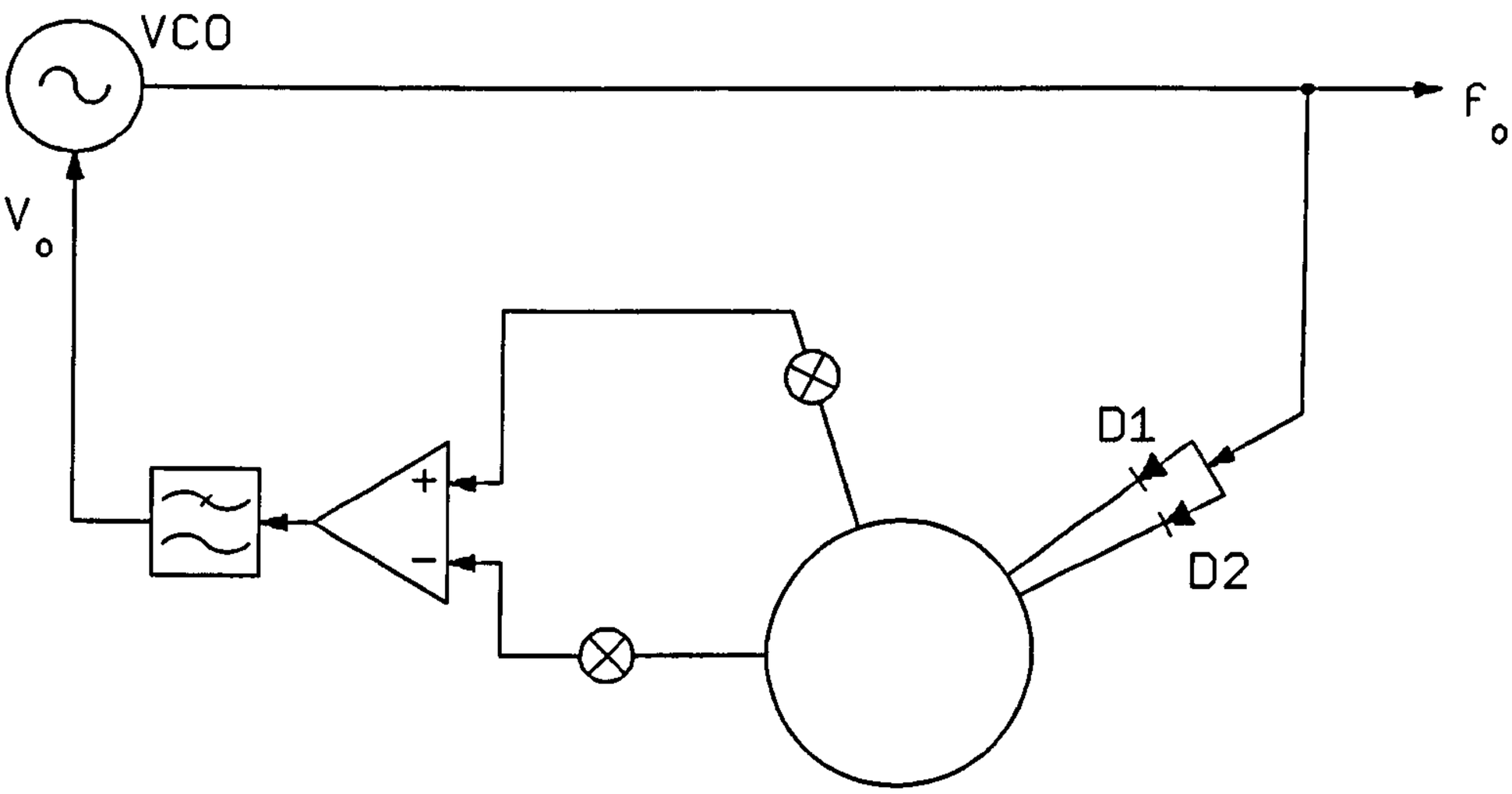

Figure 6.2: **Frequency control circuit showing a dual-feed microstrip ring**

sions were chosen to give a nominal centre frequency of 10GHz, and output port impedances of 50Ω. The input port was not matched. Chip capacitors were surface mounted across gaps in the ring to permit independent biasing of the two PIN diodes. The DC bias connections were made externally to the microstrip circuit using conventional coaxial bias- tees. For measurement, the microstrip circuit was mounted on a standard Omni-Spectra test fixture with coaxial-to-microstrip transitions used to make the external connections.

6.4 Test conditions

The test conditions were essentially the same as those described in Chapter 5 for the switched delay-line circuit. Additional measurements were made on the dual-feed circuit to find the settling time and the transient response overshoot. These measurements were made by monitoring the voltage output from the discriminator when the diodes were switched using a low frequency

	Single feeds	Digital feed
Selected frequencies (GHz)	9.9,10.0 10.1,10.2	10.0,10.1 10.2
Phase noise reduction (5kHz off carrier)	~13dB	~13dB
Stabilization ratio	5	5
Settling time (PIN diode: ON→OFF) (100MHz step)	340μs	360μs
Settling time (PIN diode: OFF→ON) (100MHz step)	350μs	353μs
Voltage (frequency) overshoot (PIN diode: ON→OFF) (100MHz step)	120%	140%
Voltage (frequency) overshoot (PIN diode: OFF→ON) (100MHz step)	44%	39%

Figure 6.3: **Summary of typical measured results**

pulse generator. The voltage changes seen at the output of the discriminator, before the low-pass filter, are directly proportional to the frequency changes in the oscillator output, assuming the system to be linear. Since only small frequency steps, less than 2% of the carrier frequency, are being investigated, the assumption of a quasi-linear system is valid.

6.5 Results and discussion

A summary of the typical results for the two circuits investigated is shown in Fig. 6.3, above. The single feed and digital feed columns refer to the circuits shown schematically in Fig. 6.1, p. 187 and Fig. 6.2, p. 189 respectively. In the case of the multi-feed ring with four selectable inputs, switching the

PIN diodes gave four predictable frequencies, separated by constant intervals. This demonstrated the ability of the circuit to provide linear frequency control. Since the four inputs were split, with two on either side of the ring, so as to minimise coupling between the input lines it was necessary to reverse the polarity of the inputs to the differential amplifier when switching from one side of the ring to the other. This was done manually for the present measurements although it would be simple to arrange for this to be performed automatically through a switching network linked to the switching control of the PIN diodes. Thus in practice this would not impose any limitation on the operation or usefulness of the circuit. However, there are clearly some limitations to the number of feed arms to the ring and hence to the number of selectable frequencies. In particular the spacing of the feed arms must be sufficient to prevent unwanted coupling. Moreover, the theory has shown that as the position of the feed port is varied, with respect to the output ports, so the slope of the discriminator response changes. Ultimately, with the feed port located symmetrically between the output ports, the slope would be zero and the discriminator function would vanish. The slope of the discriminator response is important if the same order of stabilization and phase noise reduction is to be maintained for all selected frequencies, as would be required in a practical situation. However these limitations could be overcome by making the ring larger, or cascading several rings, thereby providing a greater range of selectable frequencies. For the dual-feed circuit, the results show that the three possible diode state combinations yielded three frequencies with approximately equal intervals between them. In both circuits the magnitude of the frequency steps can be changed by altering the sensitivity of the feedback amplifier. The oscillator remained stabilized at all of the selected frequencies and a typical plot of the relative phase noise, showing the effect of stabilization, is reproduced in Fig. 6.4, p. 192. A phase noise reduction of approximately 13dB was observed 5kHz off the carrier and this is consistent with a measured stabilization ratio of 5. The absolute values of phase noise were not calculated since these are functions of the particular test oscillator being used and are not of primary interest here. It should also be noted that using this method of measurement, the measured value is the effective sum of the FM and AM noise from the oscillator. Since we are primarily concerned with the reduction in phase noise due to the sta-

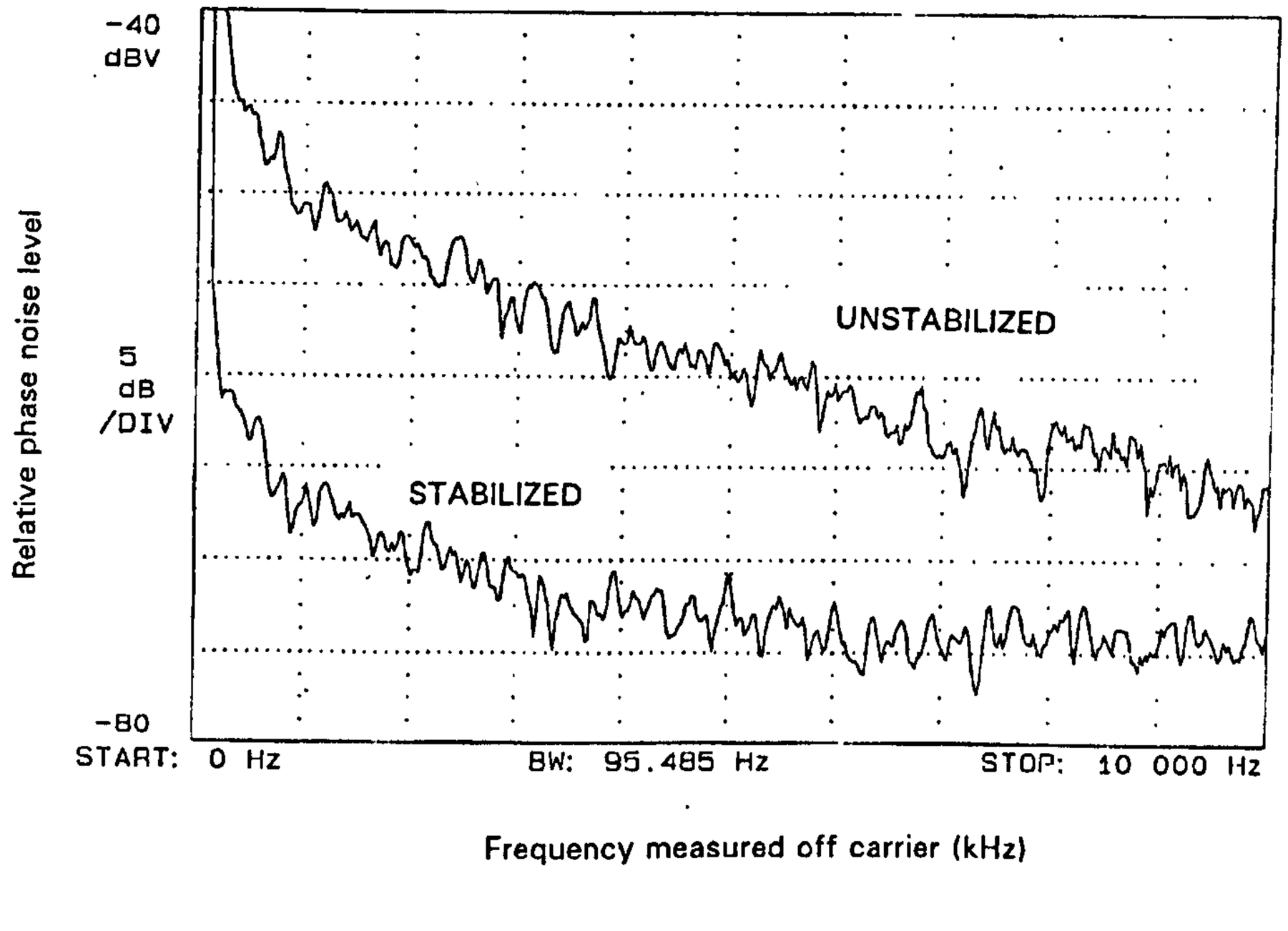

Figure 6.4: **Measured phase noise**

bilizing effect of the feedback network, the presence of the AM noise is not particularly significant, as this component of noise should be the same with the circuit locked or unlocked. Generally, the AM noise from an oscillator will be less than the FM noise and will only have a small effect on the result. For interest, the AM noise of the oscillator being used for the tests was measured, and the response is shown in Fig. 6.5, p. 193. The values of the AM noise values are left in dBV so that a general comparison can be made with the previous phase noise values. Although the AM noise was measured with the same system as the phase noise, i.e. with the same bandwidths and detector efficiencies, but with the frequency discriminator removed, an exact comparison must include the sensitivity of the frequency discriminator. In this case the AM and FM noise could be expressed relative to the carrier level in units of dBc/Hz. This was not done for the present work, which was primarily concerned with the phase noise reduction and where it was evident that the AM noise was relatively small. Fig. 6.6, p. 194 shows the magnitude of the phase noise suppression, plotted as a function of frequency. It can be

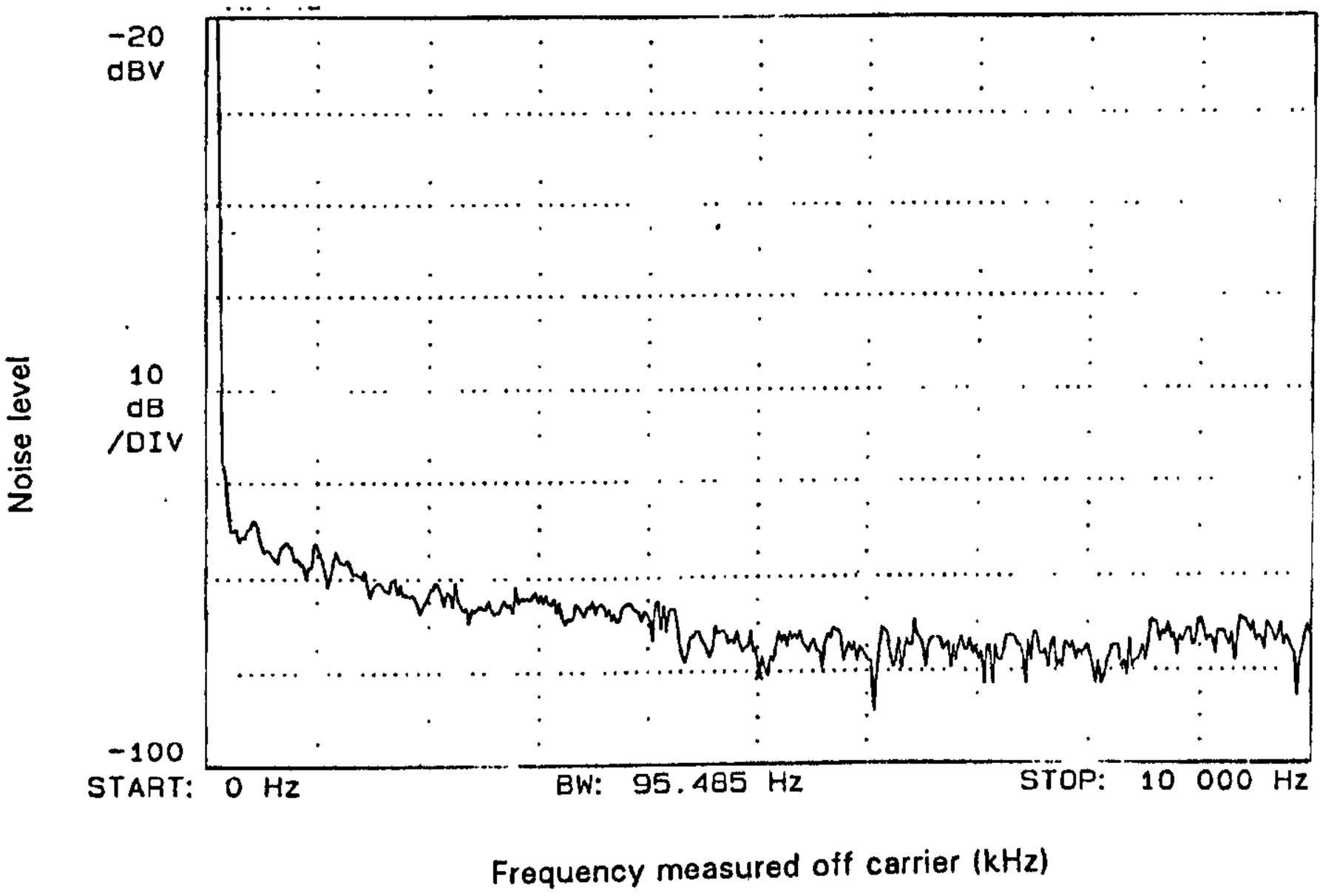

Figure 6.5: **Measured AM noise**

seen that there is a decrease in suppression as the frequency increases. This is due to the low-pass filter in the feedback loop. For these measurements the filter used was a simple active 2-pole low-pass filter with a 3dB cut-off frequency at 8kHz.

Although the principal aim of the work has been to investigate methods of controlling the frequency of an oscillator, rather than to achieve frequency agile oscillators with a fast response time, additional measurements were made for completeness on the settling time of the oscillator controlled by the new microstrip circuits. As CRAWFORD [24] points out the definition of settling time tends to vary according to the application. He quotes examples of QPSK systems, where the settling time is defined as that which enables the frequency of the oscillator to settle to within 0.1 radians of the steady state final phase. A somewhat more stringent specification is given for analogue cellular telephone systems where the time is that for the oscillator to settle within 100Hz of the steady state value of frequency. In the present work, the settling times have been calculated from the measured time responses on the

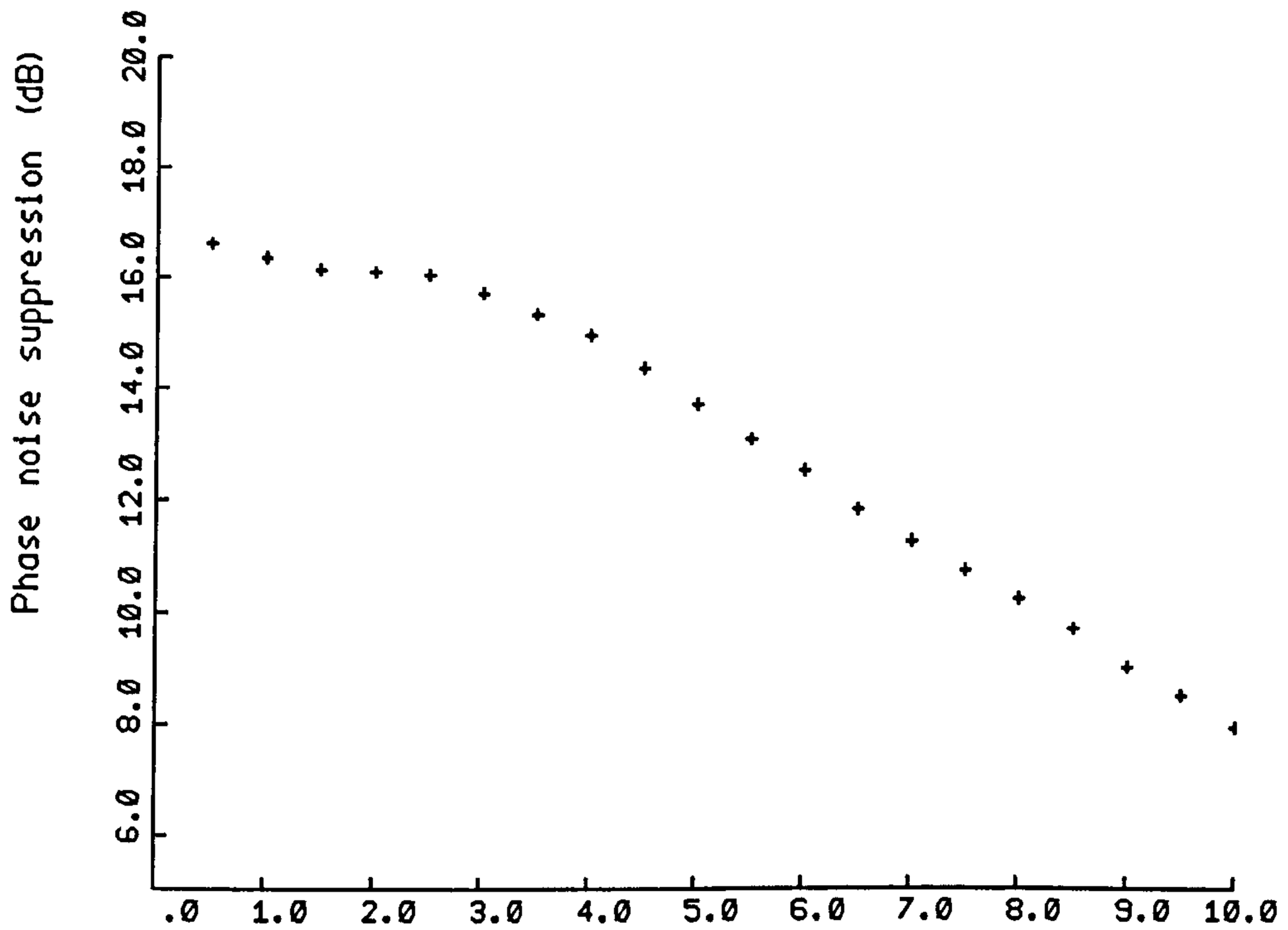

Figure 6.6: **Phase noise suppression**

basis of the time taken for the oscillator to settle within 10% of the frequency step value. It can be seen from the measured data in Fig. 6.3, p. 190 that the transient behaviour of both circuit configurations was very similar in respect of the speed of response. This is not unexpected since the principal difference between the circuits was in the configuration of the microstrip feed network, while the active or band-limited components which primarily determine the transient behaviour were the same in both cases.

The measured transient responses of the oscillator due to a 100MIIz step in frequency produced by the dual-feed circuit are shown in Fig. 6.7, p. 195 and Fig. 6.8, p. 196. Also shown in these figures are the corresponding switching edges of the PIN diode control voltage obtained from the pulse generator. The rise and fall times of the pulse generator output were mea-

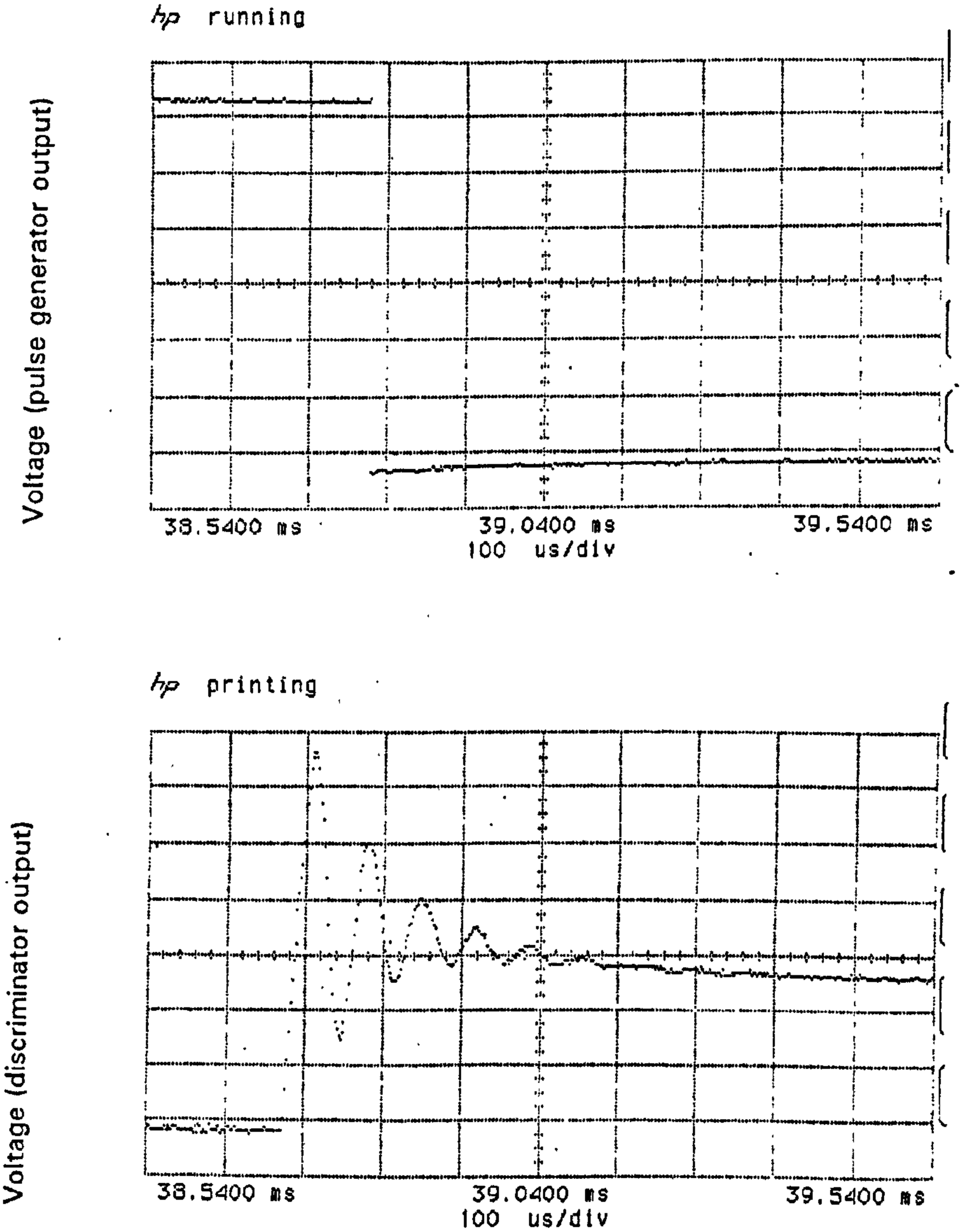

Figure 6.7: **Transient response when PIN diode turned OFF**

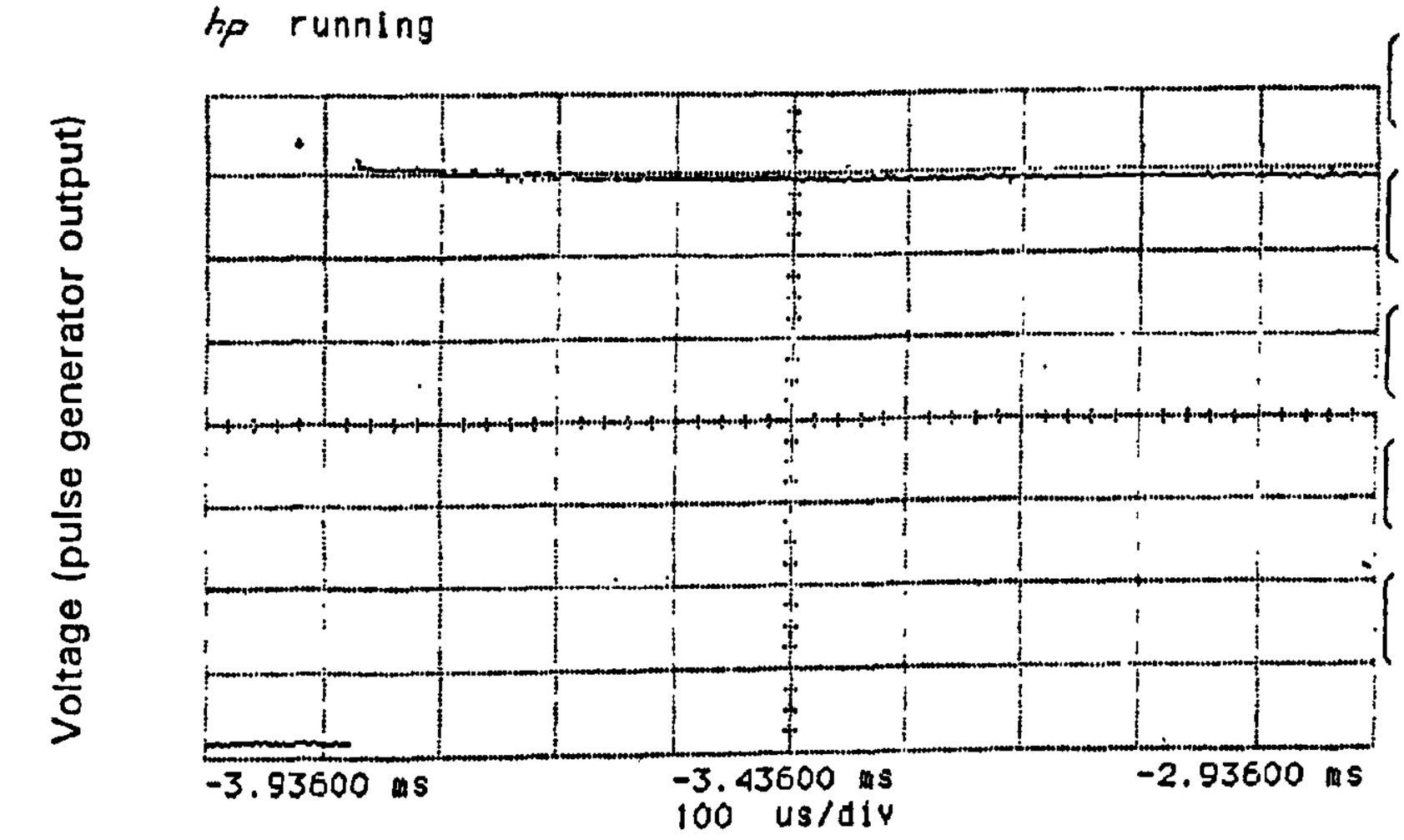

Figure 6.8: **Transient response when PIN diode turned ON**

sured separately and found to be less than $12\mu s$. Since there always has to be at least one diode switched on in these circuits, the responses were obtained by biasing one diode permanently on and using the pulse generator to switch the state of another diode. This biasing strategy was necessary because in the test circuits all the diodes were mounted in the same sense, i.e. with all the cathodes connected together. Thus turning one diode on and another off would have required two independent switching waveforms, with the pulse edges very closely synchronized to avoid spurious transient effects. In the measured responses the rear edge of the switching waveform corresponds to the diode being turned off and the front edge to the diode being turned on. The settling time for each edge is essentially the same. This would be expected since the only difference is in the behaviour of the PIN depletion region when the charge plasma is being formed and when the region is swept clear by a reverse bias. Any differences associated with the response time of the junction in these two circumstances are related to the lifetime of the carriers. This is of the order of a few micro-seconds, which is very much less than the total measured settling time. Thus the difference in PIN junction behaviour due to the rising and falling edges of the switching waveform would not be observable. It would also be expected that the settling time would be a function of the frequency step size, with a large step causing a large perturbation of the signal in the feedback loop and hence a long settling time. This was confirmed by measurement and the measured variation in settling time due to different frequency steps is plotted in Fig. 6.9, p. 198 for both pulse edges. The figure shows the same order of settling time for both switching edges, for a given frequency increment. It can also be seen that the settling time exhibits a quasi-linear relationship with frequency step size. The random variation in the measured values is largely due to the problems in reading the settling time values from a digitized display waveform and is not of particular significance.

It is interesting to note that the percentage transient overshoot is greater for the rear edge switching, i.e. with the diode being turned off. This difference in transient behaviour for the two switching edges was observed for all of the measured frequency steps and for both test circuits. Since these transient overshoot effects occur in a short time, which is comparable with the lifetime of the carriers, it could be concluded that they are due to differences

Frequency step (MHz)	Settling time (PIN on→off) (μS)	Settling time (PIN off→on) (μS)
10	173	173
25	199	211
50	239	245
100	341	352

Figure 6.9: **Measured variation of settling time with frequency step size**

in the behaviour of the junction during turn-on and turn-off which have been alluded to previously. The observed effect suggests that it takes relatively more time to sweep charges from the depletion region, thereby causing the circuit to respond more slowly during the initial turn-off period.

The absolute values of the transient overshoot should be a function of the loop bandwidth. This was confirmed by removing the low-pass filter and repeating the transient measurements. The resulting responses are shown in Fig. 6.10, p. 199. The maximum overshoot was reduced by 66 per cent for the leading edge and 54 per cent for the trailing edge. It is also noticeable that there is less ringing in the settling period. In practical situations the choice of low-pass filter response, and in particular the cut-off frequency, will be a compromise between having a fast response time, which requires a high cut-off value, and good suppression of spurious frequencies in the system, which requires a low cut-off value.

Although the transient behaviour of the system was not a primary concern of the work, the results show that the system is behaving in a predictable manner and that there are no spurious effects due to the use of the new circuit configuration.

It will be noted that the settling times quoted in Fig. 6.3, p. 190 are rather long, and in a practical situation would impose severe limitations on

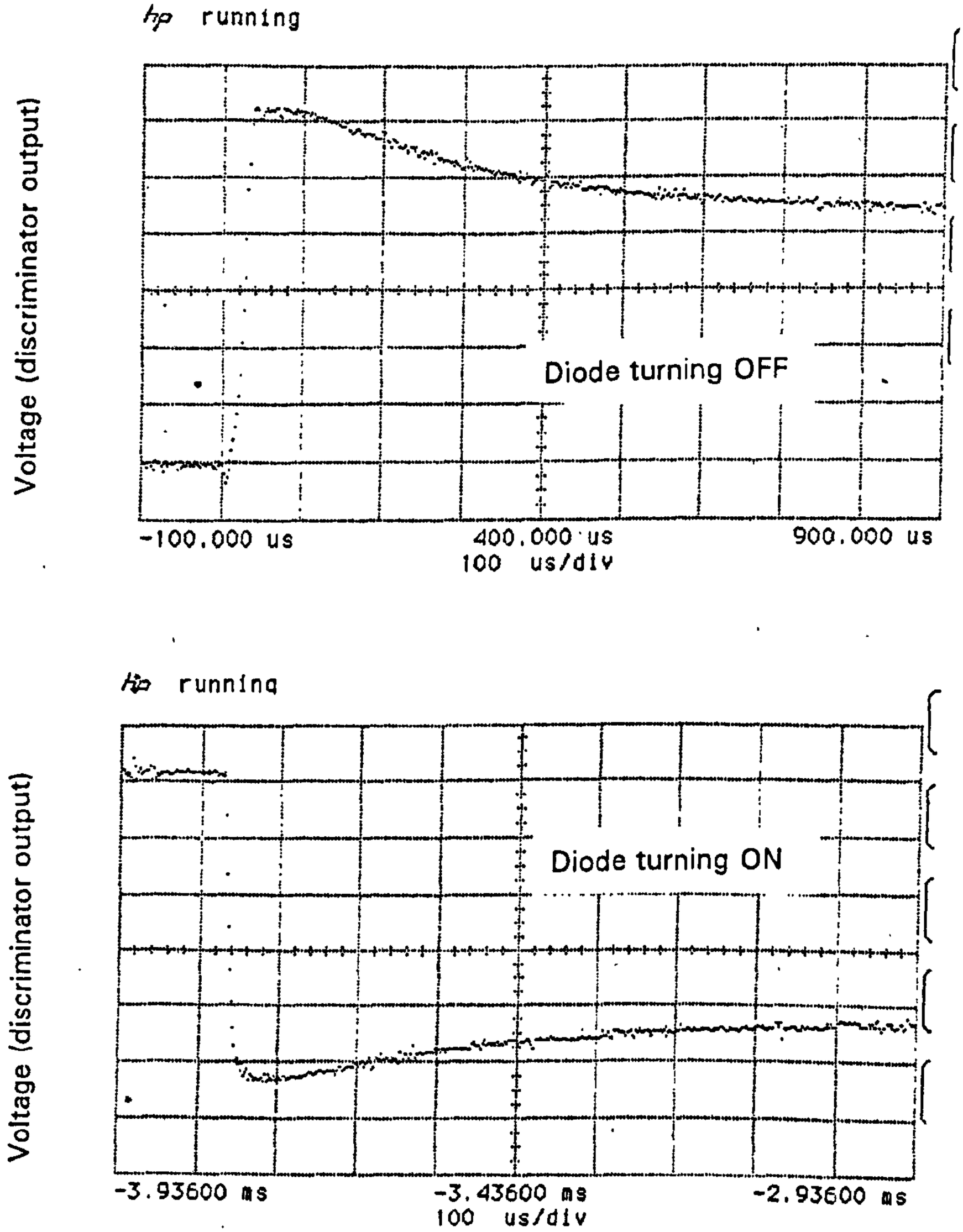

Figure 6.10: **Measured transient responses due to a 100MHz frequency step,with low-pass filter removed from feedback loop**

the circuit application since the period of the switching or modulating signal must necessarily be greater than the settling time. In the present work the settling times were dominated by the response of the oscillator, which itself exhibit a long settling time when subjected to a direct switching through the FM control port. This particular oscillator had been used for all of the phase noise measurements and was deliberately retained for the time response measurements so that all of the results were taken with the same source.

6.6 Conclusions

A new circuit technique for controlling the frequency of an oscillator, whilst maintaining frequency stabilization, has been established and confirmed through practical measurement. The technique, based on the switching of the input port in a three-port microstrip ring, has been extended to provide digital control of the oscillator frequency. The technique appears very attractive because of its simplicity, lack of frequency constraints and the potential to be implemented in an MMIC format.

Chapter 7

Overview discussion

7.1 Summary

The previous chapters have each included a detailed discussion on the individual aspects of the work. This present chapter provides a more general overview of the project and reflects on the outcomes of the work in relation to the original aims.

7.2 Terms of reference

The original intention of the work was to show that the delay-line method of stabilizing an oscillator could successfully be implemented in a microstrip format and to extend the technique to permit control of the frequency of an oscillator. Although significant emphasis has been placed on the development of several new circuit techniques, the original terms of reference were adhered to and these new circuit techniques were eventually combined to provide digital control of the frequency of a microwave oscillator.

7.3 Frequency control strategies

Chapters 5 and 6 introduced two different methods of implementing frequency control of an oscillator, one using a switched phase shifter and the other switched input ports on a three-port ring. Both circuits gave similar performance. In each case predictable frequency changes could be obtained;

the oscillator remained stabilized at each frequency position and only one PIN diode was needed to achieve each frequency change. This means that for a digital control system only one PIN diode is needed for each digital bit. Comparing the two methods, that based on switching the port positions seems more attractive, in that it is less demanding in fabrication terms, since it does not involve any small gaps in the microstrip geometry. In this circuit the precision with which frequencies can be selected depends primarily on locating a particular point of excitation of the ring. In practice this would be done at the mask making stage of the fabrication process, and consequently the excitation point could be located with high accuracy.

It was mentioned in chapter 6 that the frequency selection capability of the switched port arrangement could be increased by cascading several rings. Fig. 7.1, p. 203 shows such a cascaded arrangement. The four diodes controlling the feed paths to each ring generate $2^4 - 1$ different voltage levels, giving a total of 225 levels at the output of the final summing amplifier, i.e. 8 diodes would permit the selection of 225 different frequencies.

7.4 Circuit techniques

The two new circuit techniques which were developed, the single PIN diode phase shifter and the three-port ring, yielded predictable results. The phase shifter provided a far more compact design than traditional switched line or loaded line techniques, and because of this would seem to offer particular advantages if expanded to form a multi-bit digital phase shifter. In the context of the present work, the single PIN diode was particularly useful for inclusion in a three-port ring to change the effective delay-path, since its compact form did not significantly increase the size of the ring and hence reduce the bandwidth. One possible disadvantage of this type of PIN diode phase shifter is the need to include planar DC breaks in the coupled line section to permit DC biasing of the diode. The gap in these breaks has necessarily to be small and, moreover, the dimensions are important in establishing the overall transmission phase of the component. Thus there is some disadvantage in that the device requires a particularly accurate fabrication process. The alternative to the DC breaks would be to replace the terminating short on the coupled section with a chip capacitor. Although this arrangement

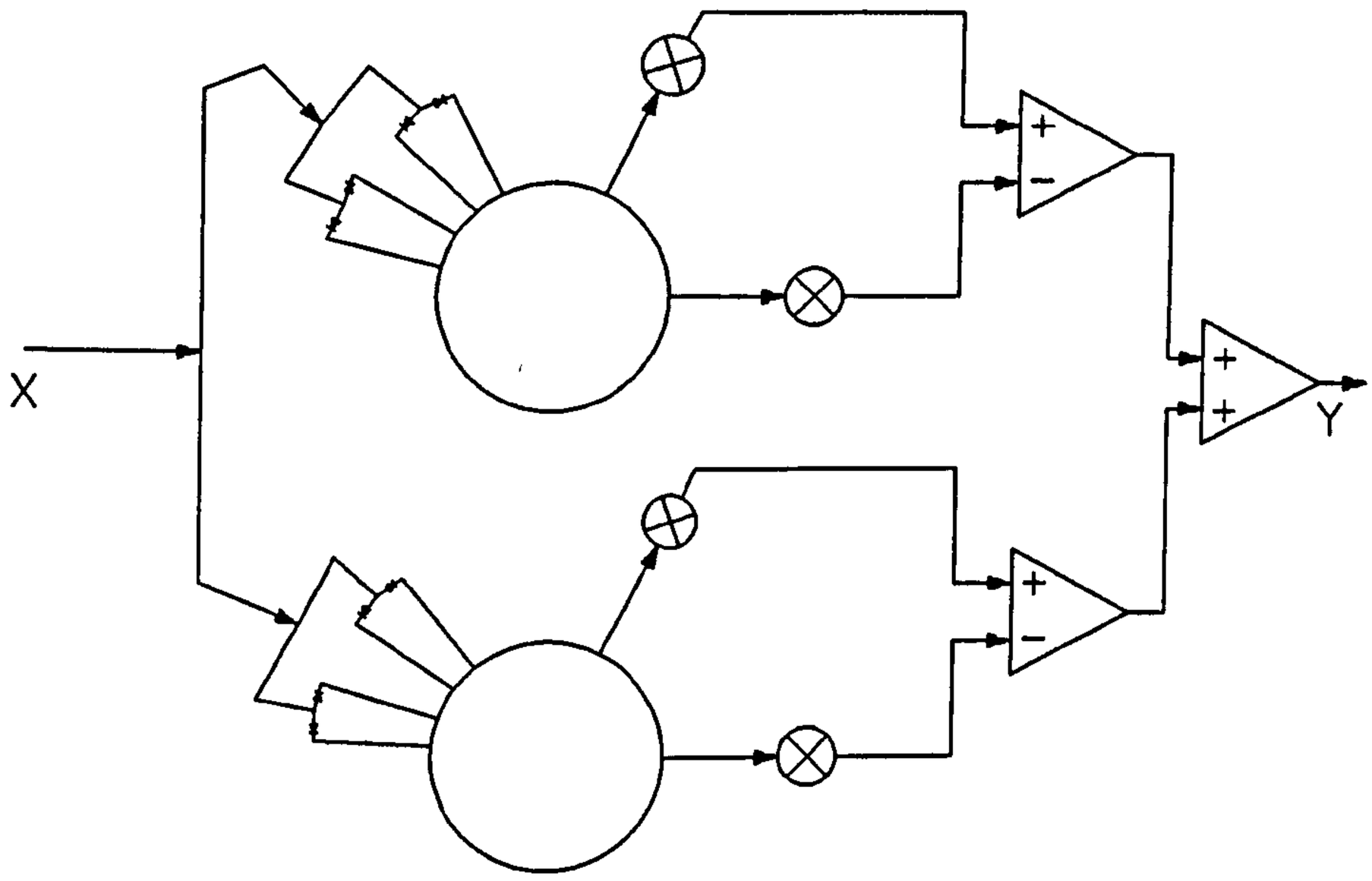

Figure 7.1: **Cascaded three-port rings to provide extended frequency selection**

was tested and found to give satisfactory results, not enough data was collected to determine whether the discontinuities due to the surface mounting of the chip capacitor, combined with the variation in the chip parameters, would be a greater source of error than that associated with limitations in the fabrication process of the narrow gaps.

The three-port ring proved to be a versatile device. Not only did it perform the original discriminator function for which it was designed, but it subsequently provided the basis for the development of a digital device based on multi-feed switching. The compact nature of the ring certainly provides a significant advantage over other microstrip discriminator structures. Its one limitation, namely the need to match the input port, should not be of consequence in practical design situations.

7.5 Theoretical analysis

Since the ultimate aim of the work was to switch microstrip circuits so as to provide small, precise changes in the frequency of an oscillator, it was necessary to have precise theoretical design information on the behaviour of simple microstrip structures. It was found necessary to extend the existing theory of coupled lines and introduce the concept of excess phase into the design DC planar breaks to achieve this. A serious source of error in the commonly quoted closed-form expressions for microstrip gap equivalent circuit values was identified in chapter 2. During the course of writing this report, a second edition of 'Microstrip Lines and Slotlines', by GUPTA, GARG AND BAHL [36] was published (in 1996) which introduced a scalar correction factor into the expression for the even mode capacitance. The correction has been introduced without comment and without reference to any previous paper. The modification goes some way to rectifying the error discussed in chapter 2, but the authors do not address the issue of the discontinuity in the even mode capacitance expression at s/w=0.3. This still exists, and indeed is more evident, with the corrected expression.

The current summing technique developed for the three-port ring not only simplified the analysis of the ring but permitted the further development of the ring to provide digital control. Without this technique it would have been very difficult to predict the behaviour of the ring with multi- port excitation.

7.6 Implementation in microstrip

It was apparent at the start of the work that there were no fundamental difficulties in implementing in microstrip a technique which had previously been established in waveguide. Whilst there were a number of unknown quantities in relation to the effects of the microstrip material, these were not seen as crucial. For example, it was important to have a stable material since the basic aim was to improve the stability of an oscillator. However, extensive information already existed in the literature on the electrical and mechanical properties of alumina, which is the standard substrate material for microstrip circuits. So the initial focus of the work was to look at simpler microstrip designs for implementing the basic circuit functions that were required, and

to make use of commonly available microstrip materials. Rather than use alumina, which tended to be expensive, soft substrate materials were used for testing the designs. It was apparent at an early stage that in order to achieve the required circuit performance, particularly in terms of precise transmission phase, it would be necessary to have a very accurate fabrication process. Several of the proposed new circuits contained narrow gaps, where dimensional errors would have a significant effect on the transmission phase and thereby on the ability of the circuit to permit precise design of delay times. Consequently, the RT/duroid range of substrates were chosen for the development of the microstrip circuits, for three reasons. Firstly, the substrate material was available with relative permittivities close to that of microwave quality alumina, thereby making the transfer of final designs to alumina straightforward, and hence producing designs whose dimensions were consistent with normal industrial practice. Secondly, the RT/duroid was known to have isotropic properties; the main rival material, Epsilam-10, was reported to exhibit significant anisotropic properties in respect of ϵ_r, due to the rolling of the copper, which would be particularly important for microstrip designs where accurate knowledge of the transmission phase was crucial. Lastly, RT/duroid material was available with the thinnest copper, $\sim 4.5\mu m$, of any pre-coated commercially available substrate. This meant that undercutting in the fabrication process would be small, and could be accurately accounted for in the design. It was found that with a wet etching process, using an acidified ferric chloride etchant, circuits could be fabricated on a reproducible basis with line and space dimensions accurate to within $\pm 2\mu m$.

Chapter 8

Conclusions and suggestions for further work

8.1 Conclusions

The original aim of the work, namely to use delay-line techniques to stabilize and control the frequency of a microwave oscillator, has been achieved. Circuits have been designed which provide digital control of the frequency of a low-noise oscillator, and the operation of these circuits has been verified through practical measurement.

Two new circuit concepts, the three port ring and the single PIN diode phase shifter, have been established, and the theoretical operation confirmed through measurements on microstrip at X-band.

A new current summing technique for analysing microstrip ring structures has been developed which is less restrictive than existing analytical methods. The new method has been shown to be particularly useful for examining the behaviour of asymmetrical microstrip ring circuits.

In-depth analyses of coupled microstrip lines and planar microstrip DC breaks have provided greater insight into the behaviour of these devices than has hitherto been available in the published literature. This has useful practical significance in terms of improved accuracy in circuit design.

Overall, the work has led to the development of a potentially powerful technique for digitally controlling the frequency of a low-noise microwave oscillator. Moreover, the novel circuit techniques which have been used in

the implementation of the frequency control system provide simple, accurate design strategies which have the potential for further development in MMICs.

8.2 Suggestions for further work

Whilst the original concepts of the work have been established, there are a number of aspects which warrant further investigation, particularly in respect of the practical implementation of the novel microstrip circuits which have been developed.

8.2.1 Frequency control using a multi-feed microstrip ring

The arrangement based on a multi-feed microstrip ring was the most promising of the frequency control circuits that were investigated. However, there is a limit to the number of frequency steps that can be achieved with this circuit due to restrictions on the number of feed points to the ring. The extent of this limitation needs to be quantified, firstly by determining the minimum spacing between the feed lines, and secondly by establishing the limits on the distribution of feed points around the ring. The minimum spacing between the feed lines will be set by the need to avoid significant unwanted coupling between these lines. At present, the effect on the discriminator responses of small levels of crosstalk between the feed lines is unknown and this needs further investigation. The crosstalk could be evaluated using conventional microstrip coupled-line theory, with a modification to account for the non-parallel line structure. Alternatively, a modified feed geometry with parallel lines could be considered, which would make the analysis more tractable. The limitations on the distribution of the feed points around the ring will be determined by the requirements of bandwidth, phase noise suppression and and the linearity of the frequency steps. Each of these three parameters is affected by the slope of the discriminator response, which will change as the feed point is moved around the ring. Clearly, therefore, the distribution of feed points must be restricted so as to obtain essentially the same performance for each frequency selected. A relatively straightforward extension to the current summing technique should yield a generalized theory of operation

which relates the bandwidth, phase noise suppression and frequency step size to the feed positions. This would provide the circuit designer with useful, precise design information.

8.2.2 Noise analysis of delay-line stabilised oscillator

One of the principal features of the delay-line stabilised oscillator is the reduction in phase noise which is obtained. However, there has not been a detailed noise analysis of this type of circuit, using transmission line components, reported in the literature. Such an analysis would therefore seem to be a logical extension of the present work, which has established the principle of operation of this type of circuit. Where more general analyses of of the noise properties of feedback stabilised oscillators have been reported, they have used an essentially linear technique. To obtain a rigorous understanding of the noise properties of this type of circuit a non-linear analysis is needed which considers the cumulative effect of the wideband noise spectrum generated by a single noise sinusoid in the system. It is by no means obvious that uniform noise suppression will occur within the pass-band of the low-pass filter located in the feedback network, and an exact analysis is necessary to establish the precise noise response under closed-loop conditions. Recently, RIZZOLI ET AL [37] reported a full non-linear analysis of near carrier noise in discriminator-stabilized microwave oscillators. This appears to have been the only attempt to address the non-linear aspects of this class of stabilized oscillator. Their approach, which was based on a harmonic-balance method, yielded good agreement between measured and simulated data for a discriminator-stabilized dielectric-resonator oscillator. It would be worthwhile extending this approach to include the delay-line stabilized circuit. An alternative approach worth considering would be to make use of autocorrelation theory, since the circuit has the form of a standard autocorrelator.

8.2.3 Switching analysis

For many applications the switching speed of an oscillator is of paramount significance. A high response time will limit the modulation capabilities of the oscillator and restrict its use. The circuits in the present work were

designed primarily to give well-defined frequency changes, rather than a fast response. However, some switching measurements were made and the results were explainable in term of the general circuit behaviour, but the settling times were excessively large. Although the slow response may in part have been due to the sweep oscillator being used, which itself had a poor response, it would be worth investigating the effect on the settling time of using a different PIN diode, of lower junction capacitance, and modifying the bias network.

8.2.4 Current summing analysis

Whilst the current summing technique proved a convenient and powerful technique for analysing asymmetric ring structures, the analysis presented in chapter 4 for three-port rings needs some expansion to include the effects of discontinuities associated with the structure. In particular, the effect of the T-junction discontinuities needs to be considered. Although the T-junction is a very common microstrip feature, and a number of equivalent circuits are available in the literature, there is little reported information on the practical transmission phases of this type of junction. In the current work, where the main theme has been to develop devices where the voltage controlled frequency steps have sizes determined primarily by the line geometry, the transmission phases of the circuit components is of particular importance. It would be useful to develop a comprehensive set of frequency-dependent scattering coefficients covering a range of microstrip T-junction geometries.

8.2.5 Single PIN diode phase shifter

The principal limitation of the PIN diode phase shifters investigated, was that their performance was restricted to phase changes in the vicinity of 0° or 360°. To make full use of this phase shifter concept further work is needed to extend the degrees of freedom in the design. This could be done by modifying the geometry of the matching section, so as to give a greater difference in performance when the diode is switched from the off to the on state, thereby suppressing one of the propagating modes. A further possibility would be to develop a geometry which would load one of the propagating modes as was done for the even mode in chapter 2.

8.2.6 Digital phase shifter, using cascaded single PIN diode phase shifters

It was envisaged that the compactness of the single PIN diode phase shifter, together with the need for only one switching element, would make this circuit particularly suitable for expansion into a digital device, wherein a number of single PIN diode phase shifters could be connected in cascade. Using this technique an n-bit digital device could be constructed with only n active switching elements. In addition to assessing practically the performance of such a device it would be useful to extend the basic analysis to include the effects on performance of interactions between closely phase shifting elements. Three sources of interaction need to be investigated: (i) direct electromagnetic coupling between the various coupled line sections; (ii) multiple reflections along the main transmission path; (iii) evanescent field coupling.

8.2.7 The microstrip gap

At an early stage in the work a significant error was found in the widely quoted closed-form expressions for the capacitance values in microstrip gap equivalent circuits. While the error can to some extent be rectified by including a scalar value in the expressions, they still contain a significant discontinuity. It would be worthwhile, in terms of gaining practical design information, to model a microstrip gap using a modern commercial simulator, such as HFSS, and from the results of this to generate a more up-to-date-set of circuit design equations.

Appendix A

A.1 Exact analysis of coupled-line phase shifters

Equation 2.1 can be expanded to give

$$V_{1e} = V_{4e}\cos\theta_e + jI_{4e}Z_{oe}\sin\theta_e \tag{A.1}$$

$$I_{1e} = jV_{4e}Y_{oe}\sin\theta_e + I_{4e}\cos\theta_e \tag{A.2}$$

and similarly 2.2 gives

$$V_{1o} = V_{4o}\cos\theta_o + jI_{4o}Z_{oo}\sin\theta_o \tag{A.3}$$

$$I_{1o} = jV_{4o}Y_{oo}\sin\theta_o + I_{4o}\cos\theta_o. \tag{A.4}$$

The boundary conditions are

$$V_{4o} = V_{3o} = 0 \tag{A.5}$$

$$I_{4e} = I_{3o} = 0. \tag{A.6}$$

Substituting the boundary conditions into equations A.1 to A.4 gives

$$V_{1e} = V_{4e}\cos\theta_e \tag{A.7}$$

$$I_{1e} = jV_{4e}Y_{oe}\sin\theta_e \tag{A.8}$$

and

$$V_{1o} = jI_{4o}Z_{oo}\sin\theta_o \tag{A.9}$$

$$I_{1o} = I_{4o}\cos\theta_o. \tag{A.10}$$

The input impedance at port 1 is given by

$$Z_{in,1} = \frac{V_{1e}+V_{1o}}{I_{1e}+I_{1o}}$$

$$= \frac{V_{1e} + V_{1o}}{jV_{4e}Y_{oe}\sin\theta_e + I_{4o}\cos\theta_o}$$

$$= \frac{V_{1e} + V_{1o}}{j\frac{V_{1e}}{\cos\theta_e}Y_{oe}\sin\theta_e + \frac{V_{1o}}{jZ_{oo}\sin\theta_o}\cos\theta_o}$$

$$= \frac{V_{1e} + V_{1o}}{j(V_{1e}Y_{oe}\tan\theta_e - V_{1o}Y_{oo}\cot\theta_o)} \qquad \text{(A.11)}$$

Now, if Z_{1e} and Z_{1o} are the input impedances at port 1 for the even and odd modes respectively, then

$$V_{1e} = \frac{Z_{1e}}{Z_{1e} + Z_o}\frac{V}{2} \qquad \text{(A.12)}$$

$$V_{1o} = \frac{Z_{1o}}{Z_{1o} + Z_o}\frac{V}{2}. \qquad \text{(A.13)}$$

Also, from equations A.7 and A.8

$$Z_{1e} = \frac{V_{1e}}{I_{1e}} = -jZ_{oe}\cot\theta_e \qquad \text{(A.14)}$$

and

$$Z_{1o} = \frac{V_{1o}}{I_{1o}} = jZ_{oo}\tan\theta_o \qquad \text{(A.15)}$$

Substituting from equations A.12 through A.15 into equation A.11 we obtain, after straightforward manipulation

$$Z_{in,1} = \frac{2Z_{oe}Z_{oo}\cot\theta_e\tan\theta_o - jZ_o(Z_{oe}\cot\theta_e - Z_{oo}\tan\theta_O)}{2Z_o - j(Z_{oe}\cot\theta_e - Z_{oo}\tan\theta_O)}. \qquad \text{(A.16)}$$

The input reflection coefficient, S_{11}, is given by

$$S_{11} = \frac{Z_{in,1} - Z_o}{Z_{in,1} + Z_o}. \qquad \text{(A.17)}$$

It should be noted that if we put $\theta_o = \theta_e = \theta$, the expression for $Z_{in,1}$ becomes

$$Z_{in,1} = \frac{2Z_{oe}Z_{oo} - jZ_o(Z_{oe}\cot\theta - Z_{oo}\tan\theta)}{2Z_o - j(Z_{oe}\cot\theta - Z_{oo}\tan\theta)} \qquad \text{(A.18)}$$

and then, if

$$Z_o = \sqrt{Z_{oe}Z_{oo}} \qquad \text{(A.19)}$$

we obtain

$$Z_{in.1} = Z_o \qquad \text{(A.20)}$$

which is the nominal matched condition.

The transmission coefficient representing transmission between ports 1 and 2 is given by

$$\frac{V_2}{V_1} = \frac{V_{2e} + V_{2o}}{V_{1e} + V_{1o}} \tag{A.21}$$

From considerations of symmetry, equation A.21 can be written as

$$\begin{aligned} \frac{V_2}{V_1} &= \frac{V_{1e} - V_{1o}}{V_{1e} + V_{1o}} \\ &= \frac{\frac{Z_{1e}}{Z_{1e}+Z_o} - \frac{Z_{1o}}{Z_{1o}+Z_o}}{\frac{Z_{1e}}{Z_{1e}+Z_o} + \frac{Z_{1o}}{Z_{1o}+Z_o}}. \end{aligned} \tag{A.22}$$

Thus, substituting from equations A.14 and A.15 we obtain

$$\frac{V_2}{V_1} = -j\frac{Z_o(Z_{oe}\cot\theta_e - Z_{oo}\tan\theta_o)}{2Z_{oe}Z_{oo}\tan\theta_o\cot\theta_e - jZ_o(Z_{oe}\ cot\theta_e - Z_{oo}\tan\theta_o)}. \tag{A.23}$$

From equation A.23 the transmission phase change is obtained as

$$\phi = \frac{\pi}{2} + \tan^{-1}\left[\frac{Z_o(Z_{oe}\cot\theta_e - Z_{oo}\tan\theta_o)}{2Z_{oe}Z_{oo}\tan\theta_o\cot\theta_e}\right]. \tag{A.24}$$

This is the exact expression for insertion phase. We can simplify this last expression by making assumptions about Z_{oe} and Z_{oo} and by letting $\theta_e = \theta_o = \theta$. We have already established that the approximate theory, averaging the odd and even mode velocities, yields a matched input condition when

$$Z_o = \sqrt{Z_{oe}Z_{oo}}. \tag{A.25}$$

Substituting these simplifying conditions into equation A.24 gives

$$\phi = \frac{\pi}{2} + \tan^{-1}\left[\frac{Z_{oe}\cot\theta - Z_{oo}\tan\theta}{2sqrtZ_{oe}Z_{oo}}\right] \tag{A.26}$$

whence

$$\cot\phi = \frac{Z_{oo}\tan\theta - Z_{oe}\cot\theta}{2sqrtZ_{oe}Z_{oo}}. \tag{A.27}$$

Using the trigonometric relationship

$$\cot^2\phi = \frac{\cos^2\phi}{1 - \cos^2\phi} \tag{A.28}$$

we obtain

$$\cos\phi = \pm\frac{Z_{oo}\tan\theta - Z_{oe}\cot\theta}{Z_{OO}\tan\theta + Z_{oe}\cot\theta'}. \tag{A.29}$$

Now we know that $\phi = 0$ when $\theta = 0$, hence

$$\cos\phi = \frac{\frac{Z_{oe}}{Z_{oo}} - \tan^2\theta}{\frac{Z_{oe}}{Z_{oo}} + \tan^2\theta} \tag{A.30}$$

or

$$\phi = \cos^{-1}\left[\frac{\rho - \tan^2\theta}{\rho + \tan^2\theta}\right] \tag{A.31}$$

where

$$\rho = \frac{Z_{oe}}{Z_{oo}}. \tag{A.32}$$

Equation A.31 thus gives the approximate insertion phase of the coupler.

A.2 Dispersion relationships for parallel-coupled microstrip lines

The dispersion relationships given by GETSINGER [14] are, for the even mode

$$\epsilon_{r,eff,e}(f) = \epsilon_r - \frac{\epsilon_r - \epsilon_{r,eff}(0)}{1 + G_e\left(\frac{f^2}{f_{p,e}^2}\right)} \tag{A.33}$$

$$f_{p,e} = \frac{Z_{oe}}{4\mu_o h} \tag{A.34}$$

$$G_e = 0.6 + 0.0045 Z_{oe} \tag{A.35}$$

where

$\epsilon_{r,eff,e}(f)$ is the frequency dependent effective relative permittivity of the even mode

$\epsilon_{r,eff}(0)$ is the effective relative permittivity of the even mode at zero frequency

ϵ_r is the relative permittivity of the substrate

Z_{oe} is the characteristic impedance of the even mode at zero frequency

μ_o is the permeability of free space

h is the substrate thickness

G is an empirical parameter.

The corresponding expressions for the frequency dependent effective relative permittivity of the odd mode are

$$\epsilon_{r,eff,o}(f) = \epsilon_r - \frac{\epsilon_r - \epsilon_{r,eff}(0)}{1 + G_o\left(\frac{f^2}{f_{p,o}^2}\right)} \quad \text{(A.36)}$$

$$f_{p,o} = \frac{Z_{oo}}{\mu_o h} \quad \text{(A.37)}$$

$$G_o = 0.6 + 0.018 Z_{oo} \quad \text{(A.38)}$$

The parameters in the odd mode expressions are defined in the same way as for the even mode.

A.3 Curve-fitted expressions for gap capacitance

The values of the capacitor element values in Fig. 2.13, p. 54 can be expressed in terms of odd and even mode capacitances, C_o and C_e, such that

$$C_e = 2C_1 \quad \text{(A.39)}$$

and

$$C_o = C_1 + 2C_2 \quad \text{(A.40)}$$

giving

$$C_1 = \frac{C_e}{2} \quad \text{(A.41)}$$

$$C_2 = \frac{C_o - C_1}{2} \quad \text{(A.42)}$$

The closed-form expressions given by GARG AND BAHL [19] to evaluate the values of C_o and C_e for a gap spacing of s in a microstrip track of width w on a substrate of thickness h are:

$$\frac{C_o}{w} = \left[\frac{s}{w}\right]^{m_o} e^{k_o} \quad \text{(A.43)}$$

$$\frac{C_e}{w} = \left[\frac{s}{w}\right]^{m_e} e^{k_e} \quad \text{(A.44)}$$

where C_o/w and C_e/w are in pF/m and where

for $0.1 \leq s/w \leq 1.0$

$$m_o = \frac{w}{h}\left[0.619\log\left(\frac{w}{h}\right) - 0.3853\right] \tag{A.45}$$

$$k_o = 4.26 - 1.453\log\left(\frac{w}{h}\right) \tag{A.46}$$

for $0.1 \leq s/w \leq 0.3$

$$m_e = 0.8675 \tag{A.47}$$

$$k_e = 2.043\left(\frac{w}{h}\right)^{0.12} \tag{A.48}$$

for $0.3 \leq s/w \leq 1.0$

$$m_e = \frac{1.565}{\left(\frac{w}{h}\right)^{0.16}} - 1 \tag{A.49}$$

$$k_e = 1.97 - 0.03\frac{h}{w}. \tag{A.50}$$

The expressions were originally developed for $\epsilon_r = 9.6$, but GARG AND BAHL [19] provided scaling factors for other values of ϵ_r in the range $2.5 \leq \epsilon_r \leq 15$ in the form

$$C_e(\epsilon_r) = C_e(9.6)\left(\frac{\epsilon_r}{9.6}\right)^{0.9} \tag{A.51}$$

$$C_o(\epsilon_r) = C_o(9.6)\left(\frac{\epsilon_r}{9.6}\right)^{0.8}. \tag{A.52}$$

Appendix B

B.1 Photographs of a selection of test circuits

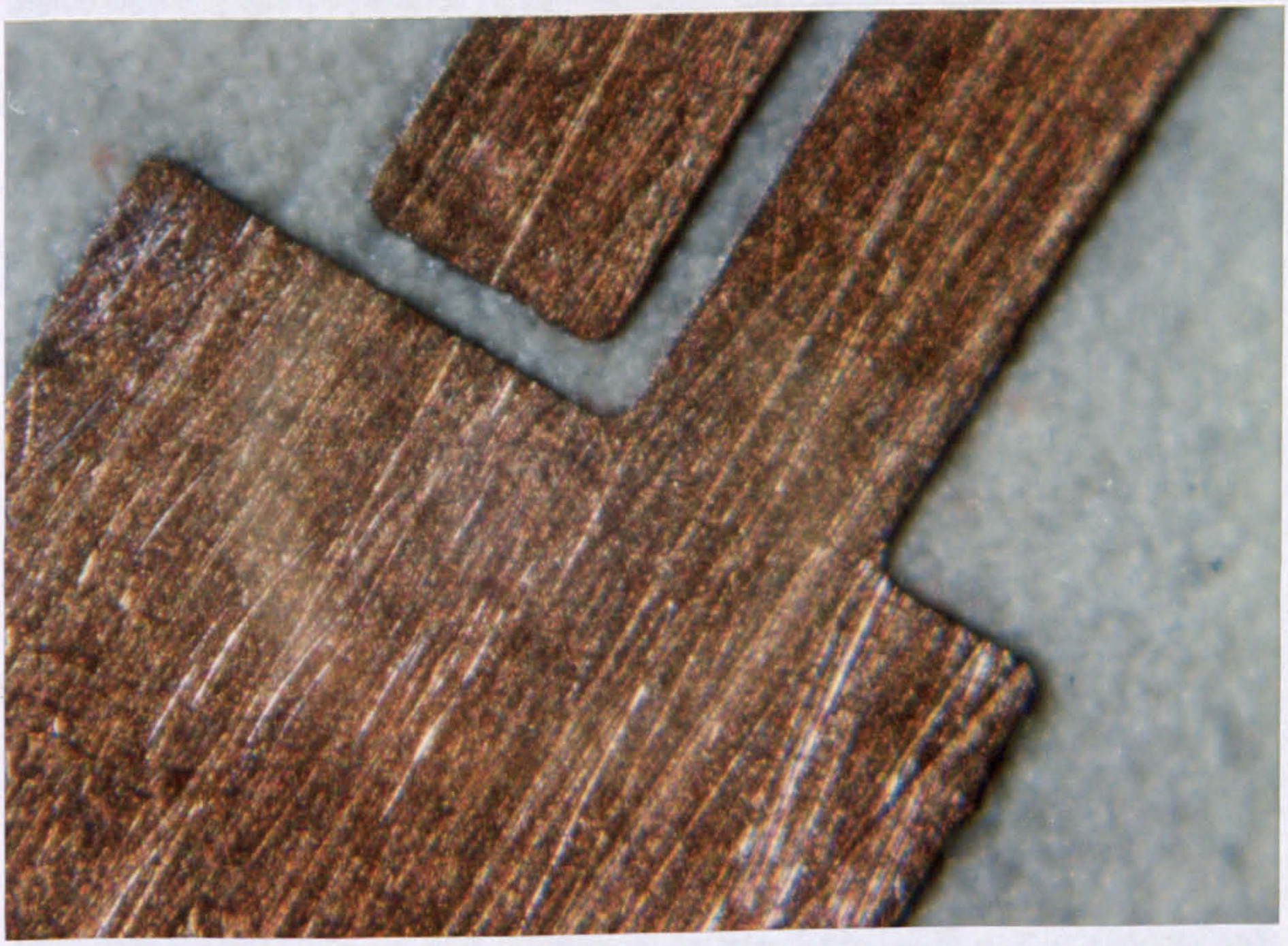

Figure B.1: **Partial view of a finger break in a 50Ω microstrip line, showing the quality of etching of a $30\mu m$ gap. (Magnification: x200)**

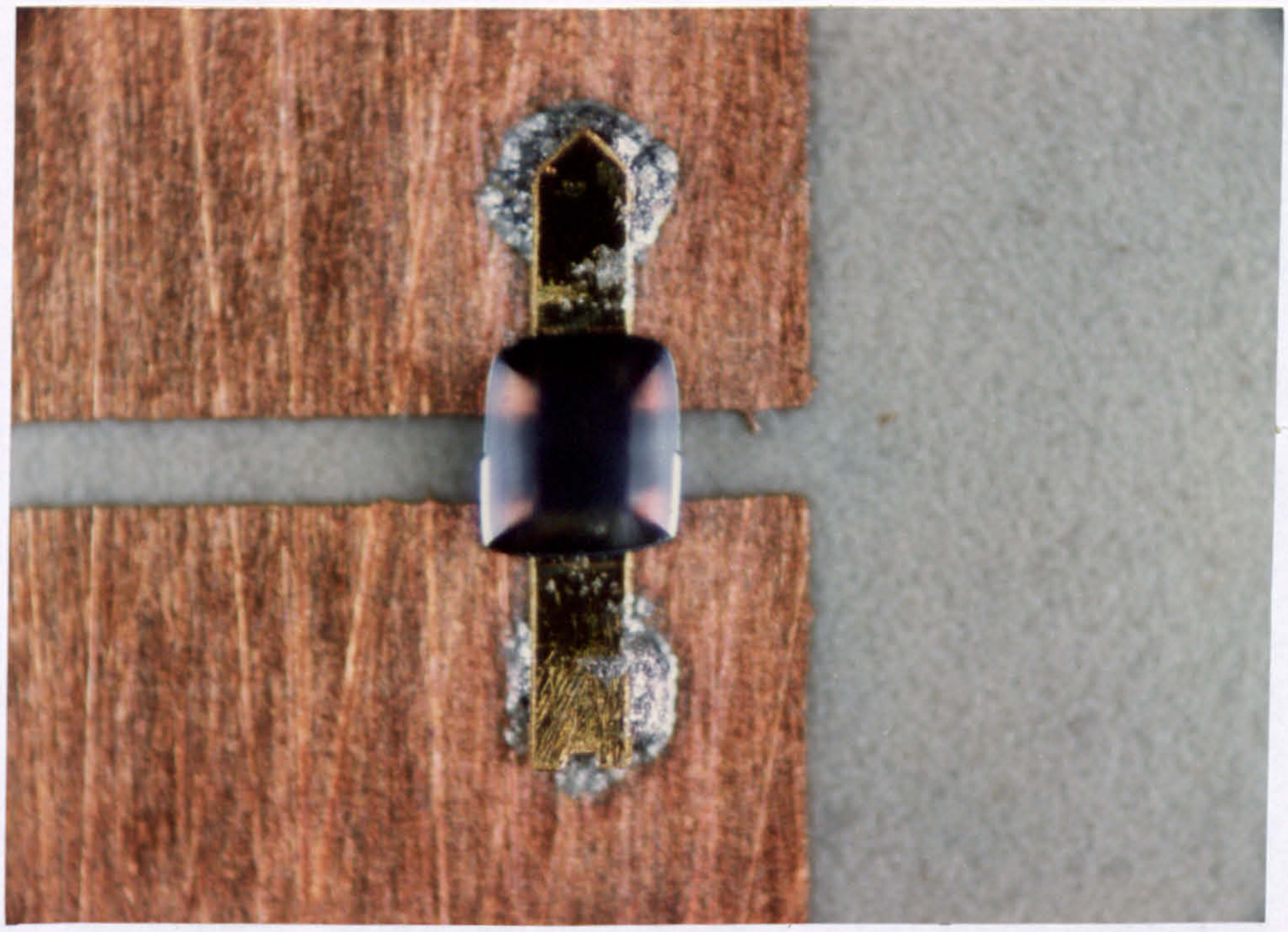

Figure B.2: **Beam-lead PIN diode mounted across a** $100\mu m$ **gap. (Magnification: x100)**

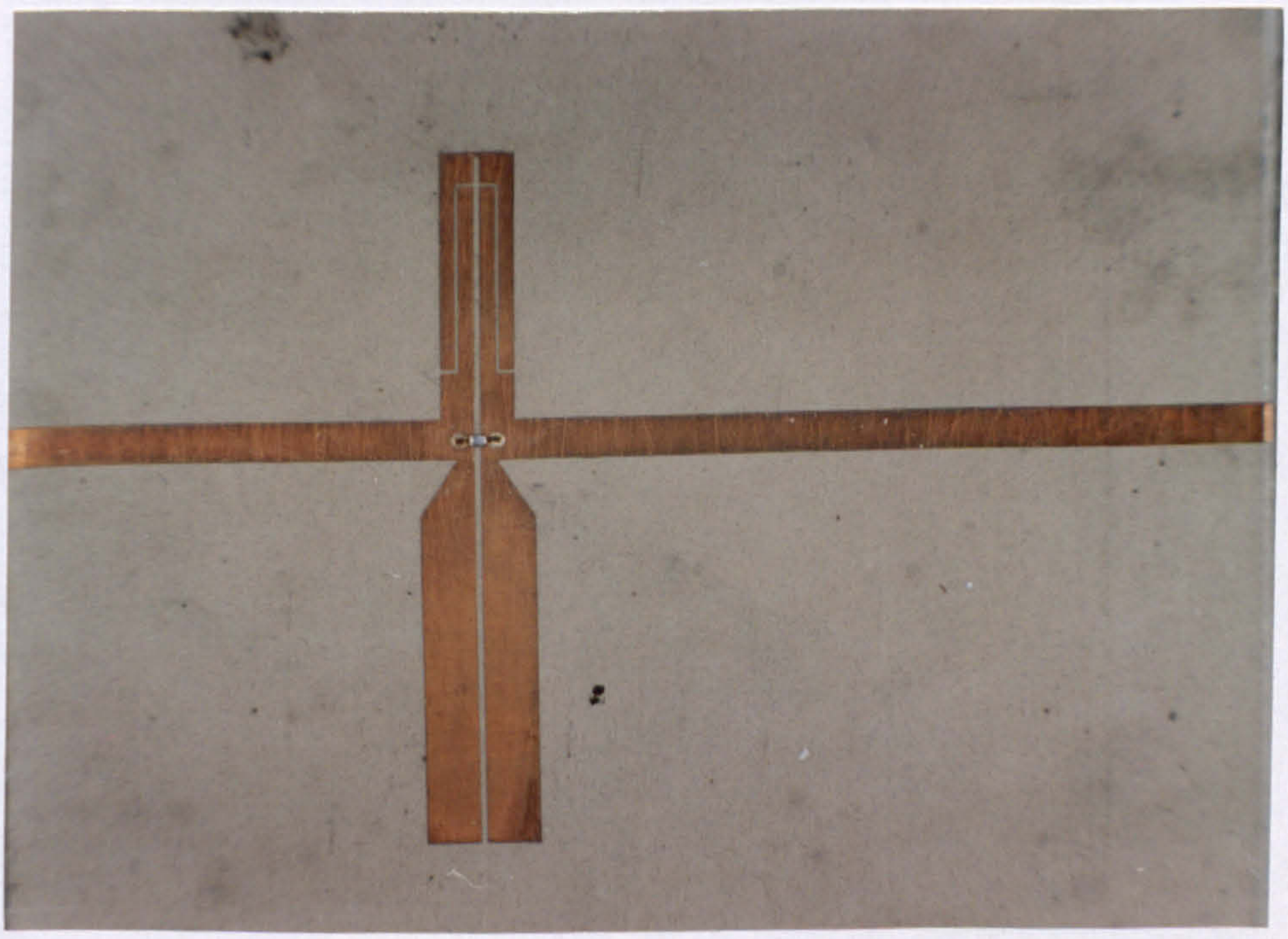

Figure B.3: **10GHz single PIN diode phase shifter. (Magnification: x7.7)**

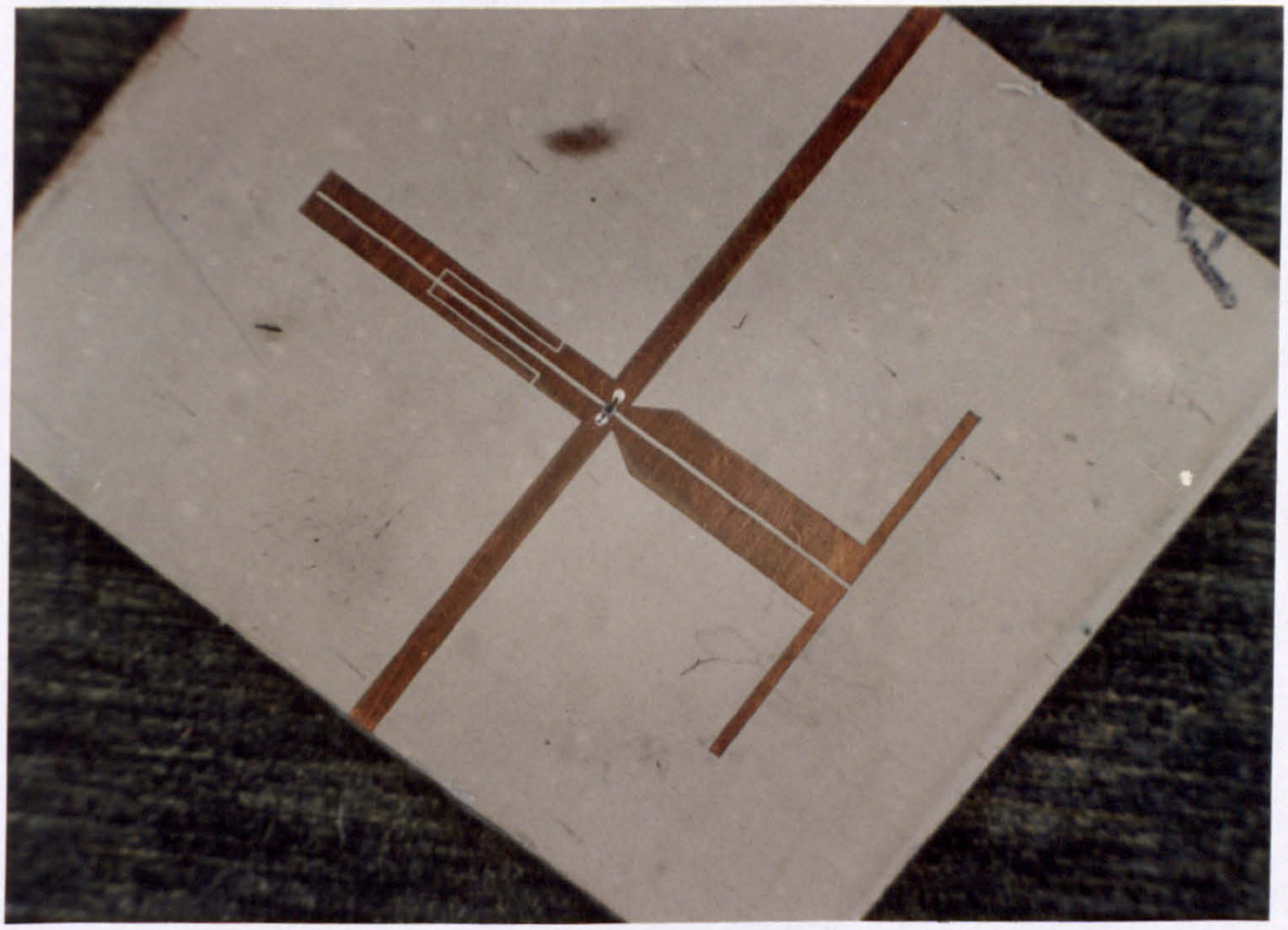

Figure B.4: **10GHz single PIN diode phase shifter with even mode loading. (Magnification: x5.6)**

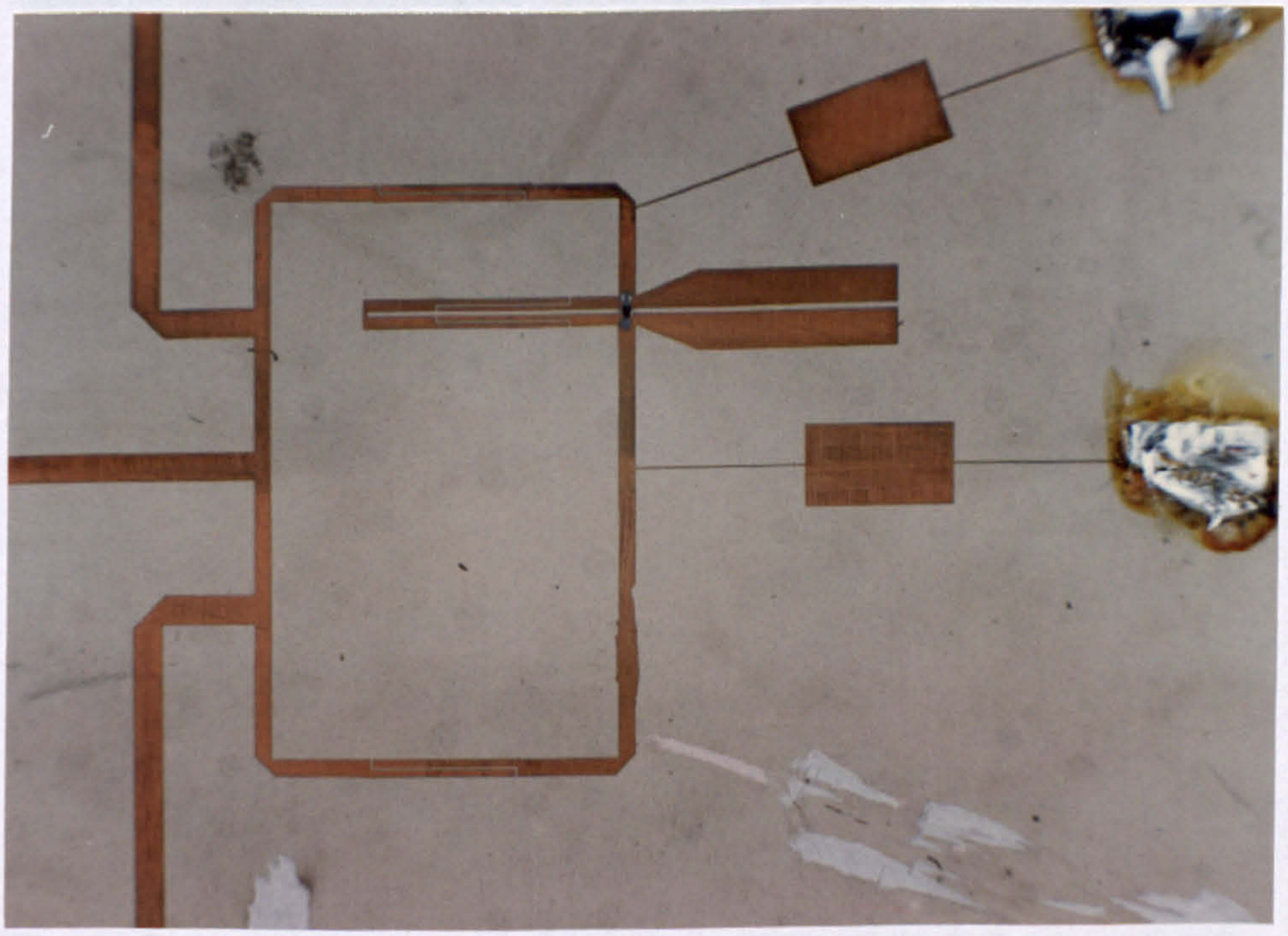

Figure B.5: **10GHz three-port ring incorporating a single PIN diode phase shifter. (Magnification: x5.6)**

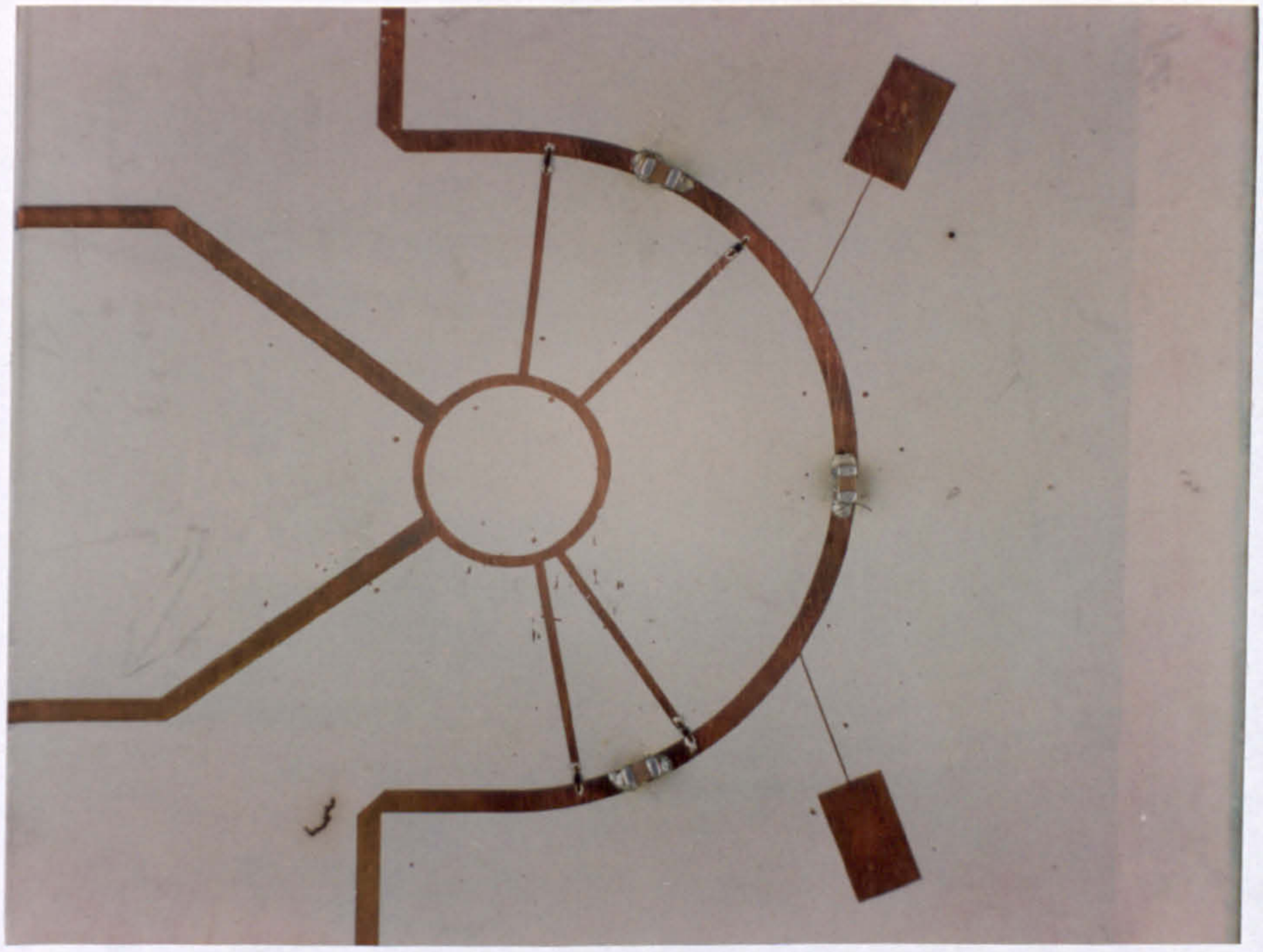

Figure B.6: **10GHz multi-feed microstrip ring. (Magnification: x4.4)**

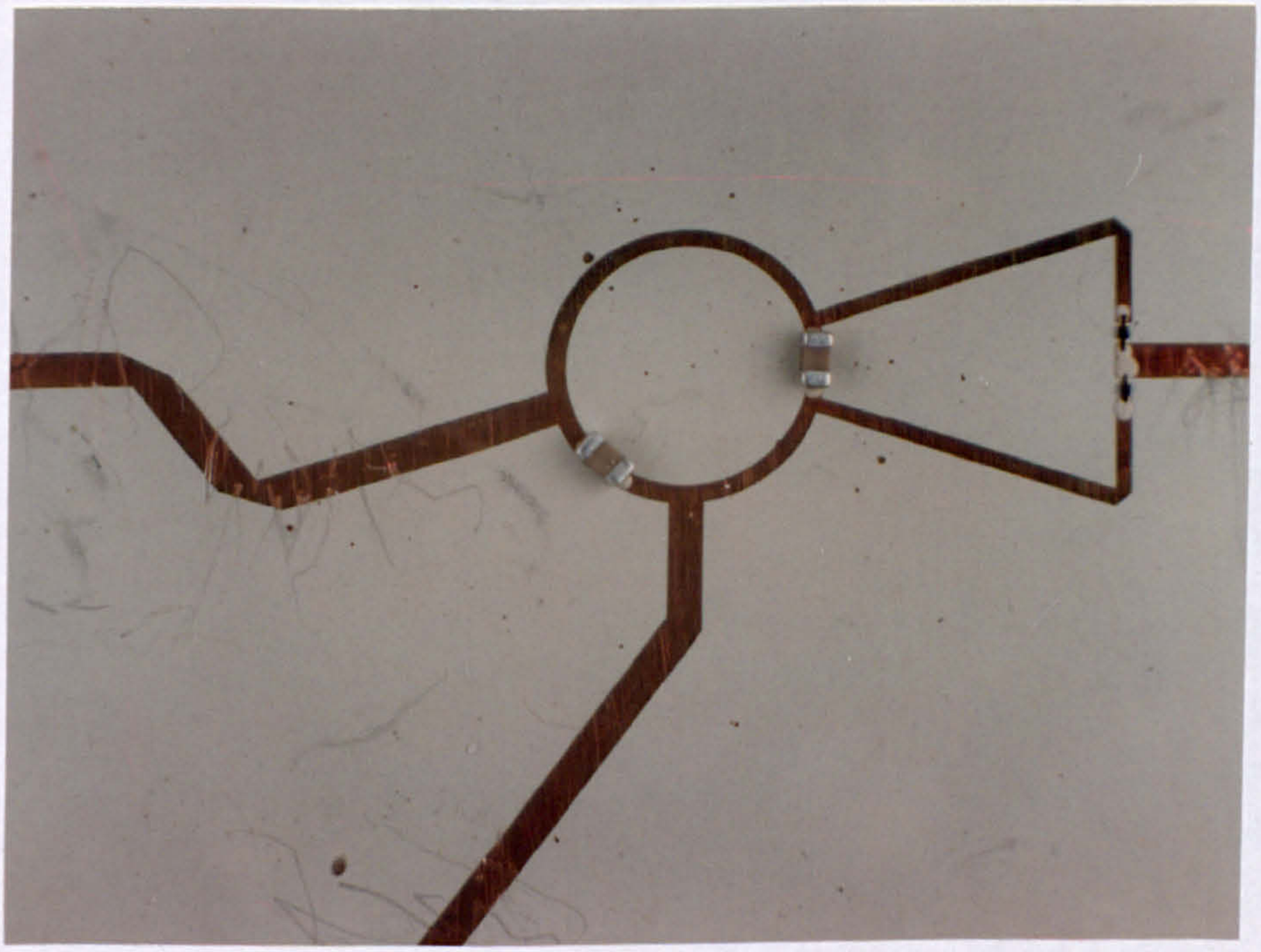

Figure B.7: **10GHz microstrip ring with digital feed network. (Magnification: x6.4)**

Appendix C

C.1 Publications

The following list of publications resulted from the work described in this thesis. For the convenience of the reader, scanned copies of the various articles are given in this appendix.

1. Free, C.E. and Aitchison, C.S., 'Excess phase in microstrip DC blocks', Electronics Lett., 1984, Vol. 20, No 21, pp892-893.

2. Free, C.E. and Aitchison, C.S., Single PIN diode X-band phase shifter', Electronics Lett., 1985, Vol. 21, No. 4, pp128-129.

3. Free, C.E. and Aitchison, C.S., 'Three-port ring discriminator', Electronics Lett., 1986, Vol. 22, No. 3, pp123-125.

4. Free, C.E. and Aitchison, C.S., 'Microwave oscillator control using a switched delay-line technique', Proc. IEEE MTT-Symposium, Orlando, May 1995, pp79-82.

5. Free, C.E. and Aitchison, C.S., 'Improved analysis and design of coupled-line phase shifters', 1995, IEEE Trans., MTT-43, No. 9, pp2126-2131.

6. Free, C.E. and Aitchison, C.S., 'Analysis of microstrip ring structures', Electronics lett., 1996, Vol. 32, No. 10, pp903-904.

7. Free, C.E. and Aitchison, C.S., 'A digitally controlled microwave oscillator', Proc. 26th European Microwave Conference, 1996, Prague, pp677-680.

in the framework of the exponential model of monthly exceedances rather than from a large number of single-year worst-month statistics. However, before making use of the model it should be verified that the cumulative distributions of monthly exceedances can be represented reasonably by exponentials.

F. DINTELMANN

Forschungsinstitut der Deutschen Bundespost
6100 Darmstadt, W. Germany

31st August 1984

References

1 CRANE, R. K., and DEBRUNNER, W. E.: 'Worst-month statistics', *Electron. Lett.*, 1978, **14**, pp. 38–40
2 BRUSSAARD, G., and WATSON, P. A.: 'Annual and annual-worst-month statistics of fading on earth satellite paths at 11·5 GHz', *ibid.*, 1978, **14**, pp. 278–280
3 CCIR Report 723-1 (MOD-I): 'Worst-month statistics'. Conclusions of the interim meeting of study group 5, Geneva, 1983, pp. 68–70
4 MAWIRA, A.: 'Statistics of rain rates, some worst-month considerations', *Ann. Télécommun.*, 1980, **35**, pp. 423–428
5 SEGAL, B.: 'The estimation of worst-month precipitation attenuation probabilities in microwave systems design', *ibid.*, 1980, **35**, pp. 429–433

EXCESS PHASE IN MICROSTRIP DC BLOCKS

Indexing terms: Microwave devices and components, Microstrip

The letter gives details of excess phase calculations and measurements on microstrip DC breaks. Published microstrip discontinuity data has been used to develop an equivalent circuit which yields very good agreement between experimental and theoretical phase results over the frequency range 8 to 12 GHz.

Introduction: The use of the conventional microstrip finger break is widespread in microwave circuit designs. One aspect of the finger break performance which does not appear to have been addressed in the literature is that of excess phase; i.e. the difference between the phase change through the break and through the same physical length of 50 Ω microstrip line. There are a number of applications where it is important to be able to predict the excess phase with some degree of accuracy.

Theoretical and experimental results are presented for two microstrip DC blocks of slightly different geometry, the conventional finger break and a simple zig-zag slit. The two configurations are shown in Figs. 2*b* and 3*b*. In each case the measured excess phase is compared with theory.

Theory: The total phase change through the finger breaks investigated may conveniently be divided into two parts: (*a*) the phase change through the coupled line section; (*b*) the additional phase due to the end discontinuities.

The calculation of the phase change through the coupled lines is straightforward from the analysis of coupled, open-circuited microstrip lines[1] and is given by $\angle S_{21}$, where

$$S_{21} = \frac{2Z_{21}}{(Z_{11}+1)(Z_{22}+1) - Z_{12}Z_{21}}$$

and

$$Z_{11} = Z_{22} = -j\,\frac{Z_{0e}+Z_{0o}}{2}\,\frac{\cot\theta}{Z_0}$$

$$Z_{12} = Z_{21} = -j\,\frac{Z_{0e}-Z_{0o}}{2}\,\frac{\operatorname{cosec}\theta}{Z_0}$$

Z_0 is the characteristic impedance of the main microstrip line, θ is the electrical length of the coupled section, Z_{0e} and Z_{0o} are the even- and odd-mode characteristic impedances of the coupled line.

The latter expressions were the basis for the VSWR calculation for the finger break originally reported by Lacombe and Cohen.[2] Clearly, in a microstrip finger break, each of the fingers is not terminated in a pure open circuit, and some addition to the above expressions is needed to account for end effects.

Three discontinuity components may be identified as being associated with each finger end, namely: (i) an inductive component related to the narrowing of the main 50 Ω track to form the finger; (ii) capacitive coupling between the finger end and the adjacent 50 Ω track end; (iii) fringing capacitances at the track ends. An equivalent circuit of the form shown in Fig. 1 may be deduced to represent the discontinuity at each finger end.

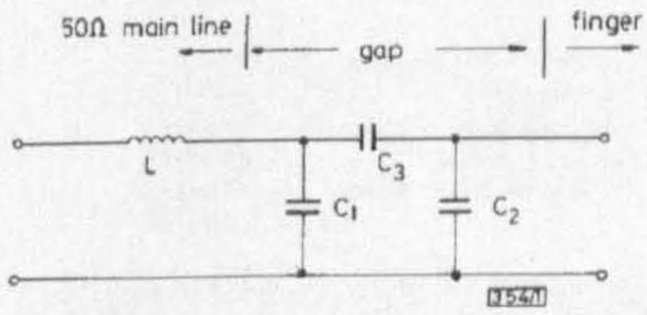

Fig. 1 *Equivalent circuit for coupled line end discontinuities*

Hammerstad and Bekkadal[3] have given expressions which enable the individual elements of the circuit of Fig. 1 to be calculated from the microstrip geometry and hence to be represented by some equivalent line lengths.

Results: The circuits shown in Figs. 2*a* and 3*a* were fabricated on RT/Duroid 6010, which had a substrate thickness of 635 μm and a relative permittivity of 10·4.

Table 1 gives the calculated element values for the equivalent circuit of Fig. 1; data are presented for the two DC breaks investigated. Converting the values from Table 1 into the appropriate equivalent line lengths gave total additional line lengths of 140 and 200 μm to represent the discontinuities of

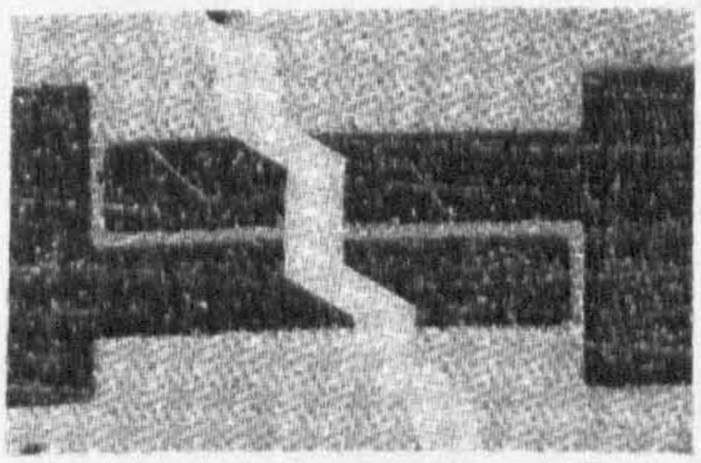

Fig. 2
a Test circuit: photograph shows enlargement of principal features of 3·06 mm finger break
b Comparison of measured and theoretical excess phase for 3·06 mm finger break

Table 1 VALUES OF DISCONTINUITY EQUIVALENT CIRCUIT ELEMENTS DEFINED IN FIG. 1

	L	C_1	C_2	C_3
	pH	pF	pF	pF
Finger break	74	0·0015	0·0018	0·020
Zig-zag slit	44	0·0030	0·0030	0·024

the finger break and zig-zag slit, respectively. The measured and calculated excess phases are compared in Figs. 2*b* and 3*b*, over the frequency range 8 GHz to 12 GHz. In each case graph A is the calculated excess phase neglecting the end correction and B the calculated excess phase including the end correction in the form of the above specified additional line lengths.

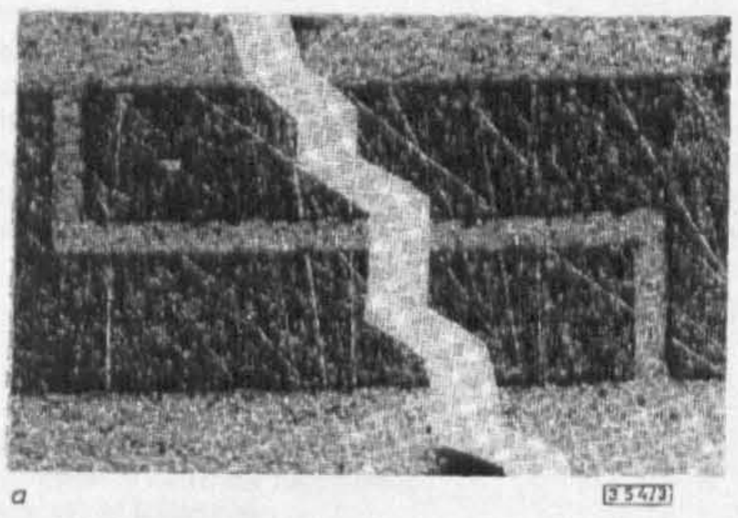

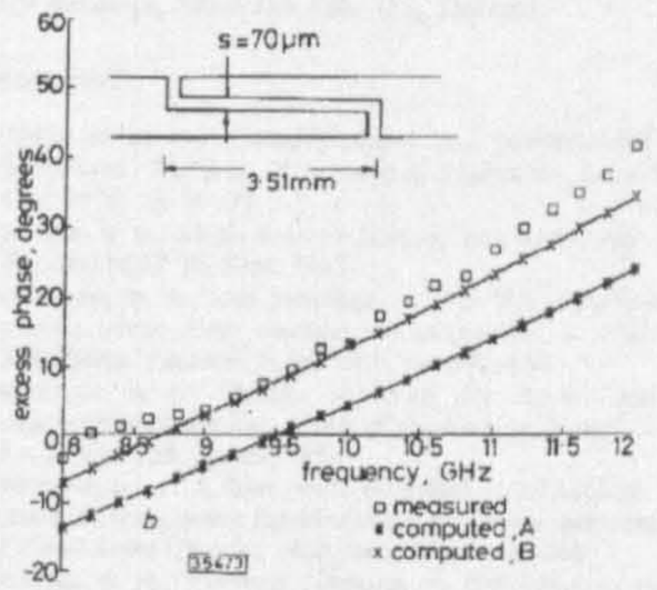

Fig. 3

a Test circuit: photograph shows enlargement of principal features of 3·51 mm zig-zag slit

b Comparison of measured and theoretical excess phase for 3·51 mm zig-zag slit

The measured values were obtained with an HP 8410 network analyser. It is evident from the results that there is good agreement between the measured excess phases and those computed theoretically with appropriate end corrections. It should be noted that the finger break has a smaller excess phase than the zig-zag slit.

Insertion loss measurements performed on the two different configurations of DC break gave comparable results (~0·3 dB) over X-band.

Conclusions: The excess phase has been shown to be significant, over X-band, for the popularly used microstrip DC finger break. Moreover, end effects have been shown to contribute significantly to the total excess phase. An equivalent circuit has been deduced to represent the discontinuities which yields good agreement between experimental and measured values of phase. The agreement has been shown to hold for two microstrip DC blocks of slightly different geometry.

C. E. FREE
C. S. AITCHISON

Department of Electronics
Chelsea College
Pulton Place, London SW6 5PR, England

2nd August 1984

References

1 EDWARDS, T. C.: 'Foundations for microstrip circuit design' (John Wiley & Sons, 1981)
2 LACOMBE, D., and COHEN, J.: 'Octave-band microstrip DC blocks', *IEEE Trans.*, 1972, **MTT-20**, pp. 555–556
3 HAMMERSTAD, E. O., and BEKKADAL, F.: 'A microstrip handbook'. ELAB report STF44 A74169, N7034, University of Trondheim, Norway, 1975

AUGER RECOMBINATION IN LONG-WAVELENGTH QUANTUM-WELL LASERS

Indexing terms: Lasers and laser applications, Semiconductor lasers

A formula for the ratio of the Auger recombination rates in quantum-well and bulk structures is derived. Significant changes in the Auger recombination in long-wavelength lasers are not expected on using a quantum well instead of a conventional double heterostructure unless the carrier density is reduced.

The advent of long-wavelength quantum-well lasers[1] is of considerable importance for sources in long-haul optical-fibre communication systems operating in the region of 1·55 μm because the quantum size effect provides extra degrees of freedom, namely the quantum-well width and barrier height, for device optimisation. In the development of such devices, some of the important problems will be to maximise the luminescent efficiency and minimise the threshold current and its sensitivity to temperature. Since Auger recombination is the only alternative recombination path to radiative recombination in idealised material (i.e. free of midgap levels) and is known to contribute in part to the temperature sensitivity of the threshold current of conventional long-wavelength bulk lasers,[2,3] its study in relation to the above development problems is highly relevant.

Ab initio calculations of Auger recombination using standard theory[4] are unreliable at present even in bulk material because of the many drastic approximations made, e.g. isotropic parabolic bands[5] and oversimplified estimates of overlap integrals.[6–8] Calculations of Auger recombination in quantum wells already published by other authors[9–11] contain yet further approximations and concentrate on presenting numerical as opposed to analytic results. However, it is reasonable to assume that the comparison of Auger recombination rates in bulk material and a quantum well can be more reliably calculated. A formula displaying the effects of size quantisation on Auger recombination would be very useful in giving guidelines for laser design, and such a formula is presented in this letter.

Consider the so-called CHCC process (see Fig. 1) in which an electron in the conduction band recombines with a hole in the heavy-hole band, the energy and momentum so liberated being taken up by a conduction-band electron moving further up the conduction band. While this specifies the Auger recombination process to be discussed precisely in the bulk, further specification is needed in a quantum well. Both the conduction and heavy-hole bands are subdivided into sub-bands in a quantum well. Provided size quantisation effects are sufficiently strong, i.e. the well is not too wide and the heterojunction barriers are sufficiently high, then the majority of carriers will be in their lowest sub-bands. It will be assumed that the Auger electron also remains in the lowest conduction sub-band during the recombination process.

An analytic result for the Auger recombination rate for the above quantum-well process has been derived in detail elsewhere by the authors.[12] The calculation used exactly the same assumptions, e.g. isotropic parabolic bands etc., as the calculation by Haug *et al.*[13] for the CHCC Auger recombination rate in bulk material, who also obtained an analytic result. Denote by R_{QW} the CHCC Auger recombination rate per unit volume previously derived by the authors in the wide-well width limit[12] which, in fact, works remarkably well for the quantum-well widths commonly of practical interest (in the

measured by moving the array of ten probes. The pad array must be subject to the constraints that probes must never overlap scribe channels. The example showing Fig. 1 includes most of the basic device structures required for process evaluation, including transistors of several aspect ratios, and features to characterise resistivity,[3] linewidth,[4] misalignment,[5] contact resistance[6,7] and capacitance.

Conclusions: A new concept in test chip design has been presented which removes the requirement for the relay matrix which is the most unreliable component in a parametric tester. At a cost of £10-30 000, it is also one of the most expensive parts of the test system. A potential source of noise is also eliminated, so the overall result is an increase in system performance with a significantly reduced capital cost. This is achieved at the expense of longer testing times due to increased prober movement and a reduced packing density on the PCC. The type of system which will suit a given test facility is dependent on a large number of parameters such as cost, accuracy, throughput, reliability, range of processes handled and chip area available.[8] Bearing this in mind, the above approach will, in many situations, provide a viable alternative to the present generation of parametric testers.

A. J. WALTON
J. M. ROBERTSON
R. HOLWILL
M. B. MOORE

Edinburgh Microfabrication Facility
Department of Electrical Engineering
University of Edinburgh
Kings Buildings, Edinburgh EH9 3JL, Scotland

22nd November 1984

References

1 BUEHLER, M. G.: 'Comprehensive test pattern with modular test structures: The 2 by *N* probe-pad approach', *Solid State Technol.*, Oct. 1979, pp. 89–94
2 MOORE, M. B.: 'High access efficiency test structures'. M Sc. Project Report: MSP 18, Sept. 1983
3 BUEHLER, M. G., and THURBER, W. R.: 'An experimental study of various cross sheet resistor test structures', *J. Electrochem. Soc.: Solid State Technol.*, April 1978, pp 645–650
4 BUEHLER, M. G.: 'Bridge and Van der Pauw sheet resistors for characterizing the line width of conducting layers', *J. Electrochem. Soc.*, 1978, 125, pp. 650–654
5 PERLOFF, D. S.: 'A four point electrical measurement technique for characterizing mask superposition errors on semiconductor wafer', *J. Solid State Circuits*, 1978, SC-13, pp 436–444
6 BERGER, H. H.: 'Contact diffusion on diffused resistors'. IEEE Int. Solid State Circuits Conference, Penn, USA, 1969, pp. 160–161
7 PROCTOR, S. J., LINDHOLM, L. W., and MAZER, J. A.: 'Direct measurement of interfacial contact resistance and interfacial contact layer uniformity', *IEEE Trans.*, 1983, ED-30, pp. 1535–1542
8 LEVIS, M.: 'System comparisons can simplify selection of parametric testers', *Electronics*, 26th January 1984

SINGLE PIN DIODE X-BAND PHASE SHIFTER

Indexing terms: Microwave devices and components, Phase shifters

A new design of microstrip phase shifter is described which uses only one PIN diode per bit of phase shift. Results are presented for a representative device which show good agreement between experimental and theoretical results at X-band. In particular, the device has been shown to yield a useful 20% bandwidth centred on 10 GHz.

Introduction: Conventional designs of digitally controlled phase shifters so far reported in the literature require the use of at least two switching elements, normally PIN diodes or FETs, per bit of phase shift. The various configurations of traditional designs have been conveniently summarised by White.[1] The microstrip phase shifter described here is a departure from conventional designs in that it employs a single PIN diode. It would appear to offer advantages over existing designs in terms of reduced cost and circuit complexity.

Circuit description: The circuit of a single-bit microstrip phase shifter is shown in Fig. 1. The arrangement consists of two

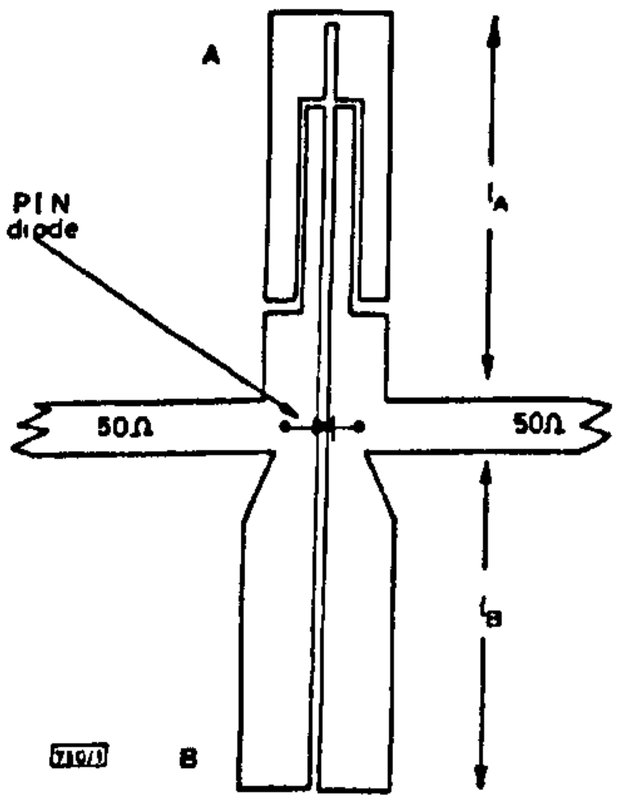

Fig. 1 *Single-bit microstrip phase shifter*

coupled line sections, A and B, with a PIN diode mounted at their intersection with the main 50 Ω line. Section A, in which the lines are connected at the remote end to form a short-circuit for the odd mode, contains two symmetrical DC breaks in the form of zig-zag slits. These permit DC biasing of the PIN diode. Section B is a high input impedance matching section.

It will be observed that section A, without the DC breaks, forms an allpass filter of the type described by Jones and Bolljohn[2] and subsequently employed by Schiffman[3] in the design of passive differential phase shifters.

Principle of operation: A specified phase change is obtained by switching the PIN diode; the frequency response is simply the difference between the phase-frequency responses of the circuit in the two diode states. The circuit is designed to be matched to the main line, at the centre frequency, in both states.

State 1: PIN diode off: In this state the two coupled line sections are effectively in parallel. The input impedance of the B section is designed to be high so that most of the signal will be transmitted through section A with a transmission phase change determined mainly by l_A. The equivalent circuit is shown in Fig. 2.

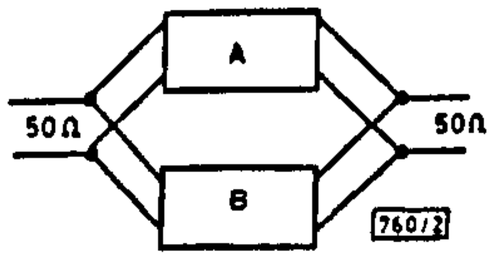

Fig. 2 *Equivalent circuit: PIN diode off*

State 2: PIN diode on: The nominal short-circuit presented by the PIN diode in the on state inhibits the formation of the odd mode on the coupled lines. In this condition, therefore, the A and B sections will behave as shunt connected stubs, each supporting an even mode. The equivalent circuit is shown in Fig. 3. The circuit parameters are chosen so that the stubs present equal and opposite input susceptances to the main line at the centre frequency, and hence cancel.

Design considerations:

Section A: The appropriate design equations are:

$$Z_0 = \sqrt{Z_{0e_A} Z_{0o_A}} \quad (1)$$

$$\phi = \cos^{-1}\left\{\frac{\rho - \tan^2 \beta l_A}{\rho + \tan^2 \beta l_A}\right\} + \delta \quad (2)$$

$$\rho = Z_{0e_A}/Z_{0o_A} \quad (3)$$

where Z_0 is the characteristic impedance of the main line (50 Ω), ϕ is the required phase change, δ is the additional

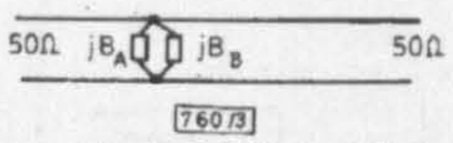

Fig. 3 *Equivalent circuit: PIN diode on*

phase introduced by DC breaks, Z_{0e_A} is the characteristic impedance of the even mode, Z_{0o_A} is the characteristic impedance of the odd mode, and ρ is a factor which determines the shape of the phase-frequency response with the diode off.

Having selected ρ, Z_{0e_A} and Z_{0o_A} are evaluated from eqns. 1 and 3; hence the line geometry for section A can be computed. The value of l_A to give the required phase change is then obtained from eqn. 2. Eqn. 2 includes a term δ to account for the excess phase due to the zig-zag slits.[4] The slits will affect the propagation of the even mode and effectively modify the electrical length of the coupled section.

Section B: The impedance presented by section B to the main line depends on Z_{0e_B}, Z_{0o_B} and l_B. These variables allow sufficient degrees of freedom to satisfy the following requirements for section B:

(*a*) With the diode off, the section should present a high impedance to the main line.

(*b*) With the diode on, $jB_B = -jB_A$ (Fig. 3).

(*c*) The overall electrical length $l_A + l_B$ should not be a multiple of π with the diode on to avoid resonances: this implies $Z_{0e_B} \neq Z_{0e_A}$.

In addition to the factors discussed above for the design of the two coupled sections, it is necessary to consider circuit discontinuities. Two sources of discontinuity were found to be significant, namely those associated with line end effects and with the T-junctions.

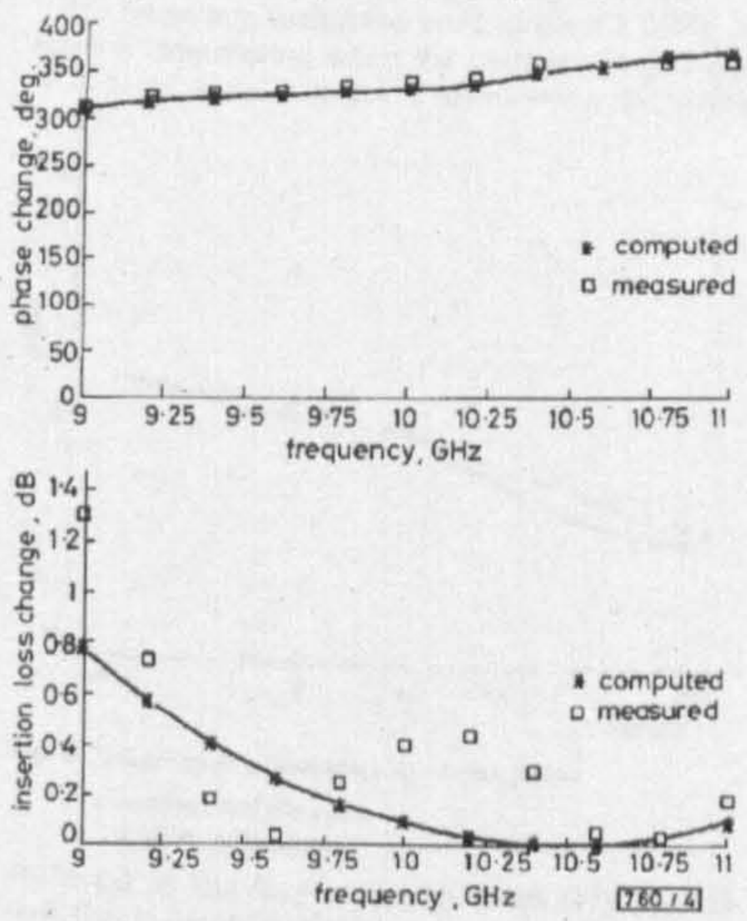

Fig. 4 *Comparison of measured and theoretical data for a single-bit phase shifter*

Test circuit details:
Section A: length $l_A = 4{\cdot}03$ mm, track widths = 490 μm, centre gap = 90 μm, DC slit gap = 45 μm, nominal slit length = 2·8 mm
Section B: length $l_B = 5{\cdot}8$ mm, track widths = 760 μm, centre gap = 90 μm

Results: Theoretical and measured data for a representative device are compared in Fig. 4, which shows the difference in phase between the two diode states. The device was fabricated on RT/Duroid 6010 which had a relative permittivity of 10·4 and a substrate thickness of 625 μm. An HP3900 beam lead PIN diode was used as the switching element. A photograph of the test circuit is given in Fig. 5. The standard deviation of

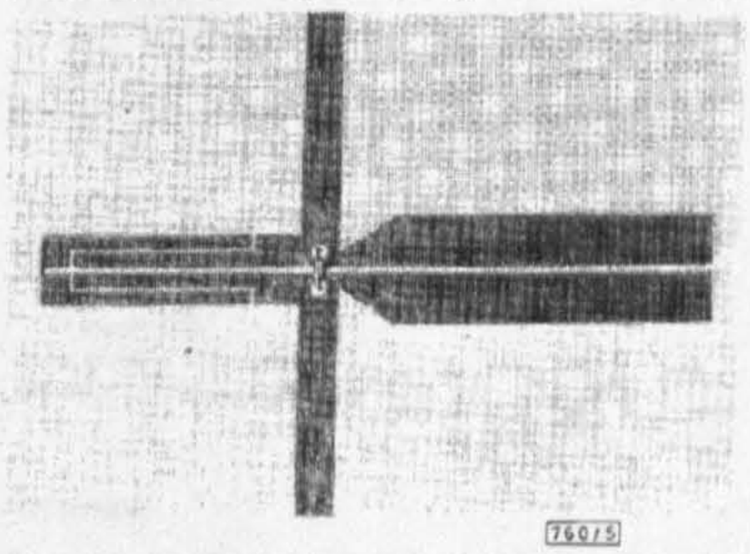

Fig. 5 *Photograph of test circuit*

the measured phase was 5·1° over the frequency range 9 to 11 GHz; the nominal design frequency was 10 GHz. The change in insertion loss (<0·5 dB) was higher than desirable, but further measurements have indicated that it could be reduced by improving the PIN diode matching in the on state.

The computed switched phase change exhibits some nonlinearity which could be reduced by optimisation of the circuit parameters.

Conclusions: A novel microstrip phase shifter has been developed, using a single PIN diode, which yields good agreement between measured and theoretical data at X-band. The performance compares well with that of other published devices using a greater number of switching elements.

The device appears attractive for the development of compact, multibit phase shifters.

C. E. FREE
C. S. AITCHISON

Electronics Department
Chelsea College
Pulton Place, London SW6 5PR, England

27th November 1984

References

1 WHITE, J. F.: 'Microwave semiconductor engineering' (Van Nos-
2 JONES, E. M. T., and BOLLJOHN, J. T.: 'Coupled strip transmission line filters and directional couplers', *IRE Trans.*, 1956, **MTT-4**, pp. 75–81
3 SCHIFFMAN, B. M.: 'A new class of broadband microwave 90° phase shifter', *ibid.*, 1958, **MTT-6**, pp. 232–237
4 FREE, C. E., and AITCHISON, C. S.: 'Excess phase in microstrip DC blocks', *Electron. Lett.*, 1984, **20**, pp. 892–893

DYNAMIC LINE BROADENING OF SEMICONDUCTOR LASERS MODULATED AT HIGH FREQUENCIES

Indexing terms: Lasers and laser applications, Semiconductor lasers

Directly modulated semiconductor lasers show a pronounced linewidth broadening. A general and simple expression for this broadening is derived and the consequences for optical communication systems are discussed.

It is well known that a directly modulated laser shows a considerable linewidth broadening, e.g. References 1–3. This fre-

simple analogic system with a comparator which could be on-chip should be able to supply the correction gate voltage. On the other hand, to use a microprocessor makes the system easier to adjust when production is considered.

Results: With $V_{gs} = -1$ V, $V_{ds} = 5$ V and $I_{ds} = 25$ mA (at $T = 20°C$), we compare in Fig. 5 the variations of the frequency when the temperature varies from $-40°C$ to $+80°C$, without (broken line) and with (solid line) stabilisation of the oscillator. In the second case, the stabilisation was made at a frequency of 7·44 GHz (corresponding to 20°C).

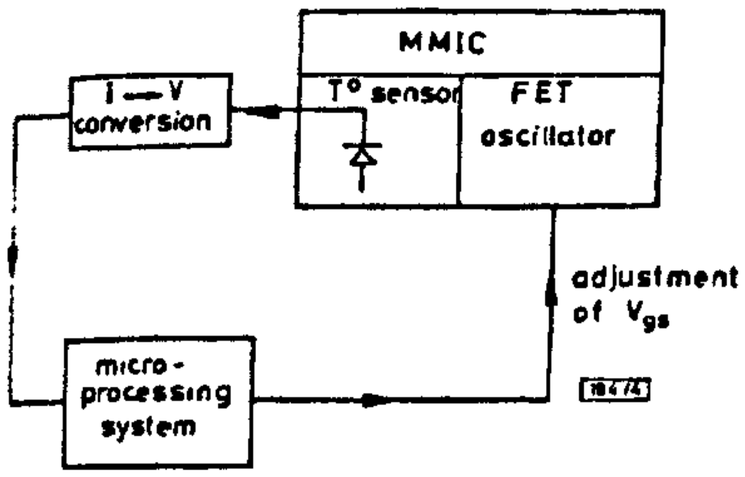

Fig. 4 *Synoptic of feedback frequency stabilisation loop*

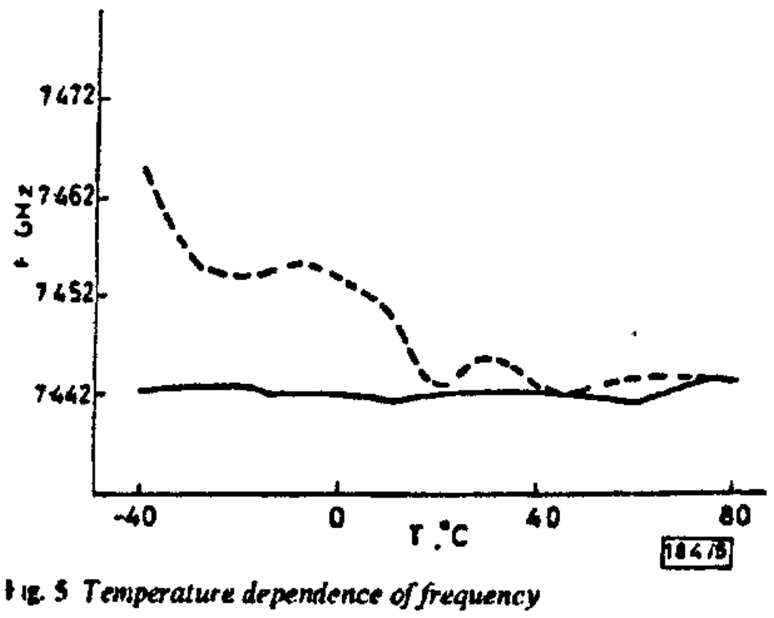

Fig. 5 *Temperature dependence of frequency*
- - without stabilisation
— with stabilisation

The frequency variations are less than 1 MHz in the whole range of temperature when the feedback loop is closed instead of 20 MHz when it is not. Furthermore, the output power is unaffected by the frequency regulation (Fig. 6). We can conclude that the stabilisation circuit is very efficient.

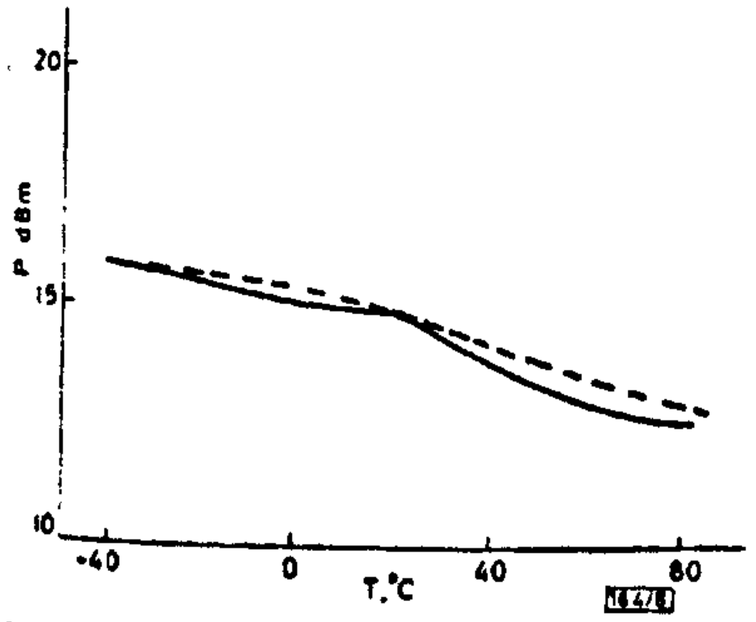

Fig. 6 *Temperature dependence of output power*
- - without stabilisation
— with stabilisation

Conclusion: We realised a GaAs MMIC including a FET oscillator and a Schottky diode which provides for the frequency stabilisation. The output power is 30 mW and remains stable in the whole range of temperature (-40 to $+80°C$). Up to now the feedback loop for stabilisation has been outside the chip and has consisted of a microprocessor, an EPROM and a DAC. The use of a microprocessor enables an efficient correction with any kind of f/T characteristic; the stabilisation loop could, however, be greatly simplified if one obtained a linear variation of the frequency against the temperature. This feature allows the oscillator to be frequency-stable to better than 1 MHz in the temperature range $-40°C$ to $+80°C$.

F. MASCART*
J. VINDEVOGHEL▲
E. CONSTANT▲
G. BLONDEL*
J. MAGARSHACK°

▲ *UST de Lille I*
Centre Hyperfréquences et Semiconducteurs
UA CNRS 287, 59655 Villeneuve D'Ascq Cedex, France

* *Sintra, DMF.*
344 avenue de la Marne
59700 Marcq en Baroeul, France

° *Thomson CSF*
Domaine de Corbeville
BP 10, 91401 Orsay, France

10th December 1985

References

1 BERTIN, R.: 'Mise au point d'un logiciel de CAO de masques pour circuits intégrés monolithiques microondes—application à la conception et à la réalisation d'un amplificateur large bande intégré'. DEA, Lille, June 1984

2 FARHAT, H.: 'Conception et réalisation en circuit intégré monolithique AsGa d'un radiomètre-microondes miniature'. Thèse Dr. Ingénieur, Lille, December 1984

THREE-PORT RING DISCRIMINATOR

Indexing terms: Microwave devices and components, Microstrip

A novel microwave discriminator is described which uses a single microstrip three-port ring. Results are presented for a representative circuit which show good agreement between theoretical and experimental results over a 20% bandwidth centred on 10 GHz. The device exhibits a narrowband match with a VSWR of 1·14 at the centre (design) frequency.

Introduction: The conventional arrangement of a passive microstrip discriminator uses hybrid rings to perform the signal splitting and combining functions, and an additional length of microstrip line to provide the required delay.

The three-port ring structure proposed in this letter, and shown connected as a discriminator in Fig. 1, achieves considerable simplicity by combining the signal splitting and delay functions in a single ring.

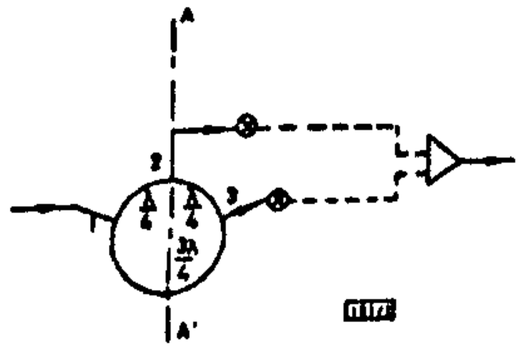

Fig. 1 *Three-port ring discriminator*

It is expected that the three-port ring device will offer a performance comparable with that of the usual dual hybrid ring arrangement, in terms of discriminator linearity and input match.

Circuit operation: Fig. 1 shows the three-port ring arrangement with the port separations specified at the design (centre) frequency. If a signal at the design frequency is applied to port

1, it follows from consideration of the port spacings that there will be equal outputs at ports 2 and 3. If the frequency is increased, the waves travelling in opposite directions around the ring will tend to move into phase at port 2 and out of phase at port 3, by virtue of the quarter-wavelength spacing between these ports. Hence the output from port 2 will increase and that from port 3 decrease. Conversely, if the frequency is decreased, the waves will move into phase at port 3 and out of phase at port 2. Thus, by combining the detected outputs at ports 2 and 3 in a differential amplifier, a discriminator response will be obtained.

The circuit in Fig. 1 shows the basic port separations, but the sensitivity of the discriminator can be improved by increasing the separation between ports 1 and 3. If the increase in separation is some multiple of λ, the circuit conditions at the centre frequency will not change.

Theory: The circuit can conveniently be analysed by applying the odd and even mode approach used for hybrid rings; see, for example, Zarbel.[1] This method of analysis makes use of a plane of symmetry through the circuit to reduce it to simpler equivalent two-port networks.

It is observed, in the three-port ring of Fig. 1, that there is geometric symmetry about the plane AA'. Thus, in-phase waves of unit amplitude applied at ports 1 and 3 will generate the even mode, and antiphase waves of unit amplitude applied at the same ports will produce the odd mode. The circuit may therefore be split along the plane of symmetry to give the two required equivalent circuits. It should be noted that taking the symmetry plane through one of the ports requires that port impedance to be doubled in the equivalent circuit. The analysis then proceeds on the lines given by Zarbel.

A particular solution for the three-port ring may be found by adding any linear combination of odd and even mode solutions.

The required solution, for a wave of unit amplitude at port 1, is given in terms of S-parameters as

$$S_{11} = \frac{T_{11e} + T_{11o}}{2{\cdot}0}$$

$$S_{21} = \frac{T_{21e} + T_{21o}}{2{\cdot}0}$$

$$S_{31} = \frac{T_{33e} - T_{33o}}{2{\cdot}0} = \frac{T_{11e} - T_{11o}}{2{\cdot}0}$$

where T_{ije} and T_{ijo} are, respectively, the odd- and even-mode reflection and transmission coefficients.

The theoretical discriminator function is obtained from $|S_{21}| - |S_{31}|$. A computer analysis, based on the above theory, showed that the best input match is obtained with a ring impedance of 70 Ω.

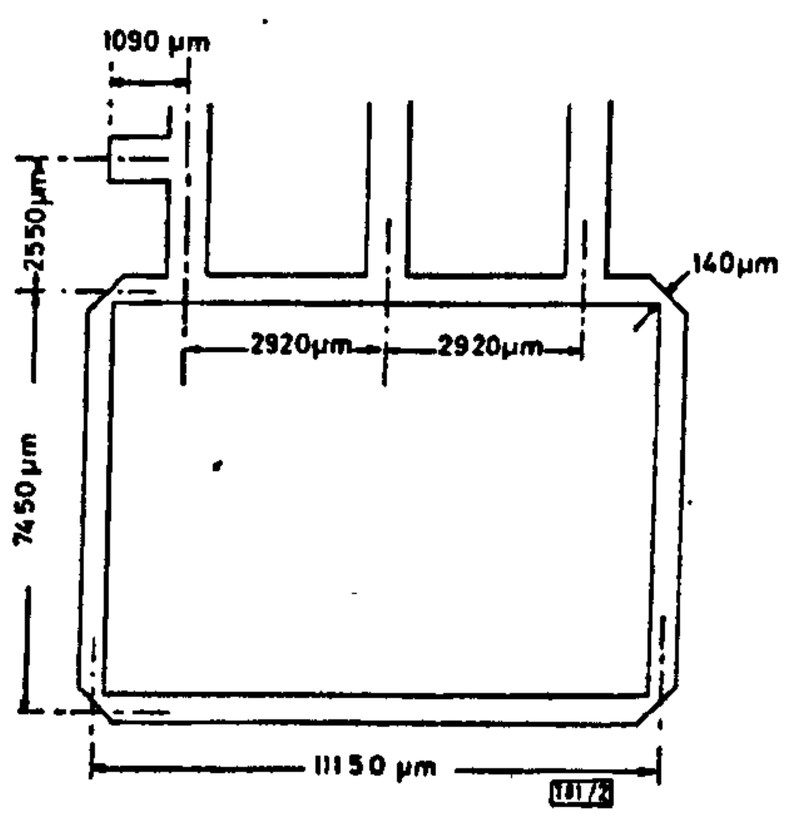

Fig. 2 *Test circuit (mean dimensions shown)*

Test circuit: The test circuit, shown dimensioned in Fig. 2, was fabricated on RT/Duroid 6010, which had a substrate thickness of 635 μm and a substrate relative permittivity of 10·4. The nominal port spacings were $\lambda/4$, $\lambda/4$ and $11\lambda/4$. Data interpolated from Easter's results[2] were used to compensate the port spacings to allow for the T-junction discontinuity effect. This compensation modified the through arm of each junction by −132 μm. For convenience the ring was made of rectangular geometry, and this necessitated a further compensation for the corner discontinuity. Using the same source as above, a value of −76 μm was obtained as the modification to the mean distance around each corner.

The port impedances were 50 Ω and the ring impedance 70 Ω. A single open-circuit stub was used to match the input to 50 Ω.

Results: The results shown in Figs. 3 and 4 were obtained using an HP 8410A network analyser. The value of $|S_{11}|$ was

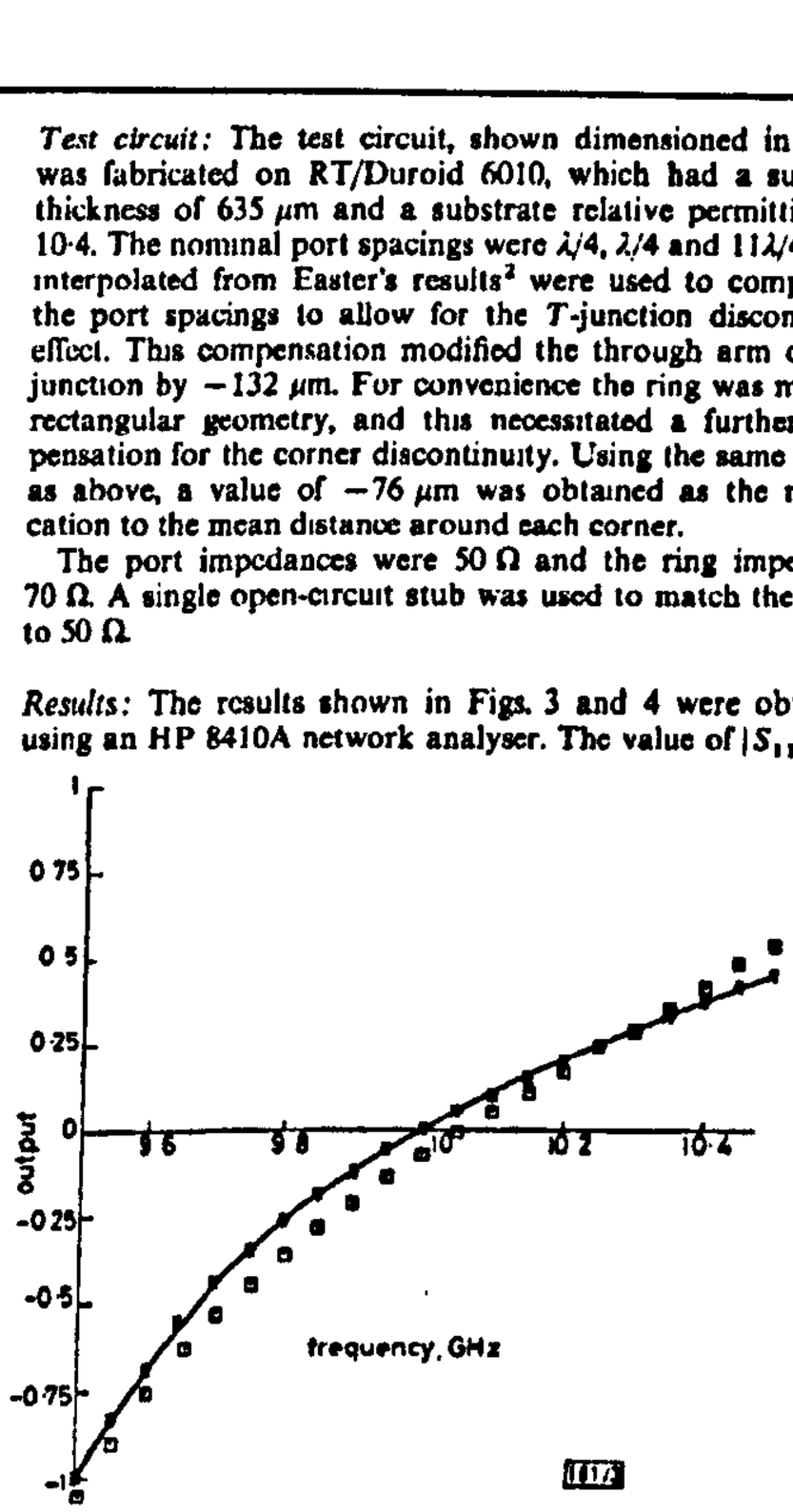

Fig. 3 *Normalised discriminator response*

□ measured
• theoretical

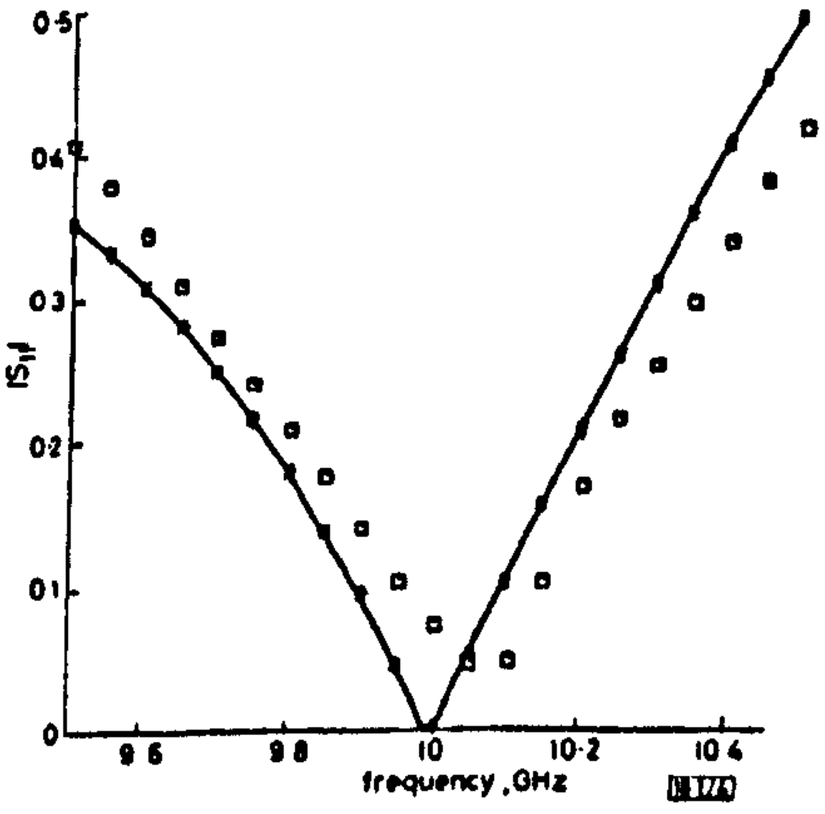

Fig. 4 *Input match of three-port ring*

□ measured
• theoretical

obtained directly, and the measured discriminator response from measured values of S_{21} and S_{31}.

The measured values of S_{11} have been corrected for the OSM coaxial to microstrip transition used on the measuring jig.

Discussion: In addition to the T-junction discontinuities affecting the port spacings, reflections within the ring caused

by the junctions were identified as a source of error. These reflections are amenable to analysis, but the results have not been included here.

The input match shown in Fig. 4 is rather narrowband, owing primarily to the use of single-stub matching, but the situation could be improved with a suitable broadband arrangement. It is also thought that the position of the input port could be optimised to eliminate the need for additional matching elements, and this is the subject of further work.

It will be noted that the theoretical discriminator response is asymmetric about the zero level. This does not impose any limitation on the application of the device, since a differential amplifier would normally be used to combine the outputs from ports 2 and 3, and an offset could be applied to the amplifier to achieve symmetrical limits for the discriminator response.

Conclusions: The proposed three-port ring has been shown to yield a useful, predictable discriminator characteristic. Although it has been shown to be possible to match the device at the centre frequency, it has the disadvantage, with single-stub tuning, of giving a narrowband match.

The reduction in circuit size offered by the three-port structure, compared with traditional designs, could be useful in MIC applications.

C. E FREE
C. S. AITCHISON*

King's College London
Electronic & Electrical Engineering Department
Chelsea Campus
Pulton Place, London SW6 5PR, United Kingdom

* Also with: ERA Technology Ltd., Cleeve Road, Leatherhead, Surrey KT22 7SA, United Kingdom

9th December 1985

References

1 ZARBEL, C. W.: 'Microwave duplexers'. MIT Radiation Laboratory Series, Vol. 14, (Boston Technical Publishers, USA, 1964), pp. 357–361
2 EASTER, B., GOPINATH, A., and STEPHENSON, I. M.: 'Theoretical and experimental methods for evaluating discontinuities in microstrip', *Radio & Electron. Eng.*, 1978, 48, pp. 73–84

APERTURE-COUPLED MICROSTRIP ANTENNA WITH A PERPENDICULAR FEED

Indexing terms: Antennas, Microstrip antennas

A new technique is described for feeding printed antennas. A microstrip antenna on one substrate is coupled through an electrically small aperture to a microstrip feed line on a perpendicularly oriented substrate. No direct connection is made to the patch. Such a geometry allows two separate substrates to be used for the antenna and feed functions. Measurements of a prototype design are presented

Introduction: Recently, an aperture-coupled microstrip antenna was reported.[1] This antenna was coupled through an aperture to a microstrip feed line on a separate parallel substrate bonded to the antenna substrate. This letter describes a variation on the aperture-coupled microstrip antenna of Reference 1, where the feed substrate is oriented perpendicular to the antenna substrate, as shown in Fig. 1. An electrically small rectangular aperture in the ground plane of the antenna substrate below the microstrip element is fed by a microstrip line on the perpendicular feed substrate. The bottom edge of the slot is connected to the ground plane of the feed substrate, and the top edge of the slot is connected to the microstrip line. This direct connection of the feed line to the aperture is very important. A number of degrees of freedom, such as slot length, width and position relative to the patch, exist to control the coupling between the feedline and the microstrip element. As will be seen, this design can easily be matched to a 50 Ω line.

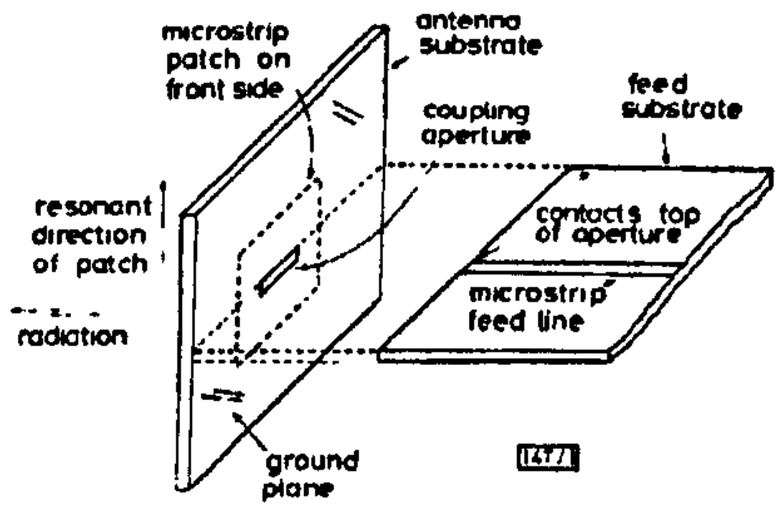

Fig. 1 *Exploded geometry of aperture-coupled microstrip antenna with perpendicular feed*

The basic antenna properties of the microstrip element are essentially the same as if the element were fed with the more conventional coaxial probe or directly connected microstrip feed line. Thus, the aperture coupling method of this letter has little effect on the radiation patterns or bandwidth of the microstrip element. As with the aperture-coupled element described in Reference 1, this new design can be used for circularly polarised elements, as well as arrays. Dual-polarised elements would probably require some sort of 'eggcrate' arrangement of the feed substrates, and so may be less practical. A number of advantages accrue from such a design, particularly for large phased arrays where active circuits for phase shifters etc. are integrated on the feed substrate:

(i) Significant space is available on the feed substrate as a result of regaining the 'depth' dimension (older waveguide arrays always used this depth for phase shifters and T/R modules).
(ii) A modular approach can be used for fabricating the feed network and associated circuitry.
(iii) The feed network and circuitry is completely isolated (by the antenna substrate's ground plane) from the radiating aperture. Spurious radiation and coupling are thus eliminated.
(iv) The use of separate antenna and feed substrates avoids the conflict of differing requirements for radiation and circuit functions, and reduces the scan blindness/bandwidth compromise.[2]

It is interesting to note that this design is analogous to a waveguide-fed microstrip element,[3] where an iris-terminated waveguide was connected at right angles to a microstrip antenna substrate. In that work, very poor matching results were obtained until the iris size was increased to the waveguide dimension. In the present design, the aperture is comparable in size to the effective cross-section of the microstrip feed line (waveguide). (The effective cross-section of the microstrip is larger than the physical width of the line due to fringing fields.)

As in Reference 1, some simple theoretical considerations can be derived easily to predict the salient features of the coupling mechanism between the microstrip-fed aperture and the microstrip antenna element. This is followed by a description of a prototype model and resulting measurements.

Basic theory of the coupling mechanism: A first-order coupling theory can be developed based on the cavity model of the microstrip antenna[4] and small-hole coupling theory.[5]

Assume the rectangular microstrip antenna is resonating in the dominant TM_{100} mode. By the cavity model,[4] the fields of this mode can be expressed as

$$E_x(x) = \frac{k_0^2}{j\omega\varepsilon_0} \cos\frac{\pi x}{a} \tag{1}$$

$$H_y(x) = \frac{\pi}{a} \sin\frac{\pi x}{a} \tag{2}$$

TU1D-3

MICROWAVE OSCILLATOR CONTROL USING A SWITCHED DELAY-LINE TECHNIQUE

Charles E. Free[1] and Colin S. Aitchison[2]

1. School of Electronic Engineering
Middlesex University
London N11 2NQ, UK

2. Dept. of Electrical Eng. & Electronics
Brunel University
Middlesex UB1 3PH, UK

ABSTRACT

A novel arrangement is described which uses an oscillator feedback network, incorporating a switched delay line, to stabilize the oscillator frequency and to permit electronic frequency selection. The circuit, which has been fabricated and tested in hybrid MIC form, makes use of two simple microstrip circuits to achieve the delay line and switching functions. A three-port discriminator is used to provide the effective delay line and single PIN diode phase shifter is used to achieve delay switching. Results are presented which show that the circuit provides good frequency stabilization, together with predictable frequency switching and a reduction in oscillator phase noise.

INTRODUCTION

The technique whereby an oscillator is stabilized using a feedback network incorporating a delay line has been well established in the literature. Generally, however, this is achieved using some form of lumped delay line, such as the bulk-wave line employed by Amblart and Peyrat [1]. The principal disadvantage of the existing techniques, particularly where SAW devices have been used, is a limitation in frequency, since suitable delay devices are not available at the higher microwave frequencies. In this paper we show that the stabilization can be achieved using a simple three-port microstrip discriminator, based on the circuit of Free and Aitchison [2] and, moreover, that the frequency of the oscillator can be altered by incorporating a switched phase shifter in the discriminator ring. Thus the basis is provided for the development of a digitally controlled oscillator, with good frequency stability, but at considerably less cost than a conventional discretely stepped frequency synthesizer. The arrangement is simple and there is no inherent frequency limitation to its operation or circuit implementation. Although a hybrid circuit has been investigated, the choice of simple circuit geometries makes the arrangement viable for integration in monolithic form.

Figure 1 shows the conventional arrangement of a delay line stabilized oscillator.

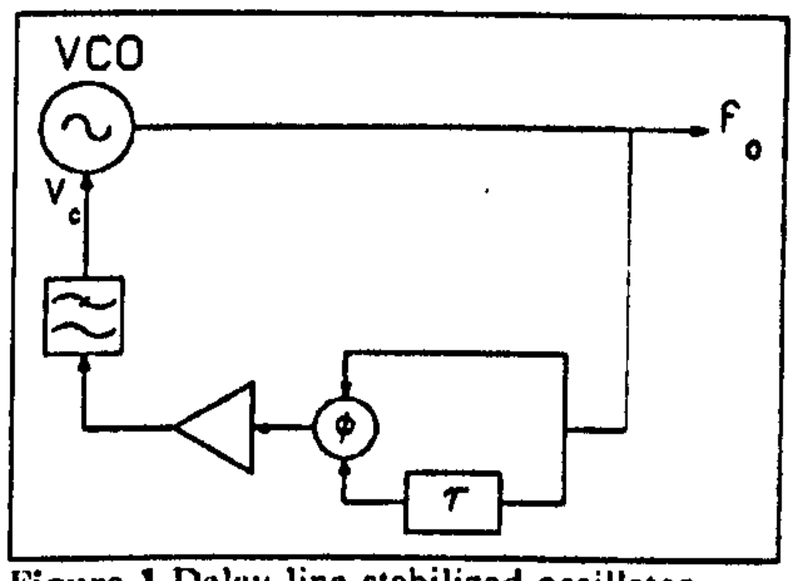

Figure 1 Delay-line stabilized oscillator

The circuit is essentially that of a microwave frequency discriminator, where the value of delay, τ, is chosen to centre the discriminator characteristic at a particular frequency. Should the oscillator frequency change, due to noise or long-term drift, then an error voltage is produced at the phase

detector output and applied as a controlling voltage to the VCO to maintain the original frequency.

If the delay is switched to a different value an offset voltage, V_e, will be produced at the feedback input to the VCO, which will lock to a new frequency, but still with the stabilization characteristics determined by the discriminator circuit. In the circuit proposed here, and shown in figure 2, the delay switching function is achieved by including a single PIN diode phase shifter, originally proposed by Free and Aitchison [3], within the ring. Thus the effective delay within the three port ring is controlled by the diode state.

One further advantage of the proposed arrangement is that the frequency stability, which depends ultimately on the delay line stability, will be high since the delay line is fabricated on relatively stable microstrip substrate. It also follows that there will be a reduction in oscillator phase noise, yielding an overall noise peformance between that of a fully variable frequency oscillator and a more complex, and expensive, conventioal frequency synthesizer.

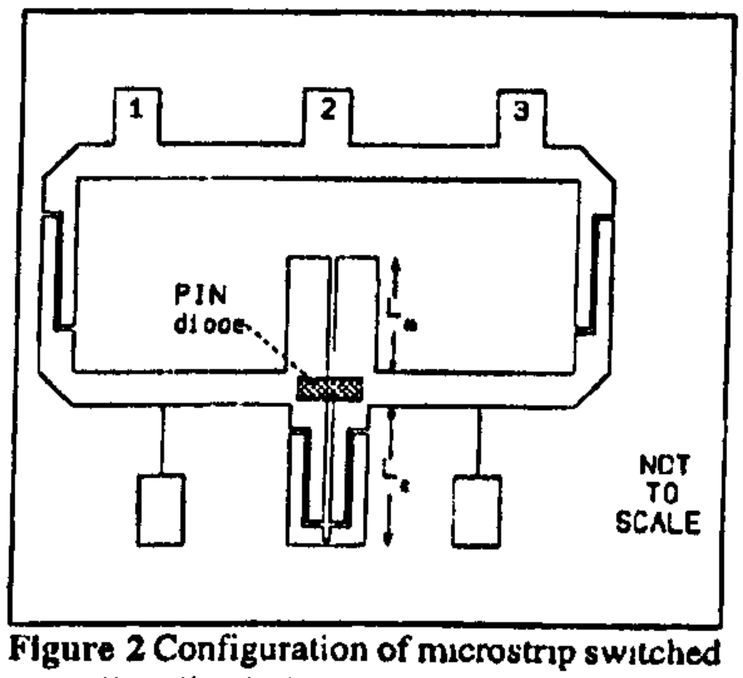

Figure 2 Configuration of microstrip switched delay-line discriminator

CIRCUIT DETAILS

The layout of the microstrip circuit investigated is shown in figure 2. The ring dimensions and port spacings were determined through the theory established in reference [2], to give input and output port impedances of 50Ω.

The oscillator output was applied to port 1 and a matched pair of coaxial detectors (HP8472A) was connected to port 2 and 3. The detector outputs were combined in a differential amplifier to yield a discriminator characteristic. It can be seen that DC finger breaks have been included in the ring to permit biasing of the PIN diode and to prevent the DC bias from affecting the two detectors. In calculating the dimensions of the ring, appropriate allowance was made for the transmission phase through the breaks, and this included the excess phase due to the finger discontinuities.

The circuit was fabricated on RT/duriod 6010, having a substrate thickness of 635μm and a relative permittivity of 10.4. A low-loss beam-lead PIN diode (HP5082-3900) was surface mounted at the centre of the single PIN diode phase shifter. The magnitude of the phase shift was determined by the length, L_e, of the coupled line region, as described in [3]. DC zig-zag breaks are shown in the coupled lines, again to permit biasing of the PIN diode. These breaks were included in both of the coupled lines to maintain the symmetry of the structure and the appropriate transmission phases included in the calculation of L_e. The matching frequency was set by the length, L_m, of the open circuited stub.

The circuit shown in figure 2 also includes two conventional bias pads.

DISCUSSION OF RESULTS

Typical results for a three port ring incorporating a single PIN diode phase shifter are summarized in table 1, with an example of the close-carrier phase noise performance for one of the PIN diode states being shown in figure 3.

Carrier frequency	11GHz
Stabilization ratio	25
Switched freq. step	30MHz
Change in input return loss between states	0.31dB
Open-loop phase noise 5kHz off carrier	-75dBc/Hz
Closed-loop phase noise 5kHz off carrier	-91dBc/Hz

Table 1: Summary of typical results

The results in the table show that a significant frequency step, 30MHz, can be achieved without a significant change in the input matching of the three-port ring between diode states. Clearly, any change in the return loss between diode states is of particular significance for this type of arrangement since any mismatch within the ring, due to the switching of the phase shifter element, will cause a change in level at the detector diodes. This means that the offset voltage will be a function of the mismatch in addition to the designed change in delay. The fact that a predictable frequency step can be achieved, with only a 0.31dB change in return loss indicates that the change in match is not significant.

The value of the stabilization ratio, measured as the frequency deviation of the oscillator to a dc control stimulus under open and closed loop conditions is a direct function of the sensitivity of the differential amplifier, and can be set to any desired value.
The bandwidth was found to be relatively narrow, of the order of 5%, as expected from [2]. This could be improved by including some form of broadband matching in the ring, following the techniques used for four-port hybrid rings.

The phase noise, shown in figure 3, was measured using an HP8472B low-frequency dynamic signal analyzer connected across the output of the low-pass filter in the feedback network. A continuous averaging function was selected on the analyzer to display the rms noise. Figure 3 shows the reduction in phase noise when the circuit is in lock. This reduction was observed in both diode states. The magnitude of the reduction is also a function of the sensitivity of the differential amplifier circuit.

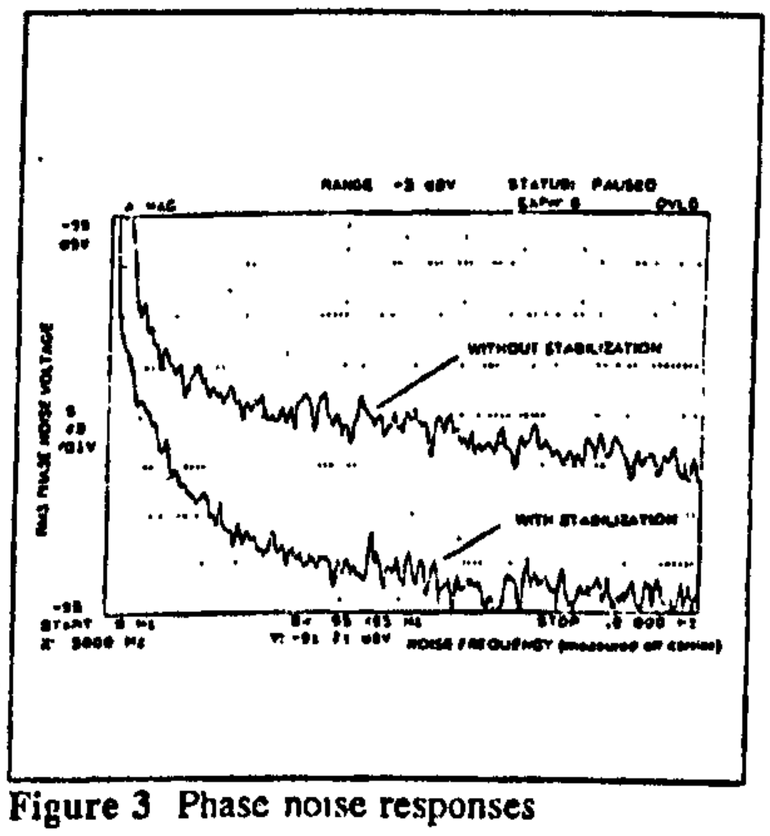

Figure 3 Phase noise responses

Table 1 gives two examples of the measured phase noise, expressed in conventional units of dBc/Hz, using values taken from figure 3. In figure 3 itself the phase noise is left as a relative level, since the absolute value of phase noise is a function of the particular test oscillator being used and is not of primary interest here.

CONCLUSIONS

The predicted functions of a delay line stabilized oscillator incorporating a frequency selection capability have been verified through practical measurement. The novel technique, together with the use of simple circuit geometries, offers

significant potential for the development of digitally controlled microwave oscillators, either in hybrid or monolithic form.

REFERENCES

1. AMBLARD, Y. and PEYRAT, A.: 'X-band bulk-wave delay line stabilized oscillator', MTT-S, June 1977, pp339-343

2. FREE, C.E. and AITCHISON, C.S.: 'Three-port ring discriminator', Electron. Lett., 1986, 22, pp.124-125

3. FREE, C.E. and AITCHISON, C.S.: 'Single PIN diode X-band phase shifter', Electron. Lett., 1985, 21, pp.128-129

2126 IEEE TRANSACTIONS ON MICROWAVE THEORY AND TECHNIQUES, VOL. 43, NO. 9, SEPTEMBER 1995

Improved Analysis and Design of Coupled-Line Phase Shifters

Charles E. Free and Colin S. Aitchison, *Fellow, IEEE*

***Abstract*—An analysis of coupled-line microstrip phase shifters is presented which shows that significant differences in theoretical performance are obtained by using an exact analysis in terms of odd and even mode propagation velocities rather than the approach in which the velocities are averaged. Measured data are presented and compared with theory over the frequency range 8–12 GHz and the agreement with theory is good.**

I. Introduction

THE CONFIGURATION of a conventional coupled-line phase shifter is shown in Fig. 1. The circuit introduces a transmission phase change between ports 1 and 2 which is a function of the coupled length, L_c. This form of circuit was employed by Schiffman [1] as part of a broadband 90° phase shifter. However, Schiffman's original work was based on stripline transmission structures, where the odd and even modes propagating along the coupled lines have equal phase velocities. Thus Schiffman was able to make use of the well known expressions for coupled-line filters developed by Jones and Bolljahn [2]. When this type of circuit has been designed in microstrip the same transmission equations are usually quoted, and the unequal odd and even mode velocities averaged to provide, theoretically, a well-behaved characteristic with zero insertion loss at all frequencies. In this paper a more exact analysis is performed, in terms of the independent odd and even mode phase changes along the coupled section and shows that for certain values of the electrical length, L_c, the insertion phase departs significantly from the ideal (average mode velocity) characteristic, and the device presents a significant mismatch at the input port. Some authors, notably Schiek and Kohler [3], have recognized the problem and suggested modifications to the basic design to compensate for the difference in the odd and even mode velocities, but there does not appear to have been any extended theoretical consideration of the simple coupled-line section to show the extent of the problem. There is a further problem which does not appear to have been addressed in the literature, namely that of establishing the actual coupled length that should be in situations where the circuit designer is inhibited from using the familiar chamfered entry by other circuit considerations.

Manuscript received November 14, 1994; revised May 25, 1995.

C. E. Free is with the School of Electronic Engineering, Middlesex University, Bounds Green Road, London N11 2NQ, UK.

C. S. Aitchison is with the Department of Electrical Engineering & Electronics, Brunel University, Uxbridge, Middlesex UB8 3PH, UK.

IEEE Log Number 9413431.

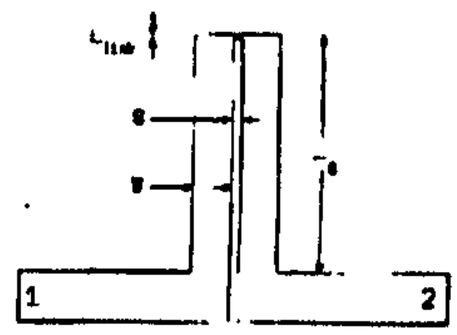

Fig. 1. Configuration of microstrip coupled-line phase shifter.

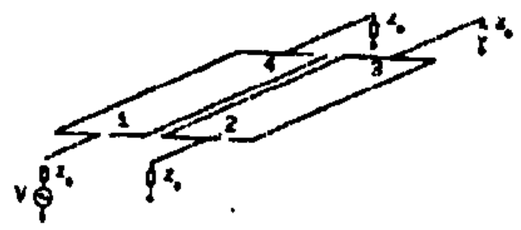

Fig. 2. Coupled microstrip lines showing port configurations.

II. Theory

The method of analysis used here follows the conventional approach adopted for coupled microstrip lines, whereby the total voltages and currents on the structure are obtained from the summation of the odd and even mode solutions. Thus the configuration of the structure shown in Fig. 2 can be reduced to two equivalent circuits as shown in Figs. 3 and 4.

Each of the lines may be analyzed using simple transmission line theory. Thus the currents and voltages at terminals 1 and 4, for the two modes, are related by

$$\begin{bmatrix} V_{1e} \\ I_{1e} \end{bmatrix} = \begin{bmatrix} \cos\theta_e & jZ_{oe}\sin\theta_e \\ jY_{oe}\sin\theta_e & \cos\theta_e \end{bmatrix} \begin{bmatrix} V_{4e} \\ I_{4e} \end{bmatrix} \tag{1}$$

and

$$\begin{bmatrix} V_{1o} \\ I_{1o} \end{bmatrix} = \begin{bmatrix} \cos\theta_o & jZ_{oo}\sin\theta_o \\ jY_{oo}\sin\theta_o & \cos\theta_o \end{bmatrix} \begin{bmatrix} V_{4o} \\ I_{4o} \end{bmatrix} \tag{2}$$

where Z_{oe} and Z_{oo} are the even and odd mode characteristic impedances, and Y_{oe} and Y_{oo} are the corresponding admittances. The relationships between the voltages and currents on the line joining ports 2 and 3 can then be deduced from symmetry. On the microstrip structure being considered, ports 3 and 4 are connected by a narrow conducting link. The link is designed to be narrow so that there will be no propagation around the end of the coupled section, but rather that the even and odd modes will be terminated by open and short circuits, respectively.

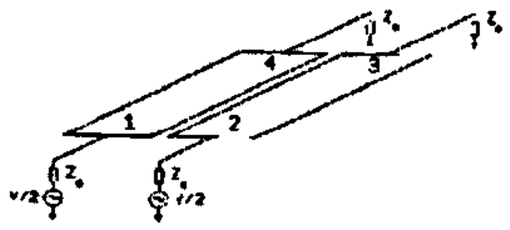

Fig. 3. Even mode equivalent circuit.

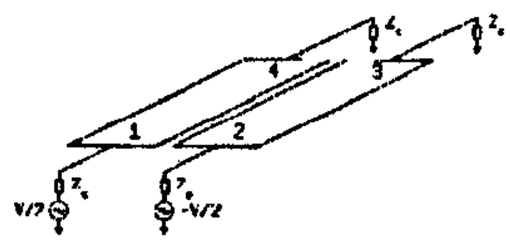

Fig 4. Odd mode equivalent circuit.

Thus the boundary conditions for the structure may be written as

$$I_{3e} = I_{4e} = 0$$
$$V_{3o} = V_{4o} = 0.$$

The transmission coefficient, V_2/V_1, for the circuit is obtained from

$$\frac{V_2}{V_1} = \frac{V_{2e} + V_{2o}}{V_{1e} + V_{1o}}. \tag{3}$$

It follows, from considerations of symmetry, that the transmission coefficient can also be written as

$$\frac{V_2}{V_1} = \frac{V_{1e} - V_{1o}}{V_{1e} + V_{1o}}$$

giving, after substitution for terminal voltages in terms of line characteristic impedances

$$\frac{V_2}{V_1} = \frac{-jZ_o(Z_{oe}\cot\theta_e + Z_{oo}\tan\theta_o)}{2Z_{oe}Z_{oo}\tan\theta_o\cot\theta_e - jZ_o(Z_{oe}\cot\theta_e - Z_{oo}\tan\theta_o)} \tag{4}$$

from which the transmission phase change is obtained as

$$\phi = \frac{\pi}{2} + \tan^{-1}\left[\frac{Z_o(Z_{oo}\tan\theta_o - Z_{oe}\cot\theta_e)}{2Z_{oe}Z_{oo}\tan\theta_o\cot\theta_e}\right]. \tag{5}$$

(The detailed derivations of (4) and (5) are given in the Appendix.)

If it is assumed that the odd and even modes have equal phase velocities, i.e., $\theta_o = \theta_e = \theta$, then (5) reduces to

$$\phi = \cos^{-1}\left[\frac{\frac{Z_{oe}}{Z_{oo}} - \tan^2\theta}{\frac{Z_{oe}}{Z_{oo}} + \tan^2\theta}\right] \tag{6}$$

which is the form quoted by Schiffman, and usually employed as an approximation in microstrip designs.

The approximations usually made in coupled-line phase shifters also extend to the match of the circuit, wherein it is assumed that the input impedance is given by

$$Z_o = \sqrt{Z_{oe}Z_{oo}}.$$

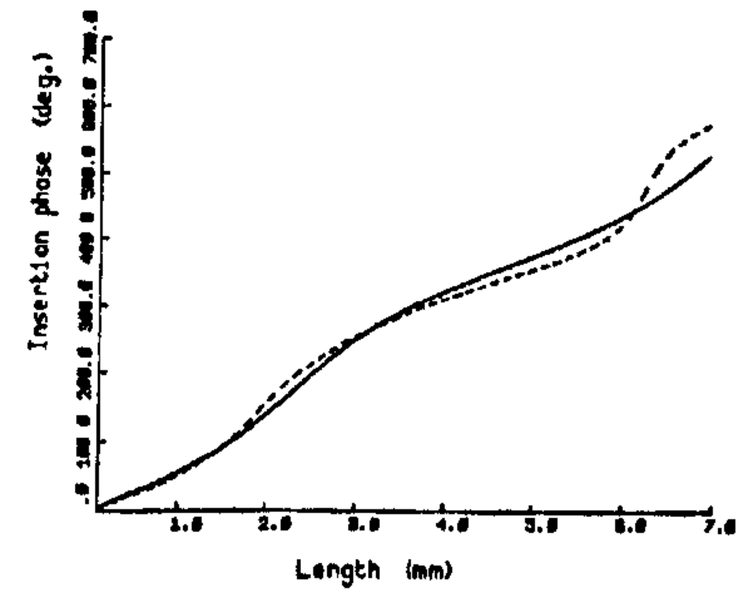

Fig. 5. Theoretical insertion phase at 12 GHz.

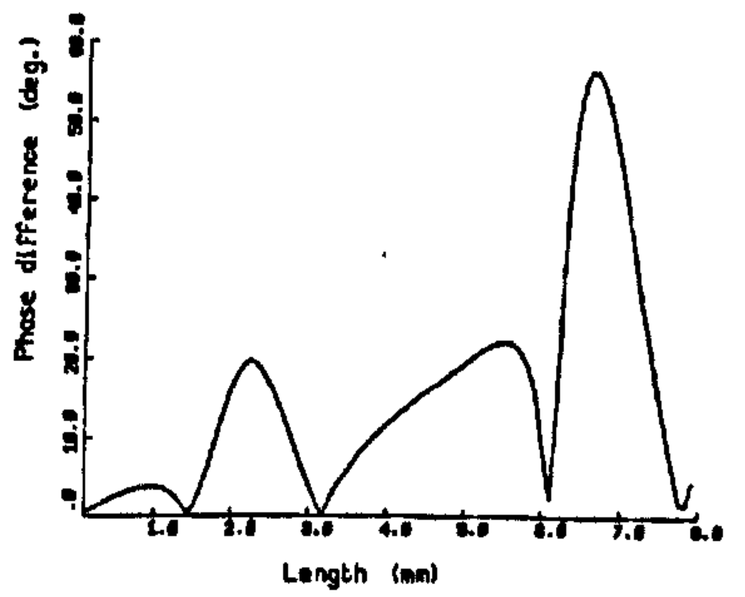

Fig. 6. Difference between exact and approximate theoretical insertion phase at 12 GHz.

It is shown in the Appendix that if the exact analysis is employed the input impedance at port 1 is frequency dependent and given by

$$Z_1 = \frac{2Z_{oe}Z_{oo}\cot\theta_e\tan\theta_o - jZ_o(Z_{oe}\cot\theta_e - Z_{oo}\tan\theta_o)}{2Z_o - j(Z_{oe}\cot\theta_e - Z_{oo}\tan\theta_o)}. \tag{7}$$

III. Comparison of Exact and Approximate Theory

Fig. 5 shows the theoretical insertion phase, computed as a function of the coupler length at 12 GHz, which results from using the approximate and exact methods of analysis. It can be seen that the exact response departs significantly from the approximate characteristic for certain lengths and, as would be expected, the difference tends to increase with the length of the coupled section. This is demonstrated more clearly in Fig. 6, where the magnitude of the of the difference between the responses has been plotted as a function of the length, and shows that the difference can be as large as 60°.

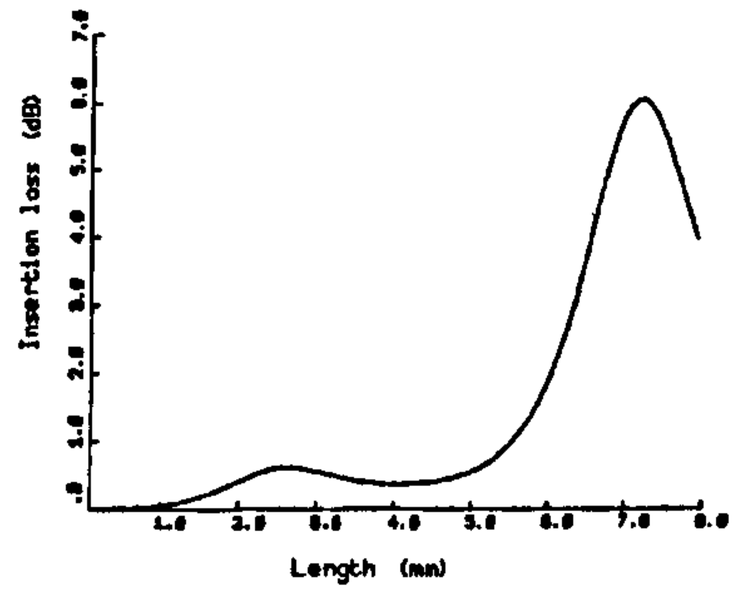

Fig. 7. Theoretical insertion loss for phase shifter at 12 GHz using exact analysis.

The approximate theory assumes that the match of the circuit is perfect, and frequency invariant. It can be seen from Fig. 7 that the exact analysis predicts significant insertion loss, due to circuit mismatch. As would be expected the highest loss occurs in the same region as the highest phase difference.

IV. Practical Design

In order to establish the validity of the new theory a number of coupled-line phase shifters of arbitrary length were designed and tested at X-band. The coupled-line geometry was chosen to give nominal input and output port impedances of 50 Ω, using $Z_o = (Z_{oe}Z_{oo})^{0.5}$. There is no unique combination of track width (w) and spacing (s) to satisfy this relationship and the actual values were selected so as to make the fabrication relatively noncritical. In calculating the values of θ_e and θ_o the Getsinger [4] model was used to account for dispersive effects. The effective length of the coupled region for the even mode was taken to be $L_c + l_{eo}$, where l_{eo} represents the effect of fringing at the remote end of the coupler and was evaluated from the well-known expression due to Hammerstad and Bekkadal [5]. In calculation for l_{eo} the effective width of the line was taken to be $2w + s$. Since the odd mode is fairly precisely terminated by the link between ports 3 and 4 no allowance was made for fringing, other than to use the full value of L_c, including L_{link}, for the odd mode on the basis that there will be some slight extension of the of the odd mode length due to the effective inductance caused by the odd mode penetrating into the narrow link.

V. Circuit Data

The test circuits were fabricated on RT/duroid 6010 having a substrate thickness of 635 μm, a track thickness of 4.5 μm, and a relative permittivity of 10.4. The actual dimensions of the circuits tested are given in Table I.

VI. Comparison of Practical Measurements with Theory

In Figs. 8–12 comparisons are presented between the theoretical insertion phase and measured data over the X-band frequency range for five couplers with different lengths. The lengths of the couplers were chosen to cover a wide range of phases, in arbitrary steps. The error bars associated with the measured data show a $\pm 1°$ measurement uncertainty. It can be seen that in all cases there is good agreement between the measured data and the predicted response based on an exact analysis. For circuit 1, with the shortest coupled length, the agreement is particularly good with the exact response well within the 1° error bounds of the measured data. For the other responses, even when the exact response lies outside the measured data error bounds the departure is small compared to the difference between the exact and approximate values. The agreement between the measured data and the exact response is emphasized by considering the shape of the responses. There are significant differences between the shapes of the approximate and exact responses, particularly for the longer coupled lengths, but in all cases the measured data points follow closely the shape of the exact response.

Figs. 11 and 12, which represent the longer coupled sections, show that the agreement between measured data and the exact response tends to worsen at the top end of the frequency band. This suggests that some dispersive effect is involved, which would naturally increase with the length of the coupled section. Getsinger's mode [4] was used to account for dispersion, but some authors, notably Easter and Gupta [6], have suggested that this model gives a slight overestimate of the effect of dispersion. This would be consistent with the results shown in

TABLE I
Test Circuit Dimensions [μm]—The Symbols are Defined in Fig. 1

CIRCUIT	L_c	L_{link}	w	s
1	759	26	465	100
2	1257	47	476	95
3	1784	10	470	.03
4	4650	52	477	109
5	6672	54	469	109

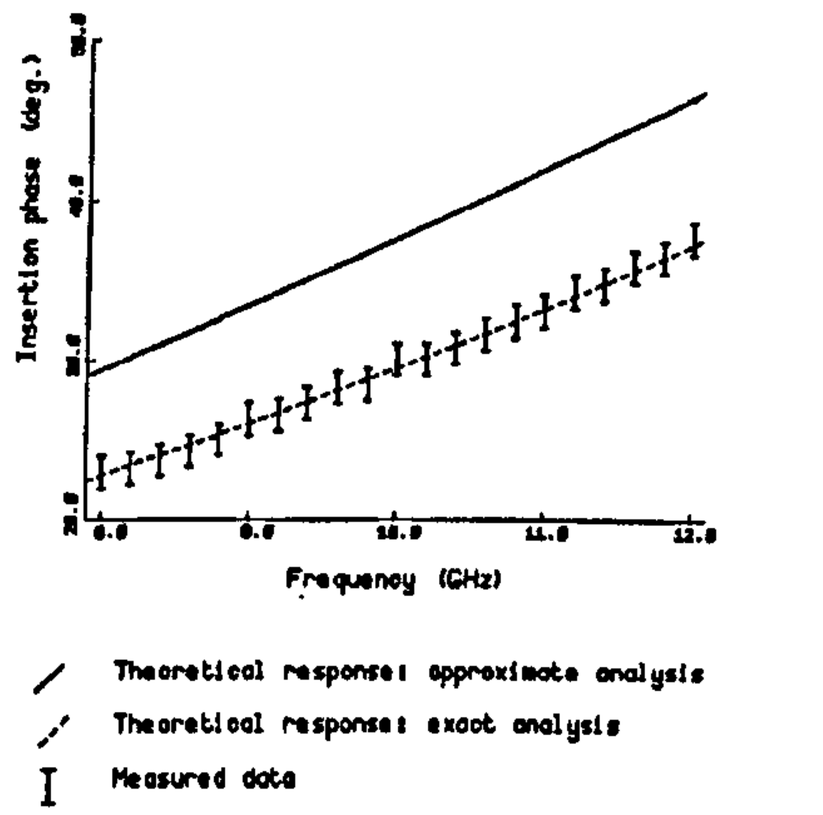

Fig. 8. Comparison of measured and theoretical data for circuit 1.

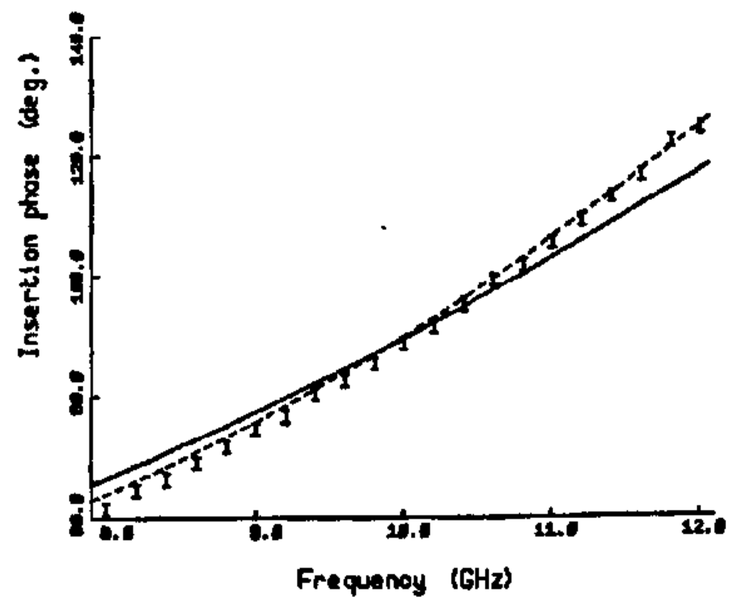

Fig. 9. Comparison of measured and theoretical data for circuit 2.

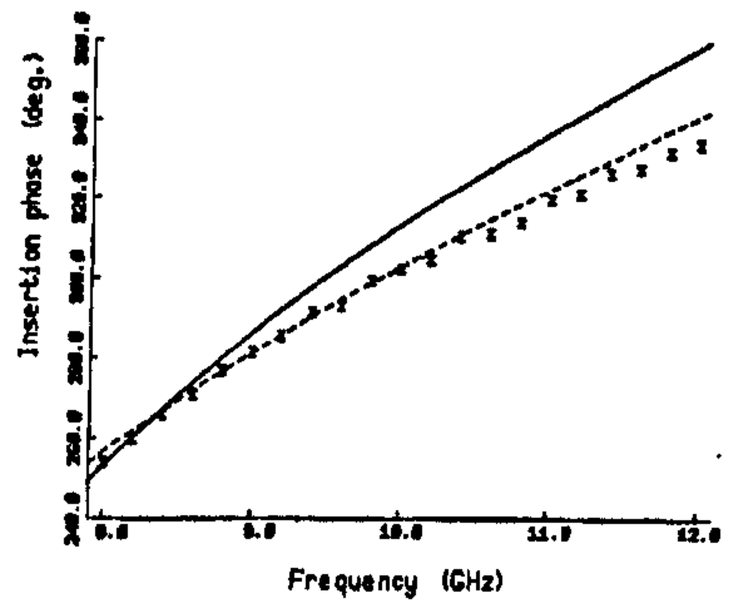

Fig. 11. Comparison of measured and theoretical data for circuit 4

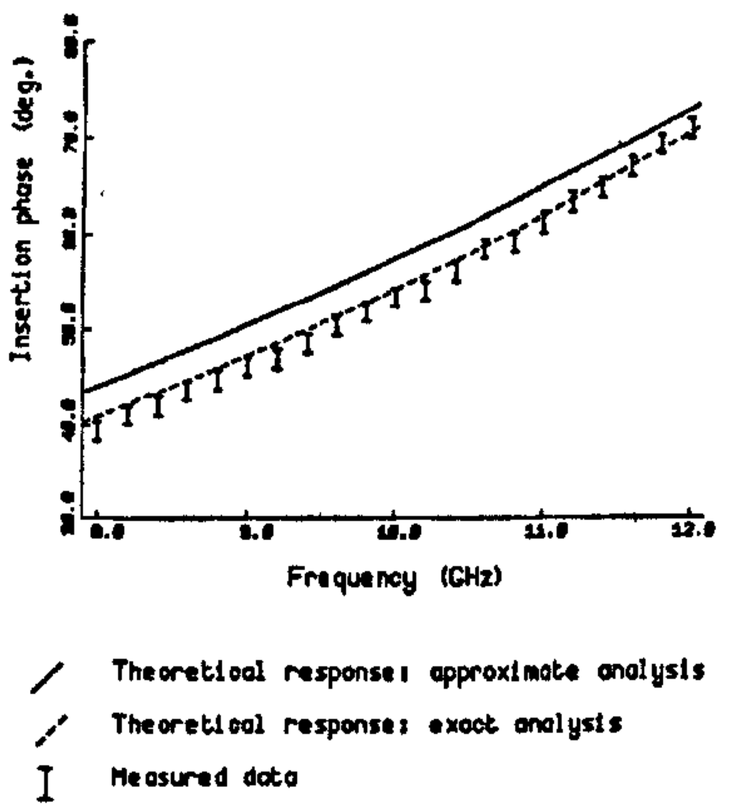

Fig. 10. Comparison of measured and theoretical data for circuit 3.

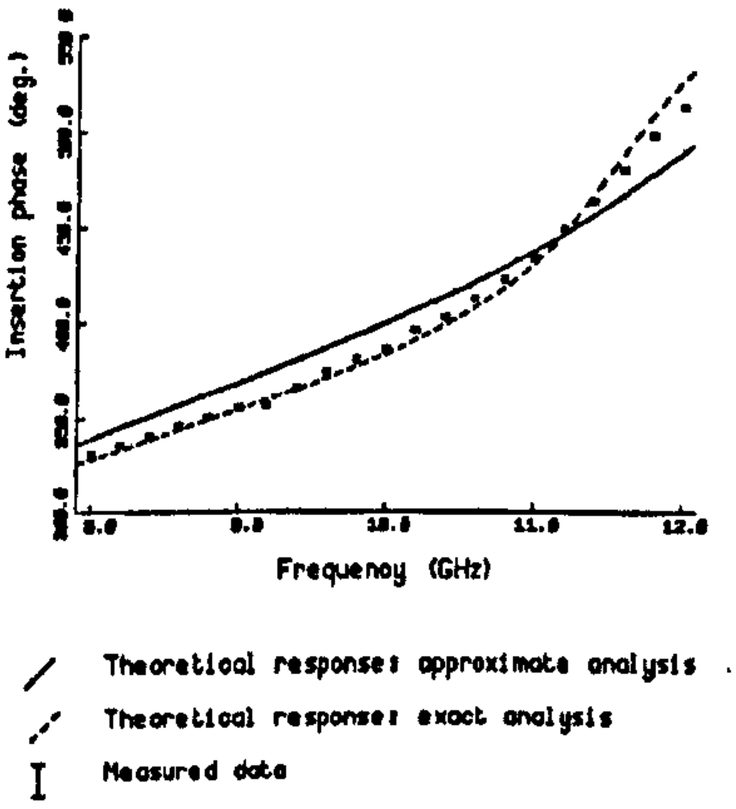

Fig. 12. Comparison of measured and theoretical data for circuit 5.

Figs. 11 and 12, where the predicted insertion phase is slightly higher than the measured data at the top end of the band. A more recent dispersion model, from Kirshning and Jansen [7], claims to provide a more accurate prediction of dispersion effects at higher microwave frequencies, and could possibly improve the fit between the measured data and exact theory in the 11–12 GHz region.

VII. Bend Discontinuity

In calculating the theoretical responses no attempt was made to model the discontinuities formed by the 90° bends at the entry to the coupled region; indeed, there do not appear to exist in the literature discontinuity models which include the combined effects of bends and coupling. However, it would appear from the results that this is an unnecessary refinement for the circuit designer and that adequate prediction of the insertion phase results from using the nominal length, L_a, together with small compensations for fringing at the remote end of the device.

It is not thought that the bend discontinuity contributed to the departure of the measured data from the exact response at the higher end of the measured band, since this effect was only noticeable for the longer coupled sections and suggested a purely length dependent effect.

VIII. Application

While the insertion phase exhibits some degree of nonlinearity with frequency, the simple coupled-line section, without the

changes in line geometry which have been introduced by some authors [3], still offers a useful and easily fabricated microstrip circuit component, which can yield very predictable results, based on an exact analysis. Moreover, its simple geometry would seem to be attractive for use at higher microwave frequencies where changes in line geometry, introduced for mode velocity compensation, would themselves introduce significant discontinuities.

IX. Conclusion

It has been shown that an exact analysis method is needed to satisfactorily predict the performance of coupled-line phase shifters and, moreover, that the device exhibits a significant mismatch under certain conditions. A comparison between measured and theoretical data shows that the new theory, based on an exact method of analysis in terms of the independent odd and even mode velocities, provides a better prediction of the nonlinear phase responses which are observed in practice.

Useful information has also been obtained on the effective length of the coupler which should be employed in practical designs.

Appendix
Exact Analysis of Coupled-Line Phase Shifter

Equation (1) can be expanded to give

$$V_{1e} = V_{4e} \cos \theta_e + jI_{1e}Z_{oe} \sin \theta_e \quad \text{(A1)}$$

$$I_{1e} = jV_{4e}Y_{oe} \sin \theta_e + I_{4e} \cos \theta_e \quad \text{(A2)}$$

and similarly (2) gives

$$V_{1o} = V_{4o} \cos \theta_o + jI_{4o}Z_{oo} \sin \theta_o \quad \text{(A3)}$$

$$I_{1o} = jV_{4o}Y_{oo} \sin \theta_o + I_{4o} \cos \theta_o. \quad \text{(A4)}$$

The boundary conditions are

$$V_{4o} = V_{3o} = 0$$
$$I_{4e} = I_{3o} = 0.$$

Substituting the boundary conditions into (A1)–(A4) gives

$$V_{1e} = V_{4e} \cos \theta e \quad \text{(A5)}$$

$$I_{1e} = jV_{4e}Y_{oe} \sin \theta_e \quad \text{(A6)}$$

and

$$V_{1o} = jI_{4o}Z_{oo} \sin \theta_o \quad \text{(A7)}$$

$$I_{1o} = I_{4o} \cos \theta_o. \quad \text{(A8)}$$

The input impedance at port 1 is given by

$$Z_{in,1} = \frac{V_{1e} + V_{1o}}{I_{1e} + I_{1o}} = \frac{V_{1e} + V_{1o}}{jV_{4e}Y_{oe} \sin \theta_e + I_{4o} \cos \theta_o} = \frac{V_{1e} + V_{1o}}{j\frac{V_{1e}}{\cos \theta_e}Y_{oe} \sin \theta_e + \frac{V_{1o}}{jZ_{oo} \sin \theta_o} \cos \theta_o} = \frac{V_{1e} + V_{1o}}{j(V_{1e}Y_{oe} \tan \theta_e - V_{1o}Y_{oo} \cot \theta_o)}. \quad \text{(A9)}$$

Now, if Z_{1e} and Z_{1o} are the input impedances at port 1 for the even and odd modes, respectively, then

$$V_{1e} = \frac{Z_{1e}}{Z_{1e} + Z_o}\frac{V}{2} \quad \text{(A10)}$$

$$V_{1o} = \frac{Z_{1o}}{Z_{1o} + Z_o}\frac{V}{2}. \quad \text{(A11)}$$

Also, from (A5) and (A6)

$$Z_{1e} = \frac{V_{1e}}{I_{1e}} = -jZ_{oe} \cot \theta_e \quad \text{(A12)}$$

and

$$Z_{1o} = \frac{V_{1o}}{I_{1o}} = jZ_{oo} \tan \theta_o. \quad \text{(A13)}$$

Substituting from (A10)–(A13) into (A9) we obtain, after straightforward manipulation, (A14) as shown at the bottom of the page.

The input reflection coefficient, S_{11}, is given by

$$S_{11} = \frac{Z_{in,1} - Z_o}{Z_{in,1} + Z_o}. \quad \text{(A15)}$$

It should be noted that if we put $\theta_e = \theta_o = \theta$, the expression for $Z_{in,1}$ becomes

$$Z_{in,1} = \frac{2Z_{oe}Z_{oo} - jZ_o(Z_{oe} \cot \theta - Z_{oo} \tan \theta)}{2Z_o - j(Z_{oe} \cot \theta - Z_{oo} \tan \theta)} \quad \text{(A16)}$$

and then, if

$$Z_o = \sqrt{Z_{oe}Z_{oo}}$$

we obtain

$$Z_{in,1} = Z_o$$

which is the nominal matched condition.

The transmission coefficient representing transmission between ports 1 and 2 is given by

$$\frac{V_2}{V_1} = \frac{V_{2e} + V_{2o}}{V_{1e} + V_{1o}}. \quad \text{(A17)}$$

$$Z_{in,1} = \frac{2Z_{oe}Z_{oo} \cot \theta_e \tan \theta_o - jZ_o(Z_{oe} \cot \theta_e - z_{oo} \tan \theta_o)}{2Z_o - j(Z_{oe} \cot \theta_e - Z_{oo} \tan \theta_o)}. \quad \text{(A14)}$$

$$\frac{V_2}{V_1} = -j\frac{Z_o(Z_{oe} \cot \theta_e - Z_{oo} \tan \theta_o)}{2Z_{oo}Z_{oo} \tan \theta_o \cot \theta_e - jZ_o(Z_{oe} \cot \theta_e - Z_{oo} \tan \theta_o)}. \quad \text{(A19)}$$

From considerations of symmetry, (A17) can be written as

$$\frac{V_2}{V_1} = \frac{V_{1e} - V_{1o}}{V_{1e} + V_{1o}} = \frac{\dfrac{Z_{1e}}{Z_{1e} + Z_o} - \dfrac{Z_{1o}}{Z_{1o} + Z_o}}{\dfrac{Z_{1e}}{Z_{1e} + Z_o} + \dfrac{Z_{1o}}{Z_{1o} + Z_o}}. \quad \text{(A18)}$$

Thus, substituting from (A12) and (A13) we obtain (A19) as shown at the bottom of the preceding page.

From (A19) the transmission phase change is obtained as

$$\phi = \frac{\pi}{2} + \tan^{-1}\left[\frac{Z_o(Z_{oe}\cot\theta_e - Z_{oo}\tan\theta_o)}{2Z_{oe}Z_{oo}\tan\theta_o\cot\theta_e}\right]. \quad \text{(A20)}$$

This is the exact expression for insertion phase. We can simplify this by making assumptions about Z_{oe} and Z_{oo} and by letting $\theta_e = \theta_o = \theta$. We have already established that the approximate theory, averaging the odd and even mode velocities, yields a matched input condition when

$$z_o = \sqrt{Z_{oe}Z_{oo}}.$$

Substituting these simplifying conditions into (A20) gives

$$\phi = \frac{\pi}{2} + \tan^{-1}\left[\frac{Z_{oe}\cot\theta - Z_{oo}\tan\theta}{2\sqrt{Z_{oe}Z_{oo}}}\right] \quad \text{(A21)}$$

whence

$$\cot\phi = \frac{Z_{oo}\tan\theta - Z_{oe}\cot\theta}{2\sqrt{Z_{oe}Z_{oo}}}.$$

Using the trigonometric relationship

$$\cot^2\phi = \frac{\cos^2\phi}{1 - \cos^2\phi}$$

we obtain

$$\cos\phi = \pm\frac{Z_{oo}\tan\theta - Z_{oe}\cot\theta}{Z_{oo}\tan\theta + Z_{oe}\cot\theta}.$$

Now we know

$$\phi = 0 \quad \text{when} \quad \theta = 0$$

hence

$$\cos\phi = \frac{\dfrac{Z_{oe}}{Z_{oo}} - \tan^2\theta}{\dfrac{Z_{oe}}{Z_{oo}} + \tan^2\theta}$$

or

$$\phi = \cos^{-1}\left[\frac{\rho - \tan^2\theta}{\rho + \tan^2\theta}\right] \quad \text{(A22)}$$

where

$$\rho = \frac{Z_{oe}}{Z_{oo}}.$$

Equation (A22) thus gives the approximate insertion phase of the coupler which should be employed in practical designs.

REFERENCES

[1] B. M. Schiffman, "A new class of broadband microwave 90° phase shifters," *IRE Trans.*, vol. MTT-6, no. 4, pp. 232–237, Apr. 1958.

[2] E. M. T. Jones and J. T. Bolljahn, "Coupled-strip transmission line filters and directional couplers," *IRE Trans.*, vol. MTT-4, no. 4, pp. 124–130, Apr. 1956.

[3] B. Schiek and J. Kohler, "A method for broadband matching of differential phase shifters," *IEEE Trans. Microwave Theory Tech.*, vol. MTT-25, no. 8, pp. 666–671, Aug. 1977.

[4] W. J. Getsinger, "Microstrip dispersion model," *IEEE Trans. Microwave Theory Tech.*, vol. 21, no. 1, pp. 34–39, Jan. 1993.

[5] E. O. Hammerstad and F. Bekkadal, "A microstrip handbook," *ELAB Report STF 44A74169, N7034*, Univ. of Trondheim—NTH, Norway 1975.

[6] B. Easter and K. C. Gupta, "More accurate model of coupled microstrip line section," *IEEE J. Microwaves, Optics and Acoustics*, vol. 3, no. 3, pp. 99–103, May 1973.

[7] M. Kirschning and R. H. Jansen, "Accurate wide-range design equations for the frequency—dependent characteristics of parallel coupled microstrip lines," *IEEE Trans. Microwave Theory Tech.* vol. MTT-32, no. 1, pp. 83–90, Jan. 1984.

Charles E. Free received the B.Sc. in electrical engineering from Aston University in the UK and the M.Sc. in communication systems.

He worked as a Research Engineer on *Q*-band communications at Marconi Research Centre, Great Baddow, England. He is now a Principal Lecturer in electronic communications at Middlesex University, London, where his research interests are mainly in microwave circuits and propagation.

Colin S. Aitchison (SM'90–F'94) received the B.Sc. from Imperial College in London in 1955.

He joined Philips Research Laboratories where he ran a research group concerned with novel microwave active components including parametric amplifiers and other solid state circuits. In 1972 he joined Chelsea College, University of London, and became Professor and Head of Department extending his research interests to include distributed amplifiers. In 1984 he joined ERA Technology to establish an active microwave research group concerned with distributed amplifiers, systems, and microwave power amplifiers. In 1989 he joined Brunel University continuing with his active research activities. He is currently Professor and Head of Department. He has published 120 papers.

Mr. Aitchison is a Fellow of the IEEE and IEE.

dual-band AR-coated crystal. The SF laser was continuously tunable from 431 to 438nm. From the practical point of view, our SF laser is particularly attractive because it combines reliable materials that are commercially available with a single-pass configuration that is simple to implement, does not require bulky and expensive optical isolators, and provides an ultra-stable and diffraction-limited beam.

8 March 1996
Electronics Letters Online No: 19960591

D. Fluck and P Günter (*Nonlinear Optics Laboratory, Institute of Quantum Electronics, Swiss Federal Institute of Technology, ETH-Hönggerberg, 8093 Zürich, Switzerland*)

References

1 BIAGGIO, I., KERKOC, P., WU, L.-S., GÜNTER, P., and ZYSSET, B.: 'Refractive indices of orthorhombic $KNbO_3$. II. Phase-matching configurations for nonlinear-optical interactions', *J. Opt. Soc. Am. B*, 1992, 9, pp. 507–517

2 FLUCK, D., PLISKA, T., and GÜNTER, P.: 'A 10mW frequency doubled diode laser at 491nm'. Proc. Advanced Solid-State Lasers, San Francisco, 1996, pp. 135–137

3 ZIMMERMANN, C., VULETIC, V., HEMMERICH, A., and HÄNSCH, T.W.: 'All solid state laser source for tunable blue and ultraviolet radiation', *Appl. Phys. Lett.*, 1995, 66, pp. 2318–2320

4 FLUCK, D., PLISKA, T., GÜNTER, P., FLEUSTER, M., BUCHAL, C., and RYTZ, D.: 'Blue light generation by frequency doubling cw diode laser radiation in ion-implanted $KNbO_3$ waveguides', *Electron. Lett.*, 1994, 30, pp. 1937–1938

5 KEA, P.N., STANDLEY, R.W., and DIXON, G.J.: 'Generation of 20mW of blue laser radiation from a diode-pumped sum-frequency laser', *Appl. Phys. Lett.*, 1993, 63, pp. 302–304

6 WIGLEY, P.G., ZHANG, Q., MIESAK, E., and DIXON, G.J.: 'High-power 467-nm passively locked signal-resonant sum-frequency laser', *Opt. Lett.*, 1995, 20, pp. 2496–2498

7 PARKE, R., WELCH, D.F., HARDY, A., LANG, R., MEHUYS, D., O'BRIEN, S., DZURKO, K., and SCIFRES, D.: '2.0W CW diffraction limited operation of a monolithically integrated master oscillator power amplifier', *IEEE Photonics Technol. Lett.*, 1993, 5, pp. 297–300

8 BOYD, G.D., and KLEINMAN, D.A.: 'Parametric interaction of focused Gaussian light beams', *J. Appl. Phys.*, 1968, 39, pp. 359–3639

Analysis of microstrip ring structures

C.E. Free and C.S. Aitchison

Indexing terms: Discriminators, Microstrip components

A new method of analysing microstip ring structures, which offers a number of advantages over existing methods, is presented In particular, the method permits the analysis of asymmetric ring networks. Results are presented which verify the technique through the consideration of symmetric and asymmetric three-port ring discriminators.

Introduction: The only method of analysing microwave ring structures that has so far been reported in the literature [1, 2] involves reducing the circuit to two equivalent two-port networks, through the establishment of a plane of symmetry. One of the equivalent circuits represents the situation when in-phase voltages are applied to symmetrical ports of the structure, and the other represents the situation when the applied voltages are in anti-phase. Then, by invoking the principle of superposition, an overall solution in terms of excitation at a single port is found by adding the solutions for the two equivalent circuits. However, this method is somewhat restrictive in that it can only be applied to circuits where there is geometric, and hence electrical, symmetry. There are some circuit components, notably the three-port ring discriminator, where this symmetry may not exist.

In the three-port ring circuit discussed by Free and Aitchison [3] there was a symmetrical arrangement of the three ports, yielding a discriminator response centred, with zero output voltage, at the design frequency. If however the input port is displaced, the shape of the discriminator response will be maintained, but with a voltage offset at the centre frequency. This offset voltage is potentially useful as a frequency control voltage when the discriminator is used to stabilise an oscillator. However, the network is no longer symmetrical, and requires a more versatile analytical approach than is currently available.

Analysis: The new approach, which does not require the structure to exhibit symmetry, involves summing the currents at each port of the network and then relating the individual currents by the transmission coefficients between and through the various circuit nodes. Thus a set of equations can be generated, from which the ratio of any two input or output currents can be found.

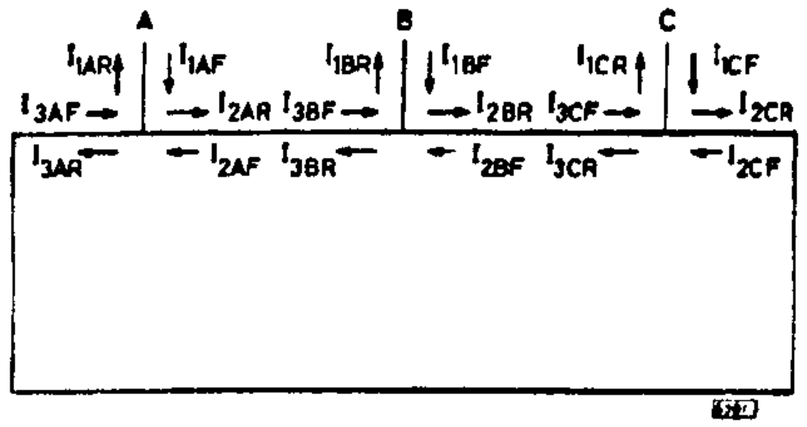

Fig. 1 *Three-port ring discriminator circuit, showing current nomenclature*

Not drawn to scale

Fig. 1 shows a three-port ring, labelled with the currents entering and leaving each node. The suffixes of the current terms indicate the port (1, 2 or 3) of each junction (A, B or C) and the direction of current flow, where *F* represents the incident wave and *R* the reflected wave. Thus at junction A we have,

$$(I_{1AF} - I_{1AR}) + (I_{2AR} - I_{2AF}) + (I_{3AF} - I_{3AR}) = 0 \quad (1)$$

If the transmission coefficients though each junction are represented by α_1 and α_2, as defined in Fig. 2, then we have a set of relationships for each junction of the form

$$I_{3AR} = \alpha_1 I_{1AF} + \alpha_2 I_{2AF} \quad (2)$$

assuming that ports 2 and 3 of each junction are correctly matched to the ring. This assumption of matching is not restrictive, and the effects of mismatching could easily be included by adding additional terms. Propagation around the ring can be represented simply by a set of equations relating the currents between adjacent ports, of the form

$$I_{3BF} = I_{2AR} e^{-j\beta d} \quad (3)$$

where β is the phase propagation constant for the ring and, in this instance, d is the spacing between ports A and B.

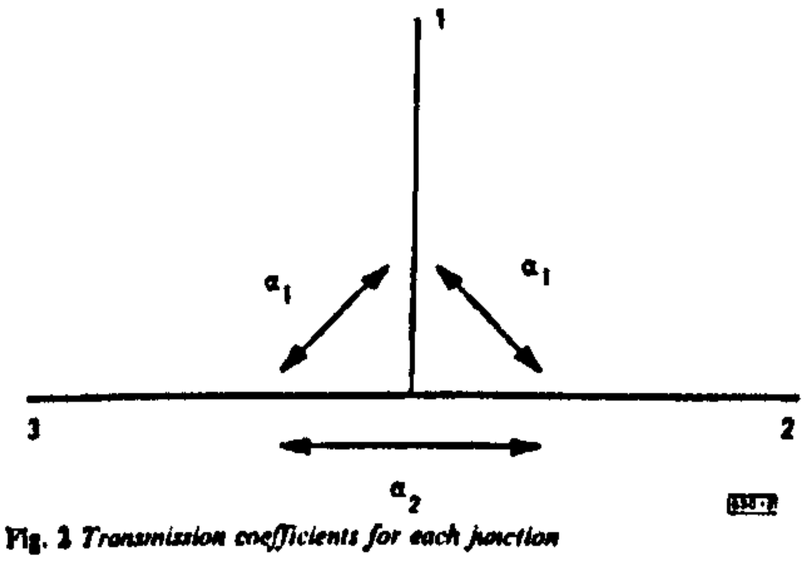

Fig. 2 *Transmission coefficients for each junction*

Thus, sets of equations based on the forms given in eqns. 1 – 3 can be written to fully represent the behaviour of any ring structure, irrespective of ring symmetry.

Three-port ring discriminator: The circuit given in Fig. 1 provides a discriminator response when a signal is applied at port *A* and the

output voltage V_o is obtained as the difference in the detected signals at ports B and C i.e.

$$V_o \propto \left|\frac{I_{1BR}}{I_{1AF}}\right| - \left|\frac{I_{1CR}}{I_{1AF}}\right| \quad (4)$$

with

$$I_{1BF} = I_{1CF} = 0$$

After some manipulation it can be shown that

$$\frac{I_{1BR}}{I_{1AF}} = \alpha_1(\alpha_2(1-\alpha_2 e^{-4\phi_1})+(1-\alpha_2)e^{-\phi_1})(1-\alpha_2^3 e^{-5\phi_1})^{-1} \quad (5)$$

$$\frac{I_{1CR}}{I_{1AF}} = \alpha_1(\alpha_2(1-\alpha_2 e^{-2\phi_1})+(1-\alpha_2)e^{-3\phi_1})(1-\alpha_2^3 e^{-5\phi_1})^{-1} \quad (6)$$

where

$$\phi_1 = \beta\frac{\lambda_o}{4}$$

and where it has been assumed that the ports of the ring have the $\lambda_o/4$ spacings defined in [3].

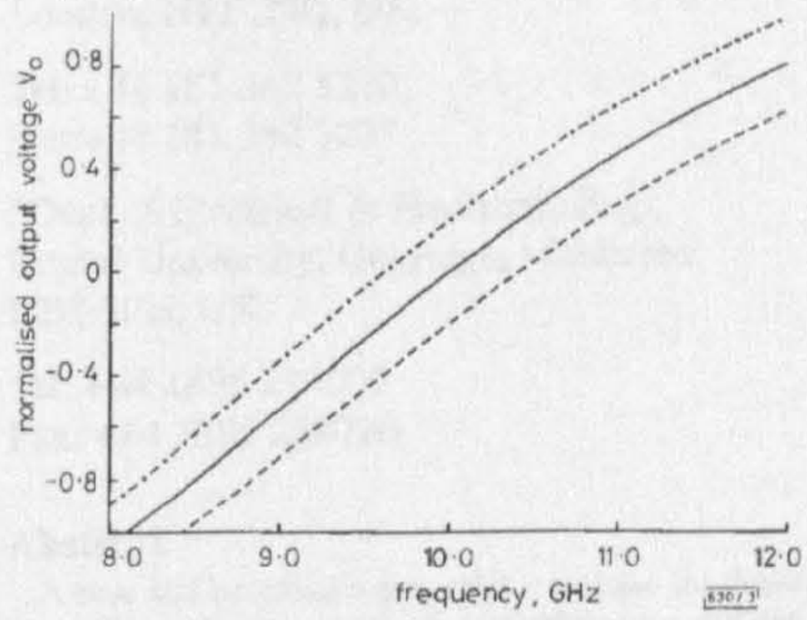

Fig. 3 *Simulated discriminator characteristic, showing effect of changing position of input port and maintaining the original circumference*

The values of δ represent fractions of design wavelength, λ_o

—— δ = 0.00
– – – – δ = 0.01
·– ·– ·– · δ = –0.01

Discussion: The discriminator response obtained using eqns. 4 – 6 is shown in Fig. 3. Also shown are the responses when the input port is displaced by δ from the original position, such that the overall ring circumference remains constant at $5\lambda_o/4$. The responses show that the new method of analysis when applied to the basic three-port ring, give results which are in agreement with those obtained using the conventional method of analysis [3]. Moreover, it has been shown that the method provides a simple analysis of asymmetric structures, as shown from the results for the ring with a displaced input port. If the conventional method was applied to the asymmetric circuit, it would be necessary to introduce a dummy port, to make the geometry symmetric, and then to seek a solution using the odd and even equivalent circuits, which made the output at the dummy port zero. Clearly this would be a more unwieldy mathematical approach, and less amenable to a computer-based solution.

The validity of the new method has also been established through analysis of the conventional four-port hybrid ring.

Conclusions: A new method of analysis of microwave ring structures has been developed, and verified through comparison with known circuit behaviour. The method is less restrictive than existing techniques and is particularly suitable for asymmetric networks.

7 March 1996
Electronics Letters Online No: 19960599

C.E. Free (*School of Electronic Engineering, Middlesex University, Bounds Green Road, London N11 2NQ, United Kingdom*)

C.S. Aitchison (*Department of Electrical and Electronic Engineering, Brunel University, Uxbridge, Middlesex UB8 3PH, United Kingdom*)

References

1 AGRAWAL, A.K., and MIKUCKI, G.F.: 'A printed-circuit hybrid-ring directional coupler for arbitrary power divisions', *IEEE Trans., Microw. Theory Tech.*, 1986, **MTT-34**, (12), pp. 1401–1407
2 COLLIN, R.E.: 'Foundations for microwave engineering' (McGraw-Hill, 2nd edn.), 1992, pp 437–442
3 FREE, C.E., and AITCHISON, C.S.: 'Three-port ring discriminator', *Electron. Lett.*, 1986, **22**, (3), pp. 123–125

Power electronics converter modelling using microwave theory and techniques

J.L. Schnaen, J. Roudet and P. Saguet

Indexing terms: Power electronics, Electromagnetic compatibility, Microwave techniques

The use of microwave theory and techniques is shown to be an attractive way to simulate EMC disturbances in power electronics converters. The approach has been validated in both the time and frequency domains.

Introduction: Power electronics consists in regulating the electrical power transfer between a source and a load by turning semiconductor switches either on or off. With the new switching capability of modern semiconductor devices (MOSFET, IGBT, MCT...) the voltage and current variations (dV/dt, dI/dt) can reach high values; concerning current variations, 400A can now be turned off in 1 μs (0.4A/ns), and predictions are made for devices with 1A/ns capability. For dV/dt, 2 or 3V/ns are relatively frequent during transitions.

These large transient phenomena induce many converter disturbances:

- large voltage surges are induced which can destroy semiconductor devices
- parasitic emitted current can disturb the converter environment, especially the surrounding low level electronics (drive circuit)
- radiated emissions.

All these disturbances are classified under the 'EMC' appellation (electromagnetic compatibility) and are to be taken into account during the converter design phase.

Simulation is a very attractive way to characterise the EMC performances of a power electronics converter because it avoids the building of a prototype and allows a great number of tests. However, the wide frequency spectrum involved in the large transient phenomena does not allow the use of classical lumped elements any more. The idea to use microwave theory appears thus as a good way to model these transients, which are at the origin of EMC disturbances.

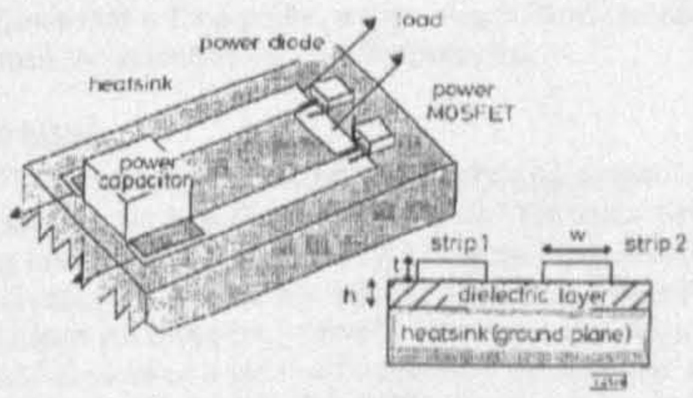

Fig. 1 *Example of a power converter implantation with the heatsink under the power PCB, acting like a ground plane. The structure looks like microstrips*

w = 1cm, h = 1.5mm, t = 35μm. Note that current is flowing from strip 1 to strip 2

Using microwave techniques in power electronics: Power electronics converters are often realised on a classical printed circuit board (PCB) of 35 or 210μm thickness. For thermal reasons (conducted and switching losses are not negligible) an aluminium heatsink is often placed under the whole PCB. As a result, the global structure looks like classical coupled microstrips (Fig. 1).

26th EuMC • 9-12 September 1996 • Hotel Hilton Atrium • Prague • Czech Republic

A digitally controlled microwave oscillator

C E Free and C S Aitchison*

School of Electronic Eng.,
Middlesex University, Bounds Green Road,
London, N11 2NQ, UK.

Tel: +44 181 362 5270
Fax:+44 181 362 5287

*Dept of Electrical & Electronic Eng.,
Brunel University, Uxbridge, Middlesex,
UB8 3PH, UK.

Tel: +44 1895 274000
Fax: +44 1895 258728

Abstract

A new and potentially powerful technique for digitally controlling the frequency of a microwave oscillator is described. The technique, which differs significantly from existing methods, makes use of a multi-feed threeport ring. The circuitry is simple and provides inherent stabilization in addition to frequency control. Measurements at X-band have been made to validate the technique, which has also been established through computer simulation.

Introduction

Delay-line techniques for achieving frequency stabilization of microwave oscillators are well known. Free and Aitchison [1] showed how the basic method could be extended to give frequency control by incorporating a switched phase shifter in the delay-line path. If a digitally controlled phase shifter were used then this method would permit digital frequency selection, although the circuit would be relatively complicated.

In this paper a different and simpler concept is proposed, whereby changes in delay are achieved by switching the feed point to a three port ring. This method has a number of advantages compared to the use of either distributed switched phase shifters or lumped delay-line elements, namely:

- circuit fabrication is made less demanding, by eliminating critical coupling gaps
- no discontinuities exist within the effective delay line path to generate reflections and hence errors in the frequency control voltage
- . the circuit permits simple, precise frequency selection where the accuracy depends mainly on the position of the feed points to a microstrip ring
- digital frequency selection is possible
- only one microwave switch is required to generate each digital bit
- the circuit occupies less substrate area than any other comparable method
- there are no frequency limitations to its implementation.

Circuit Operation

The proposed circuit is shown in figure 1. A three-port ring discriminator circuit is incorporated in the feedback path of a VCO. Two PIN diodes A and B permit the ring to fed at two different positions either independently or simultaneously.

With a single feed, and with the port spacings specified in figure 2, the control voltage V_o applied to the VCO will exhibit a frequency discriminator response as explained in reference [2]. It can be shown theoretically that if the feed position is moved without changing the overall circumference of the ring, and whilst maintaining a $\lambda/4$ spacing between the output ports, the shape of the discriminator response will not change significantly but it will be displaced in frequency from the original position. This will cause a DC offset voltage to be generated at the output of the differential amplifier and this voltage can be used to change the frequency of the oscillator. Therefore, referring to the circuit of figure 1, switching either A or B on will give a stabilized output from the VCO at one of two frequencies determined by the position of the feed ports. Moreover, the theory can be extended to show that if both diodes are switched on simultaneously a discriminator response is obtained with an offset voltage midway between the values obtained with the diodes switched individually. Hence the arrangement provides digital control of the offset voltage, and consequently of the oscillator frequency, with two feeds permitting the selection of three frequencies. It follows that n feed paths, with a single diode in each, will permit the selection of 2^n-1 frequencies.

Analysis

The conventional method of analyzing microstrip ring structures, such as the hybrid ring and the basic three-port ring discriminator, involves reducing the ring circuit to two equivalent two-port networks, and then summing the solutions for these two circuits. However, this requires the establishment of a plane of symmetry through the original circuit, as explained in Collin [3]. Such an approach is not attractive for the proposed digital control circuit, since there is no inherent plane of symmetry, and this would have to be created through the introduction of a dummy port and a solution sought which makes the signal at the dummy port zero. Therefore in the present work, a new current summing technique, recently reported by Free and Aitchison [4] was employed.

This technique requires the current entering and leaving each port to be identified as shown in figure 3. Summing the currents at each port of the network, and writing relationships for the currents flowing in the ring in terms of the transmission coefficients between and through the ports, leads to a set of linear equations from which the ratios of the currents entering and leaving any two ports can be obtained.

Results and Discussion

Using the current summing theory, computer simulations were obtained for a ring with two feeds. The three discriminator responses, corresponding to the three possible diode states are shown in figure 4. The responses are linear in the vicinity of the nominal design frequency of 10GHz, with the different diode states producing equal increments in the offset voltage, thus indicating that linear frequency control of the oscillator is possible.

Table 1 shows typical test results obtained with a microstrip circuit at X-band. The test circuit was fabricated on RT/duroid having a substrate thickness of 635 μm and a relative permittivity of 10.5. Low-loss, beam-lead PIN diodes (HPND-4005) were used as the switching elements. The distance between the PIN diodes and the ring was made $\lambda_g/2$ at the design frequency so that a feed arm containing a diode in the OFF state would reflect a high shunt impedance across the ring.

The practical results show that the three possible diode state combinations yield three frequencies with approximately equal intervals between them. The magnitude of the frequency steps can be changed by altering the sensitivity of the feedback amplifier. The oscillator remained stabilized at each frequency and a typical plot of the relative phase noise, showing the effect of stabilization, is reproduced in figure 5. A phase noise reduction of 13dB was observed 5kHz off the carrier and this is consistent with a measured stabilization ratio of 5. (The absolute values of the phase noise are a function of the particular test oscillator being used and are not of primary interest here.)

Clearly the number of frequency selection can be increased by having more feed arms to the ring, but there are some limitations. Firstly, all of the feed positions should be on the same side of the ring, otherwise the polarity of the offset voltage and the sign of the discriminator slope changes. Secondly, the spread of feed positions around the ring is limited, as the slope of the discriminator response will change, leading to a change in stabilization and hence in the phase noise reduction. Lastly, simple layout considerations restrict the number of entry points to the ring, so as to avoid unwanted coupling effects between the feed paths. However, these are not major limitations, and the basic ring circuit can always be cascaded to provide more frequency selections as shown in figure 6. In the cascaded arrangement shown, the microwave signal is applied at port X and the 4 diodes controlling the feed paths to each ring generate 2^4-1 different voltage levels, giving a total of 225 levels at the output of the final summing amplifier, i.e. 8 diodes would permit the selection of 225 different frequencies.

Conclusions

A new technique for implementing digital control of a microwave oscillator has been established and confirmed through practical measurements. The technique appears very attractive because of its simplicity, lack of frequency constraints and the potential to be implemented in an MMIC format.

References

[1] Free, C.E. and Aitchison, C.S. "Microwave oscillator control using a switched delay-line technique" IEEE MTT-Symposium, Orlando, 1995, pp79-82

[2] Free, C.E. and Aitchison, C.S. "Three-port ring discriminator" Electron. Lett., Vol 22, No 3, 1986, pp124-125

[3] Collin, R.E. Foundations for Microwave Engineering McGraw-Hill, 2nd Ed, 1992, pp437-442

[4] Free, C.E. and Aitchison, C.S. "Analysis of microstrip ring structures" Electron. Lett., Vol 32, No 10, 1996, pp903-904.

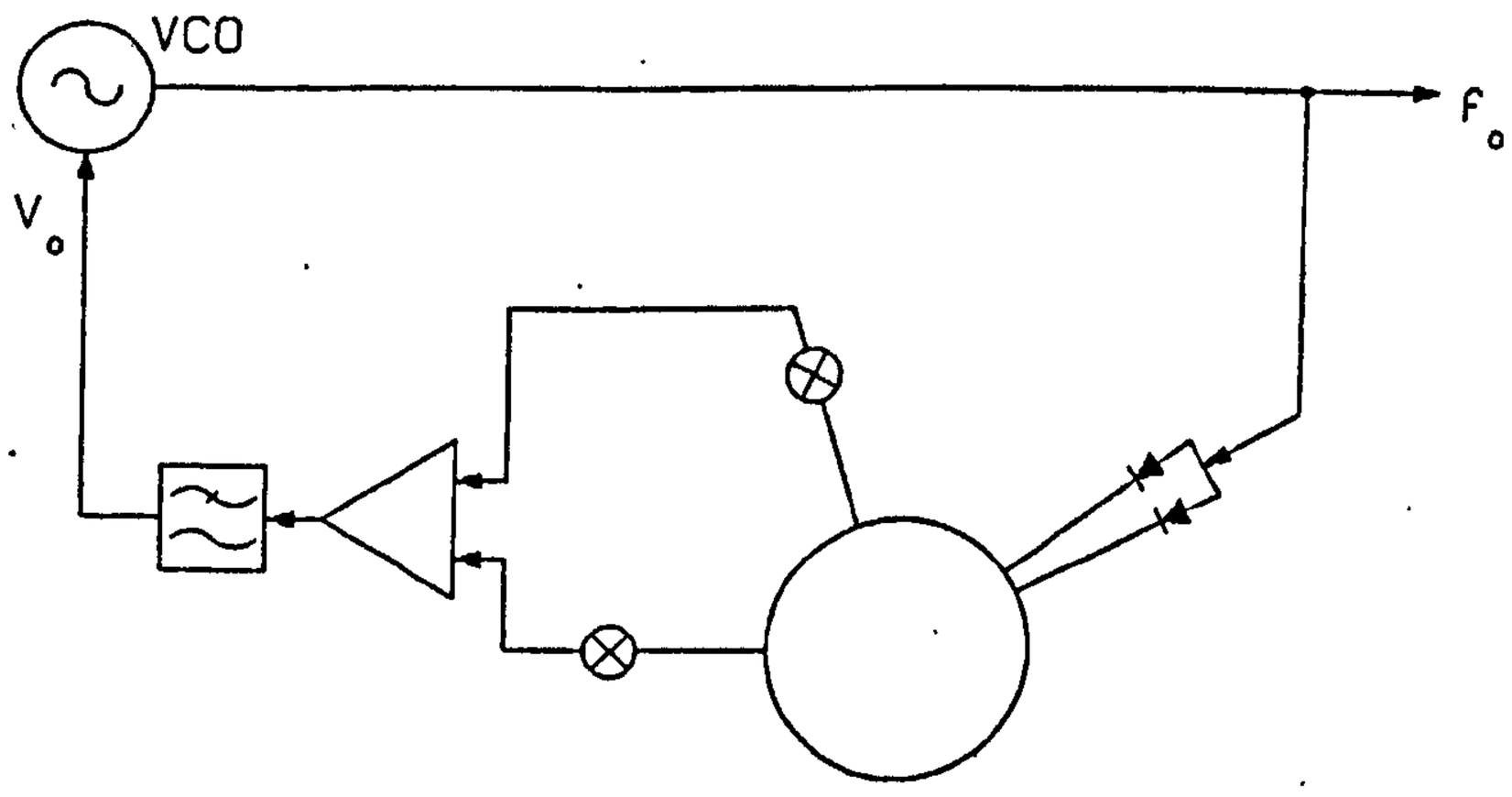

Figure 1 Frequency control circuit showing dual-fed microstrip ring.

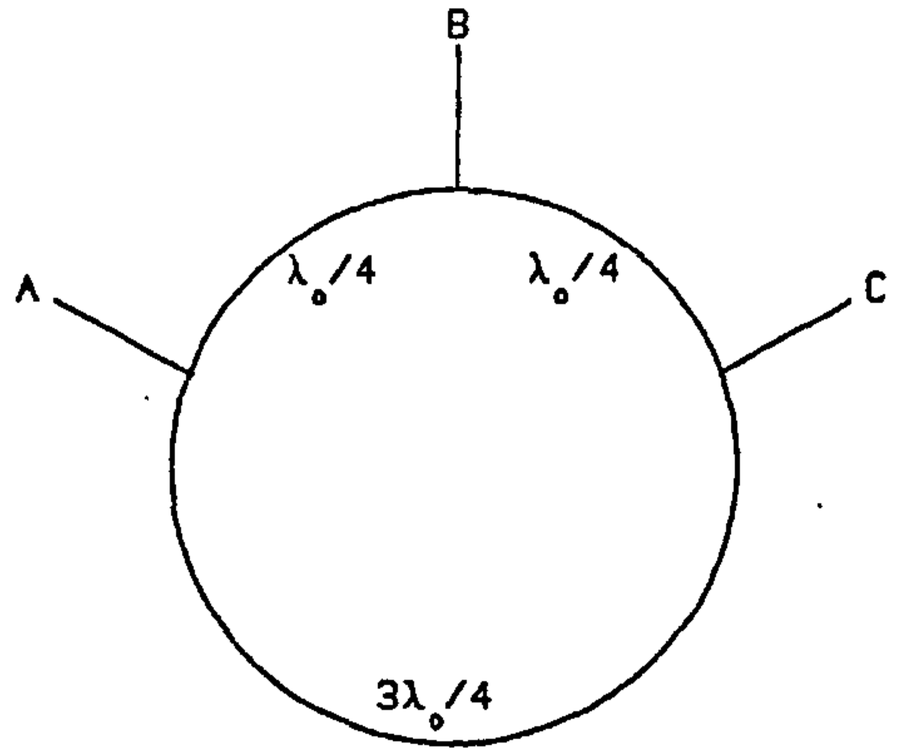

Figure 2 Port separations for a 3-port ring giving a discriminator characteristic centred on f_o ($=v_p/\lambda_o$)

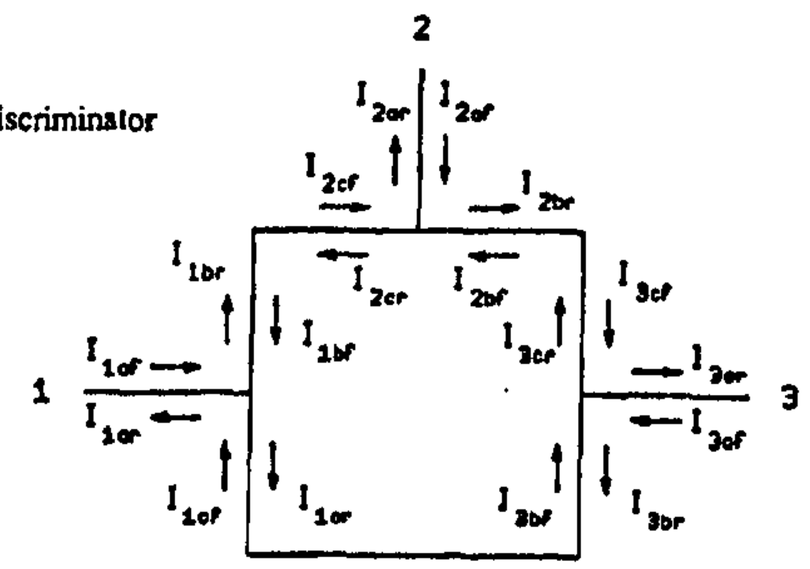

Figure 3 Current nomenclature used in the analysis of asymmetric ring structures.

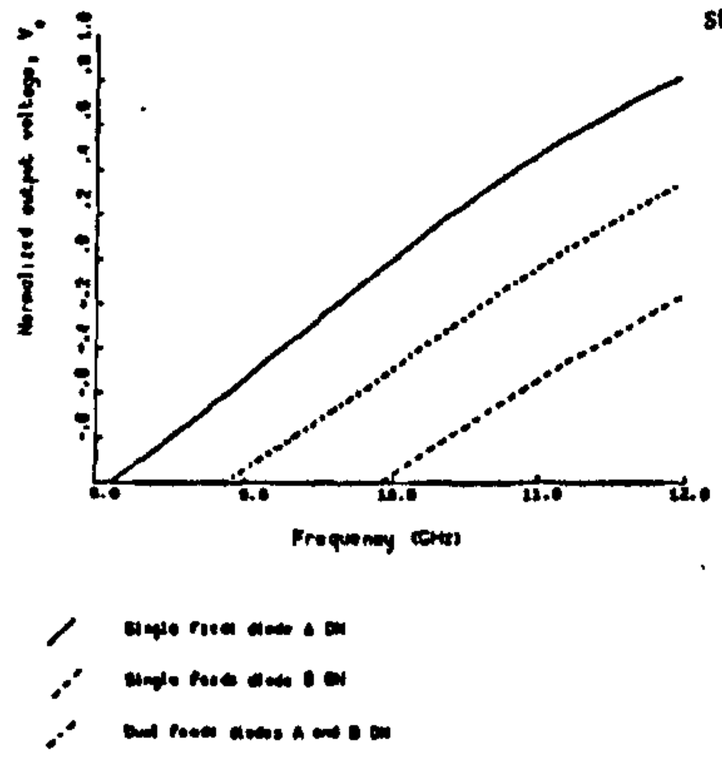

Figure 4 Simulated discriminator responses, with a feed separation of $0.05\lambda_o$ (λ_o is the ring wavelength at 10GHz)

Digitally selected frequencies (GHz)	10.0, 10.1, 10.2
Stabilization ratio	5
Phase noise reduction	−13dB

Table 1 Summary of essential results for a 2-bit system

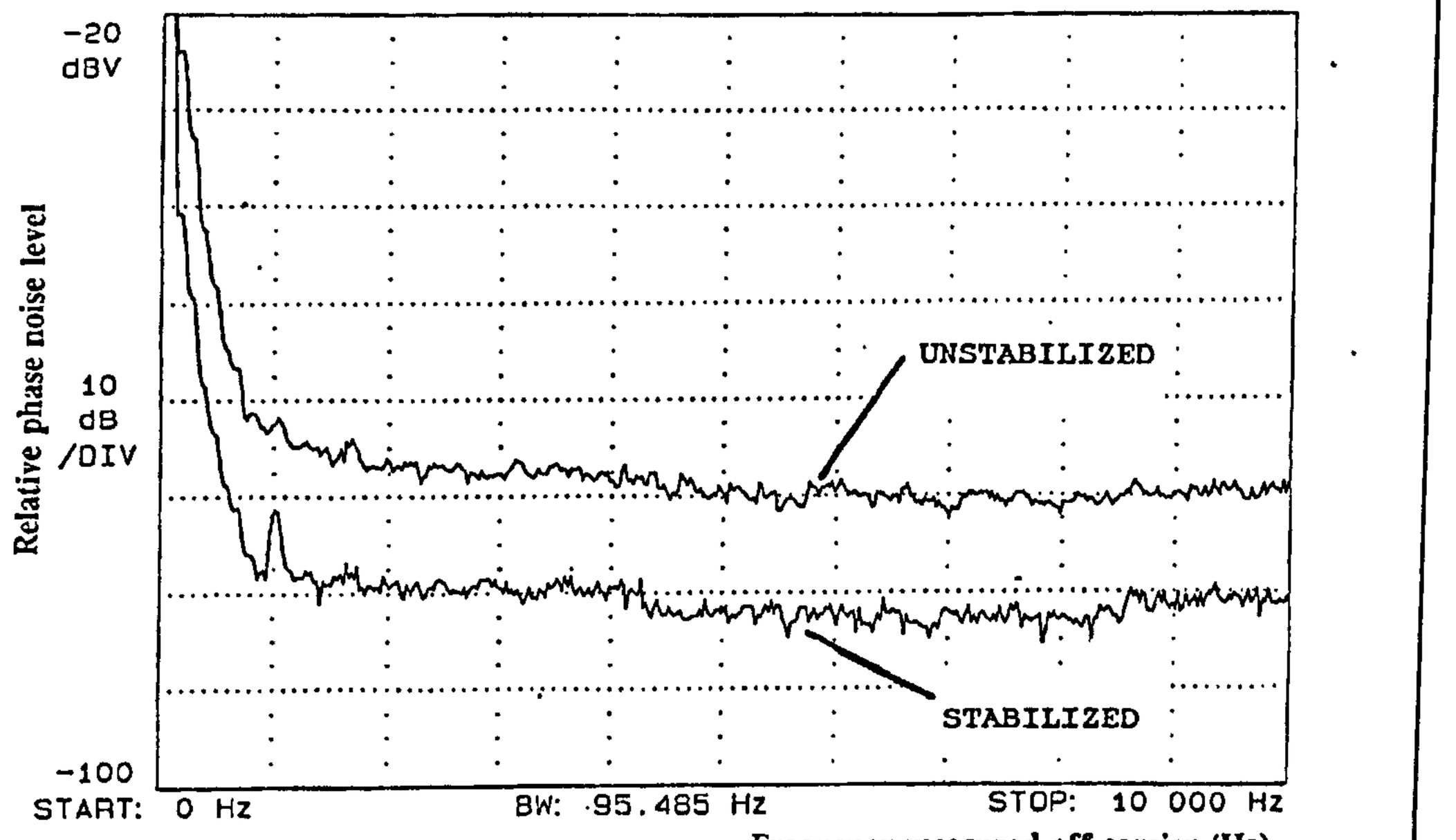

Figure 5 Typical phase noise response

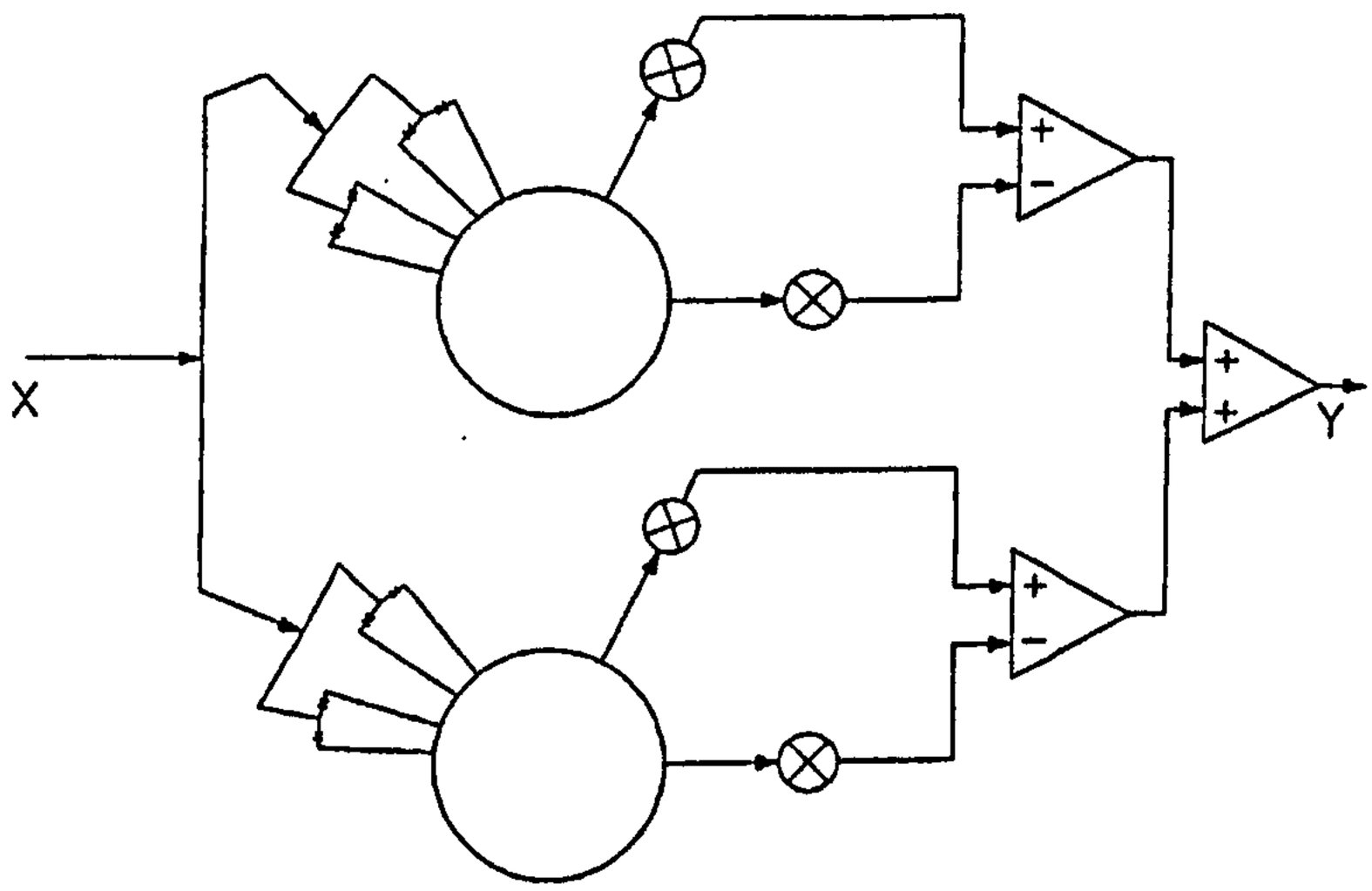

Figure 6 Cascaded three-port rings providing extended frequency selection

Bibliography

[1] UNDERHILL, M.J. 'Delay-stabilised variable oscillator.', *Electronics Lett.*, 1972 **Vol. 8**, pp115-117

[2] AITCHISON, C.S. and BATLIWALA, E.R. 'Delay-line-stabilised microwave oscillator.', *Electronics Lett.*, 1975 **Vol. 12**, pp56-57

[3] BATLIWALA, E.R. and AITCHISON, C.S. 'A low temperature dependent substrate.', *Proc. IEEE*, 1977 pp1207-1208

[4] GLANCE, B. and SNELL, W.W. 'A discriminator stabilised microstrip oscillator', *IEEE Trans.*, 1976 **MTT-10**, pp648-650

[5] AMBLARD, Y. and PEYRAT, A. 'X-band bulk-wave delay-line stabilised oscillator', *Proc. MTT-S*, 1980, pp339-341

[6] KIM, D.I. and NAITO, Y. 'Broad-band design of improved hybrid-ring 3dB directional couplers', *IEEE Trans.*, 1982 **MTT-11**, pp2040-2046

[7] AYASLI, Y., PLATZKER, A., VORHAUS, J. and REYNOLDS, L.D. 'A monolithic single-chip X-band four-bit phase shifter', *IEEE Trans.*, 1982 **MTT-30**, pp2201-2205

[8] GLANCE, B. 'A fast low-loss low-drive 14GHz microstrip p-i-n phase shifter', *IEEE Trans.*, 1980 **MTT-28**, pp669-670

[9] WILSON, K., NICHOLAS, J.M.C., McDERMOTT, G. and BURNS, J.W. 'A novel MMIC X-band phase shifter', *IEEE Trans.*, 1985 **MTT-33**, pp1572-1578

[10] JONES, E.M.T. and BOLLJAHN, J.T., 'Coupled strip transmission line filters and directional couplers', *IRE Trans.*, 1956 **MTT-4**, pp75-81

[11] SCHIFFMAN, B.M., 'A new class of broadband microwave 90° phase shifter', *IRE Trans.*, 1958, **MTT-6**, pp232-237

[12] WHITE, J. 'Microwave Semiconductor Engineering' van Nostrand Reinhold, New York, 1982

[13] SCHIEK, B. and KOHLER, J. 'A method for broadband matching of differential phase shifters' *IEEE Trans.* , 1977, **MTT-25**, pp666-671

[14] GETSINGER,W.J. 'Microstrip of parallel coupled microstrip' *IEEE. Trans.* , 1973, **MTT-21**, pp145-146

[15] HAMMERSTAD, E.O. and BEKKADAL, F. 'A Microstrip Handbook' ELAB report STF44 A74169, N7034, University of Trondheim, Norway, 1975

[16] HAMMERSTAD, E.O. and BEKKADAL, F. 'A Microstrip Handbook' ELAB report STF44 A74169, N7034, University of Trondheim, Norway, 1975

[17] LACOMBE, D and COHEN, J. 'Octave-band microstrip DC blocks' *IEEE. Trans.* , 1972, **MTT-20**, pp555-556

[18] BENEDEK, P. and SILVESTER, P. 'Equivalent capacitances for microstrip gaps and steps' *IEEE. Trans.* , 1972, **MTT-20**, pp729-733

[19] GARG, R. and BAHL, I.J. 'Microstrip discontinuities' Int. Journal of Electronics, 1978, pp81-87

[20] EASTER, B. and GUPTA, K.C. 'More accurate model of coupled microstrip line section' *IEE J. Microwaves, Optics and Acoustics*, 1973, **Vol. 3**, No. 3, pp99-103

[21] KIRSCHNING, M. and JANSEN, R.H. 'Accurate wide-range design equations for the frequecy-dependent characteristics of parallel coupled microstrip lines' *IEEE. Trans.* , 1984, **MTT-32**, pp83-90

[22] FOOKS, E.H. and ZAKAREVICIUS, R.A. 'Microwave Engineering using Microstrip Circuits' *Prentice-Hall*, 1990, pp110-112

[23] OZMEHMET, K. 'New frequency dependent equivalent circuit for gap discontinuities in microstriplines' *Proc. IEE* , 1987, **Part H**, Vol 134, No 3, pp333-335

[24] CRAWFORD, J. 'Frequency Synthesizer Design Handbook' *Artech House*, Boston, 1994, pp

[25] ZARBEL, C.W. 'Microwave Duplexers' *MIT Radiation Laboratory Series*, Vol. 14, Boston 1964, pp357-361

[26] PON, C.Y. 'Hybrid ring directional coupler for arbitrary power divisions' *IRE Trans.*, 1961, **MTT-9**, pp529-535

[27] THOMSON, A.F. and GOPINATH, A. 'Calculation of microstrip discontinuity inductances' *IEEE Trans.*, 1975, **MTT-23**, No.8, pp648-655

[28] EASTER, B., GOPINATH, A. and STEPHENSON, I.M. 'Theoretical and experimental methods for evaluating discontinuities in microstrip' *Radio and Electronic Engr.*, 1978, **48**, pp73-84

[29] MEHRAN, R. 'Frequency dependent scattering matrices of microstrip right-angle bends, T-junctions and crossings' *AEU*, 1976, **30**, pp80-82

[30] DYDYK,M. 'Master the T-junction and sharpen your MIC designs' *Microwaves*, 1972, May, pp184-186

[31] CHAPMAN, A.G. and AITCHISON, C.S. 'A broad-band model for a coaxial-to-microstrip transition' *IEEE Trans.* , 1980, **MTT-28**, No.2, pp130-136

[32] GOURLEY, S.E. and CHAPMAN, A.G. 'Broadband characterization of coaxial-to-microstrip transitions' *IEE Colloquium*, 'MIC Developments', April 1982

[33] EDWARDS, T.C. 'Foundations for microstrip circuit design' *John Wiley*, London, 1992

[34] OWENS, R.P. 'Curvature effects in microstrip ring resonators' *Electronics Letters*, 1976, **12**, No. 14, pp356-357

[35] AKELLO, R.J., EASTER, B. and STEPHENSON, I.M. 'Equivalent circuit of the asymmetric crossover junction' *Electronics Letters*, 1977, **13**, No.4, pp117-118 *Electronics Letters*, 1976, **12**, No. 14, pp356-357

[36] GUPTA, K.C., GARG, R. and BAHL, I.J. 'Microstrip Lines and Slotlines' *Artech House*, Boston, 1996

[37] RIZZOLI, V., MASTRI, F., MASOTTI, D., NERI, A. 'Full non-linear analysis of near-carrier noise in discriminator stabilized microwave oscillators' *Microwave and Optical Letters*, **6**, No.12, Dec 1993, pp907-911